3-28-2024 10:00 AM

Structure and Function of Long-COVID Evaluated Using Pulmonary Imaging

Harkiran Kaur Kooner, *The University of Westen Ontario*

Supervisor: Parraga, Grace, *The University of Western Ontario*

A thesis submitted in partial fulfillment of the requirements for the Doctor of Philosophy degree in Medical Biophysics

Abstract

The COVID-19 pandemic has resulted in millions of global respiratory infections, ranging in severity from asymptomatic to fatal. One of the many consequences of the pandemic is the emergence of long-COVID, which is an umbrella term used to describe the long-term sequelae and poor quality-of-life following recovery from acute COVID-19 infection. However, the pathophysiology and mechanisms responsible for the heterogenous manifestation of long-COVID remain poorly understood. Hyperpolarized ^{129}Xe magnetic resonance imaging (MRI) provides a non-invasive and radiation-free method to regionally visualize and quantify inhaled gas distribution and ventilation *in vivo*. A strong foundation for the use of pulmonary imaging in asthma and chronic obstructive pulmonary disease (COPD) to strengthen our grasp of disease processes suggests the utility of imaging in long-COVID. Accordingly, the objective of this thesis was to develop a deeper understanding of the structure and function of long-COVID using hyperpolarized ^{129}Xe MRI in tandem with structural computed tomography (CT) imaging. First, we investigated a group of long-COVID participants three months post-infection and observed an increased ventilation defect percent (VDP) in ever- as compared to never-COVID participants. At a follow-up visit one year later, we reported a significant improvement in VDP and the use of airways disease medication increasing the odds of quality-of-life improvement. We then contextualized CT airway sex differences in long-COVID participants by reporting similarities in CT evidence of airway remodelling for females with long-COVID and ex-smokers with and without COPD. Finally, we showed that MRI ventilation textures were predictive of one year improvement in quality-of-life, outperforming VDP and clinical measurements. Taken together, these results suggest an airways disease component to long-COVID that can help guide clinical decision making and improve patient outcomes.

Keywords

Airways, Computed Tomography, COVID-19, Long-COVID, Hyperpolarized Noble Gas Magnetic Resonance Imaging, Pulmonary Imaging, Pulmonary Structure-Function, SARS-CoV-2, Ventilation

Summary for Lay Audience

The COVID-19 pandemic was very widespread and lead to infections in millions of people around the world. After recovering from COVID-19, many people reported symptoms that did not go away or the inability to return to their normal life, we refer to this as long-COVID. Unfortunately, we still do not completely understand why these people with long-COVID continue to feel poorly. In this thesis, we used structural computed tomography (CT) and functional magnetic resonance imaging (MRI) to better understand which parts of the respiratory system could play a role in long-COVID. First, we found that patients with long-COVID had worse lung ventilation measured on MRI compared to people who were never infected with COVID-19. Then, after one year, we observed these lung ventilation measurements improved and that people who were taking respiratory medication were more likely to improve in their quality-of-life. In addition, we reported that CT measurements of the airways in the lungs are different between male and females with long-COVID, where females with long-COVID have similar measurements to females with chronic respiratory disease. Finally, we showed that patterns and texture of our ventilation MR images could be used to tell us which patients with long-COVID would improve over one year. When we take all these results together, we can say that there is some dysfunction of the airways occurring in people with long-COVID, which can help us better treat these patients.

Co-Authorship Statement

This thesis contains four manuscripts, two of which have been published in scientific journals and two of which have been submitted for publication. As first author of three of these manuscripts and co-first author alongside Marrissa J McIntosh of one of these manuscripts, I significantly contributed to all aspects of these studies as well as manuscript preparation and submission. Specifically, I made intellectual contributions to all study designs and was responsible for the organization and management of study visits. I also acquired a large portion of the pulmonary function test and imaging data. I was responsible for analyzing the hyperpolarized gas images to measure ventilation defects and segmenting all the computed tomography images to generate airway measurements. I also extracted the texture features from the ventilation gas images and generated the machine-learning models. I was responsible for statistical analysis and interpretation, as well as drafting, final approval, and submission of the manuscripts. As Principal Investigator and Supervisor, Dr. Grace Parraga provided continuous guidance and was responsible for study and experimental design, data analysis and interpretation, drafting and final revisions, and approval of the manuscripts. She is also the guarantor of study data integrity and responsible for Good Clinical Practice. The management of study visits and acquisition of pulmonary function test and imaging data were performed under the supervision of Angela Wilson. MRI of research participants was performed by David Reese. Polarization of ^{129}Xe was performed by Alexander Matheson, Maksym Sharma, Ivailo Petrov, and Tamas Lindenmaier. For each manuscript within this thesis, all co-authors approved the final draft and the specific author contributions are listed below:

Chapter 2 is an original research article entitled *"^{129}Xe MRI Ventilation Defects in ever- and never-hospitalised people with post-acute COVID-19 syndrome"* and was published in the journal *BMJ Open Respiratory Research* in 2022. This manuscript is co-authored by Harkiran K Kooner, Marrissa J McIntosh, Alexander M Matheson, Carmen Venegas, Nisarg Radadia, Terence Ho, Ehsan Haider, Norm B Konyer, Giles E Santyr, Mitchell S Albert, Alexei Ouriadov, Mohammed Abdelrazek, Miranda Kirby, Inderdeep Dhaliwal, J Michael Nicholson, Parameswaran Nair, Sarah Svenningsen, and Grace Parraga. Harkiran K Kooner and Marrissa J McIntosh are co-first authors and contributed equally to this manuscript. Marrissa J McIntosh

was responsible for data analysis and interpretation and was responsible for the first draft of the manuscript. Alexander M Matheson, Carmen Venegas, Nisarg Radadia, Norm B Konyer, and Sarah Svenningsen assisted with data acquisition. Mohammed Abdelrazek and Ehsan Haider assisted with CT acquisition and evaluated the CT data. Carmen Venegas, Terence Ho, Parameswaran Nair, Inderdeep Dhaliwal, and J Michael Nicholson were responsible for recruiting study participants and providing clinical input and interpretation of the data. Giles E Santyr, Mitchell S Albert, Alexei Ouriadov, Inderdeep Dhaliwal, J Michael Nicholson, Miranda Kirby, and Sarah Svenningsen supported the study design development and interpretation of the data.

Chapter 3 is an original research article entitled *"Post-Acute COVID-19 Syndrome: ^{129}Xe MRI Ventilation Defects and Respiratory Outcomes One Year Later"* and was published in the journal *Radiology* in 2023. This manuscript was co-authored by Harkiran K Kooner, Marrissa J McIntosh, Alexander M Matheson, Mohammed Abdelrazek, Mitchell S Albert, Inderdeep Dhaliwal, Miranda Kirby, Alexei Ouriadov, Giles E Santyr, Carmen Venegas, Nisarg Radadia, Sarah Svenningsen, J Michael Nicholson, and Grace Parraga. Marrissa J McIntosh assisted with data acquisition, analysis, and interpretation. Alexander M Matheson, Carmen Venegas, and Nisarg Radadia assisted with data acquisition. Mohammed Abdelrazek assisted with CT acquisition and evaluated the CT data. Inderdeep Dhaliwal and J Michael Nicholson were responsible for recruiting study participants and providing clinical input and interpretation of the data. Giles E Santyr, Mitchell S Albert, Alexei Ouriadov, Inderdeep Dhaliwal, J Michael Nicholson, Miranda Kirby, and Sarah Svenningsen supported the study design development and interpretation of the data.

Chapter 4 is an original research article entitled *"Chest CT Airway and Vascular Measurements in Females with Long-COVID, Ex-smokers and COPD Patients"* and was submitted to the journal *Respirology*. This manuscript was co-authored by Harkiran K Kooner, Paulina V Wyszkiewicz, Alexander M Matheson, Marrissa J McIntosh, Mohamed Abdelrazek, Inderdeep Dhaliwal, J Michael Nicholson, Miranda Kirby, Sarah Svenningsen, and Grace Parraga. Paulina V Wyszkiewicz, Alexander M Matheson, and Marrissa J McIntosh assisted with data acquisition and analysis. Mohammed Abdelrazek assisted with CT acquisition and

evaluated the CT data. Inderdeep Dhaliwal and J Michael Nicholson were responsible for recruiting study participants and providing clinical input and interpretation of the data. Inderdeep Dhaliwal, J Michael Nicholson, Miranda Kirby, and Sarah Svenningsen supported the study design development and interpretation of the data.

Chapter 5 is an original research article entitled *"^{129}Xe MRI Ventilation Textures and Longitudinal Quality-of-Life Improvements in Long-COVID"* and was published in the journal *Academic Radiology* in 2024. This manuscript was co-authored by Harkiran K Kooner, Maksym Sharma, Marrissa J McIntosh, Inderdeep Dhaliwal, J Michael Nicholson, Miranda Kirby, Sarah Svenningsen, and Grace Parraga. Maksym Sharma assisted with data acquisition, analysis, and interpretation. Marrissa J McIntosh assisted with data acquisition and analysis. Inderdeep Dhaliwal and J Michael Nicholson were responsible for recruiting study participants and providing clinical input and interpretation of the data. Inderdeep Dhaliwal, J Michael Nicholson, Miranda Kirby, and Sarah Svenningsen supported the study design development and interpretation of the data.

To our study participants who taught me the true impact of research.

Acknowledgments

First and foremost, I would like to thank my supervisor, Dr. Grace Parraga, for your endless support and mentorship throughout my graduate school experience. You always set the highest of expectations, allowing me the space and opportunity to continuously strive for new goals and grow well beyond where I thought possible. With your guidance and support, the personal, professional, and scholarly development I have experienced is unmatched by any other past opportunity in my life. Your never-ending drive and passion for research and innovation is contagious and I am grateful for the years I had to learn it from you.

To my advisory committee, Dr. Michael Nicholson, Dr. Ali Khan, and Dr. Kathleen Surry, thank you for your unwavering support and commitment to my success in graduate school and beyond. To Dr. Nicholson, thank you for your clinical insight and providing the context for our research in a real-world setting, which has become invaluable to me. To Dr. Khan, thank you for pushing my understanding of the technical details of my research, helping me to build a more complete skillset during graduate school. To Dr. Surry, thank you for always being in my corner, asking the questions I never would have considered otherwise, and for your steadfast support of my future career aspirations. I am also grateful to other mentors outside Western University, in particular Dr. Rachel Eddy and Dr. Sarah Svenningsen, for their limitless support and collaborative efforts. I would also like to thank all collaborators on the LIVECOVIDFREE study without whom this thesis would not be possible.

To all members of the Parraga lab, past and present, thank you for creating an environment that made coming into Robarts enjoyable, even in those early morning hours. To Marrissa, thank you taking me under your wing and making the transition into graduate school much less painful than it could have been. I will forever be grateful for our partnership in our research and for all I learned from you. To Maks, thank you for being an amazing senior student mentor and an even better friend. You know you helped keep me sane and I couldn't have asked for a better person to tackle this adventure with. To Alex, thank you for your mentorship from the very beginning of my graduate journey and putting up with all my friendly ribbing (you were a fun target). To Paulina, thank you for always being there for a happy chat or laugh and allowing me to mentor you in any way I could, you made it fun to come into lab every day. To

Sam and Ali, thank you for allowing me to be one of your many mentors and I wish you all the best in everything you decide to do.

To Angela, thank you for your unwavering support throughout my entire graduate experience. You have been my biggest cheerleader, always there to offer an encouraging word or sympathetic shoulder. Thank you for letting me use your office as a safe space and for the endless supply of sugar. To Hana, thank you for your clinical expertise, the endless arguments over mucus plugs, and the laughter. To Ivailo and Tamas, thank you for your contributions to our research. To Dave, thank you for making patient visits fun and always being a friendly face, no matter what. To Lauren, thank you for giving me a friend during this last year, probably when I needed it most.

Most importantly, I would like to thank my friends and family, without whom I could not have gotten to this point. To Navjot, Jasdeep, and Hardeep, thank you for your lifelong friendship and endless support for everything I decide to do. To Lauren, Kevin, Kesavi, Dana, Brett, and Jessica, thank you for making London feel like home and for the countless adventures and never-ending laughter. To my siblings, Puneet, Sharon, and Kamal, thank you for always having my back and keeping me grounded in reality. Our relationships mean more to me than I could ever articulate. To my parents, who have always been my greatest source of unconditional love and support, regardless of circumstance, and the greatest proponents of the importance of my education. To my mom, who is my favourite person to gossip with, thank you for being limitless in your faith in me and caring more about my well-being than any success or accomplishment. To my dad, thank you for always encouraging me to strive for new heights and knowing (even more than me) what I am capable of achieving. I have been blessed to have you as my parents. To all my other friends and family members, too many to name, all I can say is *thank you*.

Finally, I would like to express my gratitude to the sources of funding I have been fortunate to be recipient of. I acknowledge funding from the Natural Sciences and Engineering Research Council (NSERC), the Canadian Institutes of Health Research – Institute of Circulatory and Respiratory Health (CIHR-ICRH), Asthma Canada, the Canadian Allergy, Asthma, and Immunology Foundation (CAAIF), as well as the Western Graduate Research Scholarship.

Table of Contents

List of Tables

List of Figures

List of Equations

List of Appendices

List of Abbreviations

$\%_{pred}$ = percentage of a predicted value

6MWT = six-minute walk test

6MWD = six-minute walk distance

ACE2 = angiotensin converting enzyme 2

ADC = apparent diffusion coefficient

AUC = area under the receiver-operator curve

A_X = area of reactance

BV_5 = volume of pulmonary vessels with cross sectional area less than 5 mm^2

BV_{5-10} = volume of pulmonary vessels with cross sectional area between 5 and 10 mm^2

BV_{10} = volume of pulmonary vessels with cross sectional area greater than 10 mm^2

COPD = chronic obstructive pulmonary disease

CT = computed tomography

DL_{CO} = diffusing capacity of the lungs for carbon monoxide

ERV = expiratory reserve volume

FeNO = fraction of exhaled nitric oxide

FEV_1 = forced expiratory volume in 1-second

FO = first order

FOT = forced oscillation technique

FRC = functional residual capacity

FVC = forced vital capacity

GLCM = gray-level co-occurrence matrix

GLI = Global Lung Function Initiative

GLRLM = gray-level run-length matrix

HU = Hounsfield unit

IC = inspiratory capacity

IPAQ =International Physical Activity Questionnaire

IRV = inspiratory reserve volume

LA = lumen area

LCI = lung clearance index

MBW = multiple-breath washout

MCID = minimal clinically important difference

MERS = Middle East Respiratory syndrome coronavirus

mMRC = modified Medical Research Council

MRI = magnetic resonance imaging

NGTDM = neighbourhood gray tone difference matrix

OS = original shape

PACS = post-acute COVID-19 syndrome

PET = positron emission tomography

Pi10 = square root of wall area of a hypothetical airway of internal perimeter of 10 mm

R_5 = oscillometry measurement of total airway resistance

R_{5-19} = oscillometry measurement of distal airways resistance

R_{19} = oscillometry measurement of large airway resistance

R = airway resistance

RV = residual volume

SARS-CoV-2 = severe acute respiratory syndrome coronavirus-2

SGRQ = St. George's Respiratory Questionnaire

SPECT = single photon emission computed tomography

SpO_2 = oxygen saturation acquired using pulse oximetry

SNR = signal-to-noise ratio

TAC = total airway count

TBV = total blood volume

TLC = total lung capacity

UTE = ultra-short echo time

VC = vital capacity

VD = anatomic dead space

VDP = ventilation defect percent

VT = tidal volume

WA% = wall area percent

WHO = World Health Organization

WT = wall thickness

X_5 = oscillometry measurement of reactance at 5 Hz

X = airway reactance

Chapter 1

1 INTRODUCTION

The COVID-19 pandemic drastically impacted the world and resulted in respiratory infection in millions of people. As a result, there are global reports of persistent symptoms and poor quality-of-life enduring beyond acute infection, referred to as long-COVID. In this thesis, pulmonary magnetic resonance imaging (MRI) and computed tomography (CT) are utilized to investigate the structure and function of long-COVID in order to deepen our understanding of the potential mechanisms and pathophysiology contributing to abnormalities in the long-COVID lung.

1.1 Motivation and Rationale

The severe acute respiratory syndrome coronavirus-2 (SARS-CoV-2), colloquially referred to as COVID-19, was first discovered in December 2019.[1] The initial reports included descriptions of severe pneumonia in three patients who required hospitalization, one of whom died.[1] The infection continued to spread throughout Wuhan, China, with common symptoms at onset including fever, cough, and myalgia and leading to a diagnosis of viral pneumonia.[2] Beyond these first reports of infection, COVID-19 continued to rapidly spread to other countries worldwide, leading to the declaration of a pandemic by the World Health Organization (WHO) on March 11, 2020.[3] At this point, there were more than 118,000 global cases reported in 114 countries.[3] Despite the introduction of self-isolation guidelines, travel restrictions, and lockdowns around the world, COVID-19 infection and transmission continued to rapidly rise.[4] By the first few days of April 2020, there were over a million reported cases of COVID-19 worldwide and this number had doubled by mid-April.[4] **Figure 1-1** summarizes the increase in global COVID-19 cases over time. The first case of COVID-19 in Canada was reported at the end of January 2020[5] and by March 2023, there were more than 4.5 million cases reported.[4]

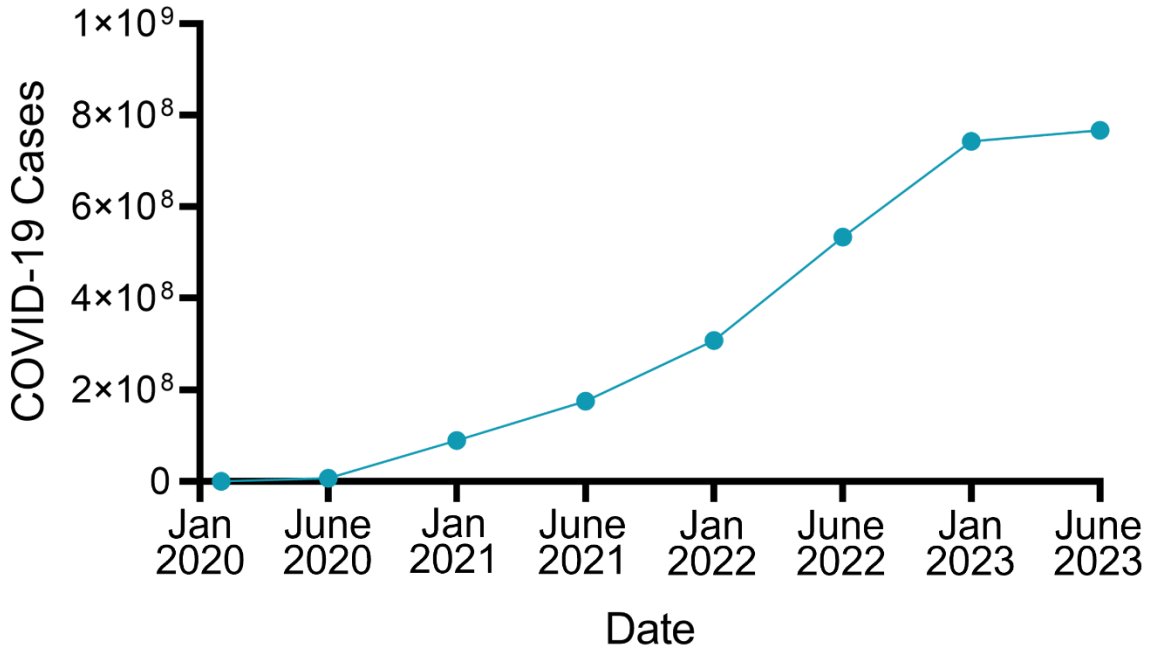

Figure 1-1. Global cases of COVID-19 infection
The number of global cases of COVID-19 infection between January 2020 and June 2023, as reported by the World Health Organization.[6]

In addition to the incredible burden and strain placed on healthcare systems by COVID-19, a new phenomenon of persistent symptoms emerged in the months following the onset of the pandemic. Residual effects following COVID-19 infection can include persistent fatigue, dyspnea, chest pain, brain fog, arthralgia, and poor quality-of-life.[7,8] Multiple terms have been coined to describe these effects, including post-acute COVID-19 syndrome,[9] post-COVID condition,[10] post-acute sequelae of COVID-19,[11] or long-COVID.[12] Although estimates for the prevalence of long-COVID vary across study population, meta analysis has reported a global pooled prevalence of up to 43% to 45% in people infected with COVID-19 regardless of hospitalization status.[13,14] Similar to the COVID-19 cases, long-COVID cases have risen over time, as illustrated in **Figure 1-2** using data from the United Kingdom. Hand in hand with the healthcare costs associated with treating patients, the economic burden includes the loss of quality-of-life and lost earnings due to the inability to return to work.[15,16] It has been

approximated that the cost of long-COVID in the United States of America can exceed upwards of $2.6 trillion USD, where the greatest proportion of the economic cost lays in the lost quality-of-life.[15,16] Unfortunately, the mechanisms and pathophysiology contributing to the persistent sequelae and enduring poor quality-of-life remain poorly understood, making treatment of these patients difficult.

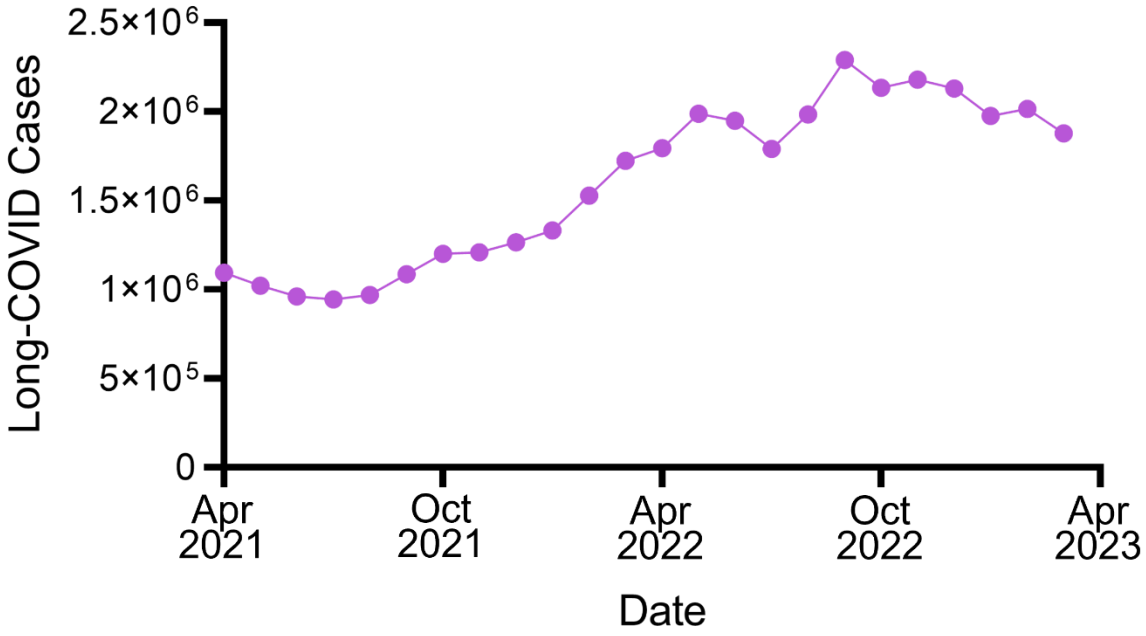

Figure 1-2. Long-COVID Cases
The number of long-COVID cases reported between April 2021 and April 2023 in the United Kingdom.[17]

The current mainstay clinical imaging approach for patients with or recovering from COVID-19 is computed tomography (CT) imaging.[18-21] However, quantitative analysis of CT imaging in patients has been restricted to density metrics, which largely inform on parenchymal abnormalities and are limited in their ability to provide functional information.[8,19-21] Pulmonary functional magnetic resonance imaging (MRI) provides a method to visualize and quantify regional inhaled gas distribution and ventilation heterogeneity *in vivo*. Hyperpolarized gas MRI provides a means to capture a real-time representation of the pulmonary ventilation in a

way that is a non-invasive, radiation-free, and requires minimal effort. Large cohort studies of patients with chronic obstructive pulmonary disease (COPD) have utilized both CT and hyperpolarized MRI to uncover the structure-function relationships in COPD and further our understanding of the disease processes.[22-26] In a similar manner, pulmonary imaging can allow us to probe the structural and functional mechanisms of long-COVID, as well as the physiological relevance of these. Accordingly, the overarching aim of this thesis is to investigate the structure and function of long-COVID in order to deepen our understanding of the potential mechanisms and pathophysiology contributing to abnormalities in the long-COVID lung. Equipped with this information, we have the potential to inform clinical decision-making, understand disease progression, and improve patient quality-of-life.

The purpose of this Chapter is to summarize the necessary background information required to motivate the original research presented in **Chapters 2-5**. First, a general overview of the respiratory system's structure and function responsibilities will be provided (**1.2**). The pathophysiology of both acute COVID-19 infection and long-COVID will be described (**1.3**) before typical clinical tools for measuring and evaluating pulmonary function will be outlined (**1.4**). Then, the currently available pulmonary imaging techniques, including all relevant quantitative imaging measurements, will be discussed (**1.5**). The majority of the aforementioned information will be contextualized with the use of more well understood chronic respiratory diseases, such as asthma and COPD. Lastly, the specific hypotheses and objectives for the thesis as a whole and for each chapter will be introduced (**1.6**).

1.2 Respiratory Structure and Function

The cardinal function of the respiratory system is gas exchange: to deliver oxygen to the blood and remove carbon dioxide. The upper respiratory tract consists of the nose and nasal passages, mouth, sinuses, pharynx, and larynx, while the trachea, bronchi, and bronchioles make up the lower respiratory tract. The lungs are contained within the thoracic cavity and supported by the diaphragmatic muscles. In combination with the abdominal wall and diaphragm, the lungs pull in air as the pressure in the airways is decreased relative to atmospheric air and a pressure gradient is formed during an inspiration maneuver. Inhaled air is breathed in through the nose or mouth and into the oropharynx before moving into the pharynx. Air then moves into the larynx before travelling into the trachea and being asymmetrically divided at the carina into the right and left main bronchi. Each bronchi branches into the secondary or lobar bronchus which branch into tertiary or segmental bronchi before eventually branching into bronchioles and alveoli. The alveoli are the site of gas exchange, where oxygen and carbon dioxide in the blood are exchanged via the pulmonary vasculature. Then, the abdominal and diaphragmatic muscles contract to increase intra-abdominal pressure and force air out of the lungs during expiration. In this section, the structure and function of the pulmonary airways, alveoli, and vasculature are presented.

1.2.1 Airways: Conducting and Respiratory Zones

The 23 generations of airways can be divided into the conducting and respiratory zones, based on the whether gases are being transported or exchanged,[27] and are summarized in **Figure 1-3**.

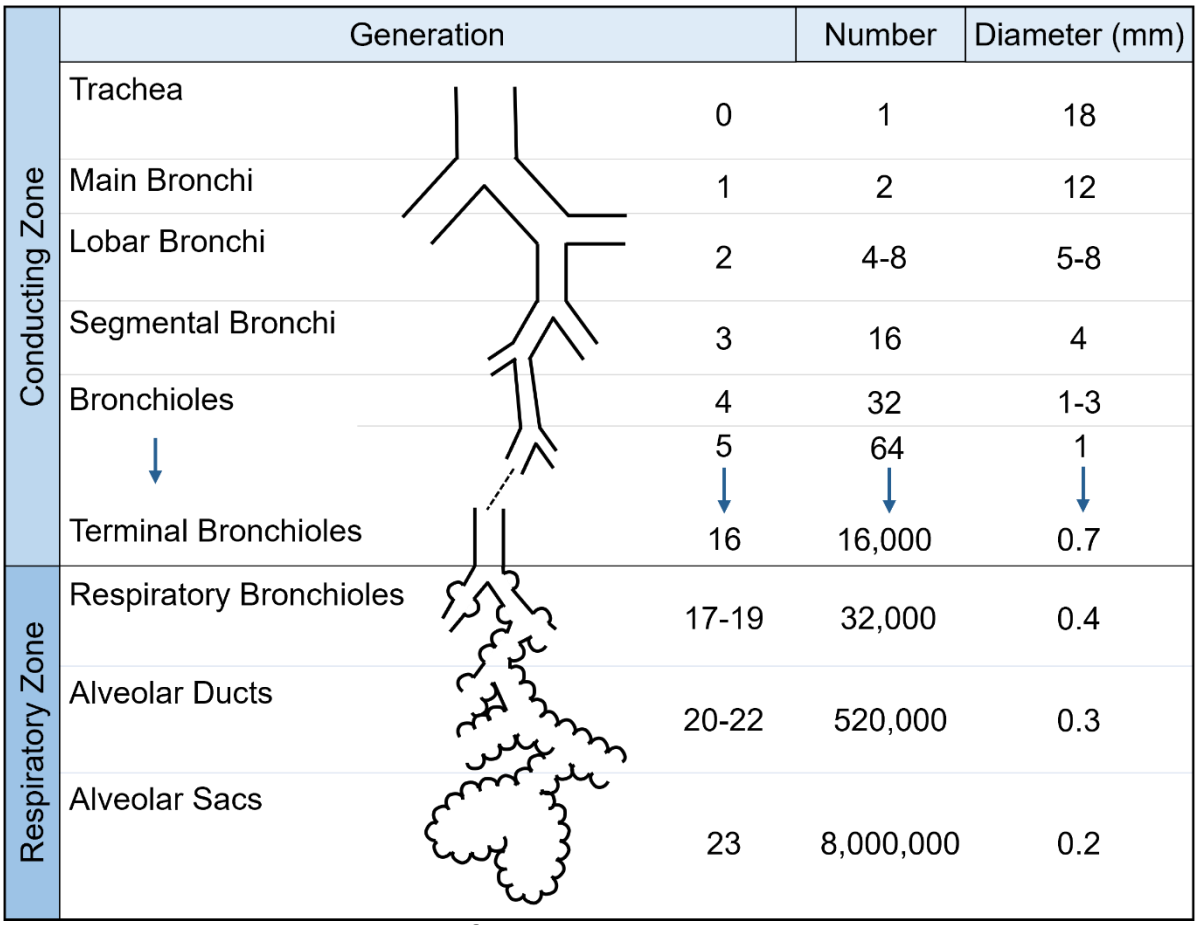

Figure 1-3. Schematic Summary of the Airway Tree Conducting and Respiratory Zones
The human airway tree, consisting of the conducting zone and respiratory zone, is depicted along with the corresponding airway generation, number, and diameter. Adapted from Nunn's Applied Respiratory Physiology, 8th Edition.[28]

Conducting Zone

The function of the conducting zone is to humidify and transport inspired air to the gas exchanging regions of the lung and is comprised of the first 16 airway generations (trachea to terminal bronchioles). The trachea, supported by C-shaped sections of cartilage and connecting bands of smooth muscle, provides a flexible passageway between the larynx and carina. Each of the two main bronchi extend into their respective lungs and divide into lobar bronchi corresponding to each lung lobe: upper, middle, and lower for the right lung and upper and lower for the left lung. The lobar bronchi divide into the segmental bronchi, which are

responsible for supplying air to the 19 distinct bronchopulmonary segments as depicted in **Figure 1-4**. These segments bifurcate into daughter branches, while the airway diameter and proportion of cartilage in the airways continues to decrease moving deeper into the lungs. Thus, the most distal airways are small and comprised entirely of smooth muscle with no cartilage. At the point of the bronchioles and beyond, the airways are now embedded in the lung parenchyma and held open through elastic forces.[28] The conducting airways also do not take part in gas exchange processes and, therefore, can be considered to be anatomic dead space such that they are areas of the lung that are ventilated but do not receive blood flow. The volume of dead space is about 150 millilitres.[29]

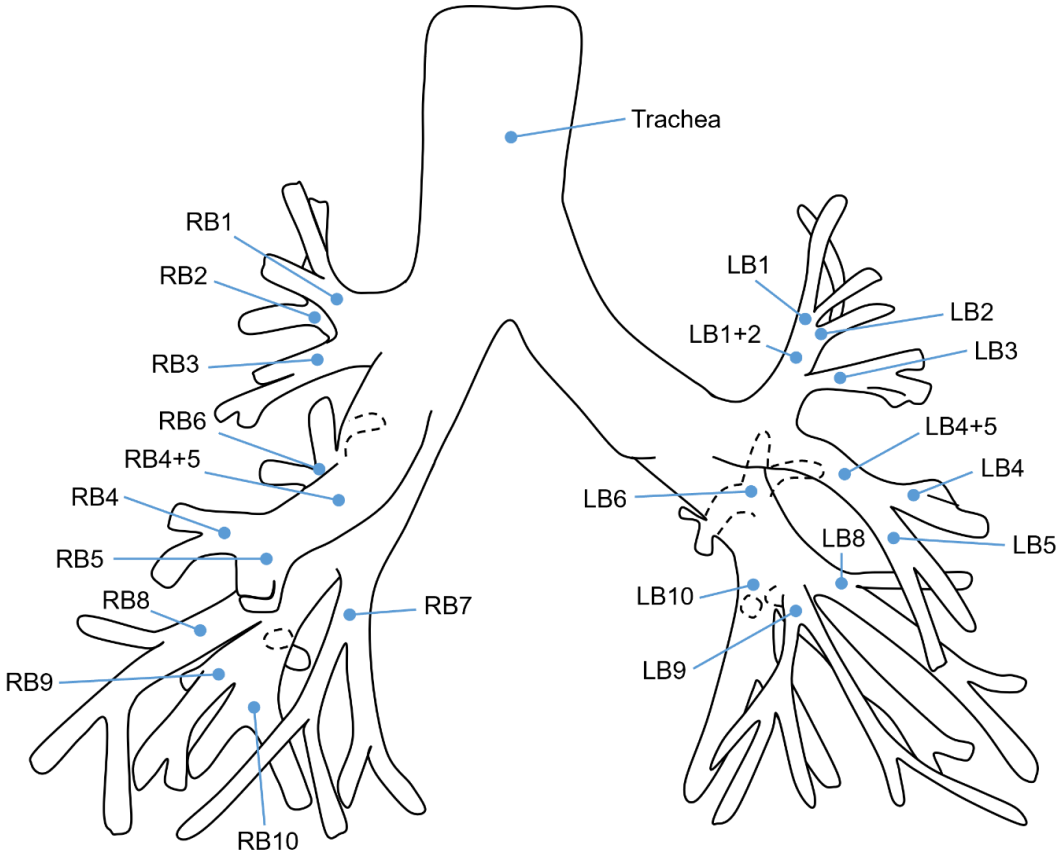

Figure 1-4. Labelled Diagram of the Airway Tree
From the trachea, the airways branch into two main bronchi and then into subsequent airways, with the 19 major airways labelled. Adapted from Tschirren et al. IEEE Trans Med Imaging (2005).[30]

Respiratory Zone

The function of the respiratory zone, consisting of airway generations 17 to 23, is to facilitate gas exchange so that oxygen can be transported into the pulmonary circulatory system and carbon dioxide can be expelled from the body. Branching from the terminal bronchioles, the respiratory bronchioles are where the first alveoli begin to appear and the function of the airways begins to transition from humidification and conduction to gas exchange. Next come the alveolar ducts, which are entirely lined with alveoli and lead to the alveolar sacs, the last generation of airways. The acinus refers to the portion of the lung distal to a terminal bronchiole, making up a distance of only a few millimetres and acting as the functional unit for gas exchange.[29] On average, the human lung contains about 30,000 acini,[31] with more than 10,000 alveoli in each acini. The cross-sectional area of the airways increases dramatically moving further down the airway tree so that, at rest, the volume of the respiratory zone is approximately two and a half to three litres, making up the majority of the lung.[29]

1.2.2 Alveoli: Site of Gas Exchange

The alveoli are small "air sacs" in the lungs where gas exchange takes place. They make up the terminal ends of the pulmonary airway tree and can be found in the respiratory bronchioles, alveolar ducts, and alveolar sacs. It is estimated that the human lung contains approximately 400 million alveoli, although this number can range from about 270 to 790 million depending on a person's height and lung volume.[32] A single alveolus has a diameter of approximately 0.2 to 0.3 millimetres, while all of the alveoli have a total surface area of about 130 square metres.[28] A dense network of capillaries surround the alveoli to create a blood-gas interface between the alveolar epithelium and capillary endothelium. The movement of oxygen and carbon dioxide through the blood-gas barrier is described by Fick's law, which states that the rate of transfer

of a gas is proportional to the surface area of the barrier and the difference in gas partial pressure between the two sides, and inversely proportional to barrier thickness.[29] The blood-gas barrier dimensions are optimal for efficient gas exchange, with a thickness of only about 0.3 micrometres and total area of 50 to 100 square metres.[29]

1.2.3 Ventilation

Ventilation is the process whereby air is inspired from the external environment, travels through the pulmonary system to the point of the alveoli, and then is expired back into the environment. Pressure gradients between the external environment and the alveoli are responsible for causing air to flow from the upper airways to the alveoli.[29] During inspiration, the diaphragm and intercostal muscles contract so that the abdominal contents move downward and forward and the rib cage is widened. This increases the volume of the chest cavity, decreases alveolar pressure, and drives air flow into the lungs. During passive expiration, the muscles relax and the lung and chest wall return to their equilibrium position so that alveolar pressure increases and air leaves the lungs. Total ventilation refers to the total volume, per unit time, of air leaving the lung during expiration and can be represented by **Equation 1-1**:[29]

Equation 1-1

$$\text{Total Ventilation [L/minute]} = \text{Breathing Rate [/min]} \cdot \text{VT [L]}$$

The tidal volume (VT) is the total amount of air that enters the lungs with each inspiration and is equal to approximately 0.5 litres on average.[29] In healthy adults, the breathing rate generally ranges from 12 to 20 breaths per minute and so, for example, if an individual takes about 16 breaths per minute, then their total ventilation is equal to 8 litres per minute. However, the entire volume does not reach the alveolar gas compartment due to the presence of 150 millilitres of anatomic dead space (VD),[29] as described previously. Alveolar ventilation refers

to the total volume of fresh air that is available for gas exchange and can be described as in **Equation 1-2**:

Equation 1-2

$$\text{Total Ventilation [L/minute]} = \text{Breathing Rate [/min]} \cdot \text{(VT - VD) [L]}$$

Hence, after accounting for dead space in our example, only 5.6 litres of fresh air are available for gas exchange every minute. It is also important to note that with every breath, 350 millilitres of fresh gas enters the alveoli; however, the alveoli still expands by the whole tidal volume due to the fact 150 millilitres of gas in the dead space is drawn into the alveoli with each breath before the fresh gas enters.[29]

1.2.4 Vasculature

The pulmonary vasculature is responsible for the transport of deoxygenated blood from the heart to the lungs and for oxygenated blood from the lungs to the heart before being transported to the rest of the body. The vasculature consists of the pulmonary arteries, capillaries, and pulmonary veins, all connected in series. Pulmonary arterioles branch from the arteries as the internal diameter becomes less than 100 micrometers and feed into the capillaries.[28] A dense network of capillaries envelops the walls of the alveoli, with a diameter of 7 to 10 micrometers which is just wide enough for a single red blood cell.[29] The thin blood-gas barrier between the capillaries and alveoli make the gas exchange process very efficient. Capillary networks pass from one alveolus to the next so that the blood travels past multiple alveoli before making its way into pulmonary venules and veins.[28] The pulmonary arteries and arterioles run parallel to the airways before transitioning into the capillaries, whereas the venules and veins lie close to the septa separating regions of the lung.

The bronchial circulation refers to the component of the systemic circulation which provides blood to the conducting airways, providing nutrition and heating for the humidification of inspired air. Of the bronchial circulation, approximately one third returns to the venous system while the remainder drains into pulmonary veins to mix with the oxygenated blood there.[28]

1.3 Pathophysiology of COVID-19 and Long-COVID

1.3.1 Acute COVID-19 Infection

The COVID-19 infection is caused by a novel coronavirus, which is named severe acute syndrome coronavirus-2 (SARS-CoV-2).[1] Coronaviruses are large, enveloped, single-stranded RNA viruses that can infect mammals, such as humans, dogs, cats, cattle, and pigs.[33,34] Prior to the detection of COVID-19, there were six coronaviruses known to infect the human species,[33] most of which cause flu-like symptoms primarily in immunocompromised patients.[34] On the other hand, two of the six are SARS-CoV and Middle East respiratory syndrome coronavirus (MERS-CoV) and these can result in fatal illness.[34] The appearance of SARS-CoV-2 is schematically represented in **Figure 1-5**; the virion has a diameter ranging from 60 to 140 nanometers and spikes with lengths of approximately 9 to 12 nanometers.[35,36] SARS-CoV and SARS-CoV-2 both bind to the angiotensin converting enzyme 2 (ACE2) receptor in the human body through the viral spike protein,[37-40] whose expression is high in the lung, heart, ileum, kidney, and bladder.[41] Once SARS-CoV-2 is bound to the host protein, the spike protein is cleaved and the virus particles enter the host cell.[40]

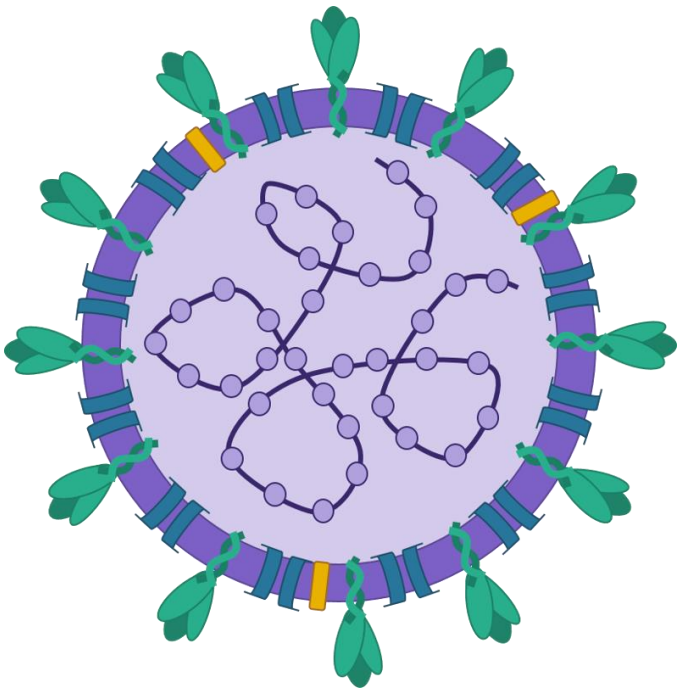

Figure 1-5. Schematic of SARS-CoV-2 Virus
The spike proteins (green) are attached to the membrane (purple), along with membrane proteins (blue) and envelope small membrane proteins (yellow). Within the structure, the RNA viral genome is contained (light purple circles represent the nucleoproteins).

In the lung, ACE2 expression is particularly increased in alveolar epithelial cells.[41] In addition, the epithelial-endothelial barrier integrity can be compromised when SARS-CoV-2 invades pulmonary capillary endothelial cells[42] and thickened alveolar walls have been observed using pathology.[43] A combination of inflamed lung tissue and pulmonary endothelial cells can lead to the formation of microthrombi and result in thrombotic complications, such as pulmonary embolism, limb ischemia, and myocardial infarction.[42,44-46]

The sequelae of COVID-19 are heterogenous, whole-body manifestations that can range from respiratory to neurological symptoms with a wide range of severities. The most common sequelae during acute COVID-19 infection are fever, cough, fatigue, dyspnea, asthenia, anosmia, and ageusia/dysgeusia.[2,47-50] Less frequent symptoms included diarrhea, confusion or brain "fog", headache, and nausea/vomiting.[2,47,48,50] Severe sequelae of COVID-19 can include acute respiratory distress syndrome, acute cardiac injury, and multiple organ failure.[2,47,48]

The radiologic findings of COVID-19 are predominantly observed with the use of planar x-ray or CT. Common x-ray findings include consolidation and ground glass opacities with bilateral chest involvement.[51-53] Reticular interstitial thickening, nodules, and pleural effusion are some less common findings on chest x-ray.[51-53] On CT, frequent findings include ground glass opacities with and without consolidation, reticulation, adjacent pleural thickening, interlobular septal thickening, and air bronchograms.[54-56] Less common CT observations are crazy paving pattern, pleural effusion, and bronchiectasis.[54,56]

1.3.2 Long-COVID

Long-COVID[12] is an umbrella term used to describe the myriad of residual, long-term effects following acute COVID-19 infection.[7-9] This syndrome is not unique to COVID-19 and is consistent with reports of persistent symptoms experienced by survivors of similar infections.[57-59] Even now, there is variation in the accepted definitions of long-COVID; however, the general consensus includes the persistence of symptoms three to four weeks beyond the onset of COVID-19 infection.[9,12] Many definitions also include two categories of long-COVID: (1) subacute or ongoing for symptoms present 4-12 weeks beyond COVID-19 infection, and (2) chronic for symptoms extending beyond 12 weeks of acute COVID-19 and not explained by an alternative diagnosis.[9,12,60,61] In addition, the occurrence of long-COVID is reported to be influenced by particular patient characteristics, such as age, sex, pre-existing health conditions, and viral factors.[9,62,63]

The causes of long-COVID are still actively under investigation; however, several hypotheses have been proposed.[64,65] It has been suggested that reservoirs of SARS-CoV-2 in tissues,[66,67] immune dysregulation,[66,68,69] infection impact on the microbiota and virome,[66,70,71] autoimmunity,[66,72,73] and microvascular blood clotting with endothelial dysfunction[66,74,75] may

play a role in the pathogenesis of long-COVID, most likely with a degree of overlap between the various pathophysiological mechanisms.[64] With regard to the respiratory system, persistent sequalae may be attributed to injury to the airways, alveoli, or endothelium of the pulmonary vasculature; long-COVID can also be the result of a combination of all three or subsequent immune reaction to the injury.[76-80] These hypotheses are strengthened by histopathologic findings of pulmonary alveolar damage and fibrosis in patients with persistent COVID-19 symptoms.[77-80] However, additional research is required to more completely understand the pathophysiology of long-COVID.[81]

Like COVID-19, long-COVID sequelae are heterogenous and can result in a multi-organ or whole-body symptoms.[9] The most commonly reported symptoms include fatigue, dyspnea, depression/anxiety, memory loss, concentration difficulties, and insomnia.[82-86] Less common long-term symptoms include cough, anosmia, ageusia, hair loss, and joint pain.[83,84,86] With respect to pulmonary function testing, decreased diffusing capacity of the lungs for carbon monoxide (DL_{CO}) is a prevalent finding in patients post-COVID-19,[87-92] which also aligns with reports of decreased oxygenation in the months following hospitalization from COVID-19 pneumonia.[8,93,94] In addition to the symptom burden associated with long-COVID, patients also reported the necessity for a reduced work load or an inability to return to employed work as result of their illness.[62,95,96]

Imaging studies of patients post-COVID-19 infection are generally predominated by patients who were hospitalized during acute infection and do not typically focus specifically on patients with long-COVID. Persistent abnormalities on chest CT images acquired one year post-infection have been reported to occur in approximately 24% to 54% of hospitalized patients, with ground-glass opacity, reticular opacity, and traction bronchiectasis findings being the

most common.[76,87,88,90,97] These radiological abnormalities also generally improve over time.[76,87,88,90,97] Moreover, in patients with long-COVID, CT imaging provided a method to identify greater air trapping as compared to healthy controls, irrespective of acute COVID-19 severity.[98]

1.4 Clinical Tools to Evaluate Pulmonary Function

Pulmonary function tests are the variety of tests that can be used to objectively evaluate and measure pulmonary function. In the context of chronic respiratory disease, these tests can be used for the purposes of disease diagnosis and monitoring. Importantly, pulmonary function tests are also non-invasive, inexpensive, and relatively simple to perform for the patient. Air flow or volume, gas transfer, perceived symptoms, and exercise capacity can be evaluated clinically and in research settings with these tests.

1.4.1 Spirometry

The most widely used of the available pulmonary function tests is spirometry, which measures the maximal volume of air that is inhaled or exhaled by the maximum effort of a patient.[99,100] The principal measurements derived from spirometry include volume or flow as a function of time.[99,100] The first of the primary measures is forced vital capacity (FVC), which is the volume of exhaled air during a maximum effort expiration starting from full inspiration and is typically expressed in litres.[99,100] Forced expiratory volume in 1-second (FEV_1) is the volume of air that is expired during the first second of the FVC maneuver, also expressed in litres.[99,100] FVC and FEV_1 can also be reported as percentage of a predicted value ($\%_{pred}$) with the use of the Global Lung Function Initiative (GLI) reference equations, which are based on a patient's age, biological sex, and height,[101] or can be reported as a ratio (FEV_1/FVC). The reference equations used for the purposes of this thesis were based on participants analyzed as part of the third

National Health and Nutrition Examination Survey (NHANES III);[102] however, it is important to note that all reference equations can be considered to be living documents which will continue to evolve over time as values for other healthy populations are added.

Either a handheld spirometer or whole-body plethysmograph may be used for completing a spirometry test. The patient is instructed to sit upright with feet flat on the floor and lips sealed completely around the mouthpiece of the spirometry device with a nose clip blocking airflow from the nostrils. The test begins with tidal breathing (normal, easy breathing) before maximal inspiration where the patient inhales rapidly to maximal inflation. The pause at full inspiration is minimal with no hesitation before the maximal expiration when the patient is instructed to blast out the air from the lungs and continue to breathe out until the air is fully expired. The volume-time plot in **Figure 1-6** summarizes the spirometry maneuver, as well as FVC and FEV_1. International guidelines[99,100] require three reproducible maneuvers (FVC and FEV_1 within 150 millilitres) be performed for a spirometry test to be considered acceptable.

In the case of restrictive disease, inspiration is typically limited during spirometry where the maximum flow rate and total exhaled volume are reduced.[29] In the case of obstructive diseases, expiration is limited with a slow flow rate in relation to lung volume.[29] In chronic respiratory diseases, such as asthma and COPD, the measures of FEV_1, FVC, and FEV_1/FVC can be reduced as a result of airway thickening and constriction, inflammation, intraluminal plugging, or airway collapse.

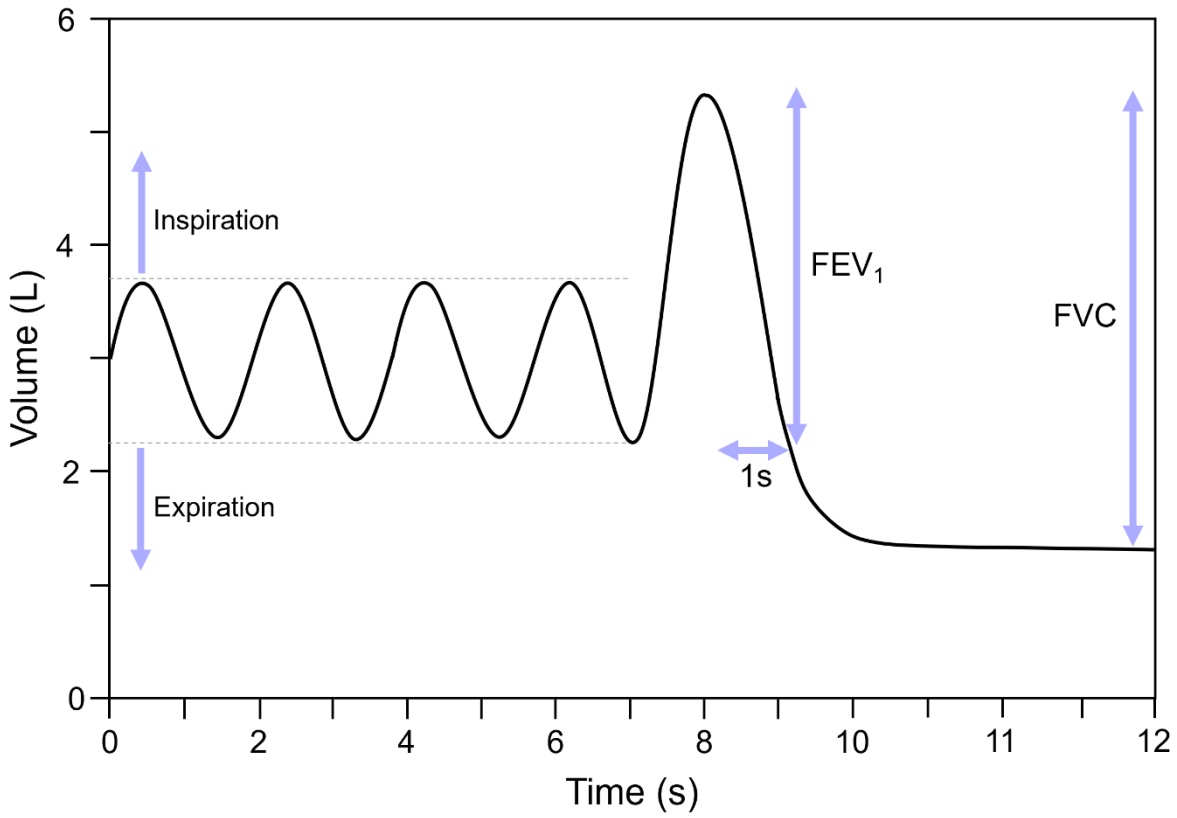

Figure 1-6. Spirometry Volume-Time Curve
Following tidal breathing, the spirometry device records the forced expiration to generate forced expiratory volume in 1-second (FEV_1) and forced vital capacity (FVC).

1.4.2 Plethysmography

A whole-body plethysmograph can be used to measure changes in volume and allows for the measurement of static lung volumes and capacities,[103] which are summarized in the volume-time plot in **Figure 1-7**. Tidal volume (VT) is the total volume of gas inspired and expired during tidal breathing. Functional residual capacity (FRC) is the volume of gas remaining in the lungs following exhalation during tidal breathing. Residual volume (RV) is the total volume of gas in the lungs following a complete expiration. Inspiratory reserve volume (IRV) is the volume of air that can inhaled with maximal effort after a normal tidal inspiration, whereas expiratory reserve volume (ERV) is the volume of air that can be exhaled with maximal effort after a normal tidal expiration. Inspiratory capacity (IC) is the volume of gas

that can be inhaled from the bottom of a normal tidal expiration. Vital capacity (VC) is the volume of gas that can be exhaled with maximal effort from the end of a complete inspiration. Lastly, total lung capacity (TLC) is the total volume of gas that can be accommodated in the lungs or the volume of gas in the lungs following maximal inspiration.

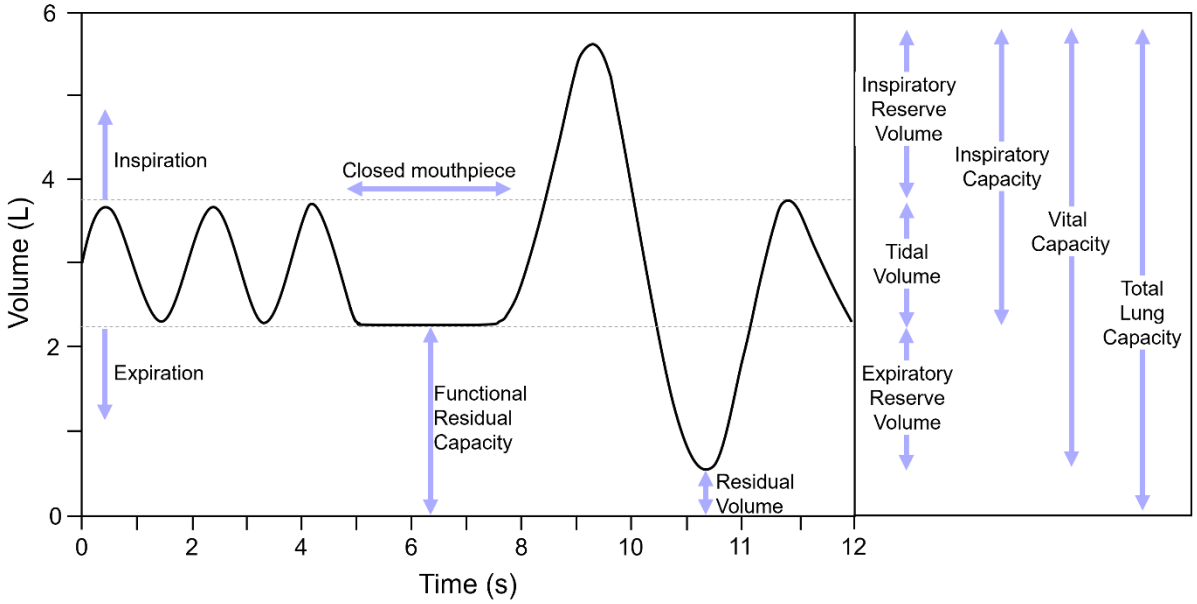

Figure 1-7 Plethysmography Volume-Time Curve
Lung volumes and capacities can be measured using a plethysmograph.

Plethysmography takes advantage of Boyle's law, which states that, for a fixed amount of gas at a constant temperature in a closed circuit, the product of volume and pressure is constant such that any changes in volume are inversely proportional to changes in pressure.[103] Plethysmography is performed with the patient seated upright in a sealed plethysmograph "body box", with nose clips on and lips sealed around the mouthpiece. In this way, volume within the plethysmograph can be kept constant so that changes in pressure are representative of changes in the lung during the breathing maneuvers being performed. The patient is instructed to begin with tidal breathing for three to four breaths before placing their hands on their cheeks to dampen pressures changes that occur in the cheeks. While the mouthpiece shutter is open, the patient performs panting maneuvers that also continue when the shutter

closes. As the shutter re-opens, the patient resumes tidal breathing before completing a full inhalation and exhalation to end the test.

In some respiratory diseases, gas trapping or air trapping can cause RV, FRC, and TLC to increase, where the ratio of RV to TLC (RV/TLC) derived from plethysmography is commonly used as an indication of air trapping. This air trapping can occur as a consequence of small airway inflammation, smooth muscle dysfunction, luminal occlusions, or loss of elastic recoil from tissue destruction.

1.4.3 Diffusing Capacity of the Lung

The diffusing capacity of the lungs for carbon monoxide (DL_{CO}) is a measurement of the efficiency of gas transfer within the lungs and can be acquired using a single-breath carbon monoxide uptake technique.[104] Carbon monoxide has a binding affinity for hemoglobin that is approximately 210-fold greater than that of oxygen and is inspired in low enough concentrations that it is does not completely saturate the hemoglobin, resulting in a constant pressure of carbon monoxide in the pulmonary capillaries.[105] Therefore, carbon monoxide is the gas chosen for this technique because its transfer is limited solely by diffusion, whereas oxygen uptake is both perfusion and diffusion limited.[105] The simplified process for carbon monoxide uptake is dependent on the diffusion properties of carbon monoxide at the alveolar capillary membrane and the binding of carbon monoxide to the hemoglobin.[104]

During the test maneuver, a test gas consisting of a mixture of 0.3% carbon monoxide, 21% oxygen, and a tracer gas (such as neon or helium) is used to calculate DL_{CO}. Once again, the patient is instructed to sit upright with nose clips on and lips sealed around the mouthpiece. The patient begins with tidal breathing, with at least four complete breaths, before exhaling completely to RV. Then, the patient is instructed to inhale the test gas rapidly and fully before

holding their breath for about eight seconds during which time the carbon monoxide will diffuse across the alveolar capillary membrane into the blood. Following the breath hold, the patient exhales and the expired gas is collected for analysis. A volume of the exhaled gas is discarded to clear the total anatomical and equipment dead space so that an alveolar gas sample can be analyzed. The concentration of carbon monoxide in the inhaled test gas is compared to that in the exhaled gas. DL_{CO} is calculated as the conductance, which is the ratio of the volume of carbon monoxide transferred from the inspired test gas to the alveolar partial pressure, and is measured as millilitres per minute per millimeter of mercury ($mL \cdot min^{-1} \cdot mmHg$). Similar to other pulmonary function test measurements, DL_{CO} can also be expressed as a percentage of the predicted value using the GLI-recommended reference equations, dependent on a patient's age, sex, and height.[106] The DL_{CO} values reported throughout this thesis were not corrected for hemoglobin concentration or alveolar volume.

The diffusing capacity of the lungs can be influenced by both structural and functional properties of the alveolar capillary membrane. For example, the thickness and area of the membrane available for gas exchange, the concentration of hemoglobin in the alveolar capillaries, or volume of blood in the capillaries all play a role in the measurement of DL_{CO}. In a clinical or research context, DL_{CO} is typically understood to represent the effective alveolar capillary surface area available for gas exchange in the lung. For instance, in COPD, DL_{CO} is commonly decreased as a result of emphysematous tissue destruction leading to reduced surface area of the alveolar capillary membrane.

1.4.4 Oscillometry

Oscillometry provides a non-invasive, effort-independent way to investigate respiratory mechanics.[107-109] The current nomenclature for oscillometry includes the forced oscillation

technique (FOT), airwave oscillometry, and impulse oscillometry. FOT oscillometry evaluates the relationship between pressure and flow with the use of forced oscillations delivered to the respiratory system.[110] The delivered waveform could be a single frequency sine wave or a combination of multiple discrete frequency sine waves.[110] Airwave oscillometry refers to advanced FOT technology which makes use of a vibrating mesh to generate multifrequency sinusoidal signal. Impulse oscillometry is an oscillometry technique where a continuous spectrum of frequencies is applied with a train of pulses.[111] In the context of this thesis, airwave oscillometry data was acquired using a commercially available tremoflo C-100 system (Thorasys, Montreal, QC, Canada).

The basis of oscillometry is the impedance of the respiratory system, which relates pressure and airflow in the lungs to indicate the extent of difficulty for air to flow in the airways.[112] It is the sum of both airway resistance (R) and airway reactance (X), where resistance provides information regarding the forward pressure and resistive elements of the conducting airways and reactance provides information regarding the elasticity of the airways and mass-inertive forces of the moving air column.[108] Oscillometry works by superimposing oscillations on the tidal breathing of a patient. Higher frequency oscillations are reflected back from the large airways while lower frequencies are reflected back from smaller airways after travelling deeper into the lung. The oscillometry measurement of total airway resistance (R_5) and the oscillometry measurement of large airway resistance (R_{19}) can be subtracted to obtain the measurement of distal airways resistance (R_{5-19}). The reactance at 5 Hz (X_5) reflects tissue elastance and inertance, while the area of reactance (A_X) takes advantage of all the frequencies used in oscillometry to provide information about the elastic properties of the lungs.

Oscillometry is performed with the patient sitting upright, with both feet planted on the ground and nose clips on. The patient is instructed to use their hands to provide firm support for their cheeks, helping to avoid shunting of the oscillations in the upper airways. Relaxed tidal breathing is commenced into the mouthpiece for approximately 16 seconds, while the device superimposes pressure oscillations on the breathing pattern. The typical oscillations usually begin around 4-5 Hz in order to avoid overlapping with the tidal breathing of the patient, which is typically 0.5 Hz or less.[112]

Oscillometry can be used as a tool to probe airway obstructions or abnormalities in both central and peripheral airways. In fact, oscillometry has been reported to sensitively detect abnormal physiology, particularly in patients with preserved spirometry measurements.[113] In addition, airway hyperreactivity or hyperresponsiveness may be identified using oscillometry measurements,[114,115] which also correlate with spirometry measures of responsiveness.[116] Moreover, oscillometry has been shown to be more sensitive than spirometry to treatment response in pediatric asthma.[117] In some cases, it also provides evidence of changes in airway function earlier than spirometry.[118] Furthermore, epidemiological studies have reported the prevalence of abnormal oscillometry in a general adult population, along with association of these measurements with respiratory symptoms,[119] even in those with normal spirometry.[120]

1.4.5 Inert Gas Washout

The inert gas washout tests, used to evaluate the ventilation heterogeneity of the lungs, can be performed using multiple-breath (MBW) and single-breath methodology.[121-123] In terms of MBW, the efficiency of ventilation distribution can be investigated by determining the efficiency of inert gas clearance from the lungs during respiration.[122,123] The inert gas chosen must satisfy the following requirements: be safe to inhale at the concentrations used, not

participate in gas exchange, and not dissolve into the blood or other tissues.[121] Nitrogen gas is most commonly used for MBW procedures with 100% oxygen gas used for the washout period, as opposed to room air. The primary measurement of ventilation heterogeneity is lung clearance index (LCI), which can be defined as the number of FRC lung turnovers necessary to decrease the inert gas concentration to 1/40th of its initial concentration.[121] LCI is calculated as the ratio of cumulative expired volume during the washout period to FRC.

During a MBW test, the patient is instructed to sit upright, wear nose clips, and seal their mouth completely around the mouthpiece. During the wash-in period, the patient breathes in the inert tracer gas during tidal breathing to a fixed volume of one litre. Then, during the washout period, the patient continues to tidal breathe to one litre until the tracer gas concentration has been reduced to 1/40th of the starting concentration. Hence, MBW requires minimal cooperation or exertion from the patient for an accurate test procedure.

The MBW test provides a method to probe the involvement of the small airways in pulmonary diseases. For instance, LCI was reported to be abnormally elevated in adults and children with asthma, even in the presence of normal spirometry,[124,125] suggesting that LCI might be sensitive to early disease processes. MBW measurements can also be predictive of airway hyperresponsiveness[126] and correlate with airflow obstruction.[127] Moreover, lung disease has also previously been detected at an earlier stage using LCI, as compared to spirometry.[128,129] In fact, early peripheral airway injury has been detected using MBW in cigarette smokers[130] and military personnel with particulate exposure.[131]

1.4.6 Fraction of Exhaled Nitric Oxide

The fraction of exhaled nitric oxide (FeNO) is an indirect measurement of airway inflammation, made via analysis of the concentration of nitric oxide in an exhaled breath.[132]

The nitric oxide measured in an exhaled breath is thought to originate in the airway epithelium as a consequence of the up-regulation of nitric oxide synthase which occurs with inflammation.[133,134] In this way, FeNO provides a measure of the up-regulation of airway inflammation.

During a FeNO maneuver, the patient sits upright with the mouthpiece firmly secured in their mouth. The patient is instructed to complete a maximal inspiration to TLC before immediately exhaling out at a constant expiratory flow rate of approximately 50 millilitres per second (±10%). The length of expiration must exceed six seconds in adults to correspond to a volume of at least 0.3 litres.

The measurement of FeNO is most commonly acquired in patients with asthma, where it has been observed to relate to eosinophilic airway inflammation,[135] predict the likelihood of corticosteroid responsiveness,[136] and may have potential for predicting airway hyperresponsiveness.[137]

1.4.7 Six-Minute Walk Test

The six-minute walk test (6MWT) provides a self-paced method to evaluate the exercise capacity of patients.[138,139] In comparison to other walking exercise tests, the 6MWT was reported to be easier to administer, well-tolerated, and reflective of daily living activities.[140] Relative to traditional pulmonary function testing, the 6MWT allows for a way to capture the extrapulmonary manifestations of respiratory diseases. The primary measurement associated with the test is the total distance walked in six-minutes (6MWD) in meters, while secondary measures include indices of fatigue, dyspnea, and oxygen saturation acquired using pulse oximetry (SpO_2) prior to and immediately following the test.

During the 6MWT, the patient should be dressed in comfortable clothes and shoes for walking; the usual walking aids for each patient should also be used during the test. The patient is instructed to comfortably walk at their own pace along a flat corridor. The corridor is marked so that the test track is 30 meters in length and the patient walks along the corridor between the makers as many times as they can. The patient is allowed to slow down or stop for rest, if necessary, but is encouraged to resume walking as soon as possible. After six minutes, the test is terminated and the total distance travelled is measured. Before and after the test, the patient is asked to rank their fatigue and dyspnea using the Borg scale.[141]

The 6MWT can be used to measure functional status in a variety of patient groups, such as those with COPD, cystic fibrosis, heart failure, vascular disease, and in elderly patients.[138,142] In people with chronic respiratory disease, 6MWD has been observed to correlate with disease severity, symptoms, quality-of-life, and physical activity.[142] In addition, lesser 6MWD has also been consistently associated with increased mortality and hospitalization in patients with chronic lung disease.[142]

1.4.8 Validated Questionnaires

The St. George's Respiratory Questionnaire (SGRQ) provides a measure of health status and has been developed for patients with chronic airflow limitation, such as those with asthma or COPD.[143] The SGRQ is a fixed format self-complete 76-item questionnaire that captures information regarding the impact of respiratory disease on a patient's symptoms, activity limitations, and daily life during the last 30 days.[143] SGRQ score has previously been used to evaluate differences among patient groups and also to investigate changes over time, where a clinically relevant change has been defined as 4 points.[144] For instance, in patients with COPD,

the SGRQ was observed to respond to both pharmacological and non-pharmacological interventions.[145-147]

The International Physical Activity Questionnaire (IPAQ) supplies a self-reported measurement of physical activity through either a short (nine items) or long form (31 items) questionnaire.[148] The questionnaire focuses on the physical activity level carried out by a patient over the last seven days, taking into account daily walking, occupational, and exercise activities.[148]

The modified Medical Research Council (mMRC) scale allows for the measurement of dyspnea level in daily practice.[149] Dyspnea is self-reported by patients using the simple and easy-to-use mMRC scale.[149] In fact, dyspnea level measured using mMRC has prognostic value and thus, has been included in the prognostic score of BODE (body mass index, airflow obstruction, dyspnea, exercise) index used for patients with COPD.[150]

1.5 Imaging of Pulmonary Structure and Function

Although pulmonary function tests provide non-invasive, inexpensive, and rapid measurements, they are limited in the fact they only inform on global lung function and cannot provide information on regional disease heterogeneity.[151,152] Furthermore, many of these conventional tests also perform poorly at predicting the presence of early disease and its progression,[22,153] as well as being insensitive to changes in the small airways.[154] In contrast, pulmonary imaging provides a method to sensitively investigate both structure and function, regionally and globally, of the lungs.

1.5.1 Planar X-ray

First discovered by Wilhelm Röntgen in 1895, the use of x-ray radiation to produce two-dimensional medical images is referred to as planar x-ray. The image is generated based on the

interaction of x-ray photons with a photon detector; the photons are made to pass from the x-ray source, through the patient, and to the detector directly opposite the x-ray tube. The x-rays are attenuated differently by the various tissues within the body so that the resultant image is a projection of the attenuating properties of all the material in the path of the x-rays. In the context of a chest x-ray, the patient is most commonly positioned so that the x-rays travel in an anterior-posterior or lateral path. Following a breath-hold image acquisition, structures such as the bone appear bright due to their high attenuation properties, while structures such as the lung parenchyma appear dark due to low attenuation of the x-rays. These medical images are also referred to as radiographs and are widely used due to the fact they are cost-effective, rapid, and provide minimal radiation exposure. A chest x-ray results in a radiation effective dose of approximately 0.01 mSv,[155] which is equivalent to 0.6% of the average annual dose acquired from the natural background radiation in Canada.[156]

In clinical practice, chest x-ray is used relatively broadly for routine pulmonary imaging. In the case of acute respiratory illness, it is indicated in patients who have a positive physical exam or other risk factors, suspected pneumonia or pneumothorax, or suspected severe acute respiratory syndrome, to name just a few indications for chest x-ray.[157] However, chest x-ray can also be used to detect hyperinflation, bronchial wall thickening, and airway mucus plugging.[158-162] In the context of COVID-19, radiographs are most commonly utilized for in-patient care during acute infection and for noting the presence of consolidation, ground-glass opacities, and viral pneumonia, often with bilateral involvement.[163,164]

1.5.2 X-ray Computed Tomography

The radiograph is limited by the fact the three-dimensional structure of the body is projected onto a two-dimensional image; x-ray CT imaging overcomes this issue by providing a method

to generate a three-dimensional representation of the anatomy. In this way, CT imaging improves the contrast of the soft tissues and adds depth information that cannot be acquired with a conventional radiograph. Following the first head CT acquisition of a patient in 1972, rapid development and technical advances have made CT the most conventionally used imaging modality for the chest and lungs.

In the 1960's, Godfrey N. Hounsfield wondered whether it would be possible to create a system that could read text on a single page in a closed book "by shining a bright light across each page from various angles and measure what came out the other end."[165] This thought formed the basis for what would become CT imaging. CT imaging measures the attenuation of x-rays, from many different angles, as they pass perpendicularly through thin sections or slices of the body. Similar to planar x-ray imaging, the x-ray source and detector array are opposite one another and, in the case of CT, rotate around a patient to acquire multiple x-ray projections at multiple angles. These measurements can then be reconstructed mathematically to generate images across contiguous cross sections of the body to provide three-dimensional information. The most common reconstruction methods include filtered back-projection and iterative reconstruction.[166]

An attenuation coefficient is calculated for each voxel, which is represented by an associated gray level in the reconstructed digital image. Hounsfield units (HU) are used to describe the attenuation by representing the tissue density as relative to that of water,[167] as shown in **Equation 1-3**:

Equation 1-3

$$\text{Hounsfield Unit [HU]} = 1000\times\left(\frac{\mu_{\text{tissue}}-\mu_{\text{water}}}{\mu_{\text{water}}}\right)$$

where μ refers to the linear attenuation coefficient for the tissue or for water. In the case of water, the HU is equal to zero, while the HU for air is approximately -1000 which appears dark on images and for bone is approximately 1000 which appears light on images. In the lungs, healthy parenchyma typically falls in the range of approximately -850 HU. CT images of the lungs are acquired while the patient is supine, during a breath hold, and following either inspiration or expiration maneuvers, dependent on the indicated evaluation. Clinically, the typical chest CT protocol results in a dose to the patient of about 7.0 mSv.[168] On the other hand, research protocol low-dose CT acquisitions are possible with an effective dose of 1.6 mSv,[22,24,25] which is similar to the average annual dose acquired from the natural background radiation in Canada.[156] More recently, advances in photon-counting CT have resulted in the possibility for ultra-high resolution pulmonary imaging with a dose on the order of 0.2 to 0.4 mSv; clinical implementation of this technology is already beginning to occur.[169,170]

In the context of pulmonary disease, the primary methods of investigation include qualitative CT findings, as well as quantification of the parenchyma, airways, and vessels using CT imaging. Similar to the radiograph, CT imaging is used to qualitatively identify ground glass opacities, consolidation, pleura and septal thickening, and reticulation in patients infected with COVID-19.[54,171,172] Quantitative CT refers to the concept of deriving CT measurements of tissue density, intensity, volume, perfusion, ventilation, and mechanics[173] that reflect the severity, degree of change, or status of a respiratory disease[174] and is summarized in **Figure 1-8**. Parenchymal CT abnormalities, such as emphysema and air trapping, can be easily quantified based on HU threshold values that represent differences in lung tissue density.[175-177] Meanwhile, computational advancements in CT image analysis have lead to the availability

of software capable of quantifying the pulmonary airway and vessel trees, which will be described in the following subsections.

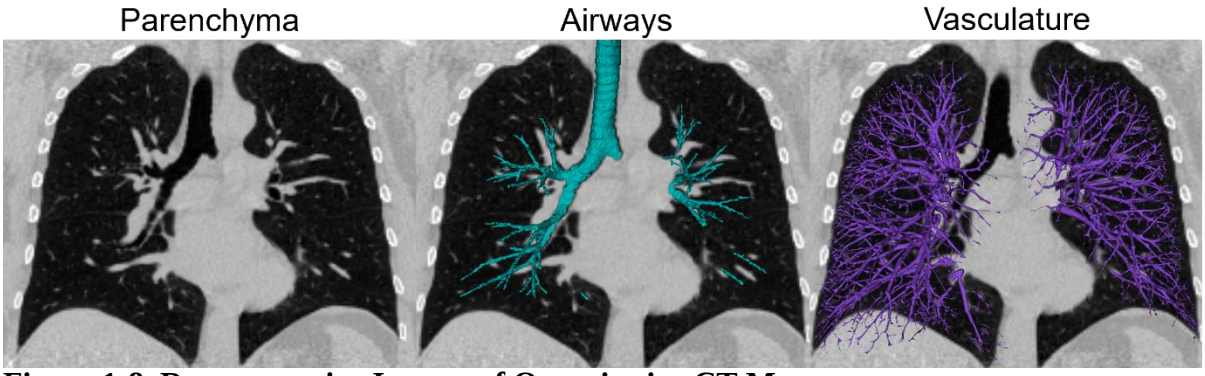

Figure 1-8. Representative Images of Quantitative CT Measurements
Quantitative CT measurements of the parenchyma (left panel) can be used to evaluate abnormalities, such as emphysema and air trapping. Quantitative CT measurements of the airways (middle panel) can be acquired following airway segmentation (shown in blue). Measurements of the pulmonary vasculature, shown in purple, can also be acquired from CT (right panel).

1.5.2.1 Airways

CT imaging provides a method of quantifying the pulmonary airway tree through segmentation and subsequent measurement of the airways, where both manual, semi-automatic, and automated segmentation processes have been developed.[30,178-184] Using an inspiratory CT acquisition, the airway tree can be segmented up to the tenth generation while the airway measurements can be reliably calculated up to the fifth and sixth generations.[30] For the purposes of this thesis, CT airway quantification was completed using commercially available software, VIDAvision software (VIDA Diagnostics Inc., Coralville, IA, USA), and hence, the details relating to this will be described.

The segmentation procedure makes use of the cylindrical properties of the airways so that the segmentation region-of-interest has a cylindrical shape and adapts to the predicted geometry of the airway branch.[30] The connectivity algorithm also takes advantage of the difference in image contrast between the airway lumen and wall, where the lumen primarily has a value of

approximately -1000 HU and the airway wall can range in value from 0 to -800 HU (the more negative values correspond to the smaller airways).[30] The measurement step of the quantification process assigns an airway tree skeleton centreline in all segmented airway segments in order to accurately detect the airway walls.[30] In this way, the cross sectional area can be computed so that minor (minimal) and major (maximal) diameters of the airways can be measured.[30] Airway measurements, such as wall area percent and wall thickness can then be calculated using **Equation 1-4** and **Equation 1-5**, respectively:

Equation 1-4

$$\text{Wall Area Percent [\%]} = 100\times\left(\frac{\text{Airway wall area [mm}^2\text{]}}{\text{Total area [mm}^2\text{]}}\right)$$

Equation 1-5

$$\text{Wall Thickness [mm]} = \text{Outer Diameter [mm]} - \text{Inner Diameter [mm]}$$

The total number of CT-visible and segmented airways can also be quantified to provide total airway count (TAC), which has been observed to associate with the number of terminal bronchioles on micro-CT.[185] Other common quantitative CT airway measurements include lumen area (LA), wall thickness (WT), wall area percent (WA%), and square root of wall area of a hypothetical airway of internal perimeter of 10 mm (Pi10).

Quantitative CT measurements of the large airways have previously been reported for both non-smokers and people with respiratory disease, such as asthma and COPD. In patients with asthma, thicker airway walls[186-189] and narrower lumens[186] have been observed relative to COPD patients and healthy control groups. Moreover, airway wall thickness increases with greater disease severity,[188,190,191] relates to pathologic airway remodelling,[191-193] and has been associated with airflow obstruction[189,192-195] and airway hyperresponsiveness.[193,196] More recently, TAC was also observed to diminish with increasing asthma severity.[197] Investigations

in patients with COPD have also revealed diminishing TAC and airway wall thinning by COPD grade[198,199] and over time.[200] Compared to never-smoker controls, patients with COPD report narrower airway lumen and fewer airways,[201-203] while airway wall thickness also relates to airflow obstruction.[201,204,205]

1.5.2.2 Parenchyma

The small airways (<2 millimeters in diameter) are difficult to directly quantify due to limitations in CT resolution. As mentioned previously, TAC does correlate with the number of micro-CT terminal bronchioles in COPD, supporting the notion that quantitative CT provides surrogate small airway measurements.[185] In addition to this, CT measurements of air trapping can also be used to indirectly evaluate small airways disease. Air trapping or gas trapping refers to the retention of gas in the lungs during expiration and, on CT, appears as decreased attenuation of the parenchyma, particularly characterized by a less than normal increase in attenuation during expiration.[206] Air trapping can be quantified as the percentage of low attenuation areas of voxels with Hounsfield units less than -856, where -856 HU is the chosen threshold because it is the value that corresponds to the normally inflated lung and so upon expiration, the measured lung attenuation should be greater than -856 HU.[207,208] Air trapping can be quantified using expiratory CT alone or in combination with co-registered inspiratory CT acquisitions.[209]

Emphysema pathologically refers to permanently enlarged distal airspaces, typically accompanied by alveolar destruction.[206] On CT, emphysema appears as regions of low attenuation, commonly without visible walls.[206] In a similar manner to air trapping, emphysema is quantified on CT using automated thresholds where -950 HU is utilized the most

often.[208] Thus, emphysema is defined as being present when the relative area of lung with Hounsfield units less than -950 is greater than 6.8%.[175]

1.5.2.3 Vasculature

The pulmonary vasculature can be quantified using CT imaging through the use of automated algorithms that generate measurements for the volume of vessels with cross sectional area less than 5 mm^2 (BV_5), between 5 and 10 mm^2 (BV_{5-10}), and greater than 10 mm^2 (BV_{10}), as well as for total blood volume (TBV).[210] CT pulmonary vascular measurements have been previously reported for patients with COPD and severe asthma and revealed vascular pruning via a decrease in small vessel volume.[211-214] These vascular abnormalities were found to associate with disease severity, poor outcomes, and exacerbations.[211-213]

1.5.3 Nuclear Medicine

Nuclear medicine imaging techniques are anchored on the principle of radiation being emitted from inside the human body and subsequently imaged, making use of radioisotopes or radiolabelled tracers. With respect to pulmonary imaging, anatomical images, such as planar x-ray or CT, are typically used to provide a reference for the medical images that measure ventilation, perfusion, and ventilation-perfusion mismatch. Scintigraphy generates a two-dimensional projection of the radioactivity in the body, emitted from inhaled or injected radiotracers that emit gamma rays. Gamma cameras detect the emitted radiation and form images typically presented as heat maps, with hot spots representing regions of high radionuclide content. The most common application of scintigraphy in pulmonary imaging is to diagnose pulmonary embolism.[215] Single photon emission computed tomography (SPECT) differs from scintigraphy in that it generates three-dimensional images of emitted gamma radiation, analogous to CT imaging as compared to planar x-ray. In this case, radiotracers are

inhaled or injected before multiple two-dimensional projections at multiple angles are acquired and reconstructed into a three-dimensional image. Positron emission tomography (PET) provides a method to acquire three-dimensional information of metabolic activity through the use of positron-emitting isotopes. Once again, the radionuclide is inhaled or injected before undergoing positron emission, which subsequently leads to an annihilation event and the two coincident gamma photons being emitted at 180° from one another. Gamma cameras detect these photons, trace back the spatial location of the source, and these are all reconstructed into a volumetric image. Relative to scintigraphy and SPECT, PET imaging is not employed as often for pulmonary applications; however, [^{13}N]nitrogen can be used to evaluate regional perfusion, shunt, aeration, ventilation, and gas trapping.[216]

1.5.4 Magnetic Resonance Imaging

MRI provides a method to produce detailed three-dimensional images of the body by manipulating and quantifying the magnetic spins of different nuclei in the body. Within a strong magnetic field, such as the one produced by an MRI scanner, the nuclei will uniformly align with the direction of the magnetic field. Radiofrequency waves (non-ionizing electromagnetic waves) can excite the nuclei so that they no longer align with the main magnetic field. As these radiofrequency waves are turned off, the nuclei relax, creating a signal as the nuclei decay back to equilibrium. This signal can be detected and measured to generate MR images. Conventional MRI generates images based on the nuclear spins of protons (^{1}H) and thus, the differences in proton density in tissues throughout the body results in excellent soft tissue contrast in the images. In the context of pulmonary imaging, there are multiple methods of utilizing MRI techniques to image both structure and function, some of which are described here.

1.5.4.1 Anatomic ^{1}H MRI

Conventional MRI can be leveraged to acquire anatomical images of the lungs; however, there are physical properties of the lungs that make this challenging. Compared to other tissues, such as those in the brain, lung tissue density is 0.1 g/cm^3, approximately ten times less than that in other tissues.[217,218] As a result, the MR signal obtained from the lungs is also ten times less than surrounding tissues. The low signal-to-noise ratio (SNR) limits the ability to acquire helpful structural information regarding the lung parenchyma.[218] In addition, the incredibly large number of tissue-air interfaces in the airways and alveoli of the lungs creates highly inhomogeneous magnetic field gradients or susceptibility artifacts.[217-219] It is therefore challenging to create sufficient signal contrast within the lungs due to the resultant rapid signal dephasing and decay. Moreover, owing to the location and function of the lungs in the chest, both cardiac and respiratory motion create artifacts in pulmonary MR images. Hence, MRI of the lungs typically results in low pulmonary signal and limited information regarding pulmonary structure.

Ultra-short echo time (UTE) MRI sequences have been developed to address some of the challenges faced in the field of pulmonary MRI.[220] This technique attempts to acquire lung tissue signal before it decays by reducing the time between radiofrequency excitation of the protons and data acquisition.[220] However, UTE MRI acquisition times on the order of minutes makes breath-hold imaging impossible and necessitates the use of some form of respiratory gating.[221] Nevertheless, UTE MRI has the potential for generating pulmonary parenchymal information that is comparable to CT. In patients with COPD and asthma, the utility of UTE MRI has been reported to be able to differentiate between and evaluate parenchymal

diseases.[222-224] In fact, bronchial wall dimensions quantified using UTE MRI were also found to be comparable to those measured on CT.[225]

1.5.4.2 Hyperpolarized Noble Gas MRI

Hyperpolarized noble gas MRI provides a means to directly visualize and quantify inhaled gas distribution to probe lung physiology and microstructure. The first hyperpolarized noble gas MR images were acquired in 1994 in excised mice lungs using ^{129}Xe gas.[226] Soon after this, the first *in vivo* images in humans were acquired using ^{3}He gas.[227,228] In the years since, there has been rapid development in the use of hyperpolarized ^{3}He and ^{129}Xe gases to image the ventilated airways and alveolar spaces.[229,230] In the case of either gas, the low spin density and small nuclear magnetic dipole moment of the gases are insufficient for an acceptable image SNR and thus, optical polarization methods are employed to increase the polarization of the gases. Spin-exchange optical pumping is a commonly used method, whereby a high-powered laser is circularly polarized, heats and irradiates a cell containing an alkali metal and the noble gas, and excites the alkali metal, typically rubidium.[231] The rubidium electrons and noble gas nuclei exchange spins via collision of the atoms, resulting in an increase of the nuclear-spin polarization of the noble gas and subsequent improvement in the MR signal.[231]

Despite the very first images leveraging ^{129}Xe gas,[226] the field of hyperpolarized noble gas MRI quickly became dominated by ^{3}He gas. Due to the greater gyromagnetic ratio (32.4 MHz/T for ^{3}He versus 11.8 MHz/T for ^{129}Xe) and achievable polarization levels (30-40% for ^{3}He versus 8-25% for ^{129}Xe) of ^{3}He compared to ^{129}Xe, superior MRI signal and image quality could be achieved. However, depleted global supply and increased cost of ^{3}He[232] has resulted in the field moving back to ^{129}Xe in recent years.[233] Regardless, the safety and tolerability of both gases has been proven in healthy and disease populations.[234-236] Hyperpolarized gas MRI

has also been validated against more traditional clinical imaging techniques, such as scintigraphy and SPECT.[237-240] As a matter of fact, ^{129}Xe MRI is now approved for clinical use in the United Kingdom and United States of America. We must also note the fact implementation of hyperpolarized gas MRI requires dedicated specialized equipment (hyperpolarizers and radiofrequency coils) and highly-trained personnel, as well as MRI systems with multinuclear capabilities.[241]

Ventilation Imaging

Ventilation imaging is the most common application of hyperpolarized gas MRI. The inhalation of hyperpolarized gas and subsequent MR imaging allows for the visualization and quantification of the regional distribution of pulmonary ventilation in a way that highlights regions of ventilation abnormalities. During image acquisition, patients are instructed to lay supine in the MR scanner, inhale the hyperpolarized gas, and hold their breath for approximately 10 to 12 seconds. In healthy patients, the inhaled gas is distributed fully and completely throughout the lung and accordingly, the ventilation MRI signal is also homogenous across the lung volume. In people with respiratory disease, the lungs do not fill completely with heterogenous inhaled gas distribution and thus, regions of image signal void are referred to as ventilation abnormalities or defects, as shown in **Figure 1-9**. Hyperpolarized gas MR images are commonly co-registered to anatomic ^{1}H MR images to define regions of ventilation heterogeneity.

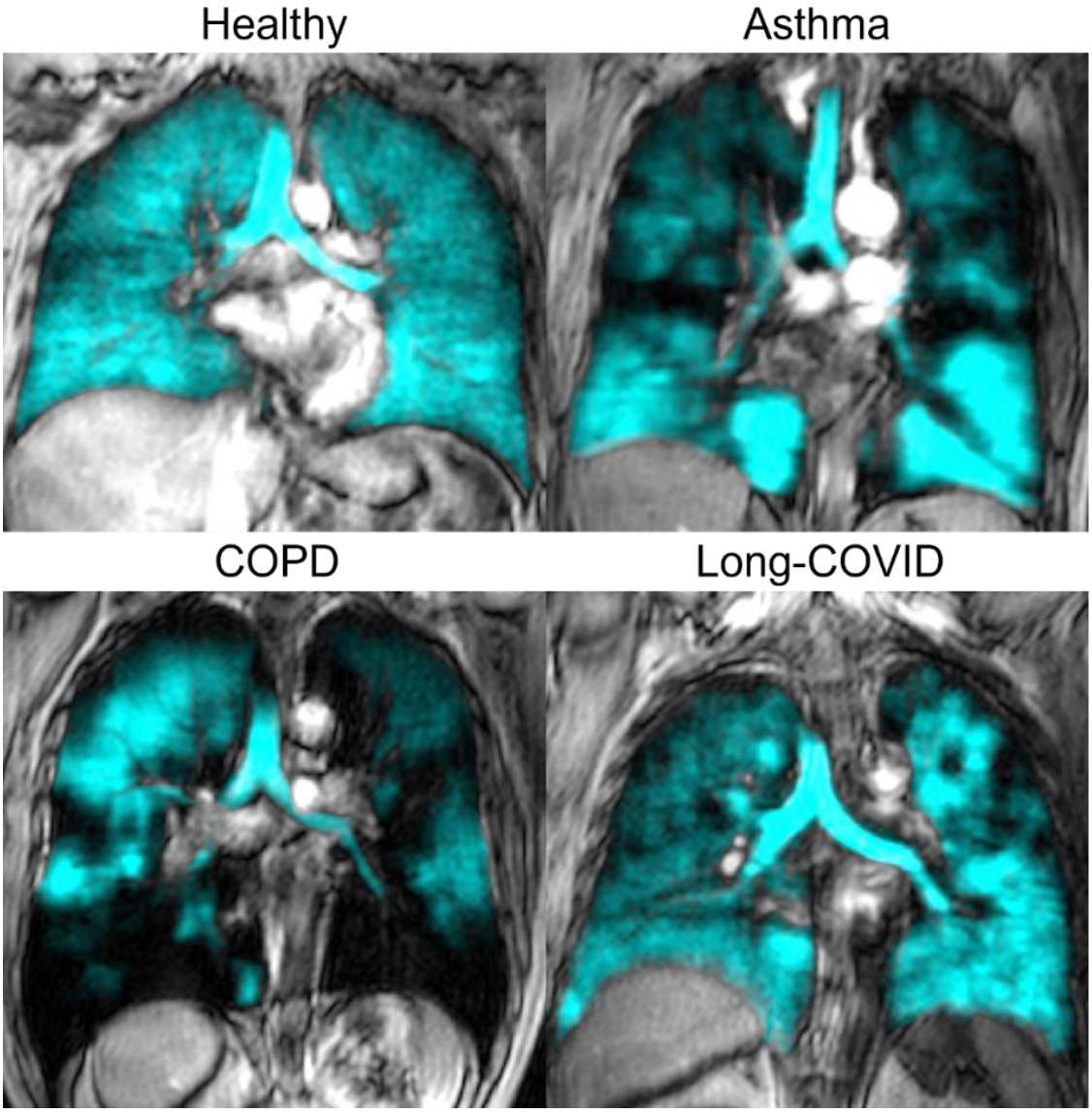

Figure 1-9. Representative ^{129}Xe MR Ventilation Images
Co-registered anatomic proton (^{1}H) and ^{129}Xe MR ventilation (cyan) images in participants with no respiratory disease, with asthma, with chronic obstructive pulmonary disease (COPD), and with long-COVID. Regions of ventilation signal void (or darkness) represent ventilation defects or abnormalities.

The initial investigations of pulmonary ventilation with hyperpolarized noble gas MRI employed the use of visual scoring systems to quantify ventilation abnormalities categorically (mild, moderate, or severe) or numerically (total number of defects).[242-244] Then, semi-automated and automated image analysis techniques were developed,[245-251] in addition to various deep learning methods in more recent years.[252-255] Using these methods, numerous

MRI biomarkers have been introduced, including ventilated volume,[245] percentage ventilation volume,[244] ventilation defect volume,[256] and ventilation defect percent (VDP).[257] VDP is the biomarker that is most commonly used and can be calculated using linear binning,[246,247] signal intensity thresholding,[251] or K-means clustering methods.[248] For the purposes of this thesis, VDP was quantified using K-means clustering, with a total of five clusters and the most hypointense signal cluster representing ventilation defects.[248] So, VDP was calculated by normalizing the volume of ventilation defects to the thoracic cavity volume,[248] as shown in **Equation 1-6**:

Equation 1-6

$$\text{Ventilation Defect Percent [\%]} = 100\times\left(\frac{\text{Ventilation defect volume [mL]}}{\text{Total thoracic cavity volume [mL]}}\right)$$

In patients with asthma, MRI ventilation defects have been shown to be reflective of airway abnormalities, including smooth muscle dysfunction,[258] airway inflammation and remodelling,[197,259,260] luminal occlusions,[261] and air-trapping.[256] Accordingly, these ventilation defects associate with asthma control,[262] airflow limitation,[243,256,258,263,264] dyspnea,[265] exacerbations and exacerbation risk,[266,267] and disease severity.[243,267] Interestingly, hyperpolarized gas MRI has also been shown to be more sensitive to respiratory disease processes than clinical measures, such as spirometry,[242,243,268] and respond to asthma treatments, including bronchodilators,[246,269,270] biological therapy,[271-274] and bronchial thermoplasty.[275,276] In patients with COPD, ventilation defects are associated with disease severity,[277] airflow obstruction,[278,279] symptoms,[280] and exercise limitation.[280] Ventilation defects have been shown improve following bronchodilation, in the absence of spirometric improvements,[281] and are predictive of COPD exacerbations.[282]

The ventilation MR images can also be analyzed using texture feature extraction tools to extract additional spatial distribution and intensity variation information by implementing mathematical algorithms. Quantification of VDP provides binary information on ventilated versus unventilated regions of the lungs and is a global measurement encompassing the entire lung volume. In contrast, texture features can provide information regarding the ventilation region's shape, voxel intensity histogram, and spatial arrangement of the intensity values at a voxel level.[283,284] These ventilation signal intensity texture and patterns could reveal additional information of the underlying pathophysiology contributing to the MRI ventilation signal. MRI ventilation texture features have been evaluated in asthma patients to evaluate bronchodilator response[285] and in COPD patients to predict lung-function decline[286] and mortality.[287] Thus, taken together, hyperpolarized gas MRI quantification of ventilation defects and ventilation texture feature analysis both provide the unique opportunity to sensitively probe airway dysfunction in people with respiratory disease.

Diffusion Weighted Imaging

The alveolar microstructure and diameter can be measured using hyperpolarized ^{3}He and ^{129}Xe diffusion weighted MRI, which is rooted upon the concept of restricted random Brownian motion (or diffusion) within the terminal airspaces. The apparent diffusion distance of the inhaled gas molecules can be quantified as the apparent diffusion coefficient (ADC)[288-290] because the alveolar wall restricts the movement or diffusion of the molecules. An increased ADC value is representative of a larger terminal acinar unit, where the diffusion path is longer, as compared to more compact acinar units.[289,291] In the case of alveolar destruction, the diffusion path will also be greater and subsequently result in a greater ADC value, as well.[289,290] This is reflected in the increasing ADC with age in healthy participants,[291] mostly likely due

to the natural aging processes of senile emphysema and terminal airway enlargement. Different timescales can also be evaluated with hyperpolarized MRI ADC values where a short timescale (order of milliseconds) coincides to diffusion within a single alveolus and a longer timescale (order of seconds) coincides to diffusion across multiple acinar airways.[292] ^{3}He and ^{129}Xe diffusion weighted MRI ADC values have been shown to reflect air trapping[293] and emphysema.[278,294,295]

Dissolved Phase Imaging

MR imaging with ^{129}Xe is particularly advantageous because it permits dissolved phase MRI. ^{129}Xe exhibits modest transmembrane solubility,[296] meaning it can diffuse from the alveoli, through the alveolar tissue barrier, and into the red blood cells, and dissolved phase MRI provides a method to simultaneously quantify it in these three compartments. When inhaled, most of the xenon remains in the lung airspaces while approximately 1-2% of the xenon diffuses into the barrier and the red blood cells,[297] termed "dissolved phase" xenon. The three compartments exhibit distinct resonance frequency shifts of ^{129}Xe,[296,298] where barrier and red blood cell spectral peaks are offset from the gas peak by approximately 198 ppm and 218 ppm, respectively.[299,300] The signal intensity of the gas, barrier, and red blood cells peaks are typically expressed as ratios with one another, where the ratio of barrier to red blood cells is thought to reflect pulmonary gas transfer efficiency and a decreased ratio may indicate diminished gas transfer.[297,298,301]

1.5.5 Overview

To summarize, both the structure and function of the lungs can be investigated with the use of pulmonary imaging techniques. In the context of this thesis, CT imaging is used to evaluate

the structure, while hyperpolarized ^{129}Xe MRI probes the function of the lungs. The measurements that can be obtained from both CT and ^{129}Xe MRI are outlined in **Table 1-1**.

Table 1-1. Summary of Imaging Modalities

Modality	Airways	Vasculature	Parenchyma
CT	• Quantified through segmentation and measurement of airways • Airway measurements include wall area, wall thickness, lumen area • Total airway count quantifies total number of CT-visible, segmented airways	• Quantified through automated measurement of pulmonary vessels • Measurements include volume of vessels with cross sectional area less than 5 mm^2 (BV_5), between 5 and 10 mm^2 (BV_{5-10}), and greater than 10 mm^2 (BV_{10}), as well as for total blood volume (TBV)	• Can be qualitatively described by radiologist (i.e. ground glass opacities, consolidation, reticulation, etc.) • Density thresholds quantify extent of air trapping (-856HU) and emphysema (-950HU)
^{129}Xe MRI	• Regional distribution of inhaled gas pulmonary ventilation defects quantified using VDP • Texture analysis tools extract additional ventilation spatial and intensity distribution information	• Dissolved phase MRI quantifies ^{129}Xe signal intensity in gas phase, alveolar tissue barrier, and red blood cells to provide gas transfer efficiency information	• Terminal airspaces quantified by ADC of inhaled gas

CT=computed tomography; MRI=magnetic resonance imaging; HU=Hounsfield unit; VDP=ventilation defect percent; ADC=apparent diffusion coefficient.

1.6 Thesis Hypotheses and Objectives

With the onset of the COVID-19 pandemic, concerns regarding the long-term consequences were inevitable. Although post-acute infection syndromes are not unique to COVID-19 and have been described historically dating back to the 1890's,[58,59] the pathophysiology responsible for the persistent sequalae remains largely unknown. Pulmonary imaging provides an opportunity to probe the structure-function relationships in long-COVID. The presence of ventilation heterogeneity and pulmonary airway abnormalities quantified with imaging may inform on the underlying pathology that contributes to the poor quality-of-life and persistent symptoms experienced by people post-COVID-19 infection. Therefore, the overarching

objective of this thesis was to utilize sensitive hyperpolarized ^{129}Xe MRI and CT measurements to interrogate the pulmonary function and structure of long-COVID as it relates to longitudinal changes, differences with biological sex, and prognostic ability.

This objective was addressed with the initiation of the LIVECOVIDFREE study, a longitudinal, multicenter study to evaluate participants with pulmonary long-COVID. The five sites were Western University, McMaster University, Toronto Metropolitan University, SickKids Hospital, and Lakehead University, where Western University and McMaster University were data acquisition sites for the data presented in this thesis. The primary outcome of the study was to determine if long-COVID participants develop long-term respiratory impairment, defined as sustained respiratory symptoms, abnormal pulmonary function testing, or lung imaging abnormalities. The study was designed in an effort to generate and provide rapid evidence-based guidance to healthcare providers, health system planners, and patients regarding monitoring to detect early signs of respiratory impairment in long-COVID and care required to prevent development of significant lung disease. The study participants enrolled as part of the LIVECOVIDFREE study encompass the long-COVID participants evaluated in all four body chapters of this thesis. The hypotheses and objectives of each chapter supporting the overarching objective of this thesis are described below.

To begin, we wondered whether there was evidence of pulmonary function and imaging abnormalities in patients with long-COVID. We hypothesized that ^{129}Xe MRI measurements would identify the presence of ventilation heterogeneity in patients with long-COVID and that MRI VDP would exhibit relationships with quality-of-life and symptoms. To this end, the objective of **Chapter 2** was to use ^{129}Xe MRI and CT to evaluate symptomatic long-COVID

patients, including never- and ever-hospitalized patients, three months post-acute COVID-19 infection.

Extending on this, we wanted to understand the longitudinal trajectory of long-COVID, specifically in the context of ventilation abnormalities and airway dysfunction, to determine whether patients could recover over time. In **Chapter 3**, we hypothesized that a decrease in ^{129}Xe MRI VDP would signify improvement in patients with long-COVID and this would relate to concurrent improvement in pulmonary function, quality-of-life, and exercise capacity. Thus, our objective was to evaluate ^{129}Xe MRI VDP, pulmonary function, quality-of-life, and exercise capacity in long-COVID patients 15 months post-infection as compared to three months post-infection.

Next, based on previous work where CT airway sex differences were associated with worse outcomes in female COPD patients,[302] we observed less total airways, narrower airway lumen, and thinner airways walls in females with long-COVID as compared to males.[303] We speculated what the potential mechanisms may be for the reported prevalence and quality-of-life deficits in females with long-COVID[304-307] and whether imaging could provide some insight. In **Chapter 4**, our objective was to compare CT airway and pulmonary vasculature measurements in females with long-COVID to female ex-smokers with and without COPD in order to contextualize the extent of possible airway and vascular remodelling present in long-COVID.

Finally, we were curious whether pulmonary imaging measurements could provide prognostic information on long-COVID outcomes. Hence, in **Chapter 5**, we hypothesized we could take advantage of the additional spatial and intensity information provided by ^{129}Xe MRI ventilation texture features to predict longitudinal quality-of-life improvement in patients with long-

COVID. Our objective was to use a combination of machine-learning and MRI ventilation texture analysis to predict SGRQ improvement at 15 months as compared to three months post-infection and evaluate how MRI textures performed relative to conventional clinical measurements as prognostic markers.

In **Chapter 6**, I outline and summarize the important observations and conclusions of **Chapters 2-5**. In addition, I include a discussion of the specific limitations of each chapter, as well as general limitations of this study. I conclude my thesis by providing an examination of the potential future directions for this research, building upon the foundation laid by this thesis.

1.7 References

1. Zhu, N., *et al.* A Novel Coronavirus from Patients with Pneumonia in China, 2019. *N Engl J Med* **382**, 727-733 (2020).

2. Huang, C., *et al.* Clinical features of patients infected with 2019 novel coronavirus in Wuhan, China. *Lancet* **395**, 497-506 (2020).

3. World Health Organization. WHO Director-General's opening remarks at the media briefing on COVID-19. (2020).

4. Dong, E., Du, H. & Gardner, L. An interactive web-based dashboard to track COVID-19 in real time. *Lancet Infect Dis* **20**, 533-534 (2020).

5. Public Health Agency of Canada. Statement by the Minister of Health on the First Presumptive Confirmed Travel-Related Case of New Coronavirus in Canada. (2020).

6. World Health Organization. WHO COVID-19 Dashboard. (2023).

7. Carfi, A., Bernabei, R., Landi, F. & Gemelli Against COVID-19 Post-Acute Care Study Group. Persistent Symptoms in Patients After Acute COVID-19. *JAMA* **324**, 603-605 (2020).

8. Huang, C., *et al.* 6-month consequences of COVID-19 in patients discharged from hospital: a cohort study. *Lancet* **397**, 220-232 (2021).

9. Nalbandian, A., *et al.* Post-acute COVID-19 syndrome. *Nat Med* **27**, 601-615 (2021).

10. Soriano, J.B., *et al.* A clinical case definition of post-COVID-19 condition by a Delphi consensus. *Lancet Infect Dis* (2021).

11. Al-Aly, Z., Xie, Y. & Bowe, B. High-dimensional characterization of post-acute sequelae of COVID-19. *Nature* **594**, 259-264 (2021).

12. National Institute of Health and Care Excellence. COVID-19 Rapid Guideline: Managing COVID-19. (NICE, 2021).

13. Chen, C., *et al.* Global Prevalence of Post-Coronavirus Disease 2019 (COVID-19) Condition or Long COVID: A Meta-Analysis and Systematic Review. *J Infect Dis* **226**, 1593-1607 (2022).

14. O'Mahoney, L.L., *et al.* The prevalence and long-term health effects of Long Covid among hospitalised and non-hospitalised populations: A systematic review and meta-analysis. *EClinicalMedicine* **55**, 101762 (2023).

15. Cutler, D.M. & Summers, L.H. The COVID-19 Pandemic and the $16 Trillion Virus. *JAMA* **324**, 1495-1496 (2020).

16. Cutler, D.M. The Costs of Long COVID. *JAMA Health Forum* **3**, e221809 (2022).

17. UK Office for National Statistics. Dataset: Prevalence of ongoing symptoms following coronavirus (COVID-19) infection in the UK. (2023).

18. Xiong, Y., *et al.* Clinical and High-Resolution CT Features of the COVID-19 Infection: Comparison of the Initial and Follow-up Changes. *Invest Radiol* **55**, 332-339 (2020).

19. Liu, M., Lv, F., Huang, Y. & Xiao, K. Follow-Up Study of the Chest CT Characteristics of COVID-19 Survivors Seven Months After Recovery. *Front Med (Lausanne)* **8**, 636298 (2021).

20. Caruso, D., *et al.* Post-Acute Sequelae of COVID-19 Pneumonia: Six-month Chest CT Follow-up. *Radiology* **301**, E396-E405 (2021).

21. Han, X., *et al.* Six-month Follow-up Chest CT Findings after Severe COVID-19 Pneumonia. *Radiology* **299**, E177-E186 (2021).

22. Vestbo, J., *et al.* Evaluation of COPD Longitudinally to Identify Predictive Surrogate End-points (ECLIPSE). *Eur Respir J* **31**, 869-873 (2008).

23. Bourbeau, J., *et al.* Canadian Cohort Obstructive Lung Disease (CanCOLD): Fulfilling the need for longitudinal observational studies in COPD. *COPD* **11**, 125-132 (2014).

24. Regan, E.A., *et al.* Genetic epidemiology of COPD (COPDGene) study design. *COPD* **7**, 32-43 (2010).

25. Couper, D., *et al.* Design of the Subpopulations and Intermediate Outcomes in COPD Study (SPIROMICS). *Thorax* **69**, 491-494 (2014).

26. Kirby, M., *et al.* Longitudinal Computed Tomography and Magnetic Resonance Imaging of COPD: Thoracic Imaging Network of Canada (TINCan) Study Objectives. *Chronic Obstr Pulm Dis* **1**, 200-211 (2014).

27. Weibel, E.R., Cournand, A.F. & Richards, D.W. *Morphometry of the human lung*, (Springer, 1963).

28. Lumb, A.B. Nunn's applied respiratory physiology. (2000).

29. West, J.B. & Luks, A.M. *West's Respiratory Physiology*, (Lippincott Williams & Wilkins, 2020).

30. Tschirren, J., Hoffman, E.A., McLennan, G. & Sonka, M. Segmentation and quantitative analysis of intrathoracic airway trees from computed tomography images. *Proc Am Thorac Soc* **2**, 484-487, 503-484 (2005).

31. Haefeli-Bleuer, B. & Weibel, E.R. Morphometry of the human pulmonary acinus. *Anat Rec* **220**, 401-414 (1988).

32. Ochs, M., *et al.* The number of alveoli in the human lung. *Am J Respir Crit Care Med* **169**, 120-124 (2004).

33. Su, S., *et al.* Epidemiology, Genetic Recombination, and Pathogenesis of Coronaviruses. *Trends Microbiol* **24**, 490-502 (2016).

34. Cui, J., Li, F. & Shi, Z.L. Origin and evolution of pathogenic coronaviruses. *Nat Rev Microbiol* **17**, 181-192 (2019).

35. Klein, S., *et al.* SARS-CoV-2 structure and replication characterized by in situ cryo-electron tomography. *Nature Commun* **11**, 5885 (2020).

36. Goldsmith, C.S., *et al.* Ultrastructural characterization of SARS coronavirus. *Emerg Infect Dis* **10**, 320-326 (2004).

37. Li, W., *et al.* Angiotensin-converting enzyme 2 is a functional receptor for the SARS coronavirus. *Nature* **426**, 450-454 (2003).

38. Walls, A.C., *et al.* Structure, Function, and Antigenicity of the SARS-CoV-2 Spike Glycoprotein. *Cell* **181**, 281-292 e286 (2020).

39. Chen, Y., Guo, Y., Pan, Y. & Zhao, Z.J. Structure analysis of the receptor binding of 2019-nCoV. *Biochem Biophys Res Commun* **525**, 135-140 (2020).

40. Yuki, K., Fujiogi, M. & Koutsogiannaki, S. COVID-19 pathophysiology: A review. *Clin Immunol* **215**, 108427 (2020).

41. Zou, X., *et al.* Single-cell RNA-seq data analysis on the receptor ACE2 expression reveals the potential risk of different human organs vulnerable to 2019-nCoV infection. *Front Med* **14**, 185-192 (2020).

42. Wiersinga, W.J., Rhodes, A., Cheng, A.C., Peacock, S.J. & Prescott, H.C. Pathophysiology, Transmission, Diagnosis, and Treatment of Coronavirus Disease 2019 (COVID-19): A Review. *JAMA* **324**, 782-793 (2020).

43. Xu, Z., *et al.* Pathological findings of COVID-19 associated with acute respiratory distress syndrome. *Lancet Respir Med* **8**, 420-422 (2020).

44. Klok, F.A., *et al.* Confirmation of the high cumulative incidence of thrombotic complications in critically ill ICU patients with COVID-19: An updated analysis. *Thromb Res* **191**, 148-150 (2020).

45. Thachil, J., *et al.* ISTH interim guidance on recognition and management of coagulopathy in COVID-19. *J Thromb Haemost* **18**, 1023-1026 (2020).

46. Tang, N., Li, D., Wang, X. & Sun, Z. Abnormal coagulation parameters are associated with poor prognosis in patients with novel coronavirus pneumonia. *J Thromb Haemost* **18**, 844-847 (2020).

47. Wang, Y., Wang, Y., Chen, Y. & Qin, Q. Unique epidemiological and clinical features of the emerging 2019 novel coronavirus pneumonia (COVID-19) implicate special control measures. *J Med Virol* **92**, 568-576 (2020).

48. Chen, N., *et al.* Epidemiological and clinical characteristics of 99 cases of 2019 novel coronavirus pneumonia in Wuhan, China: a descriptive study. *Lancet* **395**, 507-513 (2020).

49. World Health Organization. Report of the WHO-China Joint Mission on Coronavirus Disease 2019 (COVID-19). (2020).

50. Macera, M., De Angelis, G., Sagnelli, C., Coppola, N. & Vanvitelli, C.-G. Clinical Presentation of COVID-19: Case Series and Review of the Literature. *Int J Environ Res Public Health* **17**(2020).

51. Carotti, M., *et al.* Chest CT features of coronavirus disease 2019 (COVID-19) pneumonia: key points for radiologists. *Radiol Med* **125**, 636-646 (2020).

52. Pormohammad, A., *et al.* Comparison of confirmed COVID-19 with SARS and MERS cases - Clinical characteristics, laboratory findings, radiographic signs and outcomes: A systematic review and meta-analysis. *Rev Med Virol* **30**, e2112 (2020).

53. Pal, A., *et al.* Comprehensive literature review on the radiographic findings, imaging modalities, and the role of radiology in the COVID-19 pandemic. *World J Radiol* **13**, 258-282 (2021).

54. Bao, C., Liu, X., Zhang, H., Li, Y. & Liu, J. Coronavirus Disease 2019 (COVID-19) CT Findings: A Systematic Review and Meta-analysis. *J Am Coll Radiol* **17**, 701-709 (2020).

55. Zarifian, A., *et al.* Chest CT findings of coronavirus disease 2019 (COVID-19): A comprehensive meta-analysis of 9907 confirmed patients. *Clin Imaging* **70**, 101-110 (2021).

56. Ojha, V., Mani, A., Pandey, N.N., Sharma, S. & Kumar, S. CT in coronavirus disease 2019 (COVID-19): a systematic review of chest CT findings in 4410 adult patients. *Eur Radiol* **30**, 6129-6138 (2020).

57. Hui, D.S., *et al.* The 1-year impact of severe acute respiratory syndrome on pulmonary function, exercise capacity, and quality of life in a cohort of survivors. *Chest* **128**, 2247-2261 (2005).

58. Choutka, J., Jansari, V., Hornig, M. & Iwasaki, A. Unexplained post-acute infection syndromes. *Nat Med* **28**, 911-923 (2022).

59. Stefano, G.B. Historical Insight into Infections and Disorders Associated with Neurological and Psychiatric Sequelae Similar to Long COVID. *Med Sci Monit* **27**, e931447 (2021).

60. Shah, W., Hillman, T., Playford, E.D. & Hishmeh, L. Managing the long term effects of covid-19: summary of NICE, SIGN, and RCGP rapid guideline. *BMJ* **372**, n136 (2021).

61. Greenhalgh, T., Knight, M., A'Court, C., Buxton, M. & Husain, L. Management of post-acute covid-19 in primary care. *BMJ* **370**, m3026 (2020).

62. Thompson, E.J., *et al.* Long COVID burden and risk factors in 10 UK longitudinal studies and electronic health records. *Nature Commun* **13**, 3528 (2022).

63. Tsampasian, V., *et al.* Risk Factors Associated With Post-COVID-19 Condition: A Systematic Review and Meta-analysis. *JAMA Intern Med* **183**, 566-580 (2023).

64. Davis, H.E., McCorkell, L., Vogel, J.M. & Topol, E.J. Long COVID: major findings, mechanisms and recommendations. *Nat Rev Microbiol* **21**, 133-146 (2023).

65. Gupta, A., *et al.* Extrapulmonary manifestations of COVID-19. *Nat Med* **26**, 1017-1032 (2020).

66. Proal, A.D. & VanElzakker, M.B. Long COVID or Post-acute Sequelae of COVID-19 (PASC): An Overview of Biological Factors That May Contribute to Persistent Symptoms. *Front Microbiol* **12**, 698169 (2021).

67. Swank, Z., *et al.* Persistent Circulating Severe Acute Respiratory Syndrome Coronavirus 2 Spike Is Associated With Post-acute Coronavirus Disease 2019 Sequelae. *Clin Infec Dis* **76**, e487-e490 (2023).

68. Phetsouphanh, C., *et al.* Immunological dysfunction persists for 8 months following initial mild-to-moderate SARS-CoV-2 infection. *Nat Immunol* **23**, 210-216 (2022).

69. Klein, J., *et al.* Distinguishing features of long COVID identified through immune profiling. *Nature* **623**, 139-148 (2023).

70. Liu, Q., *et al.* Gut microbiota dynamics in a prospective cohort of patients with post-acute COVID-19 syndrome. *Gut* **71**, 544-552 (2022).

71. Yeoh, Y.K., *et al.* Gut microbiota composition reflects disease severity and dysfunctional immune responses in patients with COVID-19. *Gut* **70**, 698-706 (2021).

72. Arthur, J.M., *et al.* Development of ACE2 autoantibodies after SARS-CoV-2 infection. *PloS one* **16**, e0257016 (2021).

73. Wallukat, G., *et al.* Functional autoantibodies against G-protein coupled receptors in patients with persistent Long-COVID-19 symptoms. *J Transl Autoimmun* **4**, 100100 (2021).

74. Charfeddine, S., *et al.* Long COVID 19 Syndrome: Is It Related to Microcirculation and Endothelial Dysfunction? Insights From TUN-EndCOV Study. *Front Cardiovasc Med* **8**, 745758 (2021).

75. Haffke, M., *et al.* Endothelial dysfunction and altered endothelial biomarkers in patients with post-COVID-19 syndrome and chronic fatigue syndrome (ME/CFS). *J Transl Med* **20**, 138 (2022).

76. Cha, M.J., *et al.* Chronic Lung Injury after COVID-19 Pneumonia: Clinical, Radiologic, and Histopathologic Perspectives. *Radiology* **310**, e231643 (2024).

77. Aesif, S.W., *et al.* Pulmonary Pathology of COVID-19 Following 8 Weeks to 4 Months of Severe Disease: A Report of Three Cases, Including One With Bilateral Lung Transplantation. *Am J Clin Pathol* **155**, 506-514 (2021).

78. Hall, D.J., *et al.* Successful Lung Transplantation for Severe Post-COVID-19 Pulmonary Fibrosis. *Ann Thorac Surg* **114**, e17-e19 (2022).

79. Flaifel, A., *et al.* Pulmonary Pathology of End-Stage COVID-19 Disease in Explanted Lungs and Outcomes After Lung Transplantation. *Am J Clin Pathol* **157**, 908-926 (2022).

80. Li, Y., *et al.* Progression to fibrosing diffuse alveolar damage in a series of 30 minimally invasive autopsies with COVID-19 pneumonia in Wuhan, China. *Histopathology* **78**, 542-555 (2021).

81. Iwasaki, A. & Putrino, D. Why we need a deeper understanding of the pathophysiology of long COVID. *Lancet Infect Dis* **23**, 393-395 (2023).

82. Han, Q., Zheng, B., Daines, L. & Sheikh, A. Long-Term Sequelae of COVID-19: A Systematic Review and Meta-Analysis of One-Year Follow-Up Studies on Post-COVID Symptoms. *Pathogens* **11**(2022).

83. Fernandez-de-Las-Penas, C., *et al.* Prevalence of post-COVID-19 symptoms in hospitalized and non-hospitalized COVID-19 survivors: A systematic review and meta-analysis. *Eur J Intern Med* **92**, 55-70 (2021).

84. Healey, Q., Sheikh, A., Daines, L. & Vasileiou, E. Symptoms and signs of long COVID: A rapid review and meta-analysis. *J Glob Health* **12**, 05014 (2022).

85. Marjenberg, Z., *et al.* Risk of long COVID main symptoms after SARS-CoV-2 infection: a systematic review and meta-analysis. *Sci Rep* **13**, 15332 (2023).

86. Lopez-Leon, S., *et al.* More than 50 long-term effects of COVID-19: a systematic review and meta-analysis. *Sci Rep* **11**, 16144 (2021).

87. Wu, X., *et al.* 3-month, 6-month, 9-month, and 12-month respiratory outcomes in patients following COVID-19-related hospitalisation: a prospective study. *Lancet Respir Med* **9**, 747-754 (2021).

88. Han, X., *et al.* Longitudinal Assessment of Chest CT Findings and Pulmonary Function after COVID-19 Infection. *Radiology* **307**, e222888 (2023).

89. Huang, L., *et al.* 1-year outcomes in hospital survivors with COVID-19: a longitudinal cohort study. *Lancet* **398**, 747-758 (2021).

90. Tarraso, J., *et al.* Lung function and radiological findings 1 year after COVID-19: a prospective follow-up. *Respir Res* **23**, 242 (2022).

91. Zhang, H., *et al.* Lung-function trajectories in COVID-19 survivors after discharge: A two-year longitudinal cohort study. *EClinicalMedicine* **54**, 101668 (2022).

92. Schlemmer, F., *et al.* Respiratory recovery trajectories after severe-to-critical COVID-19: a 1-year prospective multicentre study. *Eur Respir J* **61**(2023).

93. Guler, S.A., *et al.* Pulmonary function and radiological features 4 months after COVID-19: first results from the national prospective observational Swiss COVID-19 lung study. *Eur Respir J* **57**, 2003690 (2021).

94. Shah, A.S., *et al.* A prospective study of 12-week respiratory outcomes in COVID-19-related hospitalisations. *Thorax* **76**, 402-404 (2021).

95. Davis, H.E., *et al.* Characterizing long COVID in an international cohort: 7 months of symptoms and their impact. *EClinicalMedicine* **38**, 101019 (2021).

96. Moens, M., *et al.* Health-related quality of life in persons post-COVID-19 infection in comparison to normative controls and chronic pain patients. *Front Public Health* **10**, 991572 (2022).

97. Luger, A.K., *et al.* Chest CT of Lung Injury 1 Year after COVID-19 Pneumonia: The CovILD Study. *Radiology* **304**, 462-470 (2022).

98. Cho, J.L., *et al.* Quantitative Chest CT Assessment of Small Airways Disease in Post-Acute SARS-CoV-2 Infection. *Radiology*, 212170 (2022).

99. Miller, M.R., *et al.* Standardisation of spirometry. *Eur Respir J* **26**, 319-338 (2005).

100. Graham, B.L., *et al.* Standardization of Spirometry 2019 Update. An Official American Thoracic Society and European Respiratory Society Technical Statement. *Am J Respir Crit Care Med* **200**, e70-e88 (2019).

101. Quanjer, P.H., *et al.* Multi-ethnic reference values for spirometry for the 3-95-yr age range: the global lung function 2012 equations. *Eur Respir J* **40**, 1324-1343 (2012).

102. Hankinson, J.L., Odencrantz, J.R. & Fedan, K.B. Spirometric reference values from a sample of the general U.S. population. *Am J Respir Crit Care Med* **159**, 179-187 (1999).

103. Wanger, J., *et al.* Standardisation of the measurement of lung volumes. *Eur Respir J* **26**, 511-522 (2005).

104. Graham, B.L., *et al.* 2017 ERS/ATS standards for single-breath carbon monoxide uptake in the lung. *Eur Respir J* **49**(2017).

105. DeCato, T.W. & Hegewald, M.J. Breathing Red: Physiology of an Elevated Single-Breath Diffusing Capacity of Carbon Monoxide. *Ann Am Thorac Soc* **13**, 2087-2092 (2016).

106. Stanojevic, S., *et al.* Official ERS technical standards: Global Lung Function Initiative reference values for the carbon monoxide transfer factor for Caucasians. *Eur Respir J* **50**(2017).

107. Dubois, A.B., Brody, A.W., Lewis, D.H. & Burgess, B.F., Jr. Oscillation mechanics of lungs and chest in man. *J Appl Physiol* **8**, 587-594 (1956).

108. King, G.G., *et al.* Technical standards for respiratory oscillometry. *Eur Respir J* **55**(2020).

109. Kaminsky, D.A., *et al.* Clinical significance and applications of oscillometry. *Eur Respir Rev* **31**(2022).

110. Oostveen, E., *et al.* The forced oscillation technique in clinical practice: methodology, recommendations and future developments. *Eur Respir J* **22**, 1026-1041 (2003).

111. Smith, H., Reinhold, P. & Goldman, M. Forced oscillation technique and impulse oscillometry. *Eur Respir J* **31**, 72 (2005).

112. Bates, J.H. *Lung mechanics: an inverse modeling approach*, (Cambridge University Press, 2009).

113. Kim, S.R., *et al.* Application of Impulse Oscillometry in Adult Asthmatic Patients With Preserved Lung Function. *Allergy Asthma Immunol Res* **12**, 832-843 (2020).

114. Naji, N., *et al.* Comparison of changes in lung function measured by plethymography and IOS after bronchoprovocation. *Respir Med* **107**, 503-510 (2013).

115. Broeders, M.E., Molema, J., Hop, W.C. & Folgering, H.T. Bronchial challenge, assessed with forced expiratory manoeuvres and airway impedance. *Respir Med* **99**, 1046-1052 (2005).

116. Seccombe, L.M., Peters, M.J., Buddle, L. & Farah, C.S. Exercise-Induced Bronchoconstriction Identified Using the Forced Oscillation Technique. *Front Physiol* **10**, 1411 (2019).

117. Larsen, G.L., *et al.* Impulse oscillometry versus spirometry in a long-term study of controller therapy for pediatric asthma. *J Allergy Clin Immunol* **123**, 861-867 e861 (2009).

118. Ribeiro, C.O., Faria, A.C.D., Lopes, A.J. & de Melo, P.L. Forced oscillation technique for early detection of the effects of smoking and COPD: contribution of fractional-order modeling. *Int J Chron Obstruct Pulmon Dis* **13**, 3281-3295 (2018).

119. Veneroni, C., *et al.* Diagnostic Potential of Oscillometry: A Population-based Approach. *Am J Respir Crit Care Med* **209**, 444-453 (2024).

120. Qvarnstrom, B., *et al.* Impulse oscillometry indices in relation to respiratory symptoms and spirometry in the Swedish Cardiopulmonary Bioimage Study. *ERJ Open Res* **9**(2023).

121. Robinson, P.D., *et al.* Consensus statement for inert gas washout measurement using multiple- and single- breath tests. *Eur Respir J* **41**, 507-522 (2013).

122. Robertson, J.S., Siri, W.E. & Jones, H.B. Lung ventilation patterns determined by analysis of nitrogen elimination rates; use of mass spectrometer as a continuous gas analyzer. *J Clin Invest* **29**, 577-590 (1950).

123. Fowler, W.S. Lung function studies; uneven pulmonary ventilation in normal subjects and in patients with pulmonary disease. *J Appl Physiol* **2**, 283-299 (1949).

124. Macleod, K.A., *et al.* Ventilation heterogeneity in children with well controlled asthma with normal spirometry indicates residual airways disease. *Thorax* **64**, 33-37 (2009).

125. Bourdin, A., *et al.* Nitrogen washout slope in poorly controlled asthma. *Allergy* **61**, 85-89 (2006).

126. Downie, S.R., *et al.* Ventilation heterogeneity is a major determinant of airway hyperresponsiveness in asthma, independent of airway inflammation. *Thorax* **62**, 684-689 (2007).

127. Thompson, B.R., *et al.* Peripheral lung function in patients with stable and unstable asthma. *J Allergy Clin Immunol* **131**, 1322-1328 (2013).

128. Horsley, A.R., *et al.* Lung clearance index is a sensitive, repeatable and practical measure of airways disease in adults with cystic fibrosis. *Thorax* **63**, 135-140 (2008).

129. Aurora, P., *et al.* Multiple-breath washout as a marker of lung disease in preschool children with cystic fibrosis. *Am J Respir Crit Care Med* **171**, 249-256 (2005).

130. Jetmalani, K., *et al.* Peripheral airway dysfunction and relationship with symptoms in smokers with preserved spirometry. *Respirol* **23**, 512-518 (2018).

131. Zell-Baran, L.M., *et al.* Multiple breath washout: A noninvasive tool for identifying lung disease in symptomatic military deployers. *Respir Med* **176**, 106281 (2021).

132. Dweik, R.A., *et al.* An official ATS clinical practice guideline: interpretation of exhaled nitric oxide levels (FENO) for clinical applications. *Am J Respir Crit Care Med* **184**, 602-615 (2011).

133. Guo, F.H. & Erzurum, S.C. Characterization of inducible nitric oxide synthase expression in human airway epithelium. *Environ Health Perspect* **106 Suppl 5**, 1119-1124 (1998).

134. Guo, F.H., *et al.* Molecular mechanisms of increased nitric oxide (NO) in asthma: evidence for transcriptional and post-translational regulation of NO synthesis. *J Immunol* **164**, 5970-5980 (2000).

135. Paoliello-Paschoalato, A.B., Oliveira, S.H. & Cunha, F.Q. Interleukin 4 induces the expression of inducible nitric oxide synthase in eosinophils. *Cytokine* **30**, 116-124 (2005).

136. Smith, A.D., *et al.* Exhaled nitric oxide: a predictor of steroid response. *Am J Respir Crit Care Med* **172**, 453-459 (2005).

137. Berkman, N., *et al.* Exhaled nitric oxide in the diagnosis of asthma: comparison with bronchial provocation tests. *Thorax* **60**, 383-388 (2005).

138. Enright, P.L. The six-minute walk test. *Respir Care* **48**, 783-785 (2003).

139. Holland, A.E., *et al.* An official European Respiratory Society/American Thoracic Society technical standard: field walking tests in chronic respiratory disease. *Eur Respir J* **44**, 1428-1446 (2014).

140. Solway, S., Brooks, D., Lacasse, Y. & Thomas, S. A qualitative systematic overview of the measurement properties of functional walk tests used in the cardiorespiratory domain. *Chest* **119**, 256-270 (2001).

141. Borg, G. *Borg's perceived exertion and pain scales*, (Human kinetics, 1998).

142. Singh, S.J., *et al.* An official systematic review of the European Respiratory Society/American Thoracic Society: measurement properties of field walking tests in chronic respiratory disease. *Eur Respir J* **44**, 1447-1478 (2014).

143. Jones, P.W., Quirk, F.H., Baveystock, C.M. & Littlejohns, P. A self-complete measure of health status for chronic airflow limitation. The St. George's Respiratory Questionnaire. *Am Rev Respir Dis* **145**, 1321-1327 (1992).

144. Jones, P.W. St. George's Respiratory Questionnaire: MCID. *COPD* **2**, 75-79 (2005).

145. Calverley, P., *et al.* Combined salmeterol and fluticasone in the treatment of chronic obstructive pulmonary disease: a randomised controlled trial. *Lancet* **361**, 449-456 (2003).

146. Jones, P.W. & Bosh, T.K. Quality of life changes in COPD patients treated with salmeterol. *Am J Respir Crit Care Med* **155**, 1283-1289 (1997).

147. Griffiths, T.L., *et al.* Results at 1 year of outpatient multidisciplinary pulmonary rehabilitation: a randomised controlled trial. *Lancet* **355**, 362-368 (2000).

148. Craig, C.L., *et al.* International physical activity questionnaire: 12-country reliability and validity. *Med Sci Sports Exerc* **35**, 1381-1395 (2003).

149. Mahler, D.A., *et al.* Development of self-administered versions of modified baseline and transition dyspnea indexes in COPD. *COPD* **1**, 165-172 (2004).

150. Celli, B.R., *et al.* The body-mass index, airflow obstruction, dyspnea, and exercise capacity index in chronic obstructive pulmonary disease. *N Engl J Med* **350**, 1005-1012 (2004).

151. Busse, W.W. Asthma diagnosis and treatment: filling in the information gaps. *J Allergy Clin Immunol* **128**, 740-750 (2011).

152. Polak, A.G., Wysoczanski, D. & Mroczka, J. Effects of homogeneous and heterogeneous changes in the lung periphery on spirometry results. *Comput Methods Programs Biomed* **173**, 139-145 (2019).

153. Cerveri, I., *et al.* Underestimation of airflow obstruction among young adults using FEV1/FVC <70% as a fixed cut-off: a longitudinal evaluation of clinical and functional outcomes. *Thorax* **63**, 1040-1045 (2008).

154. Stockley, J.A., Cooper, B.G., Stockley, R.A. & Sapey, E. Small airways disease: time for a revisit? *Int J Chron Obstruct Pulmon Dis* **12**, 2343-2353 (2017).

155. Radiation and your patient: a guide for medical practitioners. *Ann ICRP* **31**, 5-31 (2001).

156. Commission, C.N.S. Radiation doses. (2014).

157. Kirsch, J., *et al.* ACR Appropriateness Criteria® acute respiratory illness in immunocompetent patients. *J Thorac Imaging* **26**, W42-W44 (2011).

158. Thurlbeck, W.M. & Simon, G. Radiographic appearance of the chest in emphysema. *AJR Am J Roentgenol* **130**, 429-440 (1978).

159. Pipavath, S.N., Schmidt, R.A., Takasugi, J.E. & Godwin, J.D. Chronic obstructive pulmonary disease: radiology-pathology correlation. *J Thorac Imaging* **24**, 171-180 (2009).

160. Paganin, F., *et al.* Chest radiography and high resolution computed tomography of the lungs in asthma. *Am Rev Respir Dis* **146**, 1084-1087 (1992).

161. Rebuck, A.S. Radiological aspects of severe asthma. *Australas Radiol* **14**, 264-268 (1970).

162. Martinez, S., *et al.* Mucoid impactions: finger-in-glove sign and other CT and radiographic features. *Radiographics* **28**, 1369-1382 (2008).

163. Wong, C.K.H., Wong, J.Y.H., Tang, E.H.M., Au, C.H. & Wai, A.K.C. Clinical presentations, laboratory and radiological findings, and treatments for 11,028 COVID-19 patients: a systematic review and meta-analysis. *Sci Rep* **10**, 19765 (2020).

164. Sadiq, Z., Rana, S., Mahfoud, Z. & Raoof, A. Systematic review and meta-analysis of chest radiograph (CXR) findings in COVID-19. *Clin Imaging* **80**, 229-238 (2021).

165. Bates, S., Beckmann, L., Thomas, A. & Waltham, R. *Godfrey Hounsfield: Intuitive Genius of CT*, (British Institute of Radiology London, 2012).

166. Goldman, L.W. Principles of CT and CT technology. *J Nucl Med Technol* **35**, 115-128; quiz 129-130 (2007).

167. Hounsfield, G.N. Computerized transverse axial scanning (tomography). 1. Description of system. *Br J Radiol* **46**, 1016-1022 (1973).

168. Mayo, J.R., Aldrich, J. & Müller, N.L. Radiation exposure at chest CT: a statement of the Fleischner Society. *Radiology* **228**, 15-21 (2003).

169. Tsiflikas, I., *et al.* Low dose pediatric chest computed tomography on a photon counting detector system - initial clinical experience. *Pediatr Radiol* **53**, 1057-1062 (2023).

170. Ferda, J., *et al.* Computed tomography with a full FOV photon-counting detector in a clinical setting, the first experience. *Eur J Radiol* **137**, 109614 (2021).

171. Bocchino, M., Rea, G., Capitelli, L., Lieto, R. & Bruzzese, D. Chest CT Lung Abnormalities 1 Year after COVID-19: A Systematic Review and Meta-Analysis. *Radiology* **308**, e230535 (2023).

172. Rubin, G.D., *et al.* The Role of Chest Imaging in Patient Management during the COVID-19 Pandemic: A Multinational Consensus Statement from the Fleischner Society. *Radiology* **296**, 172-180 (2020).

173. Newell, J.D., Jr., Sieren, J. & Hoffman, E.A. Development of quantitative computed tomography lung protocols. *J Thorac Imaging* **28**, 266-271 (2013).

174. Quantitative Imaging Biomarkers Alliance. Vol. 2023 (Radiological Society of North America, Radiological Society of North America website, 2018).

175. Gevenois, P.A., *et al.* Comparison of computed density and microscopic morphometry in pulmonary emphysema. *Am J Respir Crit Care Med* **154**, 187-192 (1996).

176. Wang, Z., *et al.* Optimal threshold in CT quantification of emphysema. *Eur Radiol* **23**, 975-984 (2013).

177. Newman, K.B., Lynch, D.A., Newman, L.S., Ellegood, D. & Newell, J.D., Jr. Quantitative computed tomography detects air trapping due to asthma. *Chest* **106**, 105-109 (1994).

178. Wiemker, R., Blaffert, T., Bülow, T., Renisch, S. & Lorenz, C. Automated assessment of bronchial lumen, wall thickness and bronchoarterial diameter ratio of the tracheobronchial tree using high-resolution CT. in *International Congress Series*, Vol. 1268 967-972 (Elsevier, 2004).

179. Saba, O.I., Hoffman, E.A. & Reinhardt, J.M. Computed tomographic-based estimation of airway size with correction for scanned plane tilt angle. in *Medical Imaging 2000: Physiology and Function from Multidimensional Images*, Vol. 3978 58-66 (SPIE, 2000).

180. Reinhardt, J.M., Park, W., Hoffman, E.A. & Sonka, M. Intrathoracic airway wall detection using graph search and scanner PSF information. in *Medical Imaging 1997: Physiology and Function from Multidimensional Images*, Vol. 3033 93-101 (SPIE, 1997).

181. Reinhardt, J.M., D'Souza, N. & Hoffman, E.A. Accurate measurement of intrathoracic airways. *IEEE transactions on medical imaging* **16**, 820-827 (1997).

182. Wood, S.A., Hoford, J.D., Hoffman, E.A., Zerhouni, E.A. & Mitzner, W.A. Quantitative 3D reconstruction of airway and pulmonary vascular trees using HRCT. in *Biomedical Image Processing and Biomedical Visualization*, Vol. 1905 316-323 (SPIE, 1993).

183. King, G.G., Muller, N.L., Whittall, K.P., Xiang, Q.S. & Pare, P.D. An analysis algorithm for measuring airway lumen and wall areas from high-resolution computed tomographic data. *Am J Respir Crit Care Med* **161**, 574-580 (2000).

184. Prêteux, F., Fetita, C., Capderou, A. & Grenier, P. Modeling, segmentation, and caliber estimation of bronchi in high resolution computerized tomography. *Journal of Electronic Imaging* **8**, 36 (1999).

185. Kirby, M., *et al.* Computed Tomography Total Airway Count Is Associated with the Number of Micro-Computed Tomography Terminal Bronchioles. *Am J Respir Crit Care Med* **201**, 613-615 (2020).

186. Oguma, T., *et al.* Longitudinal shape irregularity of airway lumen assessed by CT in patients with bronchial asthma and COPD. *Thorax* **70**, 719-724 (2015).

187. Okazawa, M., *et al.* Human airway narrowing measured using high resolution computed tomography. *Am J Respir Crit Care Med* **154**, 1557-1562 (1996).

188. Awadh, N., Muller, N.L., Park, C.S., Abboud, R.T. & FitzGerald, J.M. Airway wall thickness in patients with near fatal asthma and control groups: assessment with high resolution computed tomographic scanning. *Thorax* **53**, 248-253 (1998).

189. Niimi, A., *et al.* Airway wall thickness in asthma assessed by computed tomography. Relation to clinical indices. *Am J Respir Crit Care Med* **162**, 1518-1523 (2000).

190. Little, S.A., *et al.* High resolution computed tomographic assessment of airway wall thickness in chronic asthma: reproducibility and relationship with lung function and severity. *Thorax* **57**, 247-253 (2002).

191. Berair, R., *et al.* Associations in asthma between quantitative computed tomography and bronchial biopsy-derived airway remodelling. *Eur Respir J* **49**(2017).

192. Kasahara, K., Shiba, K., Ozawa, T., Okuda, K. & Adachi, M. Correlation between the bronchial subepithelial layer and whole airway wall thickness in patients with asthma. *Thorax* **57**, 242-246 (2002).

193. Aysola, R.S., *et al.* Airway remodeling measured by multidetector CT is increased in severe asthma and correlates with pathology. *Chest* **134**, 1183-1191 (2008).

194. Gupta, S., *et al.* Quantitative analysis of high-resolution computed tomography scans in severe asthma subphenotypes. *Thorax* **65**, 775-781 (2010).

195. Gono, H., Fujimoto, K., Kawakami, S. & Kubo, K. Evaluation of airway wall thickness and air trapping by HRCT in asymptomatic asthma. *Eur Respir J* **22**, 965-971 (2003).

196. Siddiqui, S., *et al.* Airway wall geometry in asthma and nonasthmatic eosinophilic bronchitis. *Allergy* **64**, 951-958 (2009).

197. Eddy, R.L., *et al.* Is Computed Tomography Airway Count Related to Asthma Severity and Airway Structure and Function? *Am J Respir Crit Care Med* **201**, 923-933 (2020).

198. Kirby, M., *et al.* Total Airway Count on Computed Tomography and the Risk of Chronic Obstructive Pulmonary Disease Progression. Findings from a Population-based Study. *Am J Respir Crit Care Med* **197**, 56-65 (2018).

199. Smith, B.M., *et al.* Comparison of spatially matched airways reveals thinner airway walls in COPD. The Multi-Ethnic Study of Atherosclerosis (MESA) COPD Study and the Subpopulations and Intermediate Outcomes in COPD Study (SPIROMICS). *Thorax* **69**, 987-996 (2014).

200. Wyszkiewicz, P.V., *et al.* Reduced Total Airway Count and Airway Wall Tapering after Three-Years in Ex-Smokers. *COPD* **20**, 186-196 (2023).

201. Matsuoka, S., Kurihara, Y., Yagihashi, K., Hoshino, M. & Nakajima, Y. Airway dimensions at inspiratory and expiratory multisection CT in chronic obstructive pulmonary disease: correlation with airflow limitation. *Radiology* **248**, 1042-1049 (2008).

202. Berger, P., *et al.* Airway wall thickness in cigarette smokers: quantitative thin-section CT assessment. *Radiology* **235**, 1055-1064 (2005).

203. Grydeland, T.B., *et al.* Quantitative computed tomography measures of emphysema and airway wall thickness are related to respiratory symptoms. *Am J Respir Crit Care Med* **181**, 353-359 (2010).

204. Nakano, Y., *et al.* Computed tomographic measurements of airway dimensions and emphysema in smokers. Correlation with lung function. *Am J Respir Crit Care Med* **162**, 1102-1108 (2000).

205. Hasegawa, M., *et al.* Airflow limitation and airway dimensions in chronic obstructive pulmonary disease. *Am J Respir Crit Care Med* **173**, 1309-1315 (2006).

206. Austin, J.H., *et al.* Glossary of terms for CT of the lungs: recommendations of the Nomenclature Committee of the Fleischner Society. *Radiology* **200**, 327-331 (1996).

207. Jain, N., *et al.* Quantitative computed tomography detects peripheral airway disease in asthmatic children. *Pediatric pulmonology* **40**, 211-218 (2005).

208. Lynch, D.A. & Al-Qaisi, M.A. Quantitative computed tomography in chronic obstructive pulmonary disease. *J Thorac Imaging* **28**, 284-290 (2013).

209. Kirby, M., *et al.* A Novel Method of Estimating Small Airway Disease Using Inspiratory-to-Expiratory Computed Tomography. *Respiration* **94**, 336-345 (2017).

210. Estepar, R.S., *et al.* Computational Vascular Morphometry for the Assessment of Pulmonary Vascular Disease Based on Scale-Space Particles. *Proc IEEE Int Symp Biomed Imaging*, 1479-1482 (2012).

211. Estepar, R.S., *et al.* Computed tomographic measures of pulmonary vascular morphology in smokers and their clinical implications. *Am J Respir Crit Care Med* **188**, 231-239 (2013).

212. Washko, G.R., *et al.* Arterial Vascular Pruning, Right Ventricular Size, and Clinical Outcomes in Chronic Obstructive Pulmonary Disease. A Longitudinal Observational Study. *Am J Respir Crit Care Med* **200**, 454-461 (2019).

213. Ash, S.Y., *et al.* Pruning of the Pulmonary Vasculature in Asthma. The Severe Asthma Research Program (SARP) Cohort. *Am J Respir Crit Care Med* **198**, 39-50 (2018).

214. Matsuoka, S., *et al.* Quantitative CT measurement of cross-sectional area of small pulmonary vessel in COPD: correlations with emphysema and airflow limitation. *Acad Radiol* **17**, 93-99 (2010).

215. Parker, J.A., *et al.* SNM practice guideline for lung scintigraphy 4.0. *J Nucl Med Technol* **40**, 57-65 (2012).

216. Musch, G. & Venegas, J.G. Positron emission tomography imaging of regional pulmonary perfusion and ventilation. *Proc Am Thorac Soc* **2**, 522-527, 508-529 (2005).

217. Bergin, C.J., Glover, G.M. & Pauly, J. Magnetic resonance imaging of lung parenchyma. *J Thorac Imaging* **8**, 12-17 (1993).

218. Wild, J.M., *et al.* MRI of the lung (1/3): methods. *Insights Imaging* **3**, 345-353 (2012).

219. Bergin, C.J., Noll, D.C., Pauly, J.M., Glover, G.H. & Macovski, A. MR imaging of lung parenchyma: a solution to susceptibility. *Radiology* **183**, 673-676 (1992).

220. Bergin, C.J., Pauly, J.M. & Macovski, A. Lung parenchyma: projection reconstruction MR imaging. *Radiology* **179**, 777-781 (1991).

221. Schmidt, M.A., *et al.* Non-breath-hold lung magnetic resonance imaging with real-time navigation. *MAGMA* **5**, 123-128 (1997).

222. Sheikh, K., *et al.* Ultrashort echo time MRI biomarkers of asthma. *J Magn Reson Imaging* **45**, 1204-1215 (2017).

223. Ma, W., *et al.* Ultra-short echo-time pulmonary MRI: evaluation and reproducibility in COPD subjects with and without bronchiectasis. *J Magn Reson Imaging* **41**, 1465-1474 (2015).

224. Ohno, Y., *et al.* Pulmonary high-resolution ultrashort TE MR imaging: Comparison with thin-section standard- and low-dose computed tomography for the assessment of pulmonary parenchyma diseases. *J Magn Reson Imaging* **43**, 512-532 (2016).

225. Benlala, I., *et al.* Evaluation of bronchial wall thickness in asthma using magnetic resonance imaging. *Eur Respir J* **59**(2022).

226. Albert, M.S., *et al.* Biological magnetic resonance imaging using laser-polarized 129Xe. *Nature* **370**, 199-201 (1994).

227. MacFall, J.R., *et al.* Human lung air spaces: potential for MR imaging with hyperpolarized He-3. *Radiology* **200**, 553-558 (1996).

228. Bachert, P., *et al.* Nuclear magnetic resonance imaging of airways in humans with use of hyperpolarized 3He. *Magn Reson Med* **36**, 192-196 (1996).

229. Fain, S.B., *et al.* Functional lung imaging using hyperpolarized gas MRI. *J Magn Reson Imaging* **25**, 910-923 (2007).

230. Stewart, N.J., *et al.* Lung MRI with hyperpolarised gases: current & future clinical perspectives. *Br J Radiol* **95**, 20210207 (2022).

231. Walker, T.G. & Happer, W. Spin-exchange optical pumping of noble-gas nuclei. *Rev Mod Phys* **69**, 629-642 (1997).

232. Shea, D.A. & Morgan, D.L. The helium-3 shortage: Supply, demand, and options for congress. (Congressional Research Service Washington, DC, 2010).

233. Woods, J.C. Mine the moon for 3He MRI? Not yet. *J Appl Physiol* **114**, 705-706 (2013).

234. Shukla, Y., *et al.* Hyperpolarized 129Xe magnetic resonance imaging: tolerability in healthy volunteers and subjects with pulmonary disease. *Acad Radiol* **19**, 941-951 (2012).

235. Driehuys, B., *et al.* Chronic obstructive pulmonary disease: safety and tolerability of hyperpolarized 129Xe MR imaging in healthy volunteers and patients. *Radiology* **262**, 279-289 (2012).

236. Lutey, B.A., *et al.* Hyperpolarized 3He MR imaging: physiologic monitoring observations and safety considerations in 100 consecutive subjects. *Radiology* **248**, 655-661 (2008).

237. Peiffer, J.D., *et al.* Hyperpolarized (129)Xe MRI, (99m)Tc scintigraphy, and SPECT in lung ventilation imaging: a quantitative comparison. *Acad Radiol* (2023).

238. Altes, T.A., *et al.* Ventilation imaging of the lung: comparison of hyperpolarized helium-3 MR imaging with Xe-133 scintigraphy. *Acad Radiol* **11**, 729-734 (2004).

239. Stavngaard, T., *et al.* Hyperpolarized 3He MRI and 81mKr SPECT in chronic obstructive pulmonary disease. *Eur J Nucl Med Mol Imaging* **32**, 448-457 (2005).

240. Doganay, O., *et al.* Time-series hyperpolarized xenon-129 MRI of lobar lung ventilation of COPD in comparison to V/Q-SPECT/CT and CT. *Eur Radiol* **29**, 4058-4067 (2019).

241. Niedbalski, P.J., *et al.* Protocols for multi-site trials using hyperpolarized (129) Xe MRI for imaging of ventilation, alveolar-airspace size, and gas exchange: A position paper from the (129) Xe MRI clinical trials consortium. *Magn Reson Med* **86**, 2966-2986 (2021).

242. Altes, T.A., *et al.* Hyperpolarized 3He MR lung ventilation imaging in asthmatics: preliminary findings. *J Magn Reson Imaging* **13**, 378-384 (2001).

243. de Lange, E.E., *et al.* Evaluation of asthma with hyperpolarized helium-3 MRI: correlation with clinical severity and spirometry. *Chest* **130**, 1055-1062 (2006).

244. Donnelly, L.F., *et al.* Cystic fibrosis: combined hyperpolarized 3He-enhanced and conventional proton MR imaging in the lung--preliminary observations. *Radiology* **212**, 885-889 (1999).

245. Woodhouse, N., *et al.* Combined helium-3/proton magnetic resonance imaging measurement of ventilated lung volumes in smokers compared to never-smokers. *J Magn Reson Imaging* **21**, 365-369 (2005).

246. He, M., Driehuys, B., Que, L.G. & Huang, Y.T. Using Hyperpolarized (129)Xe MRI to Quantify the Pulmonary Ventilation Distribution. *Acad Radiol* **23**, 1521-1531 (2016).

247. He, M., *et al.* Extending semiautomatic ventilation defect analysis for hyperpolarized (129)Xe ventilation MRI. *Acad Radiol* **21**, 1530-1541 (2014).

248. Kirby, M., *et al.* Hyperpolarized 3He magnetic resonance functional imaging semiautomated segmentation. *Acad Radiol* **19**, 141-152 (2012).

249. Tustison, N.J., *et al.* Ventilation-based segmentation of the lungs using hyperpolarized (3)He MRI. *J Magn Reson Imaging* **34**, 831-841 (2011).

250. Zha, W., *et al.* Semiautomated Ventilation Defect Quantification in Exercise-induced Bronchoconstriction Using Hyperpolarized Helium-3 Magnetic Resonance Imaging: A Repeatability Study. *Acad Radiol* **23**, 1104-1114 (2016).

251. Couch, M.J., *et al.* A two-center analysis of hyperpolarized (129)Xe lung MRI in stable pediatric cystic fibrosis: Potential as a biomarker for multi-site trials. *J Cyst Fibros* **18**, 728-733 (2019).

252. Zhang, X., *et al.* Quantification of lung ventilation defects on hyperpolarized MRI: The Multi-Ethnic Study of Atherosclerosis (MESA) COPD study. *Magnetic Resonance Imaging* **92**, 140-149 (2022).

253. Tustison, N.J., *et al.* Convolutional neural networks with template-based data augmentation for functional lung image quantification. *Acad* **26**, 412-423 (2019).

254. Astley, J.R., *et al.* A Dual-Channel Deep Learning Approach for Lung Cavity Estimation From Hyperpolarized Gas and Proton MRI. *J Magn Reson Imaging* **57**, 1878-1890 (2023).

255. Astley, J.R., *et al.* Large-scale investigation of deep learning approaches for ventilated lung segmentation using multi-nuclear hyperpolarized gas MRI. *Sci Rep* **12**, 10566 (2022).

256. Fain, S.B., *et al.* Evaluation of structure-function relationships in asthma using multidetector CT and hyperpolarized He-3 MRI. *Acad Radiol* **15**, 753-762 (2008).

257. Kirby, M., Wheatley, A., McCormack, D.G. & Parraga, G. Development and application of methods to quantify spatial and temporal hyperpolarized 3He MRI ventilation dynamics: preliminary results in chronic obstructive pulmonary disease. in *Medical Imaging 2010: Biomedical Applications in Molecular, Structural, and Functional Imaging*, Vol. 7626 762605 (International Society for Optics and Photonics, 2010).

258. de Lange, E.E., *et al.* The variability of regional airflow obstruction within the lungs of patients with asthma: assessment with hyperpolarized helium-3 magnetic resonance imaging. *J Allergy Clin Immunol* **119**, 1072-1078 (2007).

259. Svenningsen, S., *et al.* What are ventilation defects in asthma? *Thorax* **69**, 63-71 (2014).

260. Svenningsen, S., *et al.* Sputum Eosinophilia and Magnetic Resonance Imaging Ventilation Heterogeneity in Severe Asthma. *Am J Respir Crit Care Med* **197**, 876-884 (2018).

261. Svenningsen, S., *et al.* CT and Functional MRI to Evaluate Airway Mucus in Severe Asthma. *Chest* **155**, 1178-1189 (2019).

262. Svenningsen, S., Nair, P., Guo, F., McCormack, D.G. & Parraga, G. Is ventilation heterogeneity related to asthma control? *Eur Respir J* **48**, 370-379 (2016).

263. Ebner, L., *et al.* Hyperpolarized 129Xenon Magnetic Resonance Imaging to Quantify Regional Ventilation Differences in Mild to Moderate Asthma: A Prospective Comparison Between Semiautomated Ventilation Defect Percentage Calculation and Pulmonary Function Tests. *Invest Radiol* **52**, 120-127 (2017).

264. Samee, S., *et al.* Imaging the lungs in asthmatic patients by using hyperpolarized helium-3 magnetic resonance: assessment of response to methacholine and exercise challenge. *J Allergy Clin Immunol* **111**, 1205-1211 (2003).

265. Costella, S., *et al.* Regional pulmonary response to a methacholine challenge using hyperpolarized (3)He magnetic resonance imaging. *Respirol* **17**, 1237-1246 (2012).

266. Mummy, D.G., *et al.* Ventilation defects on hyperpolarized helium-3 MRI in asthma are predictive of 2-year exacerbation frequency. *J Allergy Clin Immunol* **146**, 831-839 e836 (2020).

267. Mummy, D.G., *et al.* Ventilation defect percent in helium-3 magnetic resonance imaging as a biomarker of severe outcomes in asthma. *J Allergy Clin Immunol* **141**, 1140-1141 e1144 (2018).

268. Kruger, S.J., *et al.* Hyperpolarized Helium-3 MRI of exercise-induced bronchoconstriction during challenge and therapy. *J Magn Reson Imaging* **39**, 1230-1237 (2014).

269. Svenningsen, S., *et al.* Hyperpolarized (3) He and (129) Xe MRI: differences in asthma before bronchodilation. *J Magn Reson Imaging* **38**, 1521-1530 (2013).

270. Safavi, S., *et al.* Evaluating post-bronchodilator response in well-controlled paediatric severe asthma using hyperpolarised 129Xe-MRI: A pilot study. *Respir Med* **180**, 106368 (2021).

271. Svenningsen, S., Eddy, R.L., Kjarsgaard, M., Parraga, G. & Nair, P. Effects of Anti-T2 Biologic Treatment on Lung Ventilation Evaluated by MRI in Adults With Prednisone-Dependent Asthma. *Chest* (2020).

272. Svenningsen, S., Haider, E.A., Eddy, R.L., Parraga, G. & Nair, P. Normalisation of MRI ventilation heterogeneity in severe asthma by dupilumab. *Thorax* **74**, 1087-1088 (2019).

273. McIntosh, M.J., *et al.* Asthma Control, Airway Mucus, and (129)Xe MRI Ventilation After a Single Benralizumab Dose. *Chest* **162**, 520-533 (2022).

274. McIntosh, M.J., *et al.* CT Mucus Score and (129)Xe MRI Ventilation Defects After 2.5 Years' Anti-IL-5Ralpha in Eosinophilic Asthma. *Chest* **164**, 27-38 (2023).

275. Svenningsen, S., *et al.* Bronchial thermoplasty guided by hyperpolarised gas MRI in adults with severe asthma: a 1-year pilot randomised trial. *ERJ Open Res* (2021).

276. Hall, C.S., *et al.* Single-Session Bronchial Thermoplasty Guided by (129)Xe Magnetic Resonance Imaging. A Pilot Randomized Controlled Clinical Trial. *Am J Respir Crit Care Med* **202**, 524-534 (2020).

277. Mathew, L., *et al.* Hyperpolarized 3He magnetic resonance imaging of chronic obstructive pulmonary disease: reproducibility at 3.0 tesla. *Acad Radiol* **15**, 1298-1311 (2008).

278. Kirby, M., *et al.* Hyperpolarized 3He and 129Xe MR imaging in healthy volunteers and patients with chronic obstructive pulmonary disease. *Radiology* **265**, 600-610 (2012).

279. Virgincar, R.S., *et al.* Quantitative analysis of hyperpolarized 129Xe ventilation imaging in healthy volunteers and subjects with chronic obstructive pulmonary disease. *NMR Biomed* **26**, 424-435 (2013).

280. Kirby, M., *et al.* COPD: Do Imaging Measurements of Emphysema and Airway Disease Explain Symptoms and Exercise Capacity? *Radiology* **277**, 872-880 (2015).

281. Kirby, M., *et al.* Chronic obstructive pulmonary disease: quantification of bronchodilator effects by using hyperpolarized (3)He MR imaging. *Radiology* **261**, 283-292 (2011).

282. Kirby, M., Pike, D., Coxson, H.O., McCormack, D.G. & Parraga, G. Hyperpolarized (3)He ventilation defects used to predict pulmonary exacerbations in mild to moderate chronic obstructive pulmonary disease. *Radiology* **273**, 887-896 (2014).

283. Haralick, R.M., Shanmugam, K. and Dinstein, I.H. Textural features for image classification. *IEEE Trans. Syst. Man Cybern. Syst.* **SMC-3**, 12 (1973).

284. Sharma, M., *et al.* Quantification of pulmonary functional MRI: state-of-the-art and emerging image processing methods and measurements. *Phys Med Biol* **67**(2022).

285. Zha, N., *et al.* Second-order Texture Measurements of (3)He Ventilation MRI: Proof-of-concept Evaluation of Asthma Bronchodilator Response. *Acad Radiol* **23**, 176-185 (2016).

286. Sharma, M., Westcott, A., McCormack, D. & Parraga, G. *Hyperpolarized gas magnetic resonance imaging texture analysis and machine learning to explain accelerated lung function decline in ex-smokers with and without COPD*, (SPIE, 2021).

287. Sharma, M., Wyszkiewicz, P.V., Matheson, A.M., McCormack, D.G. & Parraga, G. Chest MRI and CT Predictors of 10-Year All-Cause Mortality in COPD. *COPD* **20**, 307-320 (2023).

288. Saam, B.T., *et al.* MR imaging of diffusion of (3)He gas in healthy and diseased lungs. *Magn Reson Med* **44**, 174-179 (2000).

289. Yablonskiy, D.A., *et al.* Quantitative in vivo assessment of lung microstructure at the alveolar level with hyperpolarized 3He diffusion MRI. *Proceedings of the National Academy of Sciences of the United States of America* **99**, 3111-3116 (2002).

290. Salerno, M., *et al.* Emphysema: hyperpolarized helium 3 diffusion MR imaging of the lungs compared with spirometric indexes--initial experience. *Radiology* **222**, 252-260 (2002).

291. Altes, T.A., Mata, J., de Lange, E.E., Brookeman, J.R. & Mugler, J.P., 3rd. Assessment of lung development using hyperpolarized helium-3 diffusion MR imaging. *J Magn Reson Imaging* **24**, 1277-1283 (2006).

292. Yablonskiy, D.A., Sukstanskii, A.L., Quirk, J.D., Woods, J.C. & Conradi, M.S. Probing lung microstructure with hyperpolarized noble gas diffusion MRI: theoretical models and experimental results. *Magn Reson Med* **71**, 486-505 (2014).

293. Wang, C., *et al.* Assessment of the lung microstructure in patients with asthma using hyperpolarized 3He diffusion MRI at two time scales: comparison with healthy subjects and patients with COPD. *J Magn Reson Imaging* **28**, 80-88 (2008).

294. Mathew, L., *et al.* Hyperpolarized (3)He magnetic resonance imaging: preliminary evaluation of phenotyping potential in chronic obstructive pulmonary disease. *Eur J Radiol* **79**, 140-146 (2011).

295. Diaz, S., *et al.* Validity of apparent diffusion coefficient hyperpolarized 3He-MRI using MSCT and pulmonary function tests as references. *Eur J Radiol* **71**, 257-263 (2009).

296. Chen, R.Y., *et al.* Tissue-blood partition coefficient for xenon: temperature and hematocrit dependence. *J Appl Physiol Respir Environ Exerc Physiol* **49**, 178-183 (1980).

297. Kaushik, S.S., *et al.* Measuring diffusion limitation with a perfusion-limited gas--hyperpolarized 129Xe gas-transfer spectroscopy in patients with idiopathic pulmonary fibrosis. *J Appl Physiol* **117**, 577-585 (2014).

298. Kaushik, S.S., *et al.* Single-breath clinical imaging of hyperpolarized (129)Xe in the airspaces, barrier, and red blood cells using an interleaved 3D radial 1-point Dixon acquisition. *Magn Reson Med* **75**, 1434-1443 (2016).

299. Mugler, J.P., 3rd, *et al.* MR imaging and spectroscopy using hyperpolarized 129Xe gas: preliminary human results. *Magn Reson Med* **37**, 809-815 (1997).

300. Wagshul, M.E., *et al.* In vivo MR imaging and spectroscopy using hyperpolarized 129Xe. *Magn Reson Med* **36**, 183-191 (1996).

301. Wang, Z., *et al.* Using hyperpolarized 129Xe gas-exchange MRI to model the regional airspace, membrane, and capillary contributions to diffusing capacity. *J Appl Physiol* **130**, 1398-1409 (2021).

302. Bhatt, S.P., *et al.* Sex Differences in Airways at Chest CT: Results from the COPDGene Cohort. *Radiology*, 212985 (2022).

303. Kooner, H., *et al.* Sex Differences in CT Airway Measurements and Their Relationship to Post-Acute COVID-19 Syndrome. in *D109. THE LONG AND THE SHORT OF LONG COVID* A6791-A6791 (American Thoracic Society, 2023).

304. Borges do Nascimento, I.J., *et al.* Novel Coronavirus Infection (COVID-19) in Humans: A Scoping Review and Meta-Analysis. *J Clin Med* **9**(2020).

305. Chakravarty, D., *et al.* Sex differences in SARS-CoV-2 infection rates and the potential link to prostate cancer. *Commun Biol* **3**, 374 (2020).

306. Sylvester, S.V., *et al.* Sex differences in sequelae from COVID-19 infection and in long COVID syndrome: a review. *Curr Med Res Opin* **38**, 1391-1399 (2022).

307. Bowyer, R.C.E., *et al.* Characterising patterns of COVID-19 and long COVID symptoms: evidence from nine UK longitudinal studies. *Eur J Epidemiol* **38**, 199-210 (2023).

Chapter 2

2 ^{129}XE MRI VENTILATION DEFECTS IN EVER- AND NEVER-HOSPITALIZED PEOPLE WITH POST-ACUTE COVID-19 SYNDROME

To better understand the pulmonary pathophysiology of long-COVID, we evaluated and compared MRI ventilation defects in participants with and without long-COVID, as well as in long-COVID participants who were and were not hospitalized during acute infection.

The contents of this chapter were previously published in the journal BMJ Open Respiratory Research: HK Kooner, MJ McIntosh, AM Matheson, C Venegas, N Radadia, T Ho, E Haider, NB Konyer, GE Santyr, MS Albert, A Ouriadov, M Abdelrazek, M Kirby, I Dhaliwal, JM Nicholson, P Nair, S Svenningsen and G Parraga. ^{129}Xe MRI Ventilation Defects in ever- and never-hospitalised people with post-acute COVID-19 syndrome. BMJ Open Respiratory Research 2022; 9: e001235. doi: 10.1136/bmjresp-2022-001235. This article is available under the terms of the Creative Commons CC BY-NC License.

2.1 Introduction

Long-term symptoms and poor quality-of-life beyond the acute infectious phase of coronavirus disease 2019 (COVID-19) has been reported in a wide range of 14-89% of infected people.[1-5] These patients have been described as having long-COVID,[6] post-acute COVID-19 syndrome (PACS)[7] and post-acute sequelae of COVID-19.[8] It is perhaps not surprising that some COVID-19 patients who were hospitalized to manage severe illness also experience reduced quality-of-life, poor pulmonary function, and pulmonary imaging abnormalities well after the infection is resolved.[4,9,10] However, many patients who experienced milder symptoms and were managed at home also experience long-term symptoms.[11] Regardless, the etiology of long-term symptoms is not yet well understood, which stymies treatment options.

Computed tomography (CT) imaging has provided the mainstay imaging approach for COVID-19 diagnosis and monitoring in the infectious[12] and post-infectious phase.[13-15] While some patients experience complete radiological resolution in the months following COVID-19 infection,[13] CT fibrosis-like changes, ground-glass opacities and interstitial thickening have been reported to persist in 35-72% of patients.[14,15] Until now, quantitative CT analysis of post-

COVID patients has been limited to density metrics;[4,13-15] airway measurements have not yet been examined.

Hyperpolarized noble gas magnetic resonance imaging (MRI) provides a way to quantify the functional consequences of airway obstruction[16,17] via inhaled gas distribution abnormalities or ventilation defects.[18] Previously, single-center ^{129}Xe MRI investigations reported abnormal gas exchange[19] and mildly abnormal ventilation defect percentage[20] in previously hospitalized patients evaluated 14-254 days post-discharge. MRI ventilation defects were previously shown to reflect airway inflammation and remodelling,[16,17,21] relate to dyspnea[22] and disease severity,[23,24] predict the transition of reversible asthma to irreversible chronic obstructive pulmonary disease (COPD),[16,17] and uniquely explain asthma control scores[25] and COPD exacerbations.[26]

Our objective was to evaluate symptomatic ever-COVID patients, including never- and ever-hospitalized participants, who were experiencing post-COVID symptoms months after a positive COVID-19 test. We hypothesized that ventilation defect percent (VDP) would be significantly greater in ever- as compared to never-hospitalized COVID participants and VDP would be significantly related to quality-of-life and symptoms.

2.2 Methods

2.2.1 Participant and Public Involvement

The development of the research question and outcome measures did not involve potential participants. Results for each individual participant were provided to them directly and also provided to a member of their health care team, if requested by the participant. Overall results were disseminated to all study participants at follow-up visits and the manuscript will be shared widely with all participants, once peer-reviewed and accepted for publication.

2.2.2 Study Participants and Design

Participants were enrolled from two clinical research centers (Site 1: Robarts Research Institute, London Canada; Site 2: St Joseph's Healthcare Hamilton, Hamilton Canada) and provided written-informed consent to ethics board (HSREB # 113224, London; HiREB # 12672, Hamilton) and Health Canada approved and published protocols (www.clinicaltrials.gov NCT05014516). Participants were recruited from a local quaternary care post-COVID-19 clinic at Site 1 and through referral from healthcare providers or self-referral through advertising at Site 2. Inclusion criteria for Site 1 consisted of individuals aged 18 to 80 years, a local public health office confirmed (positive-test) case of COVID-19, persistent symptoms up to three-months post infection, including but not limited to respiratory, neurological and metabolic systems, and a clinical diagnosis of PACS. Inclusion criteria for Site 2 consisted of people aged 18 or older who recently (≤12 weeks) recovered from COVID-19 with the date of recovery confirmed in accordance with provincial and local public health unit protocols. All participants in this analysis reported post-COVID symptoms at the time of their research visit.

Never-COVID controls were recruited by local advertisement; research visits were completed during the period June-July 2021, prior to the participant's full vaccination. All never-COVID controls were recruited on the basis of a negative history for chronic cardiorespiratory illness and symptomatic respiratory illness during the period February 2020 up to and including the study visit. A subset of ever- (n=17) and never-COVID (n=6) participants evaluated here were previously evaluated for gas exchange MRI abnormalities.[27]

Ever-COVID participants at both sites completed spirometry, diffusing capacity of the lung for carbon-monoxide (DL_{CO}), ^{1}H and ^{129}Xe ventilation MR and CT imaging in addition to the

St. George's Respiratory Questionnaire (SGRQ),[28] modified Medical Research Council dyspnea scale (mMRC),[29] modified Borg scale,[30] International Physical Activity Questionnaire (IPAQ)[31] and Six-Minute-Walk-Test[32]; ever-COVID participants at Site 1 also completed multi-breath inert gas washout. Never-COVID volunteers were evaluated using vital signs, spirometry, multi-breath inert gas washout and ^{1}H and ^{129}Xe ventilation MRI.

2.2.3 Pulmonary Function Tests and Questionnaires

Participants performed spirometry for the forced expiratory volume in one second (FEV_1) and forced vital capacity (FVC) according to American Thoracic Society guidelines[33] using the EasyOne Pro LAB system (ndd Medical Technologies, Zurich, Switzerland) at Site 1 and using the Elite DX plethysmograph (MedGraphics Corporation, St. Paul, MN, USA) and/or CPFS/D USB Spirometer (MedGraphics Corporation, St. Paul, MN, USA) at Site 2. Multi-breath inert gas washout, also performed using the EasyOne Pro LAB system equipped with an ultrasonic flow and molar mass sensor, measured the lung clearance index (LCI) at Site 1.[34] DL_{CO} was also measured using the EasyOne Pro LAB system at Site 1 and the Elite DX plethysmograph at Site 2, according to European Respiratory Society guidelines.[35] In addition, SGRQ, mMRC, modified Borg scale, IPAQ and Six-Minute-Walk-Test were self-administered under the supervision of study personnel.

2.2.4 Thoracic Imaging

Anatomic ^{1}H and ^{129}Xe static ventilation MRI were acquired at both sites using 3.0 Tesla scanners (Discovery MR750; GE Healthcare, Milwaukee, USA), as previously described.[36] ^{129}Xe ventilation MRI was acquired using a flexible vest coil (Clinical MR Solutions, USA; Site 1) or asymmetric quadrature bird cage coil (custom built; Site 2).[37] Supine participants were coached to inhale a 1.0L bag (Tedlar; Jensen Inert Products, Coral Springs, FL, USA)

(400mL ^{129}Xe + 600mL ^{4}He at Site 1 or 600mL ^{129}Xe + 400mL N_2 at Site 2 and 1.0L N_2 for ^{1}H MRI) from the bottom of a tidal breath (functional residual capacity) with acquisition under breath-hold conditions. ^{129}Xe gas was polarized to 8-40% (Site 1: Xenispin 9820, Site 2: Xenispin 9800; Polarean, Durham, NC, USA).[38]

Within 30 minutes of MRI, CT was acquired as previously described[39] (Site 1: 64-slice LightSpeed VCT system, GE Healthcare, Milwaukee, WI, USA; Site 2: Discovery MI PET/CT scanner, GE Healthcare, Milwaukee, WI, USA).

2.2.5 Image Analysis

Anonymized MRI datasets were transferred from Site 2 to Site 1 for analysis using a cloud-based institutional server and were evaluated in a random order. Quantitative VDP analysis was performed with data anonymized as previously described[40] by a single expert observer (MJM) using a semi-automated segmentation software pipeline[40] generated in Matlab 2019a (Mathworks, Natick, MA, USA). VDP was generated by normalising ventilation defect volume to the ^{1}H MRI thoracic cavity volume, as previously described.[41] Abnormal VDP was defined as the upper limit of normal (95% confidence interval), previously described[42] for ^{3}He MRI; since ^{129}Xe MRI VDP is more sensitive to ventilation abnormalities as compared to ^{3}He MRI VDP,[43] this provides a conservative estimate.

CT images were analysed by a single expert (HKK) using VIDAvision software (VIDA Diagnostics Inc., Coralville, IA, USA) to generate total airway count (TAC).[16] Anatomically equivalent segmental, subsegmental and sub-subsegmental airways for all airway paths (third to fifth generation) were also used to generate airway lumen area, wall area, and wall thickness measurements.[44] CT images were also evaluated by two experienced chest radiologists (MA, Site 1 and EH, Site 2).

2.2.6 Endpoints and Statistical Analysis

The primary endpoints were: 1) ^{129}Xe MRI VDP differences between ever- and never-hospitalized COVID participants, and, 2) ^{129}Xe MRI VDP relationships with quality-of-life and exercise limitation. Secondary endpoints included the relationship for ^{129}Xe MRI VDP with CT airway measurements and with pulmonary function, and differences in quality-of-life and 6MWD in ever-COVID participants with and without abnormal VDP ≥4.3%.[42] An exploratory endpoint was the analysis of VDP in ever-COVID participants with and without a prior history of chronic respiratory illness.

SPSS (SPSS Statistics 25.0; IBM, Armonk, NJ, USA) was used for all statistical analyses. Data were tested for normality using Shapiro-Wilk tests and nonparametric tests were performed when data was not normally distributed. Differences between subgroups were evaluated using independent samples t-tests and analysis of variance. Univariate relationships were evaluated using Pearson (r) correlations for normally distributed variables and Spearman (ρ) correlations for non-normally distributed variables. The Holm-Bonferroni correction was used for multiple comparisons in univariate analyses. Results were considered statistically significant when the probability of making a type I error was less than 5% ($p<0.05$).

2.3 Results

2.3.1 Participants

A CONSORT diagram provided in **Figure 2-1** shows that from August 2020 to September 2021, 93 participants were enrolled (68 from Site 1, 25 from Site 2), including 80 ever-COVID and 13 never-COVID volunteers. Four never-COVID participants were excluded due to inflammatory disease (rheumatoid arthritis, asthma), hypertensive crisis and the detection of a large asymptomatic atrial septal defect.[45] Four COVID participants could not undergo MRI

and were also excluded from the analysis. In total, nine never- (five female, four male; mean age 36±12yr) and 76 ever-COVID participants (38 female, 38 male; mean age 53±12yr) were evaluated. COVID participants were evaluated 13.8±8.5 weeks following a positive COVID-19 test.

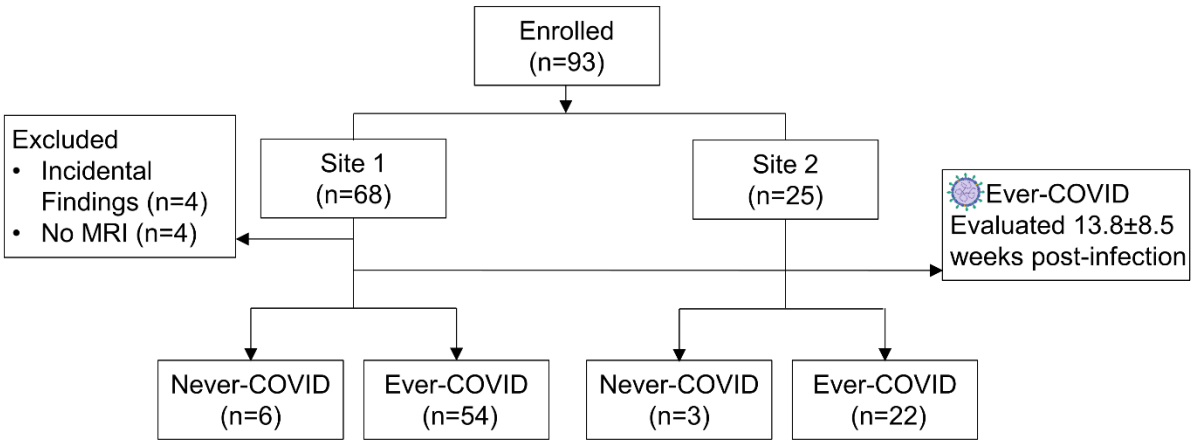

Figure 2-1. Consort Diagram
Of the 93 participants enrolled, 68 participants were enrolled from Site 1 and 25 were enrolled from Site 2. Of the 68 participants enrolled from Site 1, four were excluded due to incidental findings, four were excluded because MRI was not acquired, six were never-COVID participants and 54 were ever-COVID participants. Of the 25 participants enrolled from Site 2, three were never-COVID participants and 22 were ever-COVID participants.

Table 2-1 provides a summary of baseline characteristics for nine never- and 76 ever-COVID participants including 23 (30%) ever- and 53 (70%) never-hospitalized participants. There were significant differences for age ($p<.001$) and sex ($p=.001$) between participant subgroups. Of the 23 hospitalized participants, three required mechanical ventilation, one required non-invasive ventilation and 18 were provided supplemental oxygen during their hospital admission. In the supplement, **Table 2-3** provides baseline demographics by site and shows that the number of weeks between a positive COVID-19 test and the research visit ($p=.01$), as well as SpO_2 ($p=.01$) were significantly different between the two sites. **Table 2-4** provides a by-participant list of current medications and **Table 2-5** provides a summary of these medications.

Table 2-1. Demographic Characteristics

Parameter	Never-COVID (n=9)	All COVID Participants			
		Ever-COVID (n=76)	Ever Hospitalized (n=23)	Never Hospitalized (n=53)	Sig. p
Age years	36 (12)	53 (12)	57 (13)	52 (12)	**<.001**
Female n (%)	5 (56%)	38 (50%)	5 (22%)	33 (62%)	**.001**
BMI kg/m^2	26 (5)	30 (5)	31 (5)	29 (6)	.07
SpO_2 %	97 (2)*	97 (2)	97 (2)	97 (2)	.4
Heart rate beats/min	87 (20)*	77 (13)	82 (14)	76 (12)	.05
Blood pressure mmHg	118/79 (18/12)*	125/81 (14/10)	124/81 (15/11)	124/81 (15/9)	-
Weeks Since + COVID Test [mean/MEDIAN: min-max]	N/A	[13.8/12.0: 5.0-53.4]	[15.2/12.0: 5.0-53.4]	[13.2/12.0: 5.0-39.6]	.3
Smoking history pack-years	0 (0)	8 (18)	10 (21)	8 (16)	.3
No Prior Respiratory Illness n (%)	9 (100%)	49 (64%)	16 (70%)	33 (62%)	.5
Prior Respiratory Illness n (%)	0 (0%)	27 (36%)	7 (30%)	20 (38%)	.5
Asthma n (%)	0 (0%)	21 (26%)	5 (22%)	16 (30%)	.4
COPD n (%)	0 (0%)	6 (8%)	2 (9%)	4 (8%)	.9
Hospital Admission days	N/A	13 (16)	13 (16)	N/A	-

Values are reported as mean (SD) unless otherwise indicated.
BMI=body mass index; COPD=chronic obstructive pulmonary disease.
p=significance value for ANOVA between never-COVID, ever-hospitalized and never-hospitalized.
*n=6

2.3.2 Imaging and Other Endpoints

Figure 2-2 shows representative ^{129}Xe ventilation MRI (cyan) co-registered with anatomical ^{1}H MRI (grey-scale) for three never- and four ever-COVID participants, for which there is also representative coronal CT and segmented airway trees. For never-COVID volunteers, there was visually obvious homogeneous ventilation and VDP was <1% (P77 VDP=0.9%, P78 VDP=0.7%, P79 VDP=0.6%). For ever-COVID participants, there was visually obvious ventilation heterogeneity or defects and yellow arrows point to regions of interest with ventilation or CT abnormalities. In participant P26, there was a large ventilation defect in the right upper lobe that spatially corresponded to a radiodense region visible on CT. In participant P53, there were ventilation defects in the periphery of the upper lobes. In participants P14 and

P02, there were large ventilation defects in the lung periphery. **Table 2-6** shows CT diagnostic findings, for a subset of participants with CT reports completed by a radiologist, including ground-glass opacities (20/50, 40%), atelectasis (14/50, 28%), nodules (13/50, 26%) and bronchiectasis (11/50, 22%).

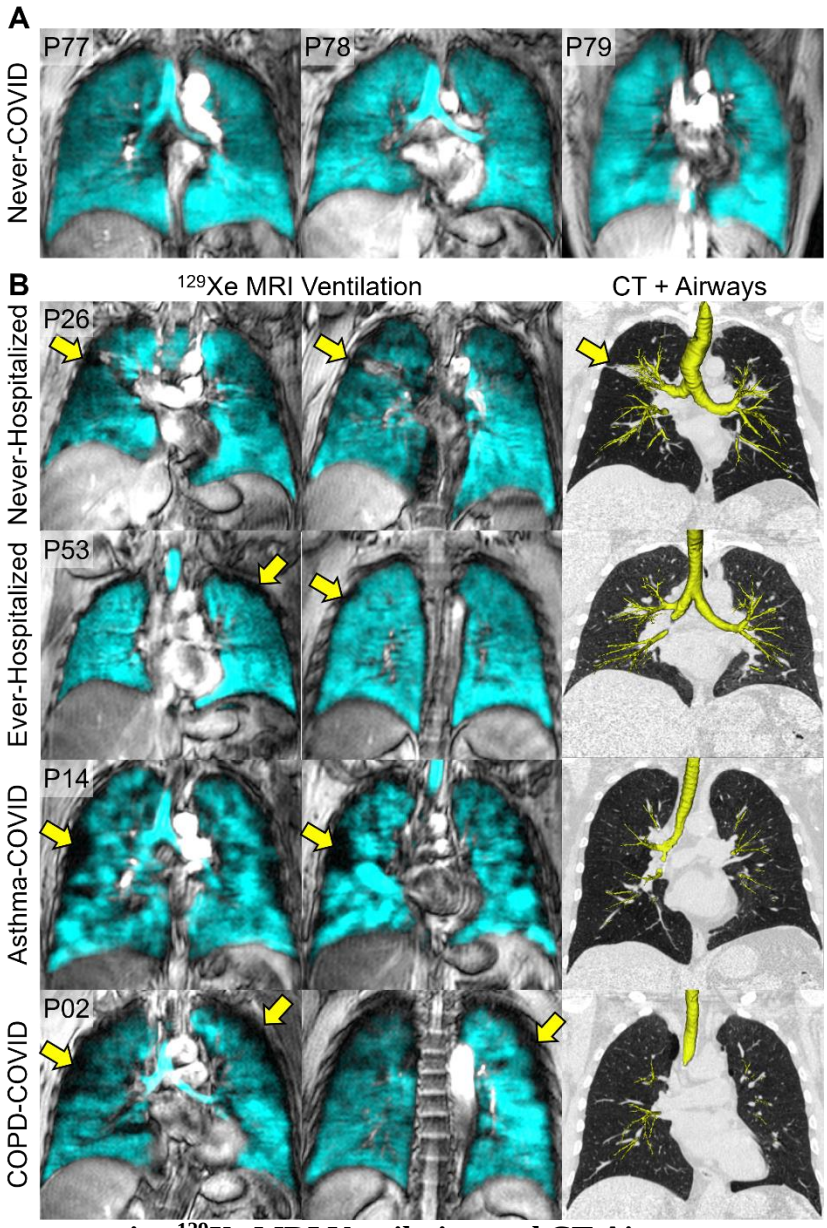

Figure 2-2. Representative ^{129}Xe MRI Ventilation and CT Airways

A. Centre coronal ^{129}Xe MRI slice (cyan) co-registered with ^{1}H MRI thoracic cavity (greyscale) in three never-COVID participants (P77: female, VDP=0.9%; P78: female, VDP=0.7%; P79: female, VDP=0.6%)

B. Two coronal ^{129}Xe MRI slices (cyan) co-registered with ^{1}H MRI thoracic cavity (greyscale) and CT with segmented airway tree in four ever-COVID participants. Yellow arrows point to MRI or CT abnormalities.

P26 was a male with no prior respiratory illness and FEV_1=95%, LCI=8.9, SGRQ=36, mMRC=1, VDP=4.2% and TAC=475.

P53 was a male with no prior respiratory illness and FEV_1=87%, LCI=8.2, SGRQ=51, mMRC=1, VDP=2.8% and TAC=301.

P14 was a female with asthma and never-hospitalized, FEV_1=71%, SGRQ=37, mMRC=0, VDP=17.7% and TAC=289.

P02 was a male with COPD and ever-hospitalized, FEV_1=96%, LCI=8.0, SGRQ=14, mMRC=0, VDP=8.0% and TAC=169.

These qualitative findings are reflected in the quantitative findings shown in **Table 2-2** which summarizes pulmonary function test, imaging, and questionnaire data. **Table 2-7** shows all pulmonary function test, imaging, and questionnaire data by site, whilst **Table 2-8** and **Figure 2-5** show these findings by previously diagnosed asthma and COPD.

As shown in **Table 2-2**, there were significant differences among subgroups for FEV_1 (p=.005), FVC (p=.004), LCI_{ao} (p=.04), DL_{CO} (p=.009), 6MWD (p=.005), post-exertional SpO_2 (p=.03) and ^{129}Xe MRI VDP (p=.03). In addition, mean VDP (≥4.3%),[44] SGRQ (≥6)[46] and LCI/LCI_{ao} (≥7.5)[47] were abnormal in ever-COVID as well as the ever- and never-hospitalized participant subgroups.

Table 2-2. Pulmonary Function, Questionnaire, and Imaging Measurements

Parameter	Never-COVID (n=9)	All COVID Participants			
		Ever-COVID (n=76)	Ever Hospitalized (n=23)	Never Hospitalized (n=53)	Sig. p
Pulmonary function					
FEV_1* $\%_{pred}$	101 (11)	85 (20)	77 (21)	88 (19)	**.005**
FVC* $\%_{pred}$	103 (10)	88 (20)	80 (18)	92 (20)	**.004**
FEV_1/FVC*	0.81 (0.04)	0.76 (0.11)	0.75 (0.14)	0.77 (0.09)	.3
LCI* n breaths	9.0 (1.4)	10.7 (3.9)	11.8 (5.0)	10.1 (3.0)	.2
LCI_{ao}* n breaths	8.0 (1.3)	9.5 (3.3)	11.4 (4.9)	8.6 (1.8)	**.04**
DL_{CO}* $\%_{pred}$	-	89 (29)	75 (23)	95 (29)	**.009**
Exercise capacity and QoL					
6MWD* m	-	454 (84)	405 (86)	471 (76)	**.005**
SpO_2 post-exertion* %	-	97 (3)	95 (5)	98 (2)	**.03**
SGRQ*	-	35 (18)	37 (15)	34 (19)	.6
mMRC*	-	1 (1)	1 (1)	1 (1)	.6
IPAQ* MET-minutes	-	4709 (4895)	3048 (3433)	5327 (5238)	.1
MRI					
VDP %	1.1 (0.9)	5.4 (7.1)	7.8 (11.1)	4.4 (4.2)	**.03**
*CT**					
TAC	-	270 (110)	294 (175)	263 (88)	.5
WA mm^2	-	66 (2)	66 (2)	66 (2)	.4
LA mm^2	-	14 (3)	15 (4)	14 (3)	.5
WT mm	-	1.4 (0.1)	1.4 (0.1)	1.4 (0.1)	.7

Values are reported as mean (SD) unless otherwise indicated.

FEV_1=forced expiratory volume in 1 second; $\%_{pred}$=percent of predicted value; FVC=forced vital capacity; LCI=lung clearance index; ao=airway opening; DL_{CO}=diffusing capacity of the lungs for carbon monoxide; QoL=quality-of-life; 6MWD=six-minute walk distance; SGRQ=St. George's Respiratory Questionnaire; mMRC=modified Medical Research Council dyspnea score; IPAQ=International Physical Activity Questionnaire; MET=metabolic equivalent; MRI=magnetic resonance imaging; VDP=ventilation defect percent; CT=computed tomography; TAC=total airway count; WA=wall area; LA=lumen area; WT=wall thickness.

p=significance value for ANOVA between never-COVID, ever-hospitalized and never-hospitalized.

FEV_1*, FVC*, FEV_1/FVC*: Never-hospitalized n=52

LCI*: Never-COVID n=5, Ever-COVID n=44, Ever-hospitalized n=16, Never-hospitalized n=28

LCI_{ao}*: Never-COVID n=5, Ever-COVID n=32, Ever-hospitalized n=10, Never-hospitalized n=22

DL_{CO}*: Ever-COVID n=64, Ever-hospitalized n=20, Never-hospitalized n=44

6MWD* and mMRC*: Ever-COVID n=66, Ever-hospitalized n=17, Never-hospitalized n=49

SpO_2 post-exertion*: Ever-COVID n=65, Ever-hospitalized n=17, Never-hospitalized n=48

SGRQ*: Ever-COVID n=64, Ever-hospitalized n=16, Never-hospitalized n=48

IPAQ*: Ever-COVID n=59, Ever-hospitalized n=16, Never-hospitalized n=43

CT*: Ever-COVID n=56 with 44 amenable to quantitative analysis, Ever-hospitalized n=9, Never-hospitalized n=35

Box and whisker plots in **Figure 2-3** show that ^{129}Xe MRI VDP was significantly greater in ever- as compared to never-COVID ($p<.001$), and in ever-hospitalized as compared to never-COVID ($p=.01$) participants and was not significantly different between never-hospitalized as compared to never-COVID participants ($p=.2$). ^{129}Xe MRI VDP was also significantly worse in ever- versus never-hospitalized COVID participants ($p=.048$). There were also significant differences for DL_{CO} ($p=.009$) and 6MWD ($p=.005$) between ever- and never-hospitalized COVID participants. **Figure 2-5** shows that ^{129}Xe MRI VDP was significantly worse in participants with prior COPD as compared to COVID patients with prior asthma ($p=.002$) and those with no prior respiratory diagnosis ($p<.001$). The 6MWD was also significantly worse ($p=.02$) in participants with prior COPD as compared to those with no prior respiratory diagnosis. Participants were dichotomized by VDP (normal VDP <4.3%, total n=49, hospitalized n=15; abnormal VDP ≥4.3%, total n=27, hospitalized n=8). As shown in **Figure 2-6**, participants with abnormal VDP also had significantly worse 6MWD ($p=.003$) and post-exertional SpO_2 ($p=.03$).

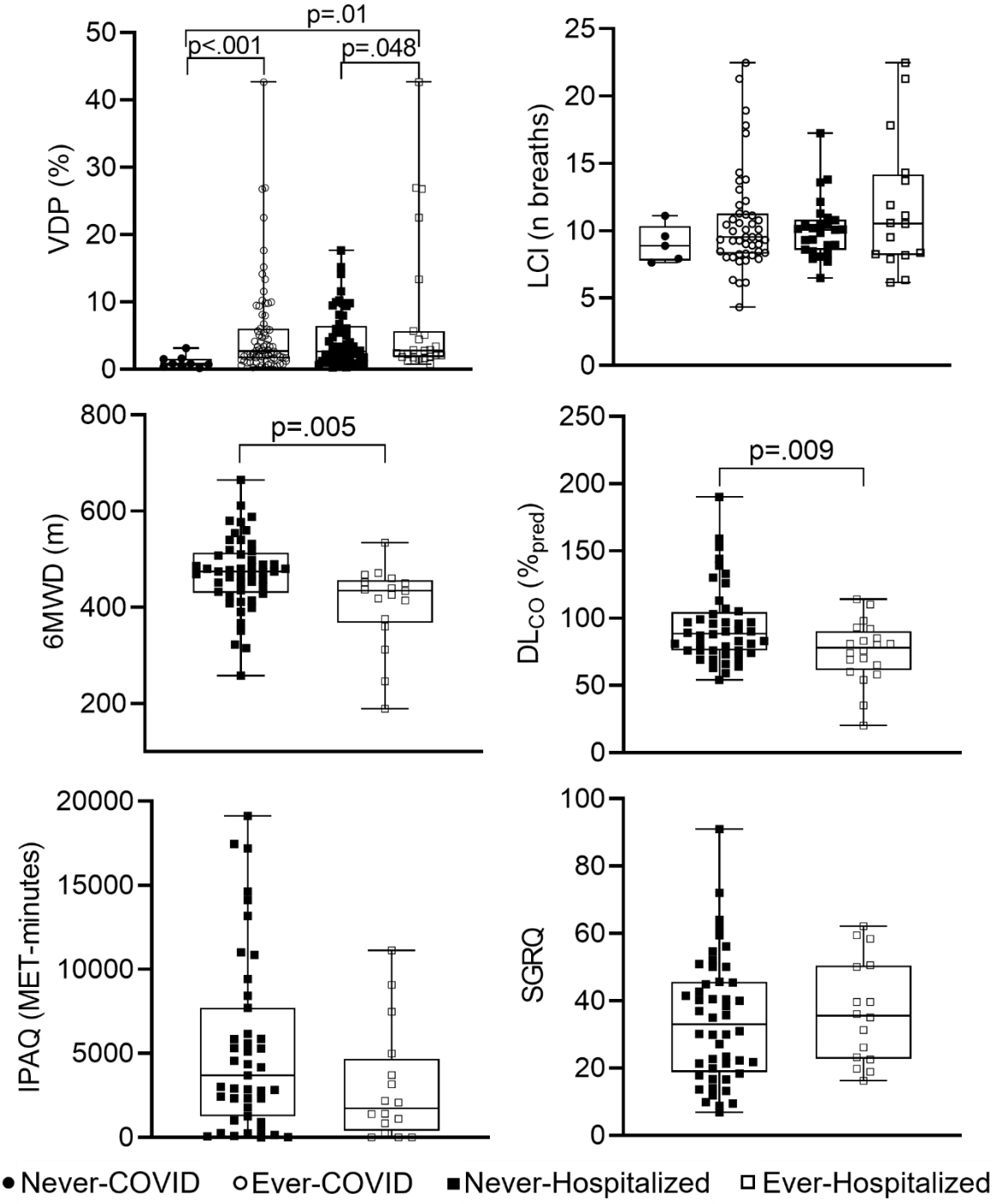

Figure 2-3. ^{129}Xe MRI VDP, pulmonary function, exercise capacity, and quality-of-life
VDP was significantly different for ever-COVID vs. never-COVID (p<.001), and ever-hospitalized vs. never-hospitalized (p=.048) and never-COVID (p=.01). 6MWD was significantly different for ever-hospitalized vs. never-hospitalized (p=.005). DL_{CO} was significantly different for ever-hospitalized vs. never-hospitalized (p=.009). LCI, IPAQ and SGRQ were not significantly different.

2.3.3 Relationships

Figure 2-4 shows linear relationships for imaging and pulmonary function measurements. For completeness and transparency, **Table 2-9** provides the Pearson or Spearman correlations for all parameters measured. As shown in Figure 4, there were significant relationships for VDP with 6MWD (ρ=-.31; p=.02) and post-exertional SpO_2 (ρ=-.43; p=.002) and for post-exertional SpO_2 with LCI (ρ=-.49; p=.01). CT measurement relationships included TAC with FEV_1/FVC (ρ=.30, p=.03), CT wall thickness with FEV_1 (r=.30, p=.046) and CT wall area with FEV_1/FVC (ρ=-.35, p=.04).

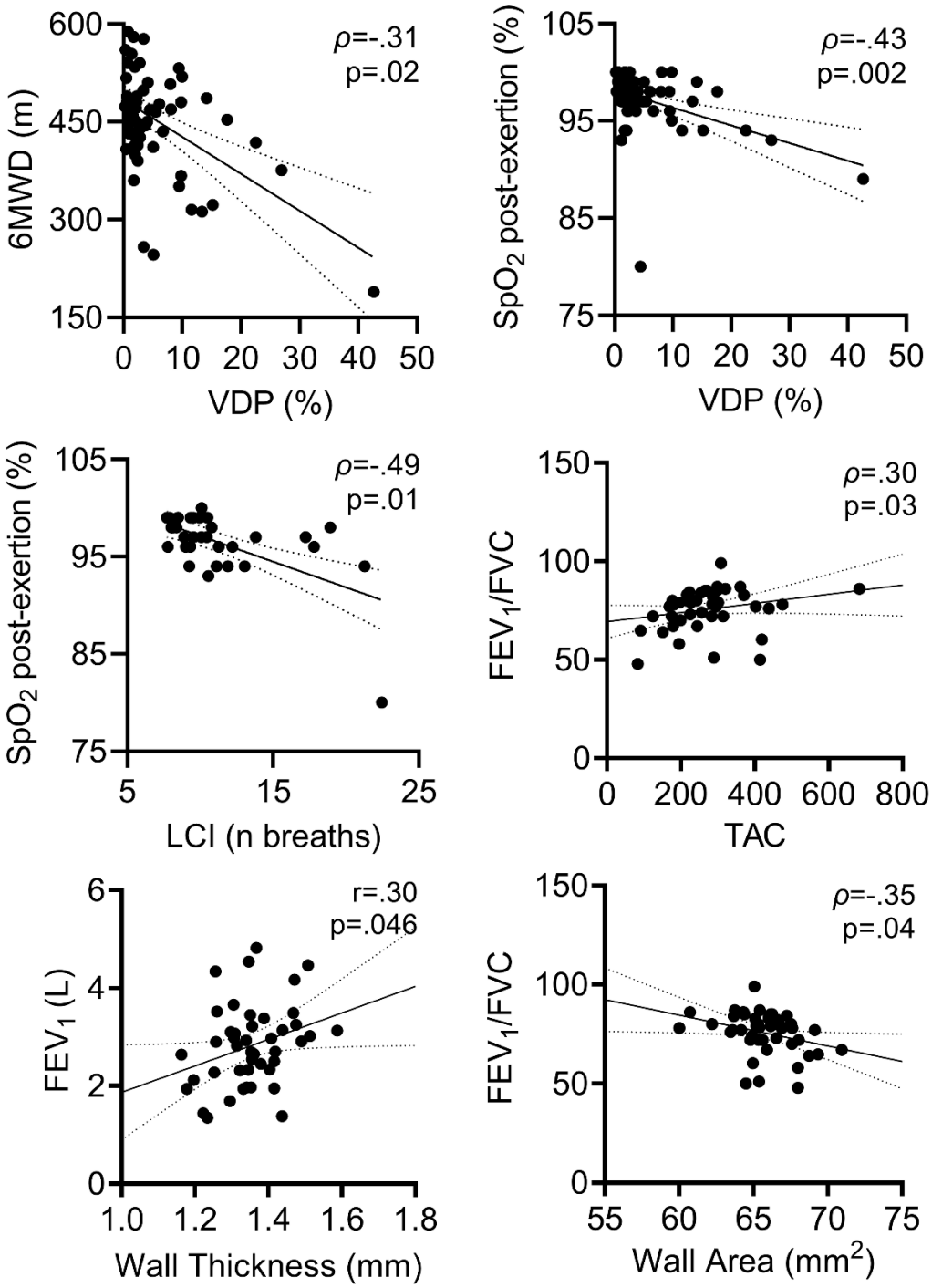

Figure 2-4. Relationships for MRI and CT Measurements
Linear correlation for VDP and 6MWD (ρ=-.31, p=.02).
Linear correlation for VDP and SpO_2 post-exertion (ρ=-.43, p=.002).
Linear correlation for LCI and SpO_2 post-exertion (ρ=-.49, p=.01).
Linear correlation for TAC and FEV_1/FVC (ρ=.30; p=.03).
Linear correlation for wall thickness and FEV_1 (r=.30; p=.046).
Linear correlation for wall area and FEV_1/FVC (ρ=-.35; p=.04).

2.4 Discussion

To our knowledge, this is the first multi-centre study that explores ventilation heterogeneity in ever- and never-hospitalized post-COVID-19 participants with persistent and serious symptoms necessitating clinical follow-up. In 76 participants, we observed: 1) significantly different (worse) MRI VDP in ever- as compared to never-COVID, and in never-hospitalized as compared to ever-hospitalized COVID participants, who also experienced significantly different (worse) DL_{CO} and 6MWD, 2) significant relationships between CT airway and spirometry measurements, and, 3) significant relationships between post-exertional SpO_2 with two measurements of ventilation heterogeneity, MRI VDP and LCI, and between MRI VDP and the 6MWD.

First, we observed that MRI VDP was significantly different in ever-COVID as compared to never-COVID participants and mean VDP in ever-COVID patients was consistent with previously reported values[20] in asymptomatic ever-hospitalized patients, post-discharge. The finding of significantly different MRI VDP in ever- as compared to never-hospitalized participants was novel as was the coincident finding of significantly different 6MWD and post-exertional SpO_2 in these participants. Previous studies have observed worse 6MWD in severe versus mild-moderate post-COVID patients,[48-50] however, the classification for mild, moderate or severe infection was not based on prior hospitalization and not all participants experienced ongoing COVID-19 symptoms. When dichotomized by VDP, 6MWD and post-exertional SpO_2 were also significantly different between groups. The link between exercise limitation, post-exertional oxygen saturation and ventilation heterogeneity in PACS is novel and points to a mechanistic relationship between persistent symptoms and airway pathologies and/or occlusion/obliteration.

Underscoring these central results was the finding of significant relationships for post-6MWD SpO_2 with MRI VDP and with LCI – both are measurements of ventilation heterogeneity that are thought to reflect airway inhalational (MRI) and exhalational (LCI) function. This is the first supportive evidence of a potential link between exercise intolerance following COVID-19 and objective (LCI and MRI VDP) and direct (MRI VDP) measurements of abnormal airway function. This evidence was also supported by the significant associations between CT findings including total airway count (reflecting airway narrowing or obliteration/occlusion), airway lumen area (narrowing or occlusion) and airway wall thickness with spirometry measurements of airflow obstruction. Recent studies have provided evidence of small airways disease in post-COVID-19 patients using the full-scale airway network flow model[51] or CT air-trapping functional small airways disease.[52] We did not acquire inspiratory-expiratory CT and thus could not quantify CT air-trapping, although the ratio of residual volume to total lung capacity (RV/TLC) was measured in 38 of our 76 participants and of these, 14 (37%) reported RV/TLC > upper limit of normal.[53] In addition, the median RV/TLC value in these 38 participants was 0.41±0.17, suggesting air-trapping, and this value was greater than the evaluation group reported by Cho et al. (median RV/TLC=0.30).[52] Taken together, these findings support the use of airways disease treatments, including inhaled combination corticosteroid-long-acting beta agonist, in post-COVID patients with persistent symptoms.

We acknowledge a number of limitations in this convenience-sample study, including the relatively small sample size. We should note that Site 1 participants were monitored over time by a long-COVID clinic designed to follow and treat long-term symptoms, including dyspnea, and this clinic referred participants to consider enrolling in the study. Hence, there is a potential for bias towards a greater number and intensity of unexplained symptoms for participants

enrolled. In addition, for most of the never-hospitalized participants enrolled, there was no prior clinical history of respiratory disease and thus first-time chest imaging and pulmonary function test results were reported. Therefore, we had to untangle any previous clinical history from the impact of COVID-19 on symptoms. Furthermore, pulmonary function tests, as well as CT and MR imaging measurements, prior to COVID-19 infection were not available, and thus, the impact of COVID-19 on existing lung function is still not completely clear. For a relatively large number of ever-COVID participants, chest CT was either declined (n=18) or not quantitatively evaluable (n=13) which also limits the generalizability of the CT results. It is also important to acknowledge that this was a multi-centre study, with participants enrolled from two relatively diverse regional healthcare systems embedded within a population of 14.7 million people served by a single universal and comprehensive health-care insurance plan. Site 1 enrollment derived from a quaternary care academic health centre serving a mainly rural population and Site 2 enrollment derived from another quaternary care academic health centre, located about 100km away from Site 1 with a mainly urban population, hence our findings may not be generalizable to other health-care jurisdictions. Moreover, we also recognise that the convenience study group we evaluated included a relatively large number of people with previously diagnosed asthma (n=21) and COPD (n=6), which is a greater proportion of patients with co-morbid obstructive lung disease than previous reports.[2-5,19,20] We expect that the presence of previous obstructive lung disease likely has complex interactions with post-COVID pulmonary measurements including MRI VDP. Importantly, there were no significant differences for SGRQ and IPAQ scores between participants with and without a previous diagnosis of obstructive lung disease, which underscores the severity of illness in PACS. Finally, as previously reported,[54] older people are at greater risk for poor COVID outcomes

and there is also a complex relationship between age and MRI VDP,[55] so age must be considered as an important factor in our results. It should also be noted that the ever-COVID group was significantly older compared to never-COVID and hence this may have influenced VDP measurements in this group. However, MRI VDP was still greater in the ever-COVID group than predicted based on age alone.[56]

In conclusion, we explored a potential role for MRI and CT pulmonary pathologies to help explain persistent and life-altering symptoms including exercise limitation in post-COVID patients. Whilst mean SGRQ score was not normal in the PACS participants studied here, spirometry, DL_{CO} and CT measurements were normal or nearly normal. This provides some context to the growing body of evidence that shows MRI VDP provides a sensitive measurement of abnormal physiology that, in the PACS participants studied here, may contribute to exercise limitation.

In this study, participants were unable to achieve pre-COVID work and day-to-day life activities, so we asked the question, is there an airways component to PACS that can be measured using MRI VDP and does this relate to quality-of-life? Yes, this exploratory study did point to a relationship between the lung pathologies that resulted in abnormal MRI VDP (or ventilation heterogeneity) as well as exercise limitation and abnormal post-exertional SpO_2. SGRQ and IPAQ scores also were highly abnormal and very similar among ever-COVID participants. The study results point to a possible airways disease explanation for the persistent symptoms experienced following COVID-19 infection, which may help improve and target treatment.

2.5 References

1. Jennings, G., Monaghan, A., Xue, F., Mockler, D. & Romero-Ortuno, R. A Systematic Review of Persistent Symptoms and Residual Abnormal Functioning following Acute COVID-19: Ongoing Symptomatic Phase vs. Post-COVID-19 Syndrome. *J Clin Med* **10**, 5913 (2021).

2. Chopra, V., Flanders, S.A., O'Malley, M., Malani, A.N. & Prescott, H.C. Sixty-Day Outcomes Among Patients Hospitalized With COVID-19. *Ann Intern Med* **174**, 576-578 (2021).

3. Shah, A.S., *et al.* A prospective study of 12-week respiratory outcomes in COVID-19-related hospitalisations. *Thorax* **76**, 402-404 (2021).

4. Huang, C., *et al.* 6-month consequences of COVID-19 in patients discharged from hospital: a cohort study. *Lancet* **397**, 220-232 (2021).

5. Mandal, S., *et al.* 'Long-COVID': a cross-sectional study of persisting symptoms, biomarker and imaging abnormalities following hospitalisation for COVID-19. *Thorax* **76**, 396-398 (2021).

6. National Institute of Health and Care Excellence. COVID-19 Rapid Guideline: Managing COVID-19. (NICE, 2021).

7. Nalbandian, A., *et al.* Post-acute COVID-19 syndrome. *Nat Med* **27**, 601-615 (2021).

8. Al-Aly, Z., Xie, Y. & Bowe, B. High-dimensional characterization of post-acute sequelae of COVID-19. *Nature* **594**, 259-264 (2021).

9. Arnold, D.T., *et al.* Patient outcomes after hospitalisation with COVID-19 and implications for follow-up: results from a prospective UK cohort. *Thorax* **76**, 399-401 (2021).

10. Halpin, S.J., *et al.* Postdischarge symptoms and rehabilitation needs in survivors of COVID-19 infection: A cross-sectional evaluation. *J Med Virol* **93**, 1013-1022 (2021).

11. Bliddal, S., *et al.* Acute and persistent symptoms in non-hospitalized PCR-confirmed COVID-19 patients. *Sci Rep* **11**, 13153 (2021).

12. Xiong, Y., *et al.* Clinical and High-Resolution CT Features of the COVID-19 Infection: Comparison of the Initial and Follow-up Changes. *Invest Radiol* **55**, 332-339 (2020).

13. Liu, M., Lv, F., Huang, Y. & Xiao, K. Follow-Up Study of the Chest CT Characteristics of COVID-19 Survivors Seven Months After Recovery. *Front Med (Lausanne)* **8**, 636298 (2021).

14. Caruso, D., *et al.* Post-Acute Sequelae of COVID-19 Pneumonia: Six-month Chest CT Follow-up. *Radiology* **301**, E396-E405 (2021).

15. Han, X., *et al.* Six-month Follow-up Chest CT Findings after Severe COVID-19 Pneumonia. *Radiology* **299**, E177-E186 (2021).

16. Eddy, R.L., *et al.* Is Computed Tomography Airway Count Related to Asthma Severity and Airway Structure and Function? *Am J Respir Crit Care Med* **201**, 923-933 (2020).

17. Eddy, R.L., Westcott, A., Maksym, G.N., Parraga, G. & Dandurand, R.J. Oscillometry and pulmonary magnetic resonance imaging in asthma and COPD. *Physiol Rep* **7**, e13955 (2019).

18. Kauczor, H.U., *et al.* Normal and abnormal pulmonary ventilation: Visualization at hyperpolarized He-3 MR imaging. *Radiology* **201**, 564-568 (1996).

19. Grist, J.T., *et al.* Hyperpolarized (129)Xe MRI Abnormalities in Dyspneic Patients 3 Months after COVID-19 Pneumonia: Preliminary Results. *Radiology* **301**, E353-E360 (2021).

20. Li, H., *et al.* Damaged lung gas exchange function of discharged COVID-19 patients detected by hyperpolarized (129)Xe MRI. *Sci Adv* **7**(2021).

21. Svenningsen, S., *et al.* Sputum Eosinophilia and Magnetic Resonance Imaging Ventilation Heterogeneity in Severe Asthma. *Am J Respir Crit Care Med* **197**, 876-884 (2018).

22. Costella, S., *et al.* Regional pulmonary response to a methacholine challenge using hyperpolarized (3)He magnetic resonance imaging. *Respirol* **17**, 1237-1246 (2012).

23. de Lange, E.E., *et al.* Evaluation of asthma with hyperpolarized helium-3 MRI: correlation with clinical severity and spirometry. *Chest* **130**, 1055-1062 (2006).

24. Mummy, D.G., *et al.* Ventilation defect percent in helium-3 magnetic resonance imaging as a biomarker of severe outcomes in asthma. *J Allergy Clin Immunol* **141**, 1140-1141 e1144 (2018).

25. Svenningsen, S., Nair, P., Guo, F., McCormack, D.G. & Parraga, G. Is ventilation heterogeneity related to asthma control? *Eur Respir J* **48**, 370-379 (2016).

26. Kirby, M., Kanhere, N., Etemad-Rezai, R., McCormack, D.G. & Parraga, G. Hyperpolarized helium-3 magnetic resonance imaging of chronic obstructive pulmonary disease exacerbation. *J Magn Reson Imaging* **37**, 1223-1227 (2013).

27. Matheson, A.M., *et al.* Persistent (129)Xe MRI Pulmonary and CT Vascular Abnormalities in Symptomatic Individuals with Post-Acute COVID-19 Syndrome. *Radiology*, 220492 (2022).

28. Jones, P.W., Quirk, F.H., Baveystock, C.M. & Littlejohns, P. A self-complete measure of health status for chronic airflow limitation. The St. George's Respiratory Questionnaire. *Am Rev Respir Dis* **145**, 1321-1327 (1992).

29. Mahler, D.A., *et al.* Development of self-administered versions of modified baseline and transition dyspnea indexes in COPD. *COPD* **1**, 165-172 (2004).

30. Borg, G.A. Psychophysical bases of perceived exertion. *Med Sci Sports Exerc* **14**, 377-381 (1982).

31. Craig, C.L., *et al.* International physical activity questionnaire: 12-country reliability and validity. *Med Sci Sports Exerc* **35**, 1381-1395 (2003).

32. Enright, P.L. The six-minute walk test. *Respir Care* **48**, 783-785 (2003).

33. Miller, M.R., *et al.* Standardisation of spirometry. *Eur Respir J* **26**, 319-338 (2005).

34. Robinson, P.D., *et al.* Consensus statement for inert gas washout measurement using multiple- and single- breath tests. *Eur Respir J* **41**, 507-522 (2013).

35. Macintyre, N., *et al.* Standardisation of the single-breath determination of carbon monoxide uptake in the lung. *Eur Respir J* **26**, 720-735 (2005).

36. Kirby, M., *et al.* Hyperpolarized 3He and 129Xe MR imaging in healthy volunteers and patients with chronic obstructive pulmonary disease. *Radiology* **265**, 600-610 (2012).

37. Farag, A., Wang, J., Ouriadov, A., Parraga, G. & Santyr, G. Unshielded and Asymmetric RF Transmit Coil for Hyperpolarized 129Xe Human Lung Imaging at 3.0 T. *Proc Intl Soc Mag Reson Med* **20**, 1233 (2012).

38. Walker, T.G. & Happer, W. Spin-exchange optical pumping of noble-gas nuclei. *Rev Mod Phys* **69**, 629-642 (1997).

39. Kirby, M., *et al.* Longitudinal Computed Tomography and Magnetic Resonance Imaging of COPD: Thoracic Imaging Network of Canada (TINCan) Study Objectives. *Chronic Obstr Pulm Dis* **1**, 200-211 (2014).

40. Kirby, M., *et al.* Hyperpolarized 3He magnetic resonance functional imaging semiautomated segmentation. *Acad Radiol* **19**, 141-152 (2012).

41. Kirby, M., Wheatley, A., McCormack, D.G. & Parraga, G. Development and application of methods to quantify spatial and temporal hyperpolarized He-3 MRI ventilation dynamics: Preliminary results in chronic obstructive pulmonary disease. *Proc. SPIE* **7626**, 762605 (2010).

42. Pike, D., Kirby, M., Guo, F., McCormack, D.G. & Parraga, G. Ventilation heterogeneity in ex-smokers without airflow limitation. *Acad Radiol* **22**, 1068-1078 (2015).

43. Svenningsen, S., *et al.* Hyperpolarized (3) He and (129) Xe MRI: differences in asthma before bronchodilation. *J Magn Reson Imaging* **38**, 1521-1530 (2013).

44. Niimi, A., *et al.* Airway wall thickness in asthma assessed by computed tomography. Relation to clinical indices. *Am J Respir Crit Care Med* **162**, 1518-1523 (2000).

45. Matheson, A.M., *et al.* Hyperpolarized ^{129}Xe pulmonary MRI and asymptomatic atrial septal defect. *Chest* **161**, e198-e201 (2022).

46. Ferrer, M., *et al.* Interpretation of quality of life scores from the St George's Respiratory Questionnaire. *Eur Respir J* **19**, 405-413 (2002).

47. Horsley, A.R., *et al.* Lung clearance index is a sensitive, repeatable and practical measure of airways disease in adults with cystic fibrosis. *Thorax* **63**, 135-140 (2008).

48. Anastasio, F., *et al.* Medium-term impact of COVID-19 on pulmonary function, functional capacity and quality of life. *Eur Respir J* **58**, 2004015 (2021).

49. Guler, S.A., *et al.* Pulmonary function and radiological features 4 months after COVID-19: first results from the national prospective observational Swiss COVID-19 lung study. *Eur Respir J* **57**, 2003690 (2021).

50. Wong, A.W., *et al.* Predictors of reduced 6-minute walk distance after COVID-19: a cohort study in Mexico. *Pulmonology* **27**, 563-565 (2021).

51. Inui, S., Yoon, S.H., Doganay, O., Gleeson, F.V. & Kim, M. Impaired pulmonary ventilation beyond pneumonia in COVID-19: A preliminary observation. *PloS one* **17**, e0263158 (2022).

52. Cho, J.L., *et al.* Quantitative Chest CT Assessment of Small Airways Disease in Post-Acute SARS-CoV-2 Infection. *Radiology*, 212170 (2022).

53. Quanjer, P.H., *et al.* Lung volumes and forced ventilatory flows. *Eur Respir J* **6 Suppl 16**, 5-40 (1993).

54. Yanez, N.D., Weiss, N.S., Romand, J.A. & Treggiari, M.M. COVID-19 mortality risk for older men and women. *BMC public health* **20**, 1742 (2020).

55. Parraga, G., Mathew, L., Etemad-Rezai, R., McCormack, D.G. & Santyr, G.E. Hyperpolarized 3He magnetic resonance imaging of ventilation defects in healthy elderly volunteers: initial findings at 3.0 Tesla. *Acad Radiol* **15**, 776-785 (2008).

56. Sheikh, K., *et al.* Pulmonary ventilation defects in older never-smokers. *J Appl Physiol* **117**, 297-306 (2014).

2.6 Supplement

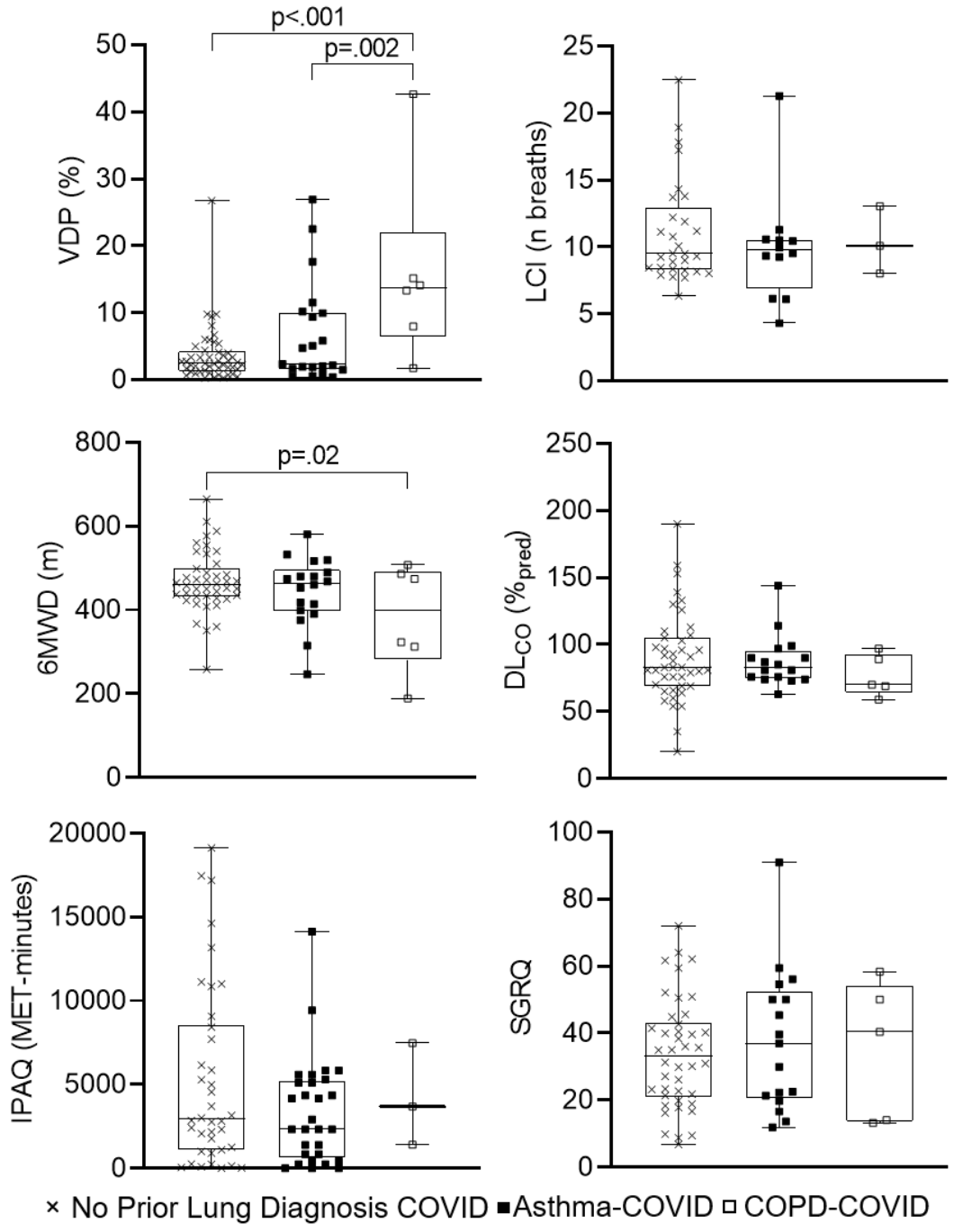

Figure 2-5. ^{129}Xe MRI VDP, pulmonary function, exercise capacity, and quality-of-life by prior respiratory illness
VDP was significantly different for COPD-COVID vs. no prior lung diagnosis COVID (p<.001) and asthma-COVID (p=.002). 6MWD was significantly different for no prior lung diagnosis COVID vs. COPD-COVID (p=.02). LCI, DL_{CO}, IPAQ and SGRQ were not significantly different between groups.

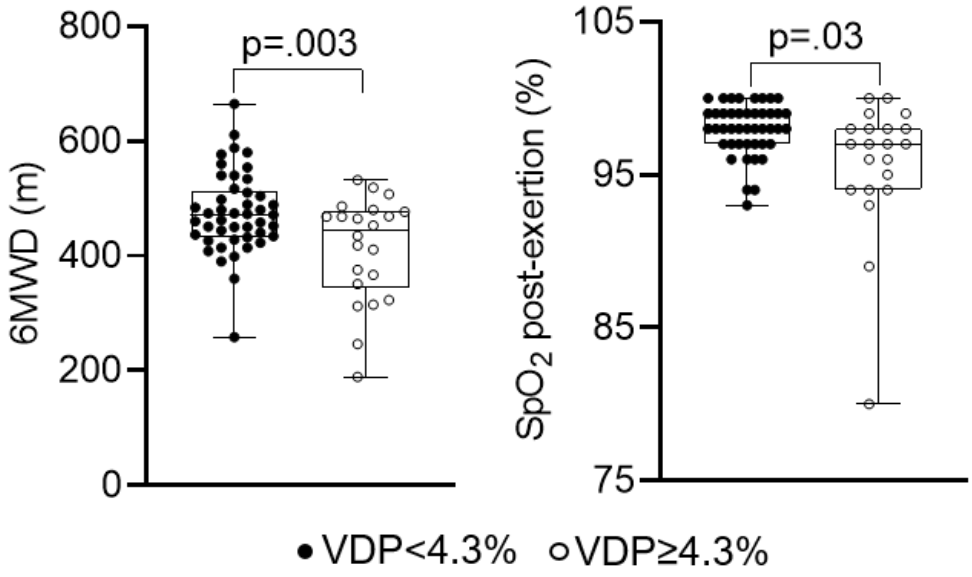

Figure 2-6. Abnormal VDP Subgroups
6MWD was significantly worse in VDP≥4.3% than VDP<4.3% (p=.003)
SpO_2 post-exertion was significantly worse in VDP≥4.3% than VDP<4.3% (p=.03)

Table 2-3. Demographic Characteristics by Site

Parameter mean (SD) [mean/MEDIAN: min-max]	Never-COVID (n=9)			Ever-COVID (n=76)		
	Site 1 (n=6)	Site 2 (n=3)	Sig. p	Site 1 (n=54)	Site 2 (n=22)	Sig. p
Age years	35 (14)	37 (6)	.8	54 (13)	50 (11)	.2
Female n (%)	3 (50)	2 (67)	.6	27 (50)	11 (50)	.9
BMI kg/m^2	25 (3)	28 (9)	.8	30 (5)	29 (6)	.2
SpO_2 %	97 (2)	ND	-	97 (2)	98 (2)	**.01**
Heart rate beats/min	87 (20)	ND	-	77 (13)	78 (14)	1.0
Blood pressure mmHg	119/18 (79/12)	ND	-	124/83 (13/10)	126/79 (16/10)	-
Weeks Since + COVID Test	N/A	N/A	-	[15/12: 5-53]	[10/9: 5-18]	**.01**
Smoking history pack-years	0 (0)	0 (0)	1.0	7 (15)	11 (23)	.4
No Prior Respiratory Illness n (%)	0 (0)	0 (0)	1.0	35 (65)	15 (64)	.9
Prior Respiratory Illness n (%)	0 (0)	0 (0)	1.0	19 (35)	8 (36)	.9
Asthma n (%)	0 (0)	0 (0)	1.0	15 (28)	6 (27)	1.0
COPD n (%)	0 (0)	0 (0)	1.0	4 (7)	2 (9)	.8
Ever-hospitalized n (%)	N/A	N/A	-	18 (33)	5 (23)	.4
Hospital Admission days	N/A	N/A	-	14 (18)	9 (4)	.5

BMI=body mass index; ND=not done; COPD=chronic obstructive pulmonary disease. p=significance value between Site 1 and Site 2.

Table 2-4. Patient Listing of Medications at Research Visit

Participant	Medications
P01	Symbicort; Salbutamol; Spiriva; Fluticasone; Warfarin; Rosuvastatin; Metoprolol; Spironolactone; Dapagliflozin/Metformin; Sitagliptin; Lorazepam
P02	None
P03	Indapamide; Gliclazide; Empagliflozin; Atorvastatin; Metformin; Sitagliptin; Tamsulosin; Ranitidine; Levothyroxine; Bisoprolol
P04	Insulin; Pregabalin; Gliclazide; Perindopril; Rosuvastatin; Sitagliptin/Metformin; Empagliflozin; Ezetimibe
P05	Formoterol-mometasone
P06	Pantoprazole; Apixaban
P07	Levothyroxine
P08	Levothyroxine; Symbicort; Trimethoprim and sulfamethoxazole
P09	Symbicort; Amitriptyline; Naproxen; Pregabalin; Rosuvastatin; Sertraline
P10	Salbutamol
P11	Olanzapine; Fluoxetine; Quetiapine; Salbutamol
P12	Symbicort
P13	None
P14	Fluticasone propionate-salmeterol; Salbutamol; Desvenlafaxine; Pantoprazole; Aripiprazole
P15	None
P16	Symbicort; Atenolol; Hydrochlorothiazide; Candesartan
P17	Metformin; Rosuvastatin; Amlodipine; Ramipril; Hydrochlorothiazide
P18	Metformin; Irbesartan; Esomeprazole; Tramadol; Azythromycin; Dexamethasone
P19	Rivarokaban; Levothyroxine; Oral Contraceptive
P20	Symbicort; Singulair; Tresiba; Jardiance; Ezetrol; Insulin; Rivaroxaban; Glumetza; Pravastatin; Colchicine; Pantaprazole
P21	Pregabalin
P22	Perindopril; Pantoprazole; Rosuvastatin; Spiriva; Ezetimibe; Amlodipine; Bimatropost; Salbutamol; Epipen
P23	Metformin; Symbicort
P24	None
P25	None
P26	Gabapentin; Canagiflozin; Levothyroxine; Saxagliptin; Dexlansoprazole; Rosuvastatin; Metformin; Symbicort
P27	Ustekinumab; Symbicort; Salbutamol
P28	Nabilone; Venlafaxine; Ferrous Gluconate; Dexlansoprazole; Rosuvastatin; Levothyroxine; Gabapentin
P29	Trazodone; Bupropion
P30	Symbicort
P31	None
P32	Cetirizine; Trazadone; Rizatriptan; Betahistine
P33	Fluticasone propionate-salmeterol; Salbutamol; Statin; Diuretic
P34	Sitagliptin; Gliclazide; Ramipril; Atrovastatin; Symbicort
P35	Anti-hypertension; Symbicort
P36	Furosemide; Ciclesonide; Lorazepam; Tamsulosin; Lamotrigine; Spiriva Respimat; Atorvastatin; Symbicort; Ferrous Gluconate; Apixaban; Flecainide; Salbutamol
P37	Triptans
P38	None
P39	Symbicort
P40	None

P41	Symbicort; Ipratropium bromide; Beclomethasone Nasal Spray
P42	Symbicort; Perindopril; Amlodiprine
P43	Symbicort
P44	Methylphenidate
P45	Furosemide; Ferrous fumurate; Candesartan; Rivaroxaban; Levothyroxine
P46	Tansulosin; Bisoprolol; Ferrous fumurate; Apixaban; Rosuvastatin; Amlodipine; Finasteride; Fluticasone
P47	Bupropion
P48	None
P49	Amitryptyline
P50	None
P51	Bupropion
P52	Formoterol-mometasone; Montelukast; Spiriva; Pantoprazole
P53	Formoterol-mometasone; Salbutamol
P54	None
P55	Losartan, Clortalidone
P56	Risedronic acid
P57	Candesartan, Rosuvastatin, Metformin
P58	Gabapentin, Amitriptyline, Clonazepam, Progesterone, Estradiol
P59	Methylphenidate, Vortioxetine
P60	None
P61	Spiriva, Symbicort
P62	None
P63	Gliclazide, Duloxetine, Advair, Semaglutide, Ipratropium bromide, Salbutamol, Pantoprazole, Ciclesonide, Spiriva, Atorvastatin, Metformin, Acetaminophen-codeine-caffeine
P64	Conjugated estrogens, Oxybutynin, Pantoprazole, Vortioxetine
P65	Perindopril
P66	Salbutamol
P67	Bisoprolol, Bupropion, Metoclopramide
P68	Fluticasone furoate, Salbutamol, Carbamazepine
P69	Formoterol-mometasone, Ferrous fumurate
P70	Rupatadine, Mometasone, Montelukast, Oral Contraceptive
P71	Fluticasone propionate
P72	Telmisartan, Bisoprolol, Thyroxine, Pantoprazole
P73	Metoprolol, Ramipril, Amlodipine, Metformin, Sitagliptin, Gliclazide, Rosuvastatin
P74	Levothyroxine, Rabeprazole, Beclometasone, Tiotropium, Salbutamol
P75	Ramipril, Budesonide, Lansoprazole, Symbicort, Rosuvastatin, Bisoprolol, Spiriva
P76	Fluticasone salmeterol, Spiriva, Fluticasone propionate, Benralizumab

Table 2-5. Summary of Medications at Research Visit

Parameter n (%)	Ever-COVID (n=76)	Ever-hospitalized (n=23)	Never-hospitalized (n=53)
None	13 (17)	2 (9)	11 (21)
SABA	10 (13)	4 (17)	6 (11)
ICS	34 (45)	12 (52)	22 (42)
LABA	30 (39)	10 (43)	20 (38)
Anticoagulant	5 (7)	2 (9)	3 (6)
Antibiotic	2 (3)	2 (9)	0 (0)
Other	52 (68)	18 (78)	34 (64)

SABA=short-acting beta-agonist; ICS=inhaled corticosteroid; LABA=long-acting beta-agonist

Table 2-6. CT Findings

Abnormality n (%)	Ever-COVID (n=50)	No Prior Lung Diagnosis COVID (n=34)	Asthma-COVID (n=13)	COPD-COVID (n=3)
Ground-Glass Opacities	20 (40)	14 (41)	5 (38)	1 (33)
Consolidation	4 (8)	2 (6)	1 (8)	1 (33)
Reticulation	2 (4)	2 (6)	0 (0)	0 (0)
Atelectasis	14 (28)	10 (29)	4 (31)	0 (0)
Emphysema	5 (10)	1 (3)	2 (15)	2 (67)
Honeycombing	1 (2)	1 (3)	0 (0)	0 (0)
Mosaic Attenuation	4 (8)	3 (9)	1 (8)	0 (0)
Bronchial Wall Thickening	1 (2)	1 (3)	0 (0)	0 (0)
Nodules	13 (26)	8 (24)	5 (38)	0 (0)
Bronchiectasis	11 (22)	8 (24)	3 (23)	0 (0)
Bronchiolectasia	1 (2)	1 (3)	0 (0)	0 (0)

Table 2-7. Pulmonary Function, Questionnaire, and Imaging Measurements by Site

Parameter	Never-COVID (n=9)			Ever-COVID (n=76)		
mean (SD)	Site 1 (n=6)	Site 2 (n=3)	Sig. p	Site 1 (n=54)	Site 2 (n=22)	Sig. p
Pulmonary function						
FEV_1* $\%_{pred}$	100 (7)	103 (17)	.7	86 (20)	81 (20)	.4
FVC* $\%_{pred}$	102 (7)	104 (16)	.9	87 (18)	92 (24)	.3
FEV_1/FVC*	0.80 (0.05)	0.84 (0.04)	.3	0.77 (0.11)	0.74 (0.11)	.2
LCI* n breaths	9.0 (1.4)	ND	-	10.7 (3.9)	ND	-
LCI_{ao}* n breaths	8.0 (1.3)	ND	-	9.5 (3.3)	ND	-
DL_{CO}* $\%_{pred}$	-	-	-	81 (21)	105 (35)	**.007**
Exercise capacity and QoL						
6MWD* m	-	-	-	435 (79)	491 (80)	**.008**
SpO_2 post-exertion* %	-	-	-	97 (3)	99 (2)	**.01**
SGRQ*	-	-	-	34 (17)	38 (19)	.4
mMRC*	-	-	-	1 (1)	1 (1)	.3
IPAQ* MET-minutes	-	-	-	4276 (4651)	5778 (5451)	.3
MRI						
VDP %	1.4 (1.0)	0.5 (0.3)	.2	6.2 (7.9)	3.6 (4.3)	.2
*CT**						
TAC	-	-	-	270 (104)	267 (139)	.9
WA mm^2	-	-	-	66 (2)	67 (3)	.4
LA mm^2	-	-	-	14 (3)	12 (3)	.2
WT mm	-	-	-	1.4 (0.1)	1.3 (0.1)	.2

FEV_1=forced expiratory volume in 1 second; $\%_{pred}$=percent of predicted value; FVC=forced vital capacity; LCI=lung clearance index; ND=not done; ao=airway opening; DL_{CO}=diffusing capacity of the lungs for carbon monoxide; QoL=quality-of-life; 6MWD=six-minute walk distance; SGRQ=St. George's Respiratory Questionnaire; mMRC=modified Medical Research Council dyspnea score; IPAQ=International Physical Activity Questionnaire; MRI=magnetic resonance imaging; VDP=ventilation defect percent; CT=computed tomography; TAC=total airway count; WA=wall area; LA=lumen area; WT=wall thickness.
p=significance value between Site 1 and Site 2.
FEV_1*, FVC* and FEV_1/FVC*: Ever-COVID Site 1 n=53
LCI*: Never-COVID n=5, Ever-COVID Site 1 n=44
LCI_{ao}*: Never-COVID n=5, Ever-COVID Site 1 n=32
DL_{CO}*: Ever-COVID Site 1 n=43, Ever-COVID Site 2 n=21
6MWD* and mMRC*: Ever-COVID Site 1 n=43
SpO_2 post-exertion*: Ever-COVID Site 1 n=43
SGRQ*: Ever-COVID Site 1 n=44, Ever-COVID Site 2 n=20
IPAQ*: Ever-COVID Site 1 n=42, Ever-COVID Site 2 n=17
CT*: Ever-COVID Site 1 n=36, Ever-COVID Site 2 n=8

Table 2-8. Characteristics by Previous Lung Disease

Parameter mean (SD) [mean/MEDIAN: min-max]	No Prior Lung Diagnosis COVID (n=49)	Asthma-COVID (n=21)	COPD-COVID (n=6)	Sig. p
Age years	52 (12)	55 (13)	59 (11)	.3
Female n (%)	23 (47)	14 (67)	1 (17)	-
BMI kg/m^2	30 (5)	28 (6)	30 (4)	.4
SpO_2 %	97 (1)	97 (2)	96 (2)	.1
Heart rate beats/min	78 (13)	75 (14)	79 (8)	.6
Blood pressure mmHg	126/82 (15/10)	124/81 (13/9)	120/78 (13/13)	-
Weeks Since + COVID Test	[14/12: 5-53]	[13/12: 6-29]	[13/13: 6-20]	.8
Smoking history pack-years	4 (11)	5 (10)	50 (27)	**<.001**
Ever-hospitalized n (%)	18 (37)	5 (24)	2 (33)	-
Hospital Admission days	14 (18)	8 (6)	7 (1)	-
Pulmonary function				
FEV_1* $\%_{pred}$	87 (18)	82 (24)	74 (24)	.3
FVC* $\%_{pred}$	88 (19)	85 (21)	96 (19)	.1
FEV_1/FVC*	0.79 (0.08)	0.75 (0.12)	0.60 (0.16)	**<.001**
LCI* n breaths	11.1 (3.9)	9.9 (4.1)	10.4 (2.5)	.7
LCI_{ao}* n breaths	9.3 (3.3)	10.0 (3.6)	8.4	.8
DL_{CO}* $\%_{pred}$	90 (33)	88 (19)	77 (16)	.6
Exercise capacity and QoL				
6MWD* m	468 (74)	445 (81)	382 (127)	.05
SpO_2 post-exertion* %	97 (3)	98 (2)	96 (4)	.6
SGRQ*	34 (16)	38 (21)	25 (21)	.7
mMRC*	1 (1)	1 (1)	1 (1)	.7
IPAQ* MET-minutes	5286 (5448)	3577 (3727)	3060 (1767)	.5
MRI				
VDP %	3.6 (4.2)	6.7 (7.6)	15.8 (14.1)	**<.001**
*CT**				
TAC	294 (117)	241 (76)	126 (61)	.06
WA mm^2	66 (2)	67 (2)	68 (2)	.08
LA mm^2	15 (3)	12 (3)	11 (1)	.09
WT mm	1.4 (0.1)	1.3 (0.1)	1.3 (0.02)	**.04**

COPD=chronic obstructive pulmonary disease; BMI=body mass index; FEV_1=forced expiratory volume in 1 second; $\%_{pred}$=percent of predicted value; FVC=forced vital capacity; LCI=lung clearance index; ao=airway opening; DL_{CO}=diffusing capacity of the lungs for carbon monoxide; QoL=quality-of-life; 6MWD=six-minute walk distance; SGRQ=St. George's Respiratory Questionnaire; mMRC=modified Medical Research Council dyspnea score; IPAQ=International Physical Activity Questionnaire; MRI=magnetic resonance imaging; VDP=ventilation defect percent; CT=computed tomography; TAC=total airway count; WA=wall area; LA=lumen area; WT=wall thickness.
p=significance value for ANOVA.
FEV_1*, FVC* and FEV_1/FVC*: Asthma-COVID n=20
LCI*: No Prior Lung Diagnosis COVID n=29, Asthma-COVID n=12, COPD-COVID n=3
LCI_{ao}*: No Prior Lung Diagnosis COVID n=22, Asthma-COVID n=4, COPD-COVID n=1
DL_{CO}*: No Prior Lung Diagnosis COVID n=43, Asthma-COVID n=16, COPD-COVID n=5
6MWD* and mMRC*: No Prior Lung Diagnosis COVID n=42, Asthma-COVID n=18
SpO_2 post-exertion*: No Prior Lung Diagnosis COVID n=42, Asthma-COVID n=17
SGRQ*: No Prior Lung Diagnosis COVID n=42, Asthma-COVID n=17
IPAQ*: No Prior Lung Diagnosis COVID n=38, Asthma-COVID n=18, COPD-COVID n=3
CT*: No Prior Lung Diagnosis COVID n=28, Asthma-COVID n=14, COPD-COVID n=2

Table 2-9. Relationships between pulmonary function tests, imaging, and quality-of-life measurements

	Days Since +COVID		Hospital Admission Days		BMI		Baseline SpO_2		FEV_1		FEV_1 %pred		FVC		FVC %pred		FEV_1/FVC		LCI		LCIao		DL_{CO} %pred		6MWD		Post SpO_2		Post Borg		Post RPE		SGRQ		IPAQ		mMRC		VDP		TAC		WA		LA		WT	
	r/ρ	p	r/ρ	p	r/ρ	p	r/ρ	p	r/ρ	p	r/ρ	p	r/ρ	p	r/ρ	p	r/ρ	p	r/ρ	p	r/ρ	p	r/ρ	p	r/ρ	p	r/ρ	p	r/ρ	p	r/ρ	p	r/ρ	p	r/ρ	p	r/ρ	p	r/ρ	p	r/ρ	p	r/ρ	p	r/ρ	p
Days Since +COVID	1.0		.3	.2	.1	.3	-.02	.8	.03	.8	.1	.4	.02	.9	-.5	**.02**	.1	.2	-.05	.8	-.06	.8	-.3	**.01**	-.2	.2	-.06	.5	.06	.6	.1	.4	.1	.3	.05	.7	.2	.2	.02	.9	.1	.5	.003	1.0	.2	.3	.3	.07
Hospital Admission Days	.3	.2	1.0		-.3	.2	-.02	.9	-.2	.4	-.2	.3	-.3	.2	-.09	.5	.5	**.02**	.5	.06	.7	**.04**	-.6	**.005**	.2	.4	-.5	.06	.01	1.0	.1	.7	-.2	.5	.2	.5	.1	.6	.2	.4	.7	**.045**	-.4	.3	.6	.08	.7	**.02**
BMI	.1	.3	-.3	.2	1.0		-.4	**.002**	-.04	.7	.1	.4	-.05	.7	.06	.6	-.08	.5	.005	1.0	-.08	.7	.2	.1	-.4	**<.001**	-.1	.3	.06	.6	.3	**.04**	.2	.06	-.1	.4	.05	.7	.2	.2	-.2	.2	.2	.3	-.1	.4	.02	.9
Baseline SpO_2	-.02	.8	-.02	.9	-.4	**.002**	1.0		.1	.3	.04	.7	.05	.7	.04	.7	.2	.1	-.3	.07	-.4	**.02**	.3	**.02**	.4	**.001**	.7	**<.001**	.1	.6	-.08	.6	-.1	.3	.2	.06	-.08	.5	-.4	**<.001**	.2	.2	-.2	.1	.2	.3	.02	.9
FEV_1	.03	.8	-.2	.4	-.04	.7	.1	.3	1.0		.7	**<.001**	.9	**<.001**	.5	**<.001**	.4	**.003**	-.4	**.01**	-.3	**.01**	.4	**.002**	.3	**.03**	.1	.3	-.2	.2	.07	.7	-.2	.1	.08	.5	-.3	**.01**	-.1	.2	.2	.3	-.03	.7	.3	.07	.3	**.046**
FEV_1 %pred	.1	.4	-.2	.3	.1	.4	.04	.7	.7	**<.001**	1.0		.5	**<.001**	.8	**<.001**	.4	**<.001**	-.3	**.048**	-.3	.07	.4	**.001**	.2	.1	.3	**.049**	-.2	.2	.2	.2	-.1	.3	.01	.9	-.1	.3	-.3	**.006**	.3	**.045**	-.3	.07	.2	.1	.2	.3
FVC	.02	.9	-.3	.2	-.05	.7	.05	.7	.9	**<.001**	.5	**<.001**	1.0		.6	**<.001**	-.05	.7	-.3	.06	-.2	.3	.3	**.03**	.2	.08	.07	.6	-.1	.3	.02	.9	-.2	.08	.1	.4	-.3	**.02**	.02	.9	.01	.9	.07	.6	.02	.3	.3	.09
FVC %pred	-.5	**.02**	-.09	.5	.06	.6	.04	.7	.5	**<.001**	.8	**<.001**	.6	**<.001**	1.0		-.2	.2	-.3	.08	-.3	.1	.4	**<.001**	.2	.2	.3	**.03**	-.1	.6	.3	**.02**	-.1	.4	.08	.6	-.1	.3	-.07	.5	.1	.4	-.02	.9	-.03	.8	-.05	.8
FEV_1/FVC	.1	.2	.5	**.02**	-.08	.5	.2	.1	.4	**.003**	.4	**<.001**	-.05	.7	-.2	.2	1.0		-.1	.4	-.2	.4	.05	.7	.1	.4	.002	1.0	-.1	.4	.1	.5	-.1	.4	-.05	.7	-.08	.5	-.2	**.04**	.3	**.03**	-.4	**.02**	.3	**.03**	.2	.3
LCI	-.05	.8	.5	.06	.005	1.0	-.3	.07	-.4	**.01**	-.3	**.048**	-.3	.06	-.3	.08	-.1	.4	1.0		.9	**<.001**	-.6	**<.001**	-.3	.08	.5	**.006**	-.1	.6	-.1	.5	.02	.9	.1	.6	.2	.3	.2	.1	.2	.5	-.3	.1	-.05	.8	-.1	.5
LCIao	-.06	.8	.7	**.04**	-.08	.7	-.4	**.02**	-.3	**.01**	-.3	.07	-.2	.3	-.3	.1	-.2	.4	.9	**<.001**	1.0		-.4	**.02**	-.2	.2	-.5	**.007**	-.09	.6	-.2	.2	-.2	.2	-.06	.8	-.08	.7	.3	.1	.05	.8	-.4	.06	.03	.9	.01	1.0
DL_{CO} %pred	-.4	**.01**	-.6	**.005**	.2	.1	.3	**.02**	.4	**.002**	.4	**.001**	.3	**.03**	.4	**<.001**	.05	.7	-.6	**<.001**	-.4	**.02**	1.0		.4	**.006**	.3	**.03**	.1	.5	.2	.3	-.02	.9	.02	.9	-.3	**.02**	-.2	.09	.09	.6	-.04	.8	-.02	.9	-.05	.8
6MWD	-.2	.2	.2	.4	-.4	**<.001**	.4	**.001**	.3	**.03**	.2	.1	.2	.08	.2	.2	.1	.4	-.3	.08	-.2	.2	.4	**.006**	1.0		.4	**<.001**	.008	1.0	-.2	.3	-.3	**.02**	.1	.3	-.3	**.02**	-.3	**.01**	.06	.7	.02	.9	-.1	.4	-.08	.6
Post SpO_2	-.07	.6	-.5	.06	-.1	.3	.7	**<.001**	.1	.4	.3	**.049**	.07	.6	.3	**.03**	.002	1.0	-.5	**.006**	-.5	**.007**	.3	**.03**	.4	**<.001**	1.0		.2	**.046**	.09	.6	.07	.6	.06	.7	.1	.4	-.4	**<.001**	-.09	.6	.04	.8	-.2	.1	-.2	.1
Post Borg	.06	.6	.01	1.0	.06	.6	.1	.6	-.2	.2	-.2	.2	-.1	.3	-.1	.6	-.1	.4	-.1	.6	-.09	.6	.1	.5	.008	1.0	.2	**.046**	1.0		.6	**<.001**	.6	**<.001**	-.2	.2	.4	**<.001**	-.02	.8	.003	1.0	.01	.5	-.2	.3	-.2	.1
Post RPE	.1	.4	.1	.7	.3	**.04**	-.08	.6	.07	.7	.2	.2	.02	.9	.3	**.02**	.1	.5	-.1	.5	-.2	.2	-.2	.3	-.2	.3	-.09	.6	.6	**<.001**	1.0		.7	**<.001**	-.2	.2	.3	**.02**	.1	.5	.1	.5	.04	.8	-.07	.7	-.05	.8
SGRQ	.1	.3	-.2	.5	.2	.06	-.1	.3	-.2	.1	-.1	.3	-.2	.08	-.1	.4	-.1	.4	.02	.9	-.2	.2	-.02	.9	-.3	**.02**	.07	.6	.6	**<.001**	.7	**<.001**	1.0		-.2	.09	.7	**<.001**	.09	.5	-.07	.6	.1	.5	-.3	.1	-.2	.2
IPAQ	.05	.7	.2	.5	-.1	.4	.2	.06	.08	.5	.01	.9	.1	.4	.08	.6	-.05	.7	.1	.6	-.06	.8	.02	.9	.1	.3	.06	.7	-.2	.2	-.2	.2	-.2	.09	1		-.1	.4	-.01	.5	.1	.5	.08	.6	-.2	.2	-.2	.2
mMRC	.2	.2	.1	.6	.05	.7	-.08	.5	-.3	**.01**	-.1	.3	-.3	**.02**	-.1	.3	-.08	.5	.2	.3	-.08	.7	-.3	**.02**	-.3	**.02**	.1	.4	.4	**<.001**	.3	**.02**	.7	**<.001**	-.1	.4	1.0		.1	.3	-.06	.7	-.04	.8	-.07	.7	-.1	.5
VDP	.02	.9	.2	.4	.2	.2	-.4	**<.001**	-.1	.2	-.3	**.006**	0.2	.9	-.07	.5	-.2	**.04**	.2	.1	.3	.1	-.2	.09	-.3	**.01**	-.4	**<.001**	-.02	.8	.1	.5	.08	.5	-.01	.5	.1	.3	1.0		-.1	.4	.3	.07	-.1	.4	-.2	.3
TAC	.1	.5	.7	**.045**	-.2	.2	.2	.2	.2	.3	.3	**.045**	.01	.9	.1	.4	.3	**.03**	.2	.5	.06	.8	.09	.6	.06	.7	-.09	.6	.003	1.0	.1	.5	-.07	.6	.1	.5	-.06	.7	-.1	.4	1.0		-.8	**<.001**	.7	**<.001**	.5	**<.001**
WA	.003	1.0	-.4	.3	.2	.3	-.2	.1	-.06	.7	-.3	.07	.07	.6	-.02	.9	-.4	**.02**	-.3	.1	-.4	.06	-.04	.8	.02	.09	.04	.8	.01	.5	.04	.8	.1	.5	.08	.6	-.04	.8	.3.	.07	-.8	**<.001**	1.0		-.7	**<.001**	-.4	**.009**
LA	.2	.3	.6	.08	-.1	.4	.2	.3	.3	.07	.2	.1	.2	.3	-.03	.8	.3	**.03**	-.05	.8	.3	.9	-.02	.9	-.1	.4	-.2	.1	-.2	.3	-.07	.7	-3	.1	-.2	.2	-.07	.7	-.1	.2	.7	**<.001**	-.7	**<.001**	1.0		.8	**<.001**
WT	.3	.07	.7	**.02**	.02	.9	.02	.9	.3	**.046**	.2	.3	.3	.09	-.05	.8	.2	.3	-.1	.5	.01	1.0	-.05	.8	-.08	.6	-.2	.1	-.2	.1	-.05	.8	-.2	.2	-.2	.2	-.1	.5	-.2	.3	.5	**.001**	-.4	**.009**	.8	**<.001**	1.0	

BMI=body mass index; FEV_1=forced expiratory volume in 1 second; $\%_{pred}$=percent of predicted value; FVC=forced vital capacity; LCI=lung clearance index; ao=airway opening; DL_{CO}=diffusing capacity of the lungs for carbon monoxide; 6MWD=six-minute walk distance; post=post-exertion (post-six minute walk test); Borg=Borg rating of perceived exertion; RPE=rated perceived exertion scale; SGRQ=St. George's respiratory capacity; IPAQ=international physical activity questionnaire; mMRC=modified medical research council dyspnea scale; VDP=ventilation defect percent; TAC=total airway count; WA=wall area; LA=lumen area; WT=wall thickness; r=Pearson correlation coefficient; ρ=Spearman correlation coefficient; p=uncorrected p value

Chapter 3

3 POST-ACUTE COVID-19 SYNDROME: ^{129}XE MRI VENTILATION DEFECTS AND RESPIRATORY OUTCOMES ONE YEAR LATER

To investigate the longitudinal trajectory of long-COVID, we evaluated the differences in MRI ventilation, pulmonary function, and quality-of-life measurements at 15-months as compared to 3-months post-COVID-19 infection in participants with long-COVID.

The contents of this chapter were previously published in the journal Radiology: HK Kooner, MJ McIntosh, AM Matheson, M Abdelrazek, MS Albert, I Dhaliwal, M Kirby, A Ouriadov, GE Santyr, C Venegas, N Radadia, S Svenningsen, JM Nicholson, and G Parraga. Post-Acute COVID-19 Syndrome: ^{129}Xe MRI Ventilation Defects and Respiratory Outcomes One Year Later. Radiology 2023; 307(2): e222557. doi: 10.1148/radiol.222557. Permission to reproduce this article was granted by the Radiological Society of North America (RSNA) and is provided in ***Appendix B****.*

3.1 Introduction

Over the past two-years, post-acute COVID-19 sequelae have been defined[1] and redefined.[2] Post-acute COVID-19 syndrome (PACS) is the umbrella term that describes continuing or new symptoms which persist four weeks or more after an acute COVID-19 infection, including respiratory, neurological and psychological symptoms.[1] While a majority of previously hospitalized people with PACS have reported improved pulmonary function and exercise capacity 12-months after infection,[3,4] at least one persistent symptom has also been reported in 41-85% patients with PACS.[5-7] Importantly, in a single center study of 30 previously hospitalized symptomatic patients 6-weeks post-discharge, treatment with oral corticosteroids significantly improved dyspnea and exercise capacity.[8] However, without a control group, it remains difficult to ascertain the influence of treatment on improvements.

Chest CT is nearly universally available and the clinical-mainstay for the evaluation of pulmonary abnormalities resultant from COVID-19 infection[9] and in people with PACS.[10] In PACS, ^{129}Xe MRI previously revealed abnormal gas exchange measurements[11-14] and

ventilation defects.[11,15] In patients with normal pulmonary function and normal or mildly abnormal chest CT,[12-15] some of these MRI findings were accompanied by highly abnormal quality-of-life scores and exercise capacity. The longitudinal trajectory of such abnormal MRI measurements and their relationship to persistent symptoms remains unclear. Hyperpolarized ^{129}Xe MRI[16] provides a way to quantify airway dysfunction, including the functional consequences of airway inflammation or remodelling in asthma.[17] In people with PACS, MRI ventilation defects were shown to be related to exercise limitation and post-exertional dyspnea.[15] Ventilation defects are temporally and spatially reproducible in people with airways disease,[18] with high reproducibility across different sites.[19] In a pilot demonstration in four asymptomatic patients with COVID-19, ^{129}Xe MRI ventilation defects improved 12-months post-infection.[20] In another investigation, full-scale airway network modelling of ventilation abnormalities differentiated dyspneic patients after COVID-19 infection.[21]

While these previous results are compelling, to our knowledge, there have been no published observations in people with PACS that link improved airway dysfunction with dyspnea and exercise capacity improvements over time. We hypothesized that in people with PACS, ^{129}Xe MRI VDP and quality-of-life scores would significantly improve 12-months after a baseline visit. Hence, our aim was to measure and compare pulmonary function, exercise capacity, quality-of-life, and ^{129}Xe MRI ventilation defect percent (VDP) in patients with PACS evaluated at 3-months and 15-months post-infection.

3.2 Methods

3.2.1 Study Participants and Design

In this prospective study, participants were recruited in a convenience series between July 2020 and August 2021 from two quaternary care centers and research sites (Site 1: Robarts Research

Institute, London Canada; Site 2: St Joseph's Healthcare Hamilton, Hamilton Canada) and all provided written-informed consent to ethics board (HSREB #113224 London; HiREB #12672, Hamilton), Health Canada-approved protocols (www.clinicaltrials.gov NCT05014516). Inclusion criteria and participant recruitment were previously described.[15] Briefly, inclusion criteria consisted of individuals aged 18 to 80 years with a public-health confirmed case of COVID-19 and persistent symptoms, including but not limited to respiratory, neurological and metabolic systems. Exclusion criteria included MRI contraindications and inability to return for follow-up.

During 3-month and 15-month visits, participants completed fractional exhaled nitric oxide, spirometry, oscillometry, multi-breath inert gas washout, diffusing capacity of the lung for carbon monoxide (DL_{CO}) and ^{129}Xe MRI. St. George's Respiratory Questionnaire (SGRQ)[22] was completed to measure respiratory-illness-related quality-of-life; modified Medical Research Council dyspnea scale,[23] modified Borg scale,[24] International Physical Activity Questionnaire,[25] and six-minute-walk-test[26] were also completed. Thoracic CT was acquired during the 3-month visit. ^{129}Xe MRI VDP and CT results acquired 3-months post-COVID-19 infection were previously reported;[15] here, we report measurements at 15-months post-COVID-19 infection and compare them with 3-month measurements.

3.2.2 Pulmonary Function Tests and Questionnaires

Participants completed spirometry for forced expiratory volume in 1-second (FEV_1) and forced vital capacity, according to American Thoracic Society guidelines,[27] using the EasyOne Pro LAB system (ndd Medical Technologies) or a whole-body plethysmograph (MedGraphics Corporation). Multi-breath inert gas washout, performed using the EasyOne Pro LAB system equipped with an ultrasonic flow and molar mass sensor, measured the lung clearance index.[28]

DL_{CO} was also measured using the EasyOne Pro LAB system or the plethysmograph, according to European Respiratory Society guidelines.[29] Oscillometry was performed according to European Respiratory Society guidelines[30] using a tremoFlo C-100 Airwave Oscillometry System (Thorasys) to measure resistance and reactance (units=cmH_2O•s/L) between 5 and 37 Hz. Post-bronchodilator measurements were performed 15 minutes after inhalation of 4×100 µg Salbutamol sulfate norflurane (Ivax Pharmaceuticals) using an AeroChamber (Trudell Medical International). Participants withheld respiratory medications before each study visit according to American Thoracic Society guidelines.[27] SGRQ, modified Medical Research Council dyspnea scale, modified Borg scale, International Physical Activity Questionnaire, and six-minute walk test were administered under study personnel supervision.

3.2.3 Thoracic MRI

Anatomic ^{1}H and ^{129}Xe static ventilation MRI were acquired using 3.0 Tesla scanners (Discovery MR750; GE Healthcare), as previously described.[15] Anatomic ^{1}H MRI was acquired using a fast-spoiled gradient-recalled-echo sequence (partial-echo acquisition; total acquisition time, 8 seconds; repetition-time msec/echo time msec, 4.7/1.2; flip-angle, 30°; field-of-view, 40×40cm^2; bandwidth, 24.4 kHz; 128×80 matrix, zero-filled to 128×128; partial-echo percent, 62.5%; 15-17×15mm slices). ^{129}Xe MRI was acquired using a three-dimensional fast-spoiled gradient-recalled echo sequence (total acquisition time, 14 s; repetition-time msec/echo time msec, 6.7/1.5; variable flip-angle; field-of-view, 40×40cm^2; bandwidth, 15.63 kHz; 128×128 matrix; 14×15mm slices) and a flexible vest coil (Clinical MR Solutions; Site 1) or asymmetric quadrature bird cage coil (custom built; Site 2). Supine participants were coached to inhale a 1.0L bag (Tedlar; Jensen Inert Products) (400mL ^{129}Xe + 600mL ^{4}He at Site 1 or 600mL ^{129}Xe + 400mL N_2 at Site 2 and 1.0L N_2 for ^{1}H MRI) from

the bottom of a tidal breath (functional residual capacity) with acquisition under breath-hold conditions. ^{129}Xe gas was polarized to 15-55% (Site 1: Xenispin 9820, Site 2: Xenispin 9800; Polarean).[15] Quantitative MRI analysis was performed (HKK, three-years experience; MJM four-years experience) using MATLAB 2019a (Mathworks), as previously described.[15]

3.2.4 Thoracic CT

Within 30 minutes of MRI, CT was acquired as previously described[15] (Site 1: 64-slice LightSpeed VCT system, GE Healthcare; Site 2: Discovery MI PET/CT scanner, GE Healthcare; parameters: 64×0.625 collimation, 120 peak kilovoltage, 100 mA, tube rotation time=500ms, pitch=1.25, standard reconstruction kernel, slice thickness=1.25mm, field-of-view=40cm^2). CT images were analyzed (HKK, three-years experience) using VIDAvision software (VIDA Diagnostics Inc.).

3.2.5 Statistical Analysis

SPSS (SPSS Statistics 25.0; IBM) was used for all statistical analyses. Sample size considerations (power 80%, two-sided significance 5% = 33 participants) are described in the supplement. Data were tested for normality using Shapiro-Wilk tests and nonparametric tests were performed for non-normally distributed data. Differences between 3- and 15-month visits were evaluated using paired samples t-tests; differences between subgroups were evaluated using independent samples t-tests and analysis of variance. Univariable relationships were evaluated using Pearson (r) for parametric data and Spearman (ρ) correlations for non-parametric data. Variables with Pearson or Spearman correlation *P* values of $\leq$0.20 were used to generate multivariable models, where significant variables included in the model were chosen using the backwards approach, to explain changes observed at 15-months. The removal criterion for the backwards method included variables with a probability of F value $\geq$0.10.

Variables were tested for collinearity and models were rejected when the variance inflation factor was ≥5. Predictors of improvements greater than the minimal clinically important difference were evaluated using binary logistic regression to generate odds ratios (OR). Results were considered statistically significant when the probability of making a type I error was less than 5% (P<0.05).

3.3 Results

3.3.1 Participant Characteristics

A CONSORT diagram provided in **Figure 3-1** shows that 76 participants with PACS (mean age, 53 years ±12[SD]; 38 male; 38 female) were evaluated at 3-months (Site 1, n=54; Site 2, n=22), as prior work has shown.[15] Of these, 17 were lost-to-follow-up, three declined, two declined COVID-19 vaccination so were not allowed to attend the follow-up visit due to institutional guidelines, and one became pregnant in the time between visits and was not eligible for MRI, and were excluded from analysis. Thus, 53 participants were evaluated at 15-months (mean age, 55 years ±18[SD]; 26 male; 27 female).

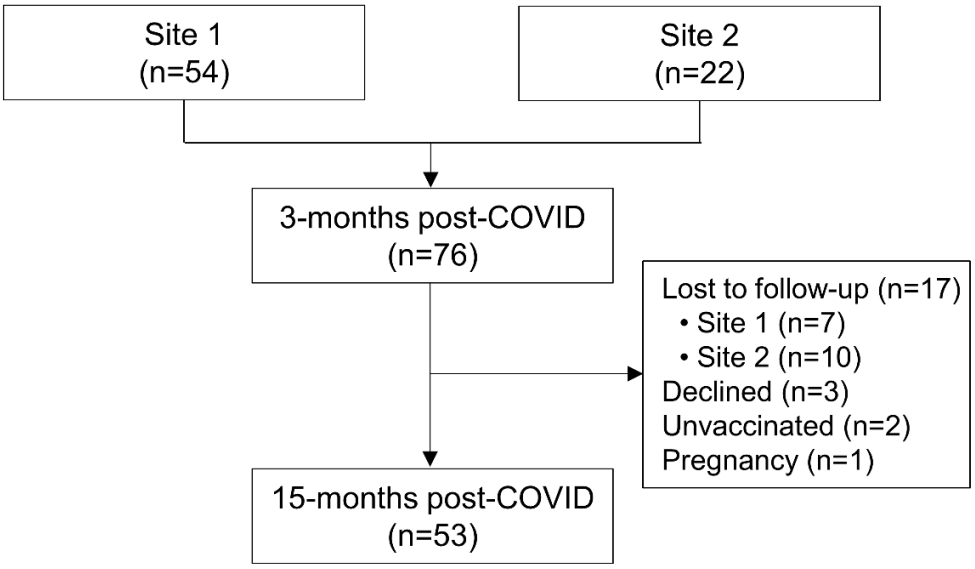

Figure 3-1. CONSORT Diagram

Table 3-1 provides demographic characteristics for participants at the 3- and 15-month visits. Biological sex was self-reported. **Table 3-4** in the supplement summarizes baseline measurements for the original study group and the subgroup attending the 15-month visit. Of the 53 participants evaluated at 15-months, 17 (32%) were hospitalized during their acute COVID-19 infection and 36 (68%) received home-based care. A summary of medications prescribed is shown in **Table 3-1** and a by-participant list is provided in **Table 3-5**. **Table 3-6** summarizes demographic characteristics by site and shows that mean SpO_2 was significantly different (96±3% vs 99±1%; *P*=.002) between sites at the 15-month post-COVID visit. **Table 3-7** and **Table 3-8** show data in subgroups dichotomized by previous hospitalization status and self-reported previous respiratory disease, respectively.

Table 3-1. Demographic Characteristics at 3-months and 15-months

Parameter	3-months post-COVID (n=53)	15-months post-COVID (n=53)	Sig. *P*
Age (y)	54 ± 14	55 ± 18	-
Age range (y)	25-84	26-85	-
Female sex n (%)	27 (51)	27 (51)	-
Male sex n (%)	26 (49)	26 (49)	-
BMI kg/m^2	31 ± 5	30 ± 5	>.99
SpO_2 %	97 ± 2	97 ± 1	>.99
Heart rate beats/min	81 ± 14	80 ± 13	.9
Blood pressure mmHg	127/83 ± 14/10	126/81 ± 15/9	-
Days Since + COVID Test	96/87: 35-275	450/441: 252-659	-
Months Since + COVID Test	3/3: 1-9	15/15: 8-22	-
Smoking history pack-years	10 ± 20	10 ± 20	-
No Previous Respiratory Disease n (%)	31 (58)	29 (55)	-
Previous Respiratory Disease n (%)	22 (42)	24 (45)	-
Asthma n (%)	17 (32)	18 (34)	-
COPD n (%)	5 (9)	6 (11)	-
Hospitalized n (%)	17 (32)	17 (32)	-
Hospital Admission days	9 ± 6	9 ± 6	-
Prescribed Respiratory Rx n (%)	29 (55)	21 (40)	>.99
ICS/LABA	26 (49)	20 (38)	>.99
SABA	13 (25)	10 (19)	.9
OCS	2 (4)	1 (2)	>.99

All data are reported as mean ± SD or mean/median: min-max.
BMI=body mass index; SpO_2=pulse oximetry estimation of arterial blood oxygen saturation made on a fingertip; COPD=chronic obstructive pulmonary disease; Rx=medical prescription; ICS=inhaled corticosteroid; LABA=long-acting beta-agonist; SABA=short-acting beta-agonist; OCS=oral corticosteroid.
P=Holm-Bonferroni corrected significance value; asterisk indicates *P*<.05.

3.3.2 15-Month Post-COVID Measurements

Figure 3-2 and **Figure 3-3** show ^{129}Xe ventilation MRI for two representative participants at 3- and 15-months. In participant P22, ventilation defects in the upper lobes were qualitatively improved at 15-months as compared with 3-months post-COVID infection. In participant P28, who required hospitalization during the acute infectious phase, wedge-shaped ventilation defects at 3-months resolved at 15-months.

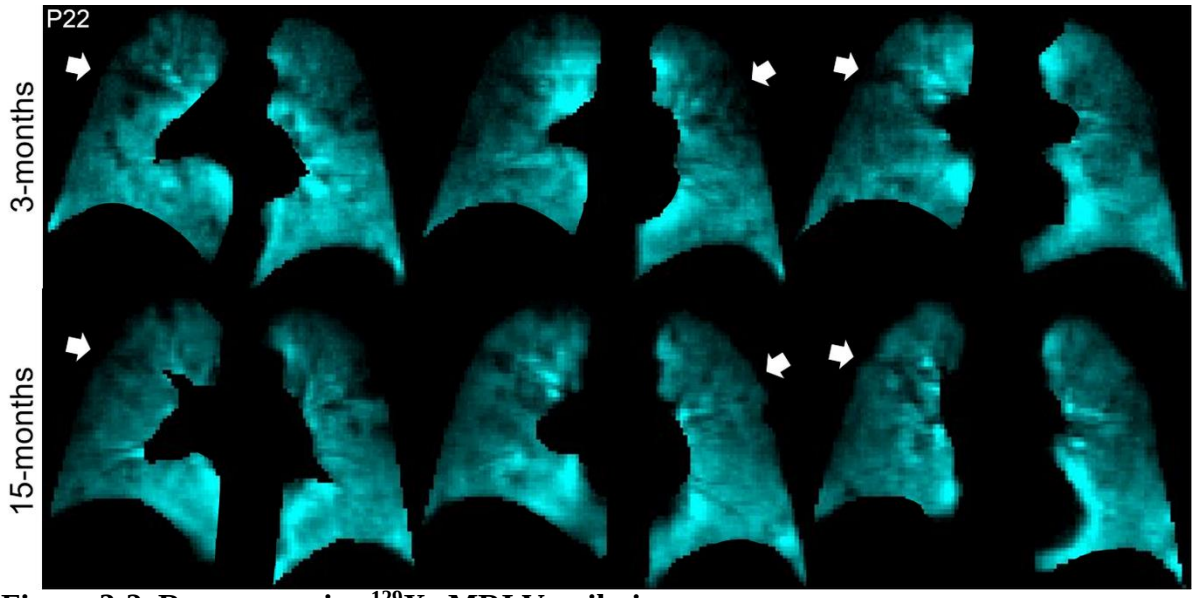

Figure 3-2. Representative ^{129}Xe MRI Ventilation
Coronal ^{129}Xe MRI slices (cyan) with white arrows pointing to MRI ventilation abnormalities that improve at follow-up. P22 is a 65-year-old male who was not hospitalized during acute infection and with 3-months/15-months post-COVID FEV_1=95%$_{pred}$/102%$_{pred}$, DL_{CO}=97%$_{pred}$/105%$_{pred}$, SGRQ=36/27, and VDP=7%/2%.

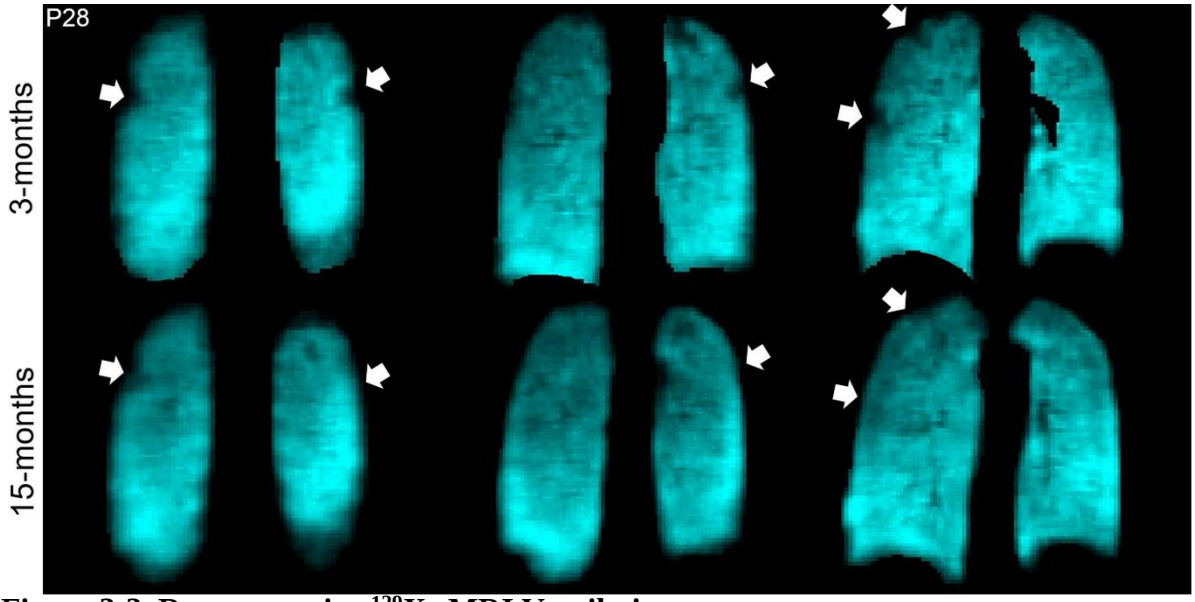

Figure 3-3. Representative ^{129}Xe MRI Ventilation
Coronal ^{129}Xe MRI slices (cyan) with white arrows pointing to MRI ventilation abnormalities that improve at follow-up. P28 is a 68-year-old female who was hospitalized for nine days during acute infection and with 3-months/15-months post-COVID FEV_1=84%$_{pred}$/100%$_{pred}$, DL_{CO}=81%$_{pred}$/91%$_{pred}$, SGRQ=59/0, and VDP=2%/0%.

Table 3-2 shows data acquired at 3- and 15-months post-COVID infection. A subset of these measurements is shown in **Figure 3-4**. In all participants with PACS, FEV_1 (85±20%$_{pred}$, 90±19%$_{pred}$; *P*=.001), FEV_1/FVC (76±11, 79±12; *P*=.003), DL_{CO} (89±29%$_{pred}$, 99±22%$_{pred}$; *P*=.002), SGRQ score (35±18, 25±20; *P*<.001) and VDP (5.4±7.1%, 4.2±6.8%; *P*=.003) were improved at 15-months as compared with 3-months post-COVID infection. Mean lung clearance index[31] (10±4, 9.7±2.6; *P*>.99) and SGRQ score[32] (35±18, 25±20; *P*<.001) remained abnormal in participants with PACS at both visits. At 15-months post-COVID infection, 34% (18/53) of participants reported VDP improvements greater than the minimal clinically important difference (2%).[33] **Table 3-9** shows all the data in participants dichotomized by VDP value at 3-month visit.

Table 3-2. Pulmonary Function, Questionnaire, and Imaging Measurements

Parameter	3-months post-COVID (n=53)	15-months post-COVID (n=53)	Sig. *P*
Pulmonary function			
FEV_1* $\%_{pred}$	84 ± 21	90 ± 19	.001*
FVC* $\%_{pred}$	87 ± 19	89 ± 16	>.99
FEV_1/FVC*	76 ± 11	79 ± 12	.003*
FeNO* ppb	24 ± 15	23 ± 21	>.99
LCI* n breaths	10 ± 4	9.7 ± 2.6	>.99
DL_{CO}* $\%_{pred}$	86 ± 21	99 ± 22	.002*
R_5* cmH_2O•s/L	3.8 ± 1.7	3.6 ± 1.3	.8
R_{19}* cmH_2O•s/L	3.0 ± 1.1	2.9 ± 0.9	.9
R_{5-19}* cmH_2O•s/L	0.9 ± 0.7	0.6 ± 0.6	.06
Exercise capacity and quality of life			
6MWD* m	441 ± 85	454 ± 79	.09
SpO_2* post-exertion %	97 ± 3	97 ± 3	.5
SGRQ*	35 ± 19	25 ± 20	<.001*
mMRC*	1 ± 1	1 ± 1	.2
IPAQ* MET-minutes	4958 ± 4336	5815 ± 6001	.09
MRI			
VDP %	5.8 ± 7.7	4.2 ± 6.8	.003*
*CT**			
TAC n	254 ± 94	-	-
WA mm^2	66 ± 2	-	-
LA mm^2	14 ± 3	-	-
WT mm	1.4 ± 0.1	-	-

All data are reported as mean ± SD.

FEV_1=forced expiratory volume in 1 second; $\%_{pred}$=percent of predicted value; FVC=forced vital capacity; FeNO=fractional exhaled nitric oxide; LCI=lung clearance index; DL_{CO}=diffusing capacity of the lungs for carbon monoxide; R_5=oscillometry measurement of total airway resistance; R_{19}=oscillometry measurement of central airway resistance; R_{5-19}=oscillometry measurement of distal airway resistance; 6MWD=six-minute walk distance; SpO_2=pulse oximetry estimation of arterial blood oxygen saturation made on a fingertip; SGRQ=St. George's Respiratory Questionnaire; mMRC=modified Medical Research Council dyspnea score; IPAQ=International Physical Activity Questionnaire; MET=metabolic equivalent; MRI=magnetic resonance imaging; VDP=ventilation defect percent; CT=computed tomography; TAC=total airway count; WA=wall area; LA=lumen area; WT=wall thickness.

P=Holm-Bonferroni corrected paired-samples significance value; asterisk indicates *P*<0.05.

FEV_1*, FVC*, FEV_1/FVC*: 3 months n=75

FeNO*: 3 months n=43, 15 months n=40

LCI*: 3 months n=44, 15 months n=41

DL_{CO}*: 3 months n=64, 15 months n=50

R_5*, R_{19}*, R_{5-19}*: 3 months n=73, 15 months n=41

6MWD*, SpO_2*, mMRC*: 3 months n=66, 15 months n=51

SGRQ*: 3 months n=64, 15 months n=51

IPAQ*: 3 months n=59, 15 months n=40

CT*: 3 months n=44

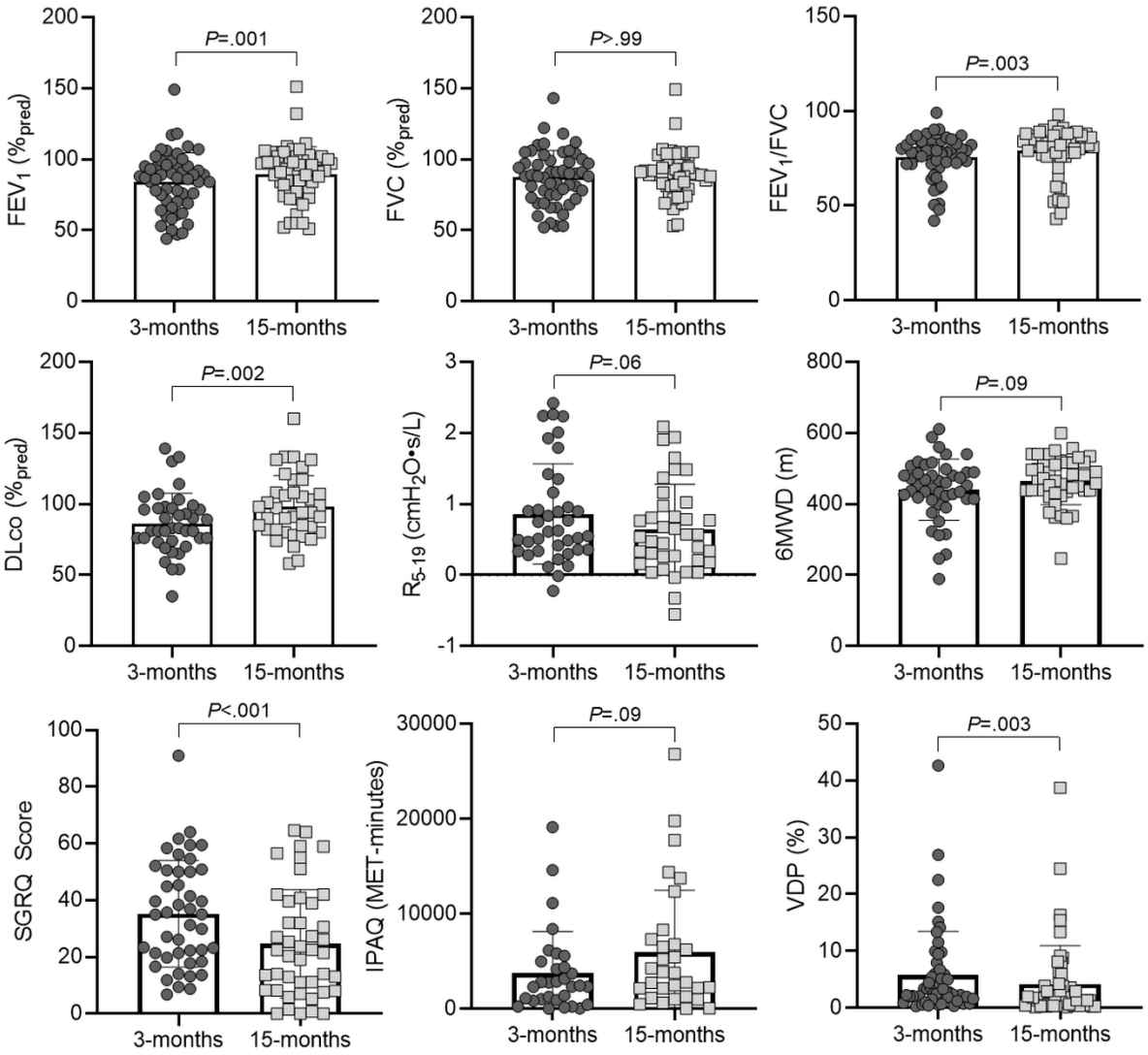

Figure 3-4.^{129}Xe MRI VDP, pulmonary function, exercise capacity, and quality-of-life Scatter plot and bar graphs show Holm-Bonferroni corrected significance for: FEV_1 (*P*=.001), FEV_1/FVC (*P*=.003), DLco (*P*=.002), SGRQ Score (*P*<.001) and VDP (*P*=.003) at 15-months as compared with 3-months post-COVID. FVC (*P*>.99), R_{5-19} (*P*=.06), 6MWD (*P*=.09) and IPAQ (*P*=.09) not significantly different.

3.3.3 Relationships and Multivariable Models

As shown in **Figure 3-7**, there were relationships at 15-months for VDP with post-exertional SpO_2 (ρ=-.36, *P*=.009) and lung clearance index (ρ=.59, *P*<.001), while the oscillometry measurement of distal airways resistance (R_{5-19}) was related to SGRQ score (ρ=.33, *P*=.04) and six-minute walk distance (6MWD) (ρ=-.42, *P*=.008). The change in VDP was related to the

change in FEV_1 (ρ=-.30, *P*=.03) and the change in lung clearance index (ρ=-.39, *P*=.03) at 15-months as compared with 3-months.

We generated multivariable models to explain the change in 6MWD, VDP and SGRQ score at 15-months and these are shown in **Table 3-3**. **Table 3-10** shows correlations for potential predictor variables of these changes. VDP (β=-.643, *P*=.006) measured at 3-months post-COVID predicted the change in 6MWD at 15-months, while CT airway wall area (β=-.298, *P*=.1) and the oscillometry measurement of distal airways resistance (β=.242, *P*=.2) also contributed to the model. CT airway wall area (β=-.401, *P*=.04), lung clearance index (β=.526, *P*=.02), and post-exertional SpO_2 (β=.696, *P*=.004) were all variables for the change in VDP at 15-months relative to 3-months. In addition, changes in DL_{CO} (β=-.463, *P*=.02) and forced vital capacity (β=-.395, *P*=.04) explained the change in SGRQ score. Some of the MRI-to-CT relationships for a single participant in **Figure 3-5** show that an abnormal left-upper-lobe anterior segmental bronchus (LB3), spatially related to ventilation defects at 3-months, showed substantial improvement, if not complete normalization at 15-months.

Table 3-3. Multivariable Linear Regression Models

Parameter	R^2	ANOVA p	Unstandardized B	Standardized β	Coefficients *p*
Δ6MWD					
Model	0.476	.004*			
Constant			55.035 ± 32.836		.1
CT WA			-0.847 ± 0.500	-.298	.1
R_{5-19}			1.408 ± 1.185	.242	.2
VDP			-0.401 ± 0.130	-.643	.006*
ΔVDP					
Model	0.626	.004*			
Constant			-114.143 ± 71.456		.1
CT WA			-1.283 ± 0.552	-.401	.04*
LCI			.816 ± 0.305	.526	.02*
Post-exertional SpO_2			1.942 ± 0.556	.696	.004*
ΔSGRQ					
Model	.357	.01*			
Constant			-5.552 ± 4.153		.2
ΔDL_{CO}			-0.446 ± 0.173	-0.463	.02*
ΔFVC			-0.537 ± 0.244	-0.395	.04*

B=unstandardized regression coefficient ± standard error; β=standardized regression coefficient; Δ=change at 15-months as compared with 3-months; 6MWD=six minute walk distance; WT=airway wall area; R_{5-19}=oscillometry measurement of distal airway resistance; VDP=ventilation defect percent; LCI=lung clearance index; SpO_2=pulse oximetry estimation of arterial blood oxygen saturation made on a fingertip; SGRQ=St. George's Respiratory questionnaire; DL_{CO}=diffusing capacity of the lungs for carbon monoxide; FVC=forced vital capacity.
Asterisk indicates $P<0.05$.

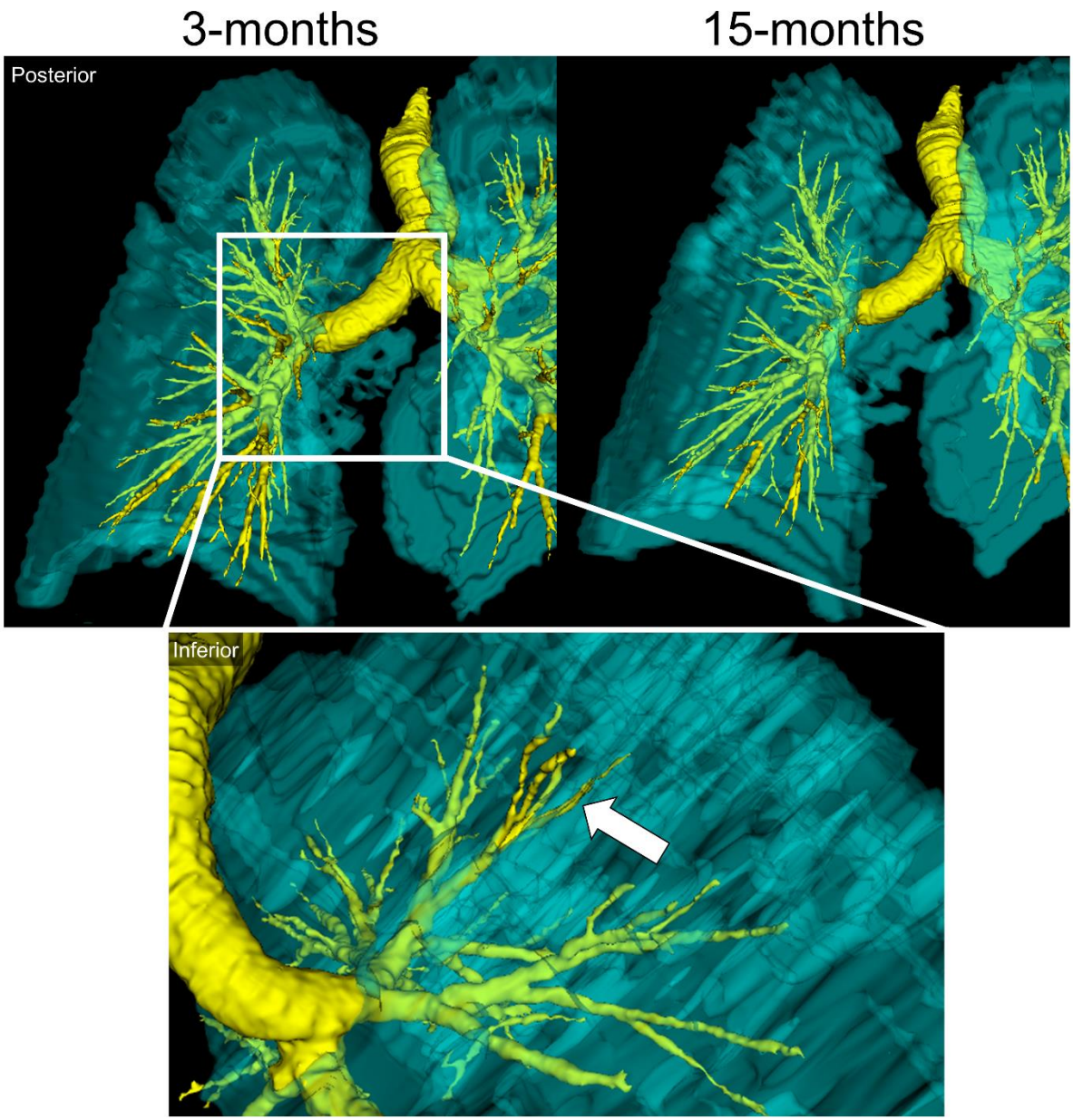

Figure 3-5. Representative ^{129}Xe MRI Ventilation and CT Airways
Three-dimensional model of ^{129}Xe MRI slices (cyan) and CT airways (yellow) of 65-year-old male who was not hospitalized during acute infection. Posterior views show ventilation abnormalities at 3-months (left) which resolve at 15-months (right). Inset shows inferior view of white arrow pointing to airway LB3, which leads to ventilation defect at 3-months.

We also retrospectively evaluated any potential influence of prescribed inhaled long-acting bronchodilator or oral and/or inhaled corticosteroids on 15-month visit improvements. Twenty-nine participants were prescribed airways-disease medications at 3-months. Of these, improvements greater than the minimal clinically important difference at 15-months were

observed for FEV_1 in 15 participants (15/29=52%), 6MWD in 15 participants (15/25=60%), SGRQ score in 20 participants (20/25=80%) and VDP in 10 participants (10/29=34%).[33-36] **Figure 3-6** shows that prescribed respiratory medication at 3-months was associated with SGRQ score improvement at 15-months (OR=4.0, 95% CI: 1.2, 13.8, *P*=.03) but was not statistically predictive of 6MWD improvement (OR=2.9, 95% CI: 0.9, 9.6, *P*=.08). There was no statistical evidence for prescribed respiratory medication at 3-months associating with improved FEV_1 (OR=1.1, 95% CI: 0.4, 3.2, *P*=.9) or VDP (OR=0.9, 95% CI: 0.3, 2.7, *P*=.9) at 15-months post-COVID infection. Notably, as shown in **Table 3-11**, the proportion of participants prescribed respiratory medication was not different (52%, 48%; *P*=.1) between those with (n=22) and without (n=31) a prior history of respiratory illness. The presence or absence of any prior history of respiratory disease, independent of treatment, was not a predictor for improved SGRQ score (OR=2.7 95% CI: 0.8, 9.1, *P*=.1), 6MWD (OR=0.8 95% CI: 0.3, 2.7, *P*=.8), FEV_1 (OR=1.5, 95% CI: 0.5, 4.31, *P*=.5) or VDP (OR=0.5, 95% CI: 0.5, 4.3, *P*=.5). **Table 3-12** shows data in participants prescribed respiratory medication at 3-months and those who were not.

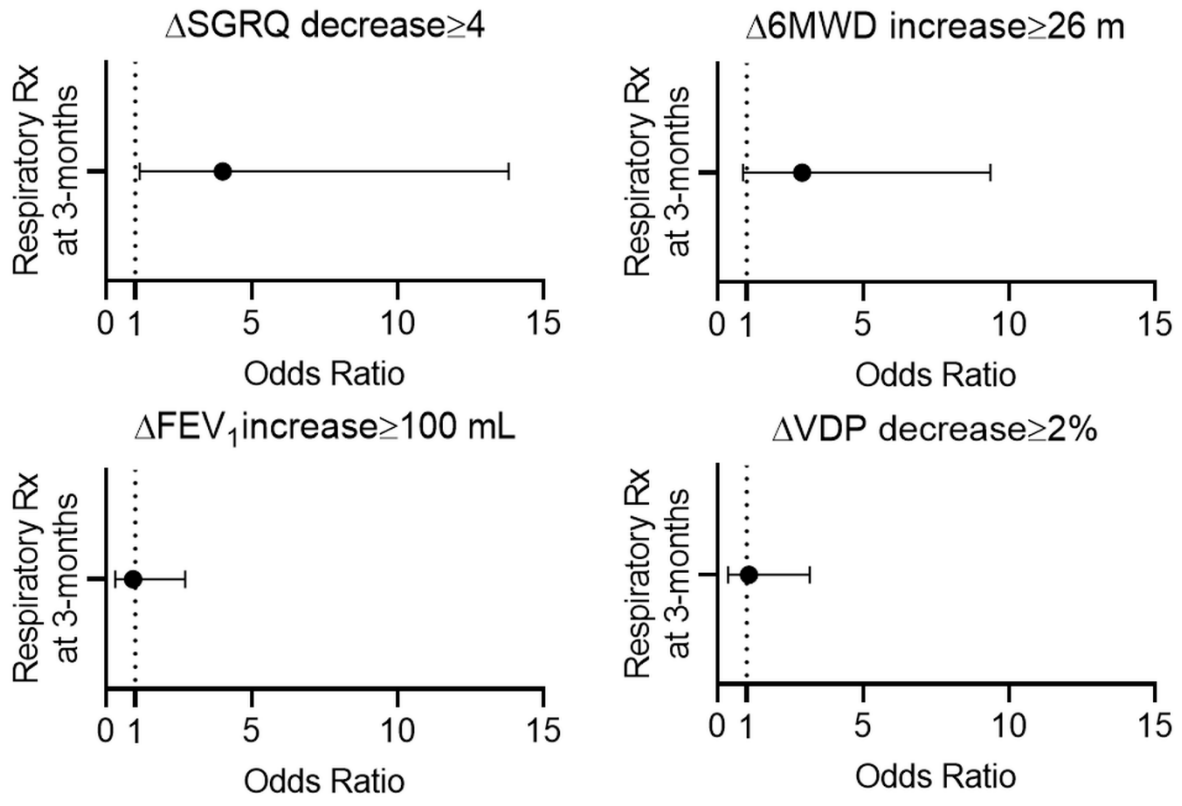

Parameter	ΔSGRQ decrease≥4 OR [95% CI]	*P*	Δ6MWD increase≥26 m OR [95% CI]	*P*	ΔFEV_1 increase≥100 mL OR [95% CI]	*P*	ΔVDP decrease≥2% OR [95% CI]	*P*
Resp. Rx at 3 months	4.0 [1.2-13.8]	.03*	2.9 [0.9-9.6]	.08	1.1 [0.4-3.2]	.9	0.9 [0.3-2.7]	.9

Figure 3-6. Treatment with respiratory medication at 3-months as a predictor of improvement > minimal clinically important difference at 15-months
Forest plots show treatment with respiratory medication at 3-months predicted improved SGRQ (OR=4.0, *P*=.03) ≥MCID at 15-months but not for 6MWD (OR=2.9, *P*=.08), FEV_1 (OR=1.1, *P*=.9), or VDP (OR=0.9, *P*=.9).
Asterisk indicates *P*<.05.

3.4 Discussion

We prospectively evaluated symptomatic participants with post-acute COVID-19 syndrome (PACS), 3- and 15-months post-COVID-19 infection using ^{129}Xe MRI, pulmonary function tests, six-minute walk test, as well as quality-of-life and exercise questionnaires. We wanted to better understand the longitudinal trajectory of abnormal MRI and other respiratory measurements, observed 3-months post-infection. We also wanted to interrogate potential mechanistic links between the lung functional pathologies we observed using MRI in

participants who presented with normal pulmonary function, but persistent symptoms, including exertional dyspnea and exercise limitation. We observed: 1) improved ^{129}Xe MRI ventilation defect percent (VDP) (5.4%, 4.2%; *P*=.003), forced expiratory volume in 1-second (FEV_1) ($85\%_{pred}$, $90\%_{pred}$; *P*=.001), diffusing capacity of the lung for carbon monoxide (DL_{CO}) ($89\%_{pred}$, $99\%_{pred}$; *P*=.002), and St. George's Respiratory Questionnaire (SGRQ) score (35, 25; *P*<.001) at 15-months compared with 3-months post-COVID infection, 2) MRI VDP (β=-.643, *P*=.006) measured at 3-months post-infection predicted six-minute walk distance (6MWD) improvement 15-months post-infection, 3) improved DL_{CO} (β=-.463, *P*=.02) and forced vital capacity (β=-.395, *P*=.04) explained the improved SGRQ score 15-months post-infection, and, 4) airways-disease therapy at 3-months strongly associated with improved quality-of-life score (odds ratio=4.0, 95% CI: 1.2, 13.8, *P*=.03) that was greater than the minimal clinically important difference at 15-months post-COVID. In this relatively large group of 53 participants, ^{129}Xe MRI VDP and SGRQ score both improved 15-months post-COVID infection; mean VDP at 15-months (4.2±6.8%) remained greater (worse) than the mean VDP values determined during the 3-month visit in a healthy never-COVID subgroup (1.1±0.9%) previously described.[15] Mean FEV_1 and $DL_{CO,}$ while both in the normal range at 3-months, also improved at 15-months. Not only were these improvements statistically significant, but the majority of participants also showed a personal improvement greater than the minimal clinically important difference.

Previous studies of longitudinal respiratory outcomes 12-months following COVID-19 infection also reported increased quality-of-life and exercise capacity.[3,4] Unfortunately, these previous studies did not uncover evidence that linked such subjective improvements with changes in pathophysiology. Because all patients in our study sample had been infected early

in the pandemic, before vaccination was possible, we could not to evaluate the relationship between different COVID-19 wave infections or vaccination status on PACS. However, we were able to demonstrate objective improvements in airway dysfunction, alongside symptom and quality-of-life changes, 15-months post-infection.

Towards our goal of understanding the drivers of post-COVID symptoms, we aimed to explore the potential relationships between symptoms and exercise limitation with MRI VDP, which in airways disease observed in asthma, reflects airway luminal dysfunction.[17] At 15-months post-infection, VDP correlated with both post-exertional SpO_2 (ρ=-.36, P=.009) and lung clearance index (ρ=.59, P<.001). This result suggested that ventilation defect improvement was coincident with improved, resting upright (versus supine for MRI) ventilation heterogeneity and O_2 saturation after the six-minute walk test. In addition, the oscillometry measurement of distal airway resistance, or R_{5-19}, which was not significantly different at 15-months (0.8±0.7cmH_2O•s/L, 0.6±0.6cmH_2O•s/L; P=.06), was related to SGRQ score (ρ=.33, P=.04) and 6MWD (ρ=-.42, P=.008), which were both improved at 15-months. Given these relationships, we were surprised that VDP did not correlate with symptoms or exercise limitations at 15-months. However, taken together, all of these results suggest that improved small airway function may play a role in improved quality-of-life and exercise capacity in some patients with PACS. Moreover, the improved MRI VDP at 15-months was also explained by CT airway wall area, lung clearance index, and post-exertional SpO_2 measurements which is consistent with the growing body of evidence pointing to small airways disease as a contributor to PACS.[37] While we have not evaluated the role of MRI gas exchange in this current study, such measurements are necessarily based on ^{129}Xe signal moving from well-ventilated lung regions to the tissue barrier and red blood cells; in participants with a predominant MRI

ventilation defect phenotype, a complete picture of the gas exchange abnormalities is impossible.

We were surprised to observe that MRI VDP, along with the oscillometry measurement of distal airways resistance, also predicted 6MWD improvements, which supported the concept of a mechanistic link between exercise intolerance and small airway dysfunction. The observation that improved DL_{CO} and forced vital capacity together explained improved SGRQ score was also consistent with previous reports in hospitalized patients with COVID-19 after discharge.[3,4] A large component of the SGRQ score evaluates exercise limitation. Thus, based on the modelling results reported here, there appears to be a complex relationship or link between exercise intolerance and quality-of-life with MRI, CT and oscillometry measurements of airway dysfunction.

Finally, our results showed that treatment with inhaled or oral airways disease medication at 3-months predicted improved quality-of-life score at 15-months that was greater than the minimal clinically important difference. As treatment of COVID-19 continues to shift from acute to chronic care, the similarities between PACS and symptomatic airways disease has placed emphasis on the treatment of the airway component of PACS.[38] Here, we provided evidence to support airways disease treatment in patients with PACS who have MRI and lung clearance index findings consistent with airways disease.

We acknowledge several study limitations. First, our study had a relatively small sample size with a potential for retention bias towards participants with persistent symptoms and poor quality-of-life. Second, we did not repeat CT imaging at 15-months and hence, were unable to measure potential CT airway, parenchymal, or pulmonary vascular changes at follow-up. Third, we did not acquire ^{129}Xe gas exchange MRI measurements in our current study, as

previously reported.[11-14] Finally, while we reported on prescribed therapies, we did not have any information about the rationale for such patient management decisions. All participants enrolled were followed by a quaternary care team based at local long-COVID clinics and were prescribed treatment plans accordingly, perhaps based on evidence of airways disease as a potential cause of PACS.[38] Thus, we note the possibility of selection bias for participants on prescribed therapy based on recruitment from these clinics.

In conclusion, in this prospective longitudinal investigation 15-months post-infection in participants with post-acute COVID-19 syndrome, we found that ^{129}Xe MRI ventilation defect percent (VDP) improvement was coincident with improved forced expiratory volume in 1-second, diffusing capacity of the lung for carbon monoxide (DL_{CO}), and St. George's Respiratory Questionnaire (SGRQ) score. MRI VDP 3-months post-infection uniquely predicted improved six-minute walk distance, 15-months post-infection, while the changes in both DL_{CO} and forced vital capacity explained the change in SGRQ-score. Treatment with respiratory medication at 3-months was strongly associated with quality-of-life score improvements at 15-months. These positive results may have implications for the monitoring and treatment of patients with PACS as the pandemic evolves.

3.5 References

1. Nalbandian, A., *et al.* Post-acute COVID-19 syndrome. *Nat Med* **27**, 601-615 (2021).

2. Montani, D., *et al.* Post-acute COVID-19 syndrome. *Eur Respir Rev* **31**(2022).

3. Lorent, N., *et al.* Prospective longitudinal evaluation of hospitalised COVID-19 survivors 3 and 12 months after discharge. *ERJ Open Res* **8**(2022).

4. Wu, X., *et al.* 3-month, 6-month, 9-month, and 12-month respiratory outcomes in patients following COVID-19-related hospitalisation: a prospective study. *Lancet Respir Med* **9**, 747-754 (2021).

5. Tran, V.T., Porcher, R., Pane, I. & Ravaud, P. Course of post COVID-19 disease symptoms over time in the ComPaRe long COVID prospective e-cohort. *Nat Commun* **13**, 1812 (2022).

6. Wynberg, E., *et al.* Evolution of Coronavirus Disease 2019 (COVID-19) Symptoms During the First 12 Months After Illness Onset. *Clin Infect Dis* **75**, e482-e490 (2022).

7. Seessle, J., *et al.* Persistent Symptoms in Adult Patients 1 Year After Coronavirus Disease 2019 (COVID-19): A Prospective Cohort Study. *Clin Infect Dis* **74**, 1191-1198 (2022).

8. Myall, K.J., *et al.* Persistent Post-COVID-19 Interstitial Lung Disease. An Observational Study of Corticosteroid Treatment. *Ann Am Thorac Soc* **18**, 799-806 (2021).

9. Kanne, J.P., *et al.* COVID-19 Imaging: What We Know Now and What Remains Unknown. *Radiology* **299**, E262-E279 (2021).

10. Solomon, J.J., Heyman, B., Ko, J.P., Condos, R. & Lynch, D.A. CT of Post-Acute Lung Complications of COVID-19. *Radiology* **301**, E383-E395 (2021).

11. Li, H., *et al.* Damaged lung gas exchange function of discharged COVID-19 patients detected by hyperpolarized (129)Xe MRI. *Sci Adv* **7**(2021).

12. Grist, J.T., *et al.* Hyperpolarized (129)Xe MRI Abnormalities in Dyspneic Patients 3 Months after COVID-19 Pneumonia: Preliminary Results. *Radiology* **301**, E353-E360 (2021).

13. Grist, J.T., *et al.* Lung Abnormalities Depicted with Hyperpolarized Xenon MRI in Patients with Long COVID. *Radiology*, 220069 (2022).

14. Matheson, A.M., *et al.* Persistent (129)Xe MRI Pulmonary and CT Vascular Abnormalities in Symptomatic Individuals with Post-Acute COVID-19 Syndrome. *Radiology*, 220492 (2022).

15. Kooner, H.K., *et al.* (129)Xe MRI ventilation defects in ever-hospitalised and never-hospitalised people with post-acute COVID-19 syndrome. *BMJ Open Respir Res* **9**(2022).

16. Albert, M.S., *et al.* Biological magnetic resonance imaging using laser-polarized 129Xe. *Nature* **370**, 199-201 (1994).

17. Svenningsen, S., *et al.* What are ventilation defects in asthma? *Thorax* **69**, 63-71 (2014).

18. de Lange, E.E., *et al.* Changes in regional airflow obstruction over time in the lungs of patients with asthma: evaluation with 3He MR imaging. *Radiology* **250**, 567-575 (2009).

19. Svenningsen, S., *et al.* Reproducibility of Hyperpolarized (129)Xe MRI Ventilation Defect Percent in Severe Asthma to Evaluate Clinical Trial Feasibility. *Acad Radiol* (2020).

20. Chen, S., *et al.* Relationship between Lung and Brain Injury in COVID-19 Patients: A Hyperpolarized (129)Xe-MRI-based 8-Month Follow-Up. *Biomedicines* **10**(2022).

21. Inui, S., Yoon, S.H., Doganay, O., Gleeson, F.V. & Kim, M. Impaired pulmonary ventilation beyond pneumonia in COVID-19: A preliminary observation. *PloS one* **17**, e0263158 (2022).

22. Jones, P.W., Quirk, F.H., Baveystock, C.M. & Littlejohns, P. A self-complete measure of health status for chronic airflow limitation. The St. George's Respiratory Questionnaire. *Am Rev Respir Dis* **145**, 1321-1327 (1992).

23. Mahler, D.A., *et al.* Development of self-administered versions of modified baseline and transition dyspnea indexes in COPD. *COPD* **1**, 165-172 (2004).

24. Borg, G.A. Psychophysical bases of perceived exertion. *Med Sci Sports Exerc* **14**, 377-381 (1982).

25. Craig, C.L., *et al.* International physical activity questionnaire: 12-country reliability and validity. *Med Sci Sports Exerc* **35**, 1381-1395 (2003).

26. Enright, P.L. The six-minute walk test. *Respir Care* **48**, 783-785 (2003).

27. Miller, M.R., *et al.* Standardisation of spirometry. *Eur Respir J* **26**, 319-338 (2005).

28. Robinson, P.D., *et al.* Consensus statement for inert gas washout measurement using multiple- and single- breath tests. *Eur Respir J* **41**, 507-522 (2013).

29. Macintyre, N., *et al.* Standardisation of the single-breath determination of carbon monoxide uptake in the lung. *Eur Respir J* **26**, 720-735 (2005).

30. King, G.G., *et al.* Technical standards for respiratory oscillometry. *Eur Respir J* **55**(2020).

31. Horsley, A.R., *et al.* Lung clearance index is a sensitive, repeatable and practical measure of airways disease in adults with cystic fibrosis. *Thorax* **63**, 135-140 (2008).

32. Ferrer, M., *et al.* Interpretation of quality of life scores from the St George's Respiratory Questionnaire. *Eur Respir J* **19**, 405-413 (2002).

33. Eddy, R.L., Svenningsen, S., McCormack, D.G. & Parraga, G. What is the minimal clinically important difference for helium-3 magnetic resonance imaging ventilation defects? *Eur Respir J* **51**(2018).

34. Jones, P.W., *et al.* Minimal clinically important differences in pharmacological trials. *Am J Respir Crit Care Med* **189**, 250-255 (2014).

35. Puhan, M.A., *et al.* The minimal important difference of exercise tests in severe COPD. *Eur Respir J* **37**, 784-790 (2011).

36. Jones, P.W. St. George's Respiratory Questionnaire: MCID. *COPD* **2**, 75-79 (2005).

37. Cho, J.L., *et al.* Quantitative Chest CT Assessment of Small Airways Disease in Post-Acute SARS-CoV-2 Infection. *Radiology*, 212170 (2022).

38. Adeloye, D., *et al.* The long-term sequelae of COVID-19: an international consensus on research priorities for patients with pre-existing and new-onset airways disease. *Lancet Respir Med* **9**, 1467-1478 (2021).

3.6 Supplement

3.6.1 Methods

Sample size was calculated as previously described[1] to achieve a power of 80% and two-sided significance value of 5%. The smallest detectable difference for ventilation defect percent (VDP) was previously determined (2% [2]) and the VDP standard deviation in the post-COVID-19 population was 2.9%.[3] Thus, the minimum sample size required was 33 participants.

3.6.2 Results

Table 3-7 shows the demographic characteristics, pulmonary function, questionnaire, and imaging measurements for ever- and never-hospitalized participants at 3- and 15-months post-infection. In the ever-hospitalized group, there was a difference in forced expiratory volume in 1 second (FEV_1) to forced vital capacity (FVC) ratio (74±14, 77±14; *P*=.04) at 15-months as compared to 3-months, while the never-hospitalized group experienced differences in St. George's Respiratory Questionnaire (SGRQ) score (34±20, 26±19; *P*=.02) and VDP (4.6±4.6, 2.9±3.6; *P*=.04).

Table 3-8 shows the demographic characteristics, pulmonary function, questionnaire, and imaging measurements for participants with and without respiratory disease prior to COVID-19 infection. The participants with no respiratory disease reported differences in the proportion of participants prescribed respiratory therapy (14 (45%), 5 (17%); *P*=.02) and combination inhaled corticosteroids and long-acting β-agonists (13 (42%), 4 (14%); *P*=.006), as well as differences in FEV_1 (89±16%$_{pred}$, 97±11%$_{pred}$; P=.009), FEV_1/FVC (79±7, 84±5; *P*=.008), diffusing capacity of the lung for carbon monoxide (DL_{CO}) (88±25%$_{pred}$, 105±22%$_{pred}$; *P*=.009), SGRQ (35±16, 21±21; *P*=.003), and VDP (3.2±2.4%, 1.5±1.1%; *P*<.001) at 15-

months compared to 3-months post-COVID. Participants with respiratory disease reported no differences in any of the measured parameters.

Table 3-9 shows the demographic characteristics, pulmonary function, questionnaire, and imaging measurements for participants dichotomized by a 3-month VDP threshold of 2.0%, which was the mode of the 3-month VDP distribution [4]. Participants with VDP≥2.0% reported differences in FEV_1 (85 ± 20 90 ± 20; *P*=.02), FEV_1/FVC (75±13, 78±14; *P*=.04), SGRQ (34±18, 23±17; *P*=.01), and VDP (8.0±8.5%, 5.3±7.9%; *P*=.004) at 15-months compared to 3-months post-COVID, while participants with VDP<2.0% reported no improvements.

Table 3-12 shows the demographic characteristics, pulmonary function, questionnaire, and imaging measurements for participants that were and were not prescribed airways-disease treatment at 3-months. Participants prescribed airways-disease treatment reported improvements in SGRQ (40±19, 27±21; *P*=.007) over 12-months, while participants not prescribed airways-disease treatment reported no differences.

3.6.3 Discussion

Importantly, participants with post-acute COVID-19 syndrome (PACS) with VDP≥2% measured during the 3-month visit experienced improved FEV_1, FEV_1/FVC, SGRQ score, and VDP 15-months as compared to 3-months post-infection.

We also report relationships for VDP with post-exertional SpO_2 (ρ=.-36, *P*=.009) and lung clearance index (ρ=.59, *P*<.001) 15-months post-COVID infection, which are consistent with similar relationships reported 3-months post-infection.[5] VDP has also been reported to be related to lung clearance index in asthma,[6] cystic fibrosis,[7] and chronic obstructive pulmonary disease (COPD).[8] Thus, it is not surprising to also observe this relationship in PACS. We note that these relationships may be driven by a few participants with greater VDP values as a result

of previous asthma and COPD diagnoses; however, VDP remains related to lung clearance index (ρ=.48, P=.002) even with the removal of these participants.

3.6.4 References

1. Kadam, P. & Bhalerao, S. Sample size calculation. *Int J Ayurveda Res* **1**, 55-57 (2010).

2. Eddy, R.L., Svenningsen, S., McCormack, D.G. & Parraga, G. What is the minimal clinically important difference for helium-3 magnetic resonance imaging ventilation defects? *Eur Respir J* **51**(2018).

3. Li, H., *et al.* Damaged lung gas exchange function of discharged COVID-19 patients detected by hyperpolarized (129)Xe MRI. *Sci Adv* **7**(2021).

4. Eddy, R.L., *et al.* Is Computed Tomography Airway Count Related to Asthma Severity and Airway Structure and Function? *Am J Respir Crit Care Med* **201**, 923-933 (2020).

5. Kooner, H.K., *et al.* (129)Xe MRI ventilation defects in ever-hospitalised and never-hospitalised people with post-acute COVID-19 syndrome. *BMJ Open Respir Res* **9**(2022).

6. Svenningsen, S., Nair, P., Guo, F., McCormack, D.G. & Parraga, G. Is ventilation heterogeneity related to asthma control? *Eur Respir J* **48**, 370-379 (2016).

7. Kanhere, N., *et al.* Correlation of Lung Clearance Index with Hyperpolarized (129)Xe Magnetic Resonance Imaging in Pediatric Subjects with Cystic Fibrosis. *Am J Respir Crit Care Med* **196**, 1073-1075 (2017).

8. Svenningsen, S., *et al.* Lung Clearance Index And Hyperpolarized 3He MRI Ventilation Heterogeneity Measurements In Non-CF Bronchiectasis And COPD. in *A103. REVOLUTIONS IN OBSTRUCTIVE LUNG DISEASE IMAGING* A2255-A2255 (American Thoracic Society, 2015).

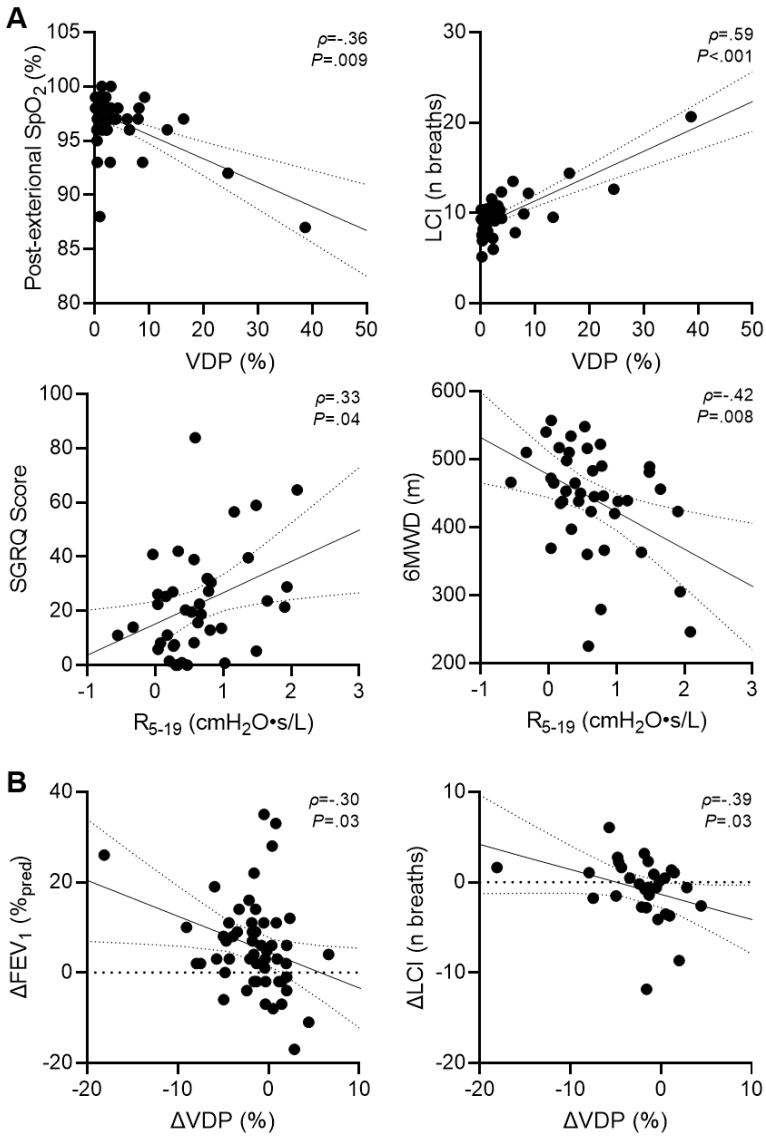

Figure 3-7. Relationships for follow-up measurements
A.
VDP at 15-months and post-exertional SpO_2 at 15-months (ρ=-.36; P=.009; Y=-0.2202X+97.75).
VDP at 15-months and LCI at 15-months (ρ=.59; P<.001; Y=11.52X+15.26).
R_{5-19} at 15-months and SGRQ score at 15-months (ρ=.33; P=.04; Y=-0.8801X+445.6).
R_{5-19} at 15-months and 6MWD at 15-months (ρ=-.42; P=.008; Y=-54.77X+477.4).
B.
15-month change in VDP and FEV_1 (ρ=-.30, P=.03; Y=-0.7945X+4.556).
15-month change in VDP and LCI (ρ=-.39, P=.03; Y=-0.2765X-1.343).

Table 3-4. Baseline Demographic Characteristics and Measurements for participants who participated at 3-months and 15-months

Parameter	With 3-month visit (n=76)	With 15-month visit (n=53)	Sig. *P*
Age years	53 ± 12	54 ± 14	>.99
Female n (%)	38 (50)	27 (51)	>.99
BMI kg/m^2	30 ± 5	31 ± 5	>.99
SpO_2 %	97 ± 2	97 ± 2	>.99
Heart rate beats/min	83 ± 14	81 ± 14	>.99
Blood pressure mmHg	125/82 ± 16/14	127/83 ± 15/10	-
Days Since + COVID Test	97/94: 35-374	96/86: 35-203	>.99
Months Since + COVID Test	3/3: 1-12	3/3: 1-9	>.99
Smoking history pack-years	8 ± 18	10 ± 20	>.99
No Previous Respiratory Disease n (%)	49 (65)	31 (59)	>.99
Previous Respiratory Disease n (%)	27 (36)	22 (42)	>.99
Asthma n (%)	21 (28)	17 (32)	>.99
COPD n (%)	6 (8)	5 (9)	>.99
Hospital Admission* days	13 ± 16	9 ± 6	>.99
Prescribed Respiratory Rx n (%)	37 (49)	29 (55)	>.99
ICS/LABA	33 (43)	26 (49)	>.99
SABA	14 (18)	13 (25)	>.99
OCS	2 (3)	2 (4)	>.99
Pulmonary function			
FEV_1* $\%_{pred}$	85 ± 18	84 ± 21	>.99
FVC* $\%_{pred}$	88 ± 20	87 ± 19	>.99
FEV_1/FVC*	76 ± 11	76 ± 11	>.99
FeNO* ppb	23 ± 14	24 ± 15	>.99
LCI* n breaths	10.5 ± 4.2	10.4 ± 3.9	>.99
DL_{CO}* $\%_{pred}$	89 ± 29	87 ± 23	>.99
R_5* cmH_2O•s/L	3.9 ± 1.7	4.0 ± 1.6	>.99
R_{19}* cmH_2O•s/L	3.1 ± 1.1	3.1 ± 1.1	>.99
R_{5-19}* cmH_2O•s/L	0.8 ± 0.7	0.8 ± 0.7	>.99
Exercise capacity and quality of life			
6MWD* m	454 ± 84	441 ± 85	>.99
SpO_2* post-exertion %	97 ± 3	97 ± 3	>.99
SGRQ*	35 ± 18	35 ± 19	>.99
mMRC*	1 ± 1	1 ± 1	>.99
IPAQ* MET-minutes	4708 ± 4894	3958 ± 4336	>.99
MRI			
VDP %	5.4 ± 7.1	5.8 ± 7.7	>.99
*CT**			
TAC n	270 ± 110	254 ± 94	>.99
WA mm^2	66 ± 2	66 ± 2	>.99
LA mm^2	14 ± 3	14 ± 3	>.99
WT mm	1.4 ± 0.1	1.4 ± 0.1	>.99

Data are reported as mean±standard deviation or mean/median: minimum-maximum.
BMI=body mass index; SpO_2=pulse oximetry estimation of arterial blood oxygen saturation made on a fingertip; COPD=chronic obstructive pulmonary disease; Rx=medical prescription;

ICS=inhaled corticosteroid; LABA=long-acting beta-agonist; SABA=short-acting beta-agonist; OCS=oral corticosteroid; FEV_1=forced expiratory volume in 1 second; $\%_{pred}$=percent of predicted value; FVC=forced vital capacity; FeNO=fractional exhaled nitric oxide; LCI=lung clearance index; DL_{CO}=diffusing capacity of the lungs for carbon monoxide; R_5=oscillometry measurement of total airway resistance; R_{19}=oscillometry measurement of central airway resistance; R_{5-19}=oscillometry measurement of distal airway resistance; 6MWD=six-minute walk distance; SpO_2=pulse oximetry estimation of arterial blood oxygen saturation made on a fingertip; SGRQ=St. George's Respiratory Questionnaire; mMRC=modified Medical Research Council dyspnea score; IPAQ=International Physical Activity Questionnaire; MET=metabolic equivalent; MRI=magnetic resonance imaging; VDP=ventilation defect percent; CT=computed tomography; TAC=total airway count; WA=wall area; LA=lumen area; WT=wall thickness.
P=Holm-Bonferroni corrected significance value for differences between participants with 3-month visit and with 15-month visit; asterisk indicates *P*<.05.
Hospital admission*: With 3-mo visit n=23, with 15-mo visit n=17
FEV_1*, FVC*, FEV_1/FVC*: With 3-mo visit n=75
FeNO*: With 3-mo visit n=43, with 15-mo visit n=33
LCI*: With 3-mo visit n=44, with 15-mo visit n=31
DL_{CO}*: With 15-mo visit n=41
R_5*, R_{19}*, R_{5-19}*: With 15-mo visit n=50
6MWD*, SpO_2*, mMRC*: With 3-mo visit n=66, with 15-mo visit n=46
SGRQ*: With 3-mo visit n=64, with 15-mo visit n=45
IPAQ*: With 3-mo visit n=59, with 15-mo visit n=43
CT*: With 3-mo visit n=44, with 15-mo visit n=33

Table 3-5. Patient Listing of Medications at Research Visit

Participant	Rx 3-months post-COVID	Rx 15-months post-COVID
P01	Symbicort; Salbutamol; Spiriva; Fluticasone; Warfarin; Rosuvastatin; Metoprolol; Spironolactone; Dapagliflozin/Metformin; Sitagliptin; Lorazepam	Aspirin; Diphenhydramine; Mometasone; Symbicort; Spiriva; Salbutamol; Warfarin; Rosuvastatin; Metoprolol; Spironolactone; Dapagliflozin/Metformin; Sitagliptin; Lorazepam
P02	None	None
P03	Indapamide; Gliclazide; Empagliflozin; Atorvastatin; Metformin; Sitagliptin; Tamsulosin; Ranitidine; Levothyroxine; Bisoprolol	Bimatoprost; Salbutamol; Indapamide; Empagliflozin; Atorvastatin; Metformin; Ranitidine
P04	Formoterol-mometasone	Tamsulosin; Colchicine
P05	Pantoprazole; Apixaban	Pantoprazole
P06	Levothyroxine	Levothyroxine; Metoprolol
P07	Symbicort; Amitriptyline; Naproxen; Pregabalin; Rosuvastatin; Sertraline	Candesartan; Amitriptyline; Naproxen; Pregabalin; Rosuvastatin; Sertraline
P08	Salbutamol	None
P09	Olanzapine; Fluoxetine; Quetiapine; Salbutamol	Olanzapine; Fluoxetine;
P10	None	None
P11	Fluticasone propionate-salmeterol; Salbutamol; Desvenlafaxine; Pantoprazole; Aripiprazole	Ezetimibe; Atorvastatin; Fluticasone propionate-salmeterol; Salbutamol; Desvenlafaxine; Pantoprazole
P12	None	None
P13	Symbicort; Atenolol; Hydrochlorothiazide; Candesartan	Tamsulosin; Pantoprazole; Propranolol; Symbicort; Atenolol; Hydrochlorothiazide; Candesartan
P14	Metformin; Rosuvastatin; Amlodipine; Ramipril; Hydrochlorothiazide	Metformin; Rosuvastatin; Amlodipine; Ramipril; Hydrochlorothiazide
P15	Metformin; Irbesartan; Esomeprazole; Tramadol; Azythromycin; Dexamethasone	Pravastatin; Metformin; Irbesartan
P16	Rivarokaban; Levothyroxine; Oral Contraceptive	Levothyroxine; Oral Contraceptive
P17	Symbicort; Singulair; Tresiba; Jardiance; Ezetrol; Insulin; Rivaroxaban; Metformin; Pravastatin; Colchicine; Pantaprazole	Tramadol; Desloratadine; Rosuvastatin; Telmisartan; Tresiba; Insulin; Rivaroxaban; Colchicine
P18	Pregabalin	Amitriptyline; Nabumetone; Pregabalin
P19	Perindopril; Pantoprazole; Rosuvastatin; Spiriva; Ezetimibe; Amlodipine; Bimatropost; Salbutamol; Epipen	Perindopril; Pantoprazole; Rosuvastatin; Spiriva; Ezetimibe; Amlodipine; Bimatropost; Salbutamol; Epipen
P20	Metformin; Symbicort	Metformin
P21	None	None
P22	Gabapentin; Canagiflozin; Levothyroxine; Saxagliptin; Dexlansoprazole; Rosuvastatin; Metformin; Symbicort	Gabapentin; Canagiflozin; Levothyroxine; Saxagliptin; Dexlansoprazole; Rosuvastatin; Metformin
P23	Ustekinumab; Symbicort; Salbutamol	Umeclidinium bromide; Ustekinumab; Symbicort; Salbutamol

P24	Nabilone; Venlafaxine; Ferrous Gluconate; Dexlansoprazole; Rosuvastatin; Levothyroxine; Gabapentin	Irbesartan; Denosumab; Nabilone; Venlafaxine; Ferrous Gluconate; Dexlansoprazole; Rosuvastatin; Levothyroxine; Gabapentin
P25	Trazodone; Bupropion	None
P26	Symbicort	None
P27	None	None
P28	Cetirizine; Trazadone; Rizatriptan; Betahistine	None
P29	Fluticasone propionate-salmeterol; Salbutamol; Statin; Diuretic	Formoterol-mometasone; Spiriva; Budesonide; Metformin
P30	Furosemide; Ciclesonide; Lorazepam; Tamsulosin; Lamotrigine; Spiriva Respimat; Atorvastatin; Symbicort; Ferrous Gluconate; Apixaban; Flecainide; Salbutamol	Diltiazem; Furosemide; Ciclesonide; Tamsulosin; Lamotrigine; Spiriva Respimat; Atorvastatin; Symbicort; Ferrous Gluconate; Apixaban; Flecainide; Salbutamol
P31	None	None
P32	Symbicort; Ipratropium bromide; Beclomethasone Nasal Spray	Statin; Symbicort
P33	Symbicort; Perindopril; Amlodiprine	Statin; Perindopril; Amlodiprine
P34	Symbicort	None
P35	Methylphenidate	Lisdexamfetamine
P36	Furosemide; Ferrous fumurate; Candesartan; Rivaroxaban; Levothyroxine	Vilanterol; Furosemide; Candesartan; Rivaroxaban; Levothyroxine
P37	Tamsulosin; Bisoprolol; Ferrous fumurate; Apixaban; Rosuvastatin; Amlodipine; Finasteride; Fluticasone	Tamsulosin; Bisoprolol; Apixaban; Rosuvastatin; Amlodipine; Finasteride; Fluticasone
P38	Amitryptyline	Symbicort
P39	Bupropion	Bupropion
P40	Formoterol-mometasone; Montelukast; Spiriva; Pantoprazole	Salbutamol; Azithromycin; Formoterol-mometasone; Spiriva;
P41	Formoterol-mometasone; Salbutamol	Formoterol-mometasone
P42	Methylphenidate, Vortioxetine	Vynase, Testosterone
P43	None	None
P44	Spiriva, Symbicort	Spiriva, Symbicort
P45	None	Metformin, Teva-lenoltec, Atrovent, Salbutamol, Pautopratole, Glicazide, Semglutide, Duloxetine, Advair, Atorvastatin, Omnaris, Spiriva
P46	Gliclazide, Duloxetine, Advair, Semaglutide, Ipratropium bromide, Salbutamol, Pantoprazole, Ciclesonide, Spiriva, Atorvastatin, Metformin, Acetaminophen-codeine-caffeine	Premarin, Diropan, Pautoprazole, Trintellix
P47	Conjugated estrogens, Oxybutynin, Pantoprazole, Vortioxetine	Coversyl
P48	Bisoprolol, Bupropion, Metoclopramide	Fluticasone vilanterol, Salbutamol, Carbamazepine, Atorvastatin, Bisoprolol
P49	Fluticasone furoate, Salbutamol, Carbamazepine	Formoterol mometasone

P50	Formoterol-mometasone, Ferrous fumurate	Symbicort, Spiriva
P51	Rupatadine, Mometasone, Montelukast, Oral Contraceptive	None
P52	Levothyroxine, Rabeprazole, Beclometasone, Tiotropium, Salbutamol	Synthroid, Beclomethasone, Salbutamol, Claritin, Tiotropium olodaterol, Salbutamol
P53	Fluticasone salmeterol, Spiriva, Fluticasone propionate, Benralizumab	Fluticasone salmeterol, Spiriva, Fluticasone propionate, Benralizumab

Site 1: P1-P41; Site 2: P42-P53.

Table 3-6. Demographic Characteristics, Pulmonary Function, Questionnaire, and Imaging Measurements at 15-months for participants at both sites

Parameter	Site 1 (n=41)	Site 2 (n=12)	Sig. *P*
Age years	56 ± 14	49 ± 13	.7
Female n (%)	(51)	(50)	>.99
BMI kg/m^2	31 ± 5	30 ± 5	>.99
SpO_2 %	97 ± 2	98 ± 1	>.99
Heart rate beats/min	80 ± 10	78 ± 21	>.99
Blood pressure mmHg	127/81 ± 14/9	123/78 ± 17/10	-
Days Since + COVID Test	461/454: 252-659	414/409: 367-506	.4
Months Since + COVID Test	15/15: 8-22	14/14: 12-17	.3
Smoking history pack-years	8 ± 17	16 ± 30	.9
No Previous Respiratory Disease n (%)	25 (61)	6 (50)	>.99
Previous Respiratory Disease n (%)	16 (39)	6 (50)	>.99
Asthma n (%)	13 (32)	4 (33)	>.99
COPD n (%)	3 (7)	2 (17)	>.99
Hospital Admission days	9 ± 7	7 ± 5	>.99
Prescribed Respiratory Rx n (%)	14 (34)	7 (58)	.9
ICS/LABA	13 (32)	7 (58)	.7
SABA	7 (17)	3 (25)	>.99
OCS	0 (0)	1 (8)	.5
Pulmonary function			
FEV_1 $\%_{pred}$	93 ± 19	81 ± 18	.3
FVC $\%_{pred}$	90 ± 16	87 ± 16	.8
FEV_1/FVC	80 ± 12	75 ± 13	.3
FeNO* ppb	23 ± 21	-	-
LCI n breaths	9.7 ± 2.6	-	-
DL_{CO}* $\%_{pred}$	98 ± 20	101 ± 29	.7
R_5 cmH_2O•s/L	3.5 ± 1.3	-	-
R_{19} cmH_2O•s/L	2.9 ± 0.9	-	-
R_{5-19} cmH_2O•s/L	0.6 ± 0.6	-	-
Exercise capacity and quality-of-life			
6MWD* m	441 ± 79	498 ± 65	.09
SpO_2* post-exertion %	96 ± 3	99 ± 1	.002*
SGRQ*	23 ± 19	36 ± 20	.08
mMRC*	1 ± 1	1 ± 1	.3
IPAQ* MET-minutes	5815 ± 6001	-	-
MRI			
VDP %	4.1 ± 7.4	4.3 ± 4.5	.2

Data are reported as mean±standard deviation or mean/median: minimum-maximum.
BMI=body mass index; SpO_2=pulse oximetry estimation of arterial blood oxygen saturation made on a fingertip; COPD=chronic obstructive pulmonary disease; Rx=medical prescription; ICS=inhaled corticosteroid; LABA=long-acting beta-agonist; SABA=short-acting beta-agonist; OCS=oral corticosteroid; FEV_1=forced expiratory volume in 1 second; $\%_{pred}$=percent of predicted value; FVC=forced vital capacity; FeNO=fractional exhaled nitric oxide; LCI=lung clearance index; DL_{CO}=diffusing capacity of the lungs for carbon monoxide; R_5=oscillometry measurement of total airway resistance; R_{19}=oscillometry measurement of central airway resistance; R_{5-19}=oscillometry measurement of distal airway resistance; 6MWD=six-minute walk distance; SpO_2=pulse oximetry estimation of arterial blood oxygen

saturation made on a fingertip; SGRQ=St. George's Respiratory Questionnaire; mMRC=modified Medical Research Council dyspnea score; IPAQ=International Physical Activity Questionnaire; MET=metabolic equivalent; MRI=magnetic resonance imaging; VDP=ventilation defect percent.
P=Holm-Bonferroni corrected significance value for differences between participants at Site 1 and Site 2; asterisk indicates *P*<.05.
FeNO*: Site 1 n=40
DL_{CO}*: Site 1 n=39, Site 2 n=11
6MWD*, SpO_2*, mMRC*: Site 1 n=40, Site 2 n=11
SGRQ*: Site 2 n=11
IPAQ*: Site 1 n=40

Table 3-7. Demographic Characteristics, Pulmonary Function, Questionnaire, and Imaging Measurements by hospitalization during acute infection

	Ever-Hospitalized (n=17)			Never-Hospitalized (n=36)		
Parameter	3-months	15-months	Sig. *P*	3-months	15-months	Sig. *P*
Age years	57 ± 14	58 ± 14	-	52 ± 14	53 ± 14	-
Female n (%)	5 (29)	5 (29)	-	22 (61)	22 (61)	-
BMI kg/m^2	31 ± 4	32 ± 4	>.99	30 ± 5	30 ± 5	>.99
SpO_2* %	96 ± 2	97 ± 1	>.99	97 ± 2	97 ± 2	>.99
Heart rate* beats/min	81 ± 13	79 ± 10	>.99	81 ± 15	80 ± 14	>.99
Blood pressure* mmHg	128/84 ± 14/11	131/81 ± 15/9	-	127/83 ± 15/9	124/81 ± 15/10	-
Days Since + COVID Test	96/84: 38-208	442/441: 252-608	-	96/90: 35-275	454/445: 360-659	-
Months Since + COVID Test	3/3: 1-7	15/15: 8-20	-	3/3: 1-9	15/15: 12-22	-
Smoking history pack-years	11 ± 24	11 ± 24	-	10 ± 19	10 ± 19	-
No Previous Respiratory Disease n (%)	10 (59)	10 (59)	-	23 (63)	21 (58)	-
Previous Respiratory Disease n (%)	7 (41)	7 (41)	-	13 (36)	15 (42)	-
Asthma n (%)	5 (29)	5 (29)	-	11 (31)	12 (33)	-
COPD n (%)	2 (12)	2 (12)	-	2 (6)	3 (8)	-
Hospital Admission days	9 ± 6	9 ± 6	-	-	-	-
Prescribed Respiratory Rx n (%)	11 (65)	9 (53)	>.99	18 (50)	12 (33)	>.99
ICS/LABA	9 (53)	8 (47)	>.99	17 (47)	12 (33)	>.99
SABA	6 (35)	6 (35)	>.99	7 (19)	4 (11)	>.99
OCS	1 (6)	0 (0)	>.99	1 (3)	1 (3)	>.99
Pulmonary function						
FEV_1 $\%_{pred}$	79 ± 20	87 ± 16	.4	86 ± 21	91 ± 20	.07
FVC* $\%_{pred}$	83 ± 17	88 ± 11	>.99	89 ± 20	90 ± 18	>.99
FEV_1/FVC*	74 ± 14	77 ± 14	.04*	77 ± 10	80 ± 11	.2
FeNO* ppb	26 ± 9	34 ± 31	>.99	23 ± 17	19 ± 14	.3
LCI* n breaths	11.0 ± 5.4	9.1 ± 2.3	>.99	10.0 ± 2.7	10.0 ± 2.0	>.99
DL_{CO}* $\%_{pred}$	78 ± 20	94 ± 23	.6	90 ± 21	100 ± 22	.07
R_5* cmH_2O•s/L	3.7 ± 1.6	3.5 ± 1.2	>.99	3.8 ± 1.8	3.7 ± 1.5	>.99
R_{19}* cmH_2O•s/L	2.4 ± 0.8	2.8 ± 0.8	>.99	3.0 ± 1.2	3.0 ± 1.0	>.99
R_{5-19}* cmH_2O•s/L	0.9 ± 0.8	0.7 ± 0.6	>.99	0.8 ± 0.7	0.6 ± 0.7	>.99
Exercise capacity and quality of life						
6MWD* m	399 ± 88	452 ± 50	.9	460 ± 78	470 ± 72	>.99
SpO_2* post-exertion %	95 ± 6	95 ± 4	>.99	97 ± 2	98 ± 1	>.99
SGRQ*	38 ± 14	21 ± 21	.4	34 ± 20	26 ± 19	.02*
mMRC*	1 ± 1	1 ± 1	>.99	1 ± 1	1 ± 1	>.99
IPAQ* MET-minutes	2952±3499	5422±4950	>.99	4099±4731	6191±7142	>.99
MRI						
VDP %	8.3 ± 11.7	7.0 ± 10.5	>.99	4.6 ± 4.6	2.9 ± 3.6	.04*

Data are reported as mean±standard deviation or mean/median: minimum-maximum.

BMI=body mass index; SpO_2=pulse oximetry estimation of arterial blood oxygen saturation made on a fingertip; COPD=chronic obstructive pulmonary disease; Rx=medical prescription; ICS=inhaled corticosteroid; LABA=long-acting beta-agonist; SABA=short-acting beta-agonist; OCS=oral corticosteroid; FEV_1=forced expiratory volume in 1 second; $\%_{pred}$=percent of predicted value; FVC=forced vital capacity; FeNO=fractional exhaled nitric oxide; LCI=lung clearance index; DL_{CO}=diffusing capacity of the lungs for carbon monoxide; R_5=oscillometry measurement of total airway resistance; R_{19}=oscillometry measurement of central airway resistance; R_{5-19}=oscillometry measurement of distal airway resistance; 6MWD=six-minute walk distance; SpO_2=pulse oximetry estimation of arterial blood oxygen saturation made on a fingertip; SGRQ=St. George's Respiratory Questionnaire; mMRC=modified Medical Research Council dyspnea score; IPAQ=International Physical Activity Questionnaire; MET=metabolic equivalent; MRI=magnetic resonance imaging; VDP=ventilation defect percent.
P=Holm-Bonferroni corrected significance value for differences between 3- and 15-months post-COVID infection; asterisk indicates *P*<.05.
SpO_2*, Heart rate*, Blood pressure*: Ever-hospitalized n=16
FVC*, FEV_1/FVC*: Never-hospitalized n=35
FeNO*: Ever-hospitalized n=11, never-hospitalized n=22
LCI*: Ever-hospitalized n=12, never-hospitalized n=19
DL_{CO}*: Ever-hospitalized n=13, never-hospitalized n=26
R_5*, R_{19}*, R_{5-19}*: Ever-hospitalized n=13, never-hospitalized n=25
6MWD*, SGRQ*: Ever-hospitalized n=12, never-hospitalized n=32
SpO_2* post-exertion: Ever-hospitalized n=12, never-hospitalized n=31
mMRC*: Ever-hospitalized n=13, never-hospitalized n=31
IPAQ*: Ever-hospitalized n=9, never-hospitalized n=22

Table 3-8. Demographic Characteristics, Pulmonary Function, Questionnaire, and Imaging Measurements by diagnosed respiratory disease

	No Respiratory Disease (n=31)			Respiratory Disease (n=22)		
Parameter	3-months	15-months	Sig. *P*	3-months	15-months	Sig. *P*
Age years	51 ± 13	52 ± 14	-	58 ± 14	59 ± 13	-
Female n (%)	15 (48)	15 (48)	-	12 (55)	12 (55)	-
BMI kg/m^2	31 ± 5	31 ± 5	>.99	30 ± 5	31 ± 5	>.99
SpO_2 %	97 ± 2	97 ± 1	.7	97 ± 2	97 ± 2	>.99
Heart rate beats/min	80 ± 14	79 ± 12	.6	83 ± 14	80 ± 14	>.99
Blood pressure mmHg	128/84 ± 13/9	129/81 ± 14/9	-	126/83 ± 16/11	123/80 ± 15/10	-
Days Since + COVID Test	101/92: 35-275	451/435: 252-659	-	89/82: 39-203	450/451: 360-542	-
Months Since + COVID Test	3/3: 1-9	15/15: 8-22	-	3/3: 1-7	15/15: 12-18	-
Smoking history pack-years	5 ± 14	5 ± 14	-	16 ± 26	16 ± 25	-
Hospitalized n (%)	10 (32)	10 (34)	-	7 (32)	7 (29)	-
Hospital Admission days	10 ± 10	10 ± 7	-	8 ± 5	8 ± 5	-
Prescribed Respiratory Rx n (%)	14 (45)	5 (17)	.02*	15 (68)	16 (67)	>.99
ICS/LABA	13 (42)	4 (14)	.006*	13 (59)	16 (67)	>.99
SABA	3 (10)	1 (3)	>.99	10 (45)	9 (38)	>.99
OCS	1 (3)	0 (0)	.9	1 (5)	1 (4)	>.99
Pulmonary function						
FEV_1 $\%_{pred}$	89 ± 16	97 ± 11	.009*	76 ± 25	82 ± 23	.6
FVC $\%_{pred}$	89 ± 17	91 ± 12	>.99	85 ± 21	89 ± 20	>.99
FEV_1/FVC	79 ± 7	84 ± 5	.008*	71 ± 15	73 ± 15	>.99
FeNO* ppb	25 ± 16	22 ± 22	>.99	22 ± 13	25 ± 19	>.99
LCI* n breaths	10.4 ± 3.8	8.8 ± 1.5	.6	10.4 ± 4.1	10.9 ± 3.2	>.99
DL_{CO}* $\%_{pred}$	88 ± 25	105 ± 22	.009*	83 ± 14	92 ± 20	>.99
R_5* cmH_2O•s/L	3.7 ± 1.5	3.4 ± 1.1	>.99	4.0 ± 1.9	3.8 ± 1.6	>.99
R_{19}* cmH_2O•s/L	2.9 ± 1.0	2.8 ± 0.8	>.99	3.0 ± 1.3	3.1 ± 1.0	.9
R_{5-19}* cmH_2O•s/L	1.0 ± 0.8	0.6 ± 0.5	.8	0.8 ± 0.7	0.7 ± 0.7	.06
Exercise capacity and quality of life						
6MWD* m	463 ± 72	461 ± 89	.4	412 ± 94	445 ± 67	.5
SpO_2* post-exertion %	97 ± 4	97 ± 2	.3	97 ± 3	96 ± 3	.8
SGRQ*	35 ± 16	21 ± 21	.003*	37 ± 22	30 ± 18	.2
mMRC*	1 ± 1	1 ± 1	.4	1 ± 1	1 ± 1	.6
IPAQ* MET-minutes	4830±5087	5897±5483	.5	2624±2410	5703±6814	.5
MRI						
VDP %	3.2 ± 2.4	1.5 ± 1.1	<.001*	9.4 ± 10.7	7.4 ± 9.1	.2

Data are reported as mean±standard deviation or mean/median: minimum-maximum.
BMI=body mass index; SpO_2=pulse oximetry estimation of arterial blood oxygen saturation made on a fingertip; Rx=medical prescription; ICS=inhaled corticosteroid; LABA=long-acting beta-agonist; SABA=short-acting beta-agonist; OCS=oral corticosteroid; FEV_1=forced

expiratory volume in 1 second; $\%_{pred}$=percent of predicted value; FVC=forced vital capacity; FeNO=fractional exhaled nitric oxide; LCI=lung clearance index; DL_{CO}=diffusing capacity of the lungs for carbon monoxide; R_5=oscillometry measurement of total airway resistance; R_{19}=oscillometry measurement of central airway resistance; R_{5-19}=oscillometry measurement of distal airway resistance; 6MWD=six-minute walk distance; SpO_2=pulse oximetry estimation of arterial blood oxygen saturation made on a fingertip; SGRQ=St. George's Respiratory Questionnaire; mMRC=modified Medical Research Council dyspnea score; IPAQ=International Physical Activity Questionnaire; MET=metabolic equivalent; VDP=ventilation defect percent.

P=Holm-Bonferroni corrected significance value for differences between 3 months and 15 months post-COVID infection; asterisk indicates *P*<.05.

FeNO*: 3-mo no resp disease n=12, 3-mo resp disease n=12, 15-mo no resp disease n=23, 15-mo resp disease n=17

LCI*: 3-mo no resp disease n=19, 3-mo resp disease n=12, 15-mo no resp disease n=23, 15-mo resp disease n=18

DL_{CO}*: 3-mo no resp disease n=25, 3-mo resp disease n=16, 15-mo no resp disease n=28, 15-mo resp disease n=22

R_5*, R_{19}*, R_{5-19}*: 3-mo no resp disease n=22, 3-mo resp disease n=16, 15-mo no resp disease n=23, 15-mo resp disease n=18

6MWD*: 3-mo no resp disease n=26, 3-mo resp disease n=20, 15-mo no resp disease n=28, 15-mo resp disease n=23

SpO_2*: 3-mo no resp disease n=26, 3-mo resp disease n=19, 15-mo no resp disease n=28, 15-mo resp disease n=23

SGRQ*: 3-mo no resp disease n=26, 3-mo resp disease n=19, 15-mo no resp disease n=28,

mMRC*: 3-mo no resp disease n=26, 3-mo resp disease n=20, 15-mo no resp disease n=28, 15-mo resp disease n=23

IPAQ*: 3-mo no resp disease n=26, 3-mo resp disease n=17, 15-mo no resp disease n=23, 15-mo resp disease n=17

Table 3-9. Demographics Characteristics, Pulmonary Function, Questionnaire, and Imaging Measurements by VDP

	3-month VDP<2.0% (n=17)			3-month VDP≥2.0% (n=36)		
Parameter	3-months	15-months	Sig. *P*	3-months	15-months	Sig. *P*
Age years	43 ± 11	44 ± 11	-	59 ± 12	60 ± 12	-
Female n (%)	10 (59)	10 (59)	-	17 (47)	17 (47)	-
BMI kg/m^2	29 ± 5	29 ± 4	.8	31 ± 5	31 ± 5	>.99
SpO_2* %	98 ± 2	98 ± 1	>.99	96 ± 2	97 ± 1	>.99
Heart rate* beats/min	89 ± 14	76 ± 12	.2	77 ± 13	81 ± 13	>.99
Blood pressure* mmHg	127/82 ± 15/11	127/81 ± 18/11	-	127/84 ± 15/9	126/81 ± 13/8	-
Days Since + COVID Test	101/94: 38-208	441/431: 252-608	-	94/86: 35-275	455/449: 360-659	-
Months Since + COVID Test	3/3: 1-7	15/14: 8-20	-	3/3 1-9	15/15: 12-22	-
Smoking history pack-years	2 ± 4	2 ± 4	-	14 ± 24	14 ± 24	-
No Previous Respiratory Disease n (%)	10 (59)	10 (59)	-	21 (58)	19 (53)	-
Previous Respiratory Disease n (%)	7 (41)	7 (41)	-	15 (42)	17 (47)	-
Asthma n (%)	7 (41)	7 (41)	-	10 (28)	11 (31)	-
COPD n (%)	0 (0)	0 (0)	-	5 (14)	6 (17)	-
Hospitalized n (%)	5 (29)	5 (29)	-	12 (33)	12 (33)	
Hospital Admission days	6 ± 4	6 ± 4	-	10 ± 7	10 ± 7	-
Prescribed Respiratory Rx n (%)	9 (53)	6 (35)	>.99	20 (56)	15 (42)	>.99
ICS/LABA	8 (47)	6 (35)	>.99	18 (50)	14 (39)	>.99
SABA	4 (24)	2 (12)	>.99	9 (25)	8 (22)	>.99
OCS	2 (12)	1 (6)	>.99	0 (0)	0 (0)	>.99
Pulmonary function						
FEV_1 $\%_{pred}$	83 ± 22	90 ± 17	.9	85 ± 20	90 ± 20	.02*
FVC* $\%_{pred}$	86 ± 20	87 ± 14	>.99	88 ± 19	91 ± 17	>.99
FEV_1/FVC*	79 ± 9	82 ± 7	>.99	75 ± 13	78 ± 14	.04*
FeNO* ppb	24 ± 15	33 ± 35	>.99	24 ± 15	20 ± 14	>.99
LCI* n breaths	9.3 ± 0.8	8.0 ± 1.5	>.99	10.7 ± 4.4	10.1 ± 2.1	>.99
DL_{CO}* $\%_{pred}$	93 ± 24	107 ± 23	.2	83 ± 20	93 ± 20	.1
R_5* cmH_2O•s/L	3.9 ± 2.0	3.5 ± 1.6	>.99	3.8 ± 1.6	3.7 ± 1.3	>.99
R_{19}* cmH_2O•s/L	3.1 ± 1.3	2.9 ± 1.0	>.99	2.9 ± 1.0	3.0 ± 0.9	>.99
R_{5-19}* cmH_2O•s/L	0.9 ± 0.8	0.6 ± 0.7	.9	0.9 ± 0.7	0.7 ± 0.6	.7
Exercise capacity and quality of life						
6MWD* m	474 ± 56	485 ± 62	>.99	427 ± 93	455 ± 68	.3
SpO_2* post-exertion %	98 ± 2	98 ± 1	>.99	96 ± 4	96 ± 3	>.99
SGRQ*	38 ± 21	29 ± 23	>.99	34 ± 18	23 ± 17	.01*
mMRC*	1 ± 1	1 ± 1	>.99	1 ± 1	1 ± 1	>.99
IPAQ* MET-minutes	3727 ± 1839	10971 ± 9214	.98	3777 ± 4918	4509 ± 4825	>.99
MRI						
VDP %	1.1 ± 0.6	1.9 ± 2.2	>.99	8.0 ± 8.5	5.3 ± 7.9	.004*

Data are reported as mean±standard deviation or mean/median: minimum-maximum.
BMI=body mass index; SpO_2=pulse oximetry estimation of arterial blood oxygen saturation made on a fingertip; COPD=chronic obstructive pulmonary disease; Rx=medical prescription; ICS=inhaled corticosteroid; LABA=long-acting beta-agonist; SABA=short-acting beta-agonist; OCS=oral corticosteroid; FEV_1=forced expiratory volume in 1 second; $\%_{pred}$=percent of predicted value; FVC=forced vital capacity; FeNO=fractional exhaled nitric oxide; LCI=lung clearance index; DL_{CO}=diffusing capacity of the lungs for carbon monoxide; R_5=oscillometry measurement of total airway resistance; R_{19}=oscillometry measurement of central airway resistance; R_{5-19}=oscillometry measurement of distal airway resistance; 6MWD=six-minute walk distance; SpO_2=pulse oximetry estimation of arterial blood oxygen saturation made on a fingertip; SGRQ=St. George's Respiratory Questionnaire; mMRC=modified Medical Research Council dyspnea score; IPAQ=International Physical Activity Questionnaire; MET=metabolic equivalent; MRI=magnetic resonance imaging; VDP=ventilation defect percent.
p=Holm-Bonferroni corrected significance value for differences between 3-months and 15-months
SpO_2*, Heart rate*, Blood pressure*: VDP≥2.0% n=35
FVC*, FEV_1/FVC*: VDP<2.0% n=16
FeNO*: VDP<2.0% n=9, VDP≥2.0% n=24
LCI*, IPAQ*: VDP<2.0% n=7, VDP≥2.0% n=24
DL_{CO}*: VDP<2.0% n=13, VDP≥2.0% n=26
R_5*, R_{19}*, R_{5-19}*: VDP<2.0% n=9, VDP≥2.0% n=29
6MWD*, VDP<2.0% n=15, VDP≥2.0% n=29
SpO_2* post-exertion: VDP<2.0% n=15, VDP≥2.0% n=28
SGRQ*, mMRC*: VDP<2.0% n=14, VDP≥2.0% n=30

Table 3-10. Correlations for Potential Predictor Variables in Linear Regression Models

	Δ6MWD		ΔVDP		ΔSGRQ	
Predictor variables 3-months post-infection	ρ	*P*	ρ	*P*	ρ	*P*
FeNO	-.11	.6	-.28	.1	-.28	.1
FEV_1 $\%_{pred}$	.18	.3	-.14	.3	-.04	.8
FVC $\%_{pred}$	.17	.3	-.02	.9	.05	.8
FEV_1/FVC	-.06	.7	-.15	.3	-.09	.6
LCI	.04	.9	.37	.04	.21	.3
DL_{CO} $\%_{pred}$	-.04	.8	-.08	.6	-.04	.8
R_5	.04	.8	.03	.9	-.11	.6
R_{19}	-.06	.7	-.03	.9	-.16	.4
R_{5-19}	.24	.2	.17	.3	.13	.5
6MWD	-.53	<.001	-.03	.9	.12	>.99
SpO_2 post-exertion	-.32	.04	.25	.1	.14	.4
SGRQ	.20	.2	.11	.5	-.39	.01
IPAQ	-.01	.9	.14	.4	-.15	.3
mMRC	.30	.05	.16	.3	-.21	.2
TAC	.02	.9	-.04	.8	.27	.1
WA	-.30	.1	-.27	.1	-.26	.2
LA	-.002	.9	-.13	.4	.32	.08
WT	-.21	.3	-.18	.3	.36	.05
VDP	.23	.1	-.55	<.001	.04	.8
ΔFeNO	.22	.2	.15	.4	.09	.6
ΔFEV_1 $\%_{pred}$	-.25	.2	-.34	.03	-.16	.4
ΔFVC $\%_{pred}$	-.05	.8	-.25	.1	-.13	.5
ΔFEV_1/FVC	.06	.7	-.05	.8	-.10	.6
ΔLCI	.03	.9	-.39	.03	.07	.8
ΔDL_{CO} $\%_{pred}$	-.13	.6	.21	.3	-.40	.06
ΔR_5	-.05	.8	.04	.8	.23	.2
ΔR_{19}	.03	.9	.14	.4	.26	.1
ΔR_{5-19}	-.11	.5	-.05	.8	.09	.6
Δ6MWD	1.0	-	.29	.1	-.23	.2
ΔSpO_2 post-exertion	.12	.5	-.11	.6	-.23	.2
ΔSGRQ	-.23	.2	.10	.6	1.0	-
ΔIPAQ	.29	.1	.16	.4	-.30	.1
ΔmMRC	-.14	.4	-.02	.9	.34	.06
ΔVDP	.1	-.11	1.0	-	.10	.6

FeNO=fractional exhaled nitric oxide; FEV_1=forced expiratory volume in 1 second; $\%_{pred}$=percent of predicted value; FVC=forced vital capacity; LCI=lung clearance index; DL_{CO}=diffusing capacity of the lungs for carbon monoxide; R_5=oscillometry measurement of total airway resistance; R_{19}=oscillometry measurement of central airway resistance; R_{5-19}=oscillometry measurement of distal airway resistance; 6MWD=six-minute walk distance; SpO_2=pulse oximetry estimation of arterial blood oxygen saturation made on a fingertip; SGRQ=St. George's respiratory capacity; IPAQ=international physical activity questionnaire; mMRC=modified medical research council dyspnea scale; TAC=total airway count; WA=wall

area; LA=lumen area; WT=wall thickness; VDP=ventilation defect percent; Δ=change from 3- to 15-months post-COVID infection; ρ=Spearman correlation coefficient; *P*=uncorrected *P* value.

Table 3-11. Prior respiratory illness and prescribed respiratory Rx

	YES Prior Respiratory Illness n=22	NO Prior Respiratory Illness n=31
YES Respiratory Rx n=29	n=15 (68%; 52%*)	n=14 (45%; 48%*)
NO Respiratory Rx n=24	n=7 (32%; 29%**)	n=17 (55%; 71%**)

*Proportion of participants prescribed Respiratory Rx

**Proportion of participants not prescribed Respiratory Rx

Table 3-12. Demographic Characteristics, Pulmonary Function, Questionnaire, and Imaging Measurements by airways-disease treatment at 3-months

	Airways-disease treatment (n=29)			No airways-disease treatment (n=24)		
Parameter	3-months	15-months	Sig. *P*	3-months	15-months	Sig. *P*
Age years	56 ± 13	57 ± 13	-	51 ± 15	52 ± 15	-
Female n (%)	16 (55)	16 (55)	-	11 (46)	11 (46)	-
BMI kg/m^2	31 ± 5	31 ± 4	>.99	30 ± 5	30 ± 5	>.99
SpO_2 %	97 ± 2	97 ± 1	.4	97 ± 2	97 ± 2	>.99
Heart rate beats/min	82 ± 13	81 ± 14	.9	80 ± 15	77 ± 11	>.99
Blood pressure mmHg	127/83 ± 13/9	125/81 ± 14/9	-	128/84 ± 16/11	128/80 ± 15/10	-
Days Since + COVID Test	99/94: 35-275	449/438: 252-659	-	93/78: 37-203	452/445: 360-551	-
Months Since + COVID Test	3/3: 1-9	15/15: 8-22	-	3/3: 1-7	15/15: 12-18	-
Smoking history pack-years	11 ± 23	11 ± 23	-	8 ± 17	8 ± 17	-
No Previous Respiratory Disease n (%)	14 (48)	13 (45)	-	17 (71)	16 (67)	-
Previous Respiratory Disease n (%)	15 (52)	16 (55)	-	7 (29)	8 (33)	-
Asthma n (%)	12 (41)	12 (41)	-	5 (21)	6 (25)	-
COPD n (%)	3 (10)	4 (14)	-	2 (8)	2 (8)	-
Hospitalized n (%)	11 (38)	11 (38)	-	6 (25)	6 (25)	-
Hospital Admission days	10 ± 7	10 ± 7	-	7 ± 5	7 ± 5	-
Pulmonary function						
FEV_1 $\%_{pred}$	79 ± 24	85 ± 21	.1	89 ± 14	95 ± 15	.1
FVC $\%_{pred}$	86 ± 23	89 ± 18	>.99	89 ± 14	90 ± 14	>.99
FEV_1/FVC*	73 ± 12	76 ± 14	.1	80 ± 9	82 ± 9	.3
FeNO* ppb	25 ± 13	28 ± 28	>.99	24 ± 17	20 ± 14	>.99
LCI* n breaths	11.4 ± 4.8	10.5 ± 2.0	>.99	9.1 ± 2.0	8.7 ± 1.8	>.99
DL_{CO}* $\%_{pred}$	82 ± 22	97 ± 21	.07	91 ± 20	99 ± 23	.4
R_5* cmH_2O•s/L	4.4 ± 1.9	4.1 ± 1.5	>.99	3.1 ± 1.2	3.1 ± 1.0	>.99
R_{19}* cmH_2O•s/L	3.3 ± 1.2	3.2 ± 1.0	>.99	2.6 ± 0.8	2.8 ± 0.8	>.99
R_{5-19}* cmH_2O•s/L	1.1 ± 0.8	0.9 ± 0.7	.1	0.5 ± 0.5	0.4 ± 0.4	>.99
Exercise capacity and quality of life						
6MWD* m	424 ± 100	458 ± 72	.3	466 ± 57	474 ± 60	>.99
SpO_2* post-exertion %	96 ± 4	96 ± 3	>.99	98 ± 1	98 ± 1	>.99
SGRQ*	40 ± 19	27 ± 21	.007*	29 ± 17	21 ± 17	.9
mMRC*	1 ± 1	1 ± 1	>.99	1 ± 1	1 ± 1	>.99
IPAQ* MET-minutes	2172 ± 2090	4423 ± 4260	.2	5466 ± 5523	7616 ± 8106	>.99
MRI						
VDP %	7.3 ± 9.7	5.7 ± 8.4	.7	4.0 ± 3.5	2.3 ± 3.3	.3

Data are reported as mean±standard deviation or mean/median: minimum-maximum.
BMI=body mass index; SpO_2=pulse oximetry estimation of arterial blood oxygen saturation made on a fingertip; COPD=chronic obstructive pulmonary disease; FEV_1=forced expiratory volume in 1 second; $\%_{pred}$=percent of predicted value; FVC=forced vital capacity; FeNO=fractional exhaled nitric oxide; LCI=lung clearance index; DL_{CO}=diffusing capacity of

the lungs for carbon monoxide; R_5=oscillometry measurement of total airway resistance; R_{19}=oscillometry measurement of central airway resistance; R_{5-19}=oscillometry measurement of distal airway resistance; 6MWD=six-minute walk distance; SpO_2=pulse oximetry estimation of arterial blood oxygen saturation made on a fingertip; SGRQ=St. George's Respiratory Questionnaire; mMRC=modified Medical Research Council dyspnea score; IPAQ=International Physical Activity Questionnaire; MET=metabolic equivalent; MRI=magnetic resonance imaging; VDP=ventilation defect percent.
P=Holm-Bonferroni corrected significance value for differences between 3-months and 15-months post-COVID infection; asterisk indicates $P<.05$.
SpO_2*, Heart rate*, Blood pressure*, FVC*, FEV_1/FVC*: No airways-disease treatment n=23
FeNO*: Airways-disease treatment n=17, no airways-disease treatment n=16
LCI*: Airways-disease treatment n=17, no airways-disease treatment n=14
DL_{CO}*: Airways-disease treatment n=21, no airways-disease treatment n=18
R_5*, R_{19}*, R_{5-19}*: Airways-disease treatment n=20, no airways-disease treatment n=18
6MWD*: Airways-disease treatment n=24, no airways-disease treatment n=20
SpO_2* post-exertion: Airways-disease treatment n=24, no airways-disease treatment n=19
SGRQ*, mMRC*: Airways-disease treatment n=25, no airways-disease treatment n=19
IPAQ*: Airways-disease treatment n=16, no airways-disease treatment n=15

Chapter 4

4 CHEST CT AIRWAY AND VASCULAR MEASUREMENTS IN FEMALES WITH LONG-COVID, EX-SMOKERS AND COPD PATIENTS

To contextualize the sex differences in CT airway and pulmonary vascular measurements in females and males with long-COVID, quantitative CT measurements in females with long-COVID were compared to female ex-smokers with and without COPD.

The contents of this chapter were submitted to the journal Respirology: HK Kooner, PV Wyszkiewicz, AM Matheson, MJ McIntosh, M Abdelrazek, I Dhaliwal, JM Nicholson, M Kirby, S Svenningsen, and G Parraga. Chest CT Airway and Vascular Measurements in Females with Long-COVID, Ex-smokers and COPD Patients. Submitted to Respirology (Manuscript ID RES-24-007).

4.1 Introduction

The coronavirus 2019 (COVID-19) pandemic has resulted in an acute disease burden which was disproportionately greater in male patients.[1-3] The male sex disparity in incidence, hospitalization, and mortality from COVID-19 has been well documented.[1,2] In contrast, females were observed to be more likely to experience persistent symptoms and poor quality-of-life, post-COVID infection,[3,4] a condition commonly referred to as post-acute COVID-19 syndrome[5] or long-COVID.[6] There have been suggestions that differences in immune function between males and females[7,8] may be partially responsible for sex differences in the expression of long-COVID. But, until now, the lung pathologies that may underly these differences have not been investigated.

Sex differences in health outcomes have also been reported in obstructive lung diseases, such as asthma and chronic obstructive pulmonary disease (COPD).[9,10] Female never-smokers are more likely to develop COPD and appear to have greater risk of COPD when accounting for age, smoking status, income, ethnicity, and education.[9] In addition, current smokers who are female experience a more rapid decline in pulmonary function as compared to males, even

when smoking fewer cigarettes.[11,12] This has been speculated to be driven by anatomical differences in lung and/or airway size resulting in a higher "dose" per cigarette for females[9] or greater concentration of tobacco smoke on the surface of the small airways.[10] In addition, the histological patterns of COPD differ in females and are predominated by small airways disease, which is characterized by smaller lumen size and thicker airway walls, rather than emphysema.[13]

Chest x-ray computed tomography (CT) imaging provides a way to quantify the architecture of the pulmonary airways and vascular tree. Although there are indirect methods to measure or estimate airway size,[14-16] quantitative CT airway segmentation yields sensitive measurements of airway wall thickness, luminal area, and the total number of airways. It is well known that there is physiologic variability in the respiratory system[15] and airway differences between females and males can be directly quantified using chest CT.[17-20] Females have been reported to have thinner airway walls[21,22] and narrower lumens[17-19] compared to males of the same size and age. Differences between females and males were also observed for CT measurements of emphysema[13,23] and airways disease[13,24] in patients with COPD. More recently, sex differences in CT airway measurements were also associated with worse outcomes in female COPD patients.[20] Quantitative chest CT measurements in patients with long-COVID also revealed sex differences.[25] In females with long-COVID, there was significantly lower total airway count, narrower airway lumen and thinner airway walls, as compared to males with long-COVID, in the absence of sex differences in pulmonary function or exercise capacity.[25] In addition, these CT airway measurements were coincident with airway dysfunction measured using ^{129}Xe magnetic resonance imaging (MRI) ventilation defect percent in the context of normal spirometry.[26,27]

To explore the potential mechanisms that underly the augmented prevalence as well as respiratory symptoms and quality-of-life deficits in females with long-COVID, chest CT airway and pulmonary vascular measurements were evaluated and compared to the same measurements in female ex-smokers and patients with COPD.

4.2 Study Design and Methods

4.2.1 Study Participants and Design

In this prospective study, participants with long-COVID were recruited 3-months post-infection in a convenience series between July 2020 and August 2021 from two quaternary care centers and research sites (Site 1: Robarts Research Institute, London Canada; Site 2: St Joseph's Healthcare Hamilton, Hamilton Canada) and all provided written-informed consent to ethics board (HSREB #113224 London; HiREB #12672, Hamilton), Health Canada-approved protocols (www.clinicaltrials.gov NCT05014516). Inclusion criteria and participant recruitment were previously described.[27] Briefly, inclusion criteria consisted of individuals aged 18 to 80 years with a public-health confirmed case of COVID-19 and persistent symptoms, including but not limited to respiratory, neurological, and metabolic systems. Exclusion criteria included MRI contraindications and inability to return for follow-up.

The comparator groups of ex-smokers with and without COPD also provided written informed consent to a study protocol approved by an ethics board (HSREB #00000984) in compliance with a Health Canada approved and registered protocol (www.clinicaltrials.gov NCT02279329). All participants were recruited from a tertiary-care academic centre and by advertisement between 2009 and 2012 as a convenience sample. Inclusion criteria included age between 50 and 85 years and a history of cigarette smoking >10 pack-years, as previously described.[28]

All participants completed spirometry, diffusing capacity of the lung for carbon monoxide (DL_{CO}), the St. George's Respiratory Questionnaire (SGRQ),[29]six-minute walk test (6MWT)[30] and thoracic CT.

4.2.2 Pulmonary Function Tests and Questionnaires

Participants completed spirometry for forced expiratory volume in 1-second (FEV_1) and forced vital capacity (FVC), according to American Thoracic Society guidelines,[31] using the EasyOne Pro LAB system (ndd Medical Technologies, Zurich, Switzerland) or a whole-body plethysmograph (MedGraphics Corporation, St. Paul, MN, USA). DL_{CO} was also measured using the EasyOne Pro LAB system or the plethysmograph, according to European Respiratory Society guidelines.[32] Post-bronchodilator measurements were performed 15 minutes after inhalation of 4×100µg Salbutamol sulfate norflurane (Ivax Pharmaceuticals, Waterford, Ireland) using an AeroChamber (Trudell Medical International, London, ON, Canada). Participants withheld respiratory medications before each study visit according to American Thoracic Society guidelines.[31] SGRQ and 6MWT were administered under supervision of study personnel.

4.2.3 Thoracic Imaging

CT was acquired, as previously described[27] (Site 1: 64-slice LightSpeed VCT system, GE Healthcare, Milwaukee, WI, USA; Site 2: Discovery MI PET/CT scanner, GE Healthcare, Milwaukee, WI, USA; parameters: 64×0.625 collimation, 120 peak kilovoltage, 100 mA, tube rotation time=500ms, pitch=1.25, standard reconstruction kernel, slice thickness=1.25mm, field-of-view=40cm^2). CT airways were evaluated (HKK, three-years experience; PVW, two-years experience) using VIDAvision software (VIDA Diagnostics Inc., Coralville, IA, USA) to generate total airway count (TAC).[33] Anatomically equivalent segmental, subsegmental, and

sub-subsegmental airways for all airway paths from the third to fifth generation were utilized to generate airway lumen area (LA) and wall thickness (WT). In addition, CT pulmonary vessels were quantitatively evaluated (HKK and AMM, two-years experience) using the Chest Imaging Platform (Brigham and Women's Hospital, Boston, MA, USA)[34] which automatically generated pulmonary vascular total blood volume (TBV), as well as the volume of blood vessels with cross sectional area <5 mm^2 (BV_5; representative of small vessels) and >10 mm^2 (BV_{10}; representative of large vessels).

4.2.4 Statistical Analysis

SPSS (SPSS Statistics 25.0; IBM, Armonk, NJ, USA) was used for all statistical analyses. Data were tested for normality using Shapiro-Wilk tests and nonparametric tests were performed for non-normally distributed data. Differences between subgroups were evaluated using independent samples tests. The Holm-Bonferroni correction was used for multiple comparisons. Differences in CT airway and pulmonary vascular measurements were evaluated using linear regression models where the imaging measurement was the dependent variable and the disease subgroup was the independent variable. Such models were adjusted for age, height, body mass index, CT total lung volume, smoking pack-years, and the presence of previously diagnosed asthma. Univariate relationships were evaluated using Pearson (r) and Spearman (ρ) correlations. Results were considered statistically significant when the probability of making a type I error was less than 5% (P<.05).

4.3 Results

4.3.1 Participant Characteristics

A CONSORT diagram provided in **Figure 4-1** shows that 51 female participants (mean age, 61±13 years) were evaluated. Of these, 21 participants were females with long-COVID (53±14 years) and 30 were female ex-smokers, including 17 ex-smokers without COPD (69±9 years) and 13 with a diagnosis of COPD (67±6 years).

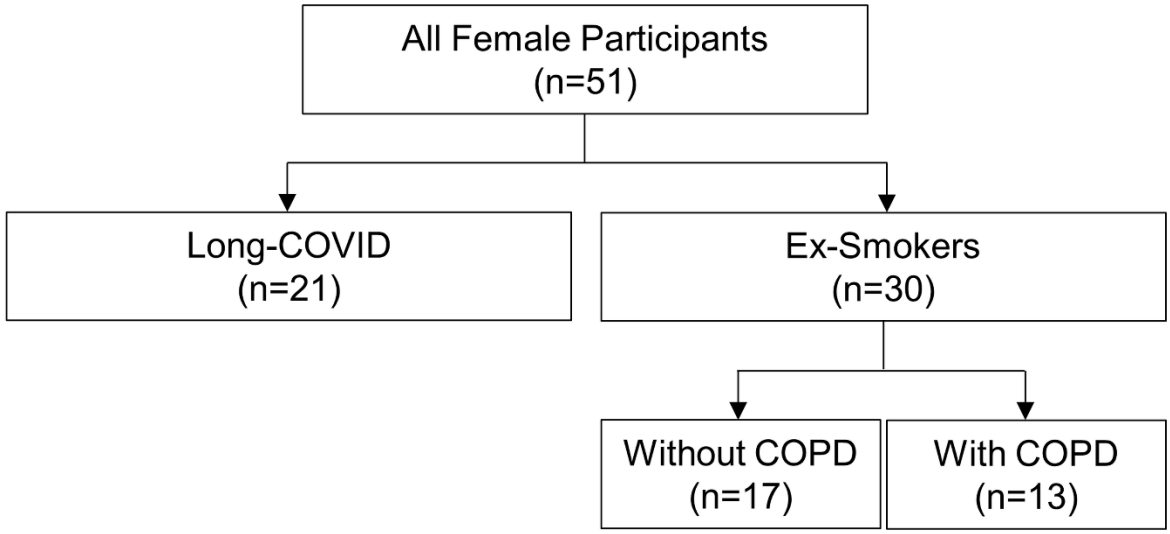

Figure 4-1. Consort Diagram
Of the 51 female participants included in the analysis, 21 were long-COVID participants and 30 were ex-smokers. Of these ex-smokers, 17 participants were ex-smokers without COPD and 13 were participants with COPD.
COPD=chronic obstructive pulmonary disease.

Table 4-1 provides demographic characteristics, pulmonary function, and quality-of-life scores for all participants, as well as the long-COVID, ex-smoker, and COPD subgroups. Biological sex was self-reported. **Table 4-1** shows age (P<.001), smoking pack-years (P<.001), and 6MWD (P=.007) were significantly different between long-COVID and ex-smoker females. In addition, for the long-COVID and COPD subgroups, there was significantly different age (P<.001), body mass index (P=.01), pack-years (P<.001), FEV_1 (P=.002), FEV_1/FVC (P<.001), DL_{CO} (P<.001), and 6MWD (P<.001).

Table 4-1. Demographic, Pulmonary Function, Quality-of-Life, and Imaging Measurements

Parameter Mean (SD)	All Female (n=51)	Long-COVID (n=21)	Ex-Smoker (n=17)	COPD (n=13)	Sig. *P*	Sig. *P**
Age years	61 (13)	53 (14)	69 (9)	67 (6)	**<.001**	**.001**
BMI kg/m^2	29 (6)	30 (5)	31 (4)	24 (4)	.2	**.01**
Pack-years	21 (23)	7 (14)	27 (17)	44 (22)	**<.001**	**<.001**
FEV_1 $\%_{pred}$	84 (25)	88 (18)	101 (21)	56 (15)	.4	**.002**
FVC $\%_{pred}$	92 (17)	92 (17)	95 (21)	86 (12)	.6	.3
FEV_1/FVC %	71 (16)	77 (10)	81 (6)	50 (11)	.6	**<.001**
DL_{CO}* $\%_{pred}$	71 (28)	92 (24)	71 (21)	46 (16)	.09	**<.001**
6MWD m	420 (94)	479 (66)	386 (101)	370 (75)	**.007**	**<.001**
SGRQ	34 (18)	36 (16)	28 (22)	39 (13)	.2	.6
CT TAC n	252 (74)	252 (76)	276 (65)	220 (77)	.5	.050
CT LA mm^2	13 (3)	12 (2)	14 (3)	12 (2)	**.006**	.7
CT WT %	18 (1)	17 (1)	18 (1)	18 (1)	.5	**.009**
CT TBV mL	232 (29)	242 (32)	228 (25)	224 (27)	.5	.6
CT BV_5 mL	121 (27)	143 (23)	109 (17)	99 (15)	**.045**	**.003**
CT BV_{10} mL	67 (13)	63 (13)	67 (12)	72 (14)	.9	**.03**
CT BV_5/TBV %	52 (9)	59 (7)	48 (6)	44 (5)	**.03**	**<.001**
CT BV_{10}/TBV %	29 (5)	26 (4)	29 (4)	32 (4)	.5	**.002**

COPD=chronic obstructive pulmonary disease; BMI=body mass index; FEV_1=forced expiratory volume in 1-second; $\%_{pred}$=percent of predicted value; FVC=forced vital capacity; DL_{CO}=diffusing capacity of the lungs for carbon monoxide; 6MWD=six-minute walk distance; SGRQ=St. George's Respiratory Questionnaire; CT=computed tomography; TAC=total airway count; LA=lumen area; WT=wall thickness; TBV=total blood volume; BV_5=blood volume for vessels with cross-sectional area less than 5 mm^2; BV_{10}=blood volume for vessels with cross-sectional area greater than 10 mm^2.

P=Holm-Bonferroni corrected significance for difference between Long-COVID and Ex-Smoker participants.

*P**=Holm-Bonferroni corrected significance for difference between Long-COVID and COPD participants.

CT Imaging Measurements *P*=significance for sex differences calculated using univariate linear models adjusted for confounders including age, height, body mass index, lung volume, smoking pack-years, and the presence of previously diagnosed asthma.

Bolded values indicate *P*<.05.

DL_{CO}*: All n=44, Long-COVID n=16, Ex-Smoker n=15

4.3.2 Chest CT Measurements

Table 4-1 also summarizes CT imaging measurements. When adjusted for age, height, body mass index, CT total lung volume, smoking pack-years and previously diagnosed asthma, there were significant differences between long-COVID and ex-smokers for LA (P=.006), BV_5 (P=.045), and BV_5/TBV (P=.03). After adjusting for the same covariates, there were differences between long-COVID and COPD patients for WT% (P=.009), BV_5 (P=.003), BV_{10} (P=.03), BV_5/TBV (P<.001), and BV_{10}/TBV (P=.002).

Figure 4-2 shows CT images for three representative female participants, one with long-COVID, a single ex-smoker and a single COPD patient. The insets show anatomically matched airways in the three participants to highlight the larger lumen area in the ex-smoker and greater wall thickness in the COPD patient, as compared to the long-COVID participant. **Figure 4-3** provides a schematic illustrating the major differences in CT measurements between the female subgroups. The top panel shows preserved airway WT and larger LA in the ex-smokers, as well as preserved LA and thicker airways wall in COPD participants, compared to long-COVID. The middle panel shows the trend of decreased TAC in females with COPD as compared to long-COVID and ex-smokers. The bottom panel shows the redistribution of blood flow from the small vessels to the large blood vessels in females with COPD as compared to the ex-smokers and females with long-COVID.

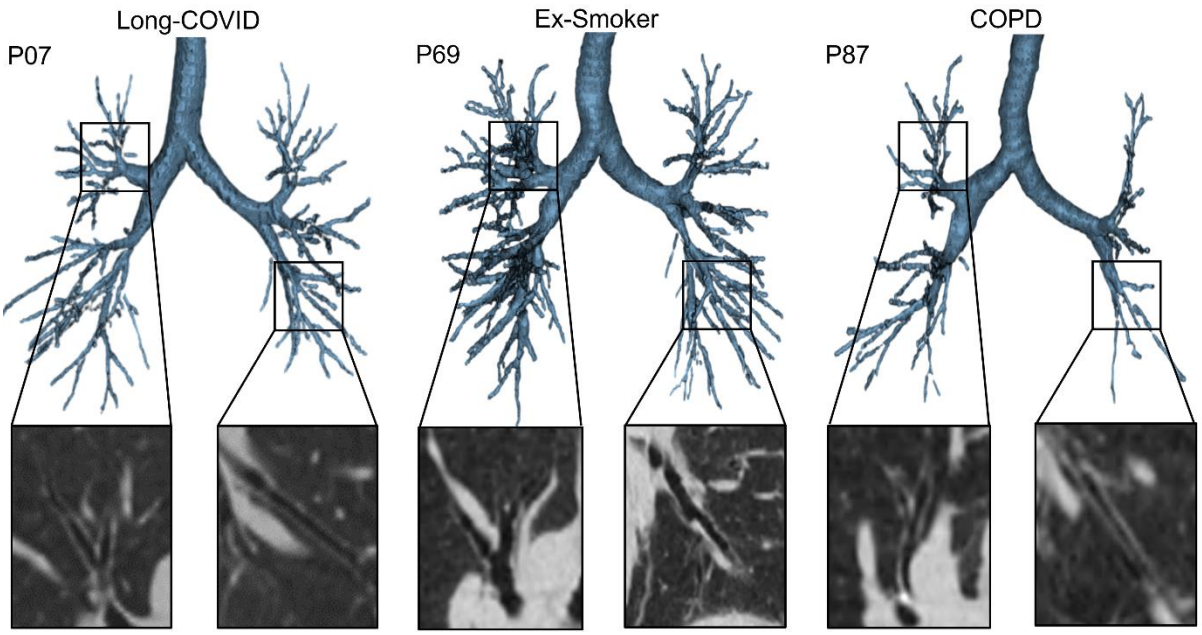

Figure 4-2. Representative CT airways in female participants
Segmented CT airway trees with insets of RB1 and LB8 airways. P07 is a 29-year-old female with no previous history of chronic lung disease, FEV_1=76%$_{pred}$, SGRQ=23, TAC=199, LA=12mm^2, and WT%=18%. P69 is a 72-year-old female who is an ex-smoker and with FEV_1=96%$_{pred}$, SGRQ=29, TAC=333, LA=21mm^2, and WT%=16%. P87 is a 72-year-old female with COPD, FEV_1=40%$_{pred}$, SGRQ=48, TAC=163, LA=9mm^2, and WT%=19%.
COPD=chronic obstructive pulmonary disease; CT=computed tomography; RB=right bronchus; LB=left bronchus; FEV_1=forced expiratory volume in 1 second; %$_{pred}$=percent of predicted value; SGRQ=St. George's Respiratory Questionnaire; TAC=total airway count; LA=lumen area; WT=wall thickness.

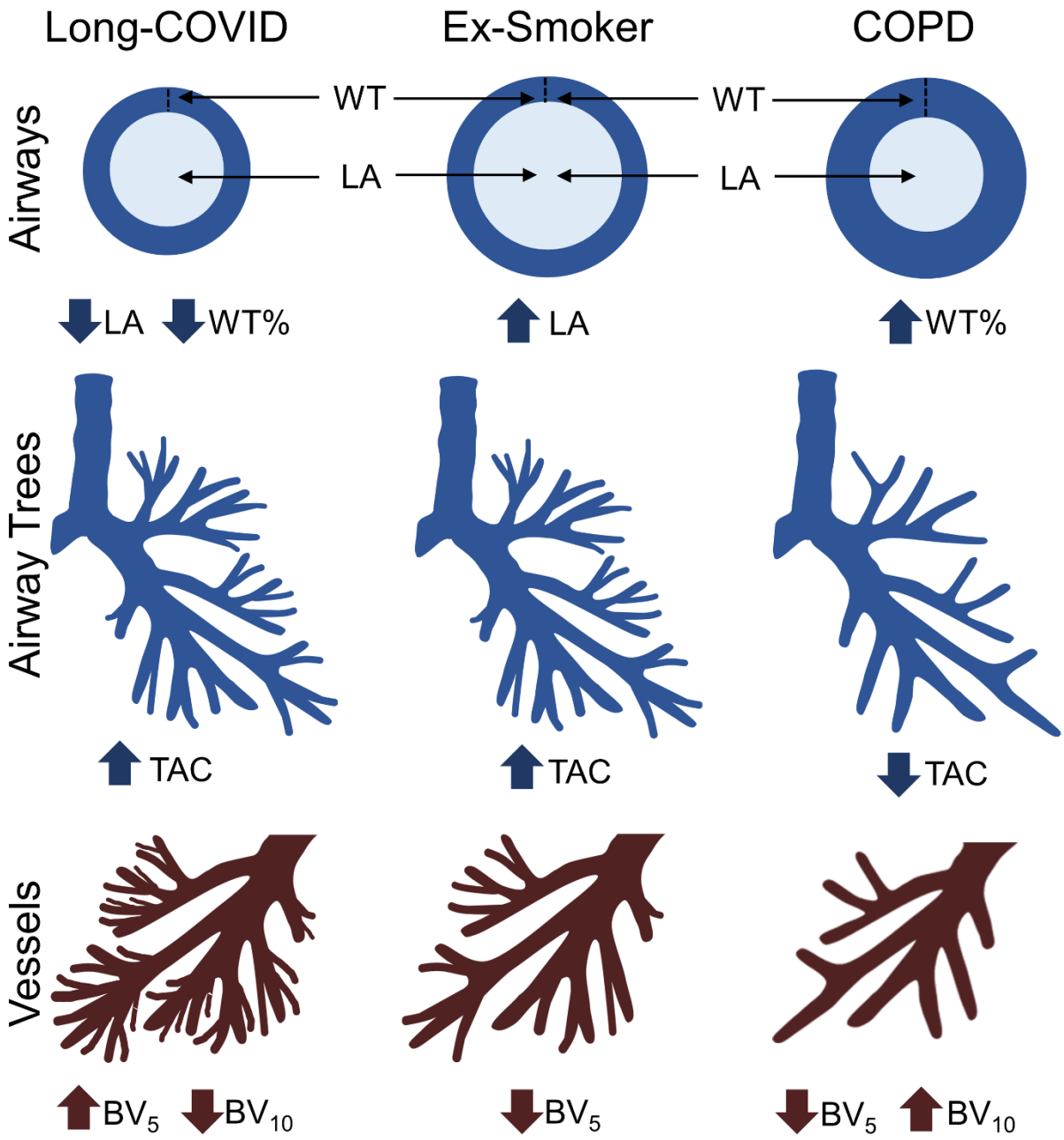

Figure 4-3. Summary Schematic of Airway and Vessel Measurements
Top panel shows reduced lumen area in female participants with long-COVID compared to ex-smokers and decreased wall thickness in female participants with long-COVID compared to COPD. The middle panel shows reduced total airway count in females with COPD, as compared to females who are ex-smokers or have long-COVID. The bottom panel shows augmented small vessel volume and reduced large vessel volume in females with long-COVID compared to ex-smoker and COPD participants.
COPD=chronic obstructive pulmonary disease; WT=wall thickness; LA=lumen area; TAC=total airway count; BV_5=blood volume for vessels with cross-sectional area less than 5 mm^2; BV_{10}=blood volume for vessels with cross-sectional area greater than 10 mm^2.

4.3.3 Relationships with Chest CT Measurements

Figure 4-4 highlights some of the important relationships for CT measurements with clinical measurements of quality-of-life and pulmonary diffusing capacity in all females investigated here. The activity score component of SGRQ significantly but weakly correlated with WT% (ρ=.29; *P*=.04), but not with LA (ρ=-.10; *P*=.5). In addition, DL_{CO} significantly correlated with WT% (ρ=-.39; *P*=.03) and strongly correlated with BV_5/TBV (ρ=.71; *P*<.001).

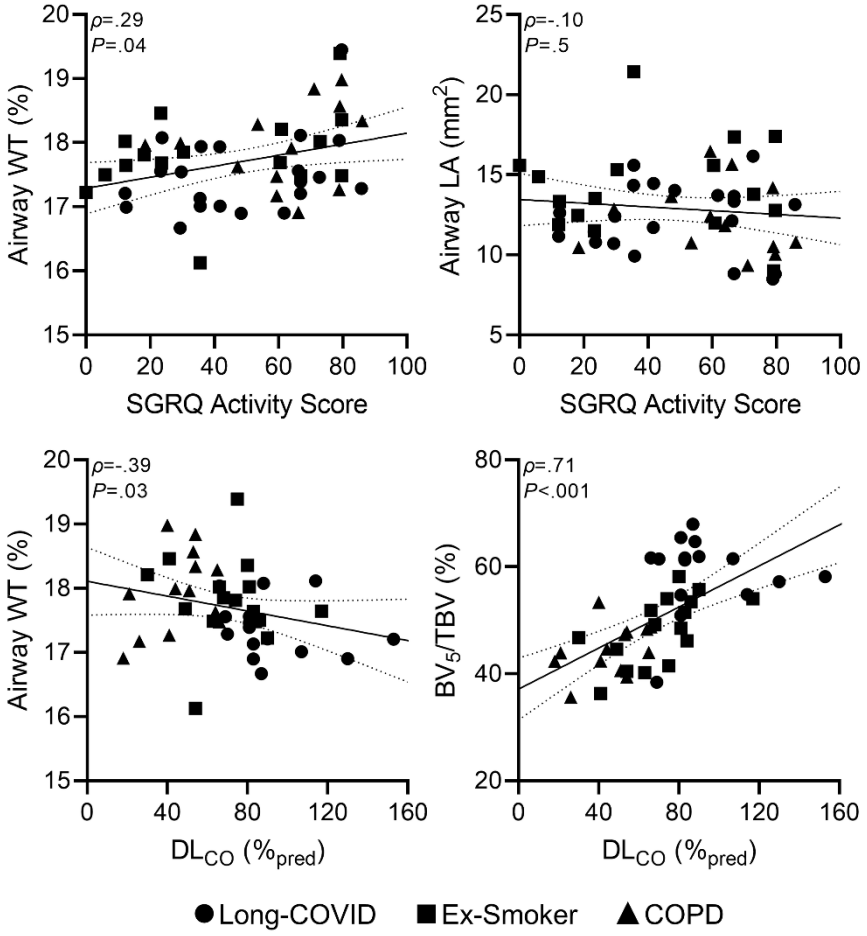

Figure 4-4. Relationships with CT Airway and Vasculature Measurements in all Females
SGRQ Activity Score significantly correlated with airway WT% (ρ=.29; *P*=.04).
SGRQ Activity Score did not significantly correlate with airway LA (ρ=-.10; *P*=.5).
DL_{CO} significantly correlated with airway WT% (ρ=-.39; *P*=.03).
DL_{CO} significantly correlated with BV_5/TBV (ρ=.71; *P*<.001).
WT=wall thickness; SGRQ=St. George's Respiratory Questionnaire; LA=lumen area; DL_{CO}=diffusing capacity of the lungs for carbon monoxide; $\%_{pred}$=percent of predicted value; BV_5=blood volume for vessels with cross-sectional area less than 5 mm^2; TBV=total blood volume.
ρ=Spearman correlation

4.4 Discussion

Chest CT measurements clearly show that in females, airway walls are thinner and the airway lumen is smaller compared to males, even when adjusting for height and lung size.[20] Such sex differences are also observed in patients with COPD with airway measurements in female patients more strongly correlated with dyspnea, quality-of-life, six-minute walk distance and all-cause mortality.[20] In patients with long-COVID, females were also recently shown to have fewer CT airways, thinner airway walls and smaller airway lumens compared to males.[25] To better understand and provide context for such sex differences in long-COVID, here we evaluated airway and pulmonary vascular measurements at a single timepoint in females with highly abnormal quality-of-life scores and long-COVID (three months post-infection) as well as female ex-smokers with and without COPD.

We observed: 1) smaller airway lumen area in females with long-COVID compared to female ex-smokers, 2) thinner airway walls in females with long-COVID compared to females with COPD, and, 3) greater small vessel volume in females with long-COVID as compared to female ex-smokers and COPD patients.

We were surprised to observe that airway lumen area was similar in females with long-COVID and COPD, and for both subgroups, the airway lumen was smaller than the calibre of the airway lumen in female ex-smokers. It is possible that the smaller lumen area in long-COVID may stem from post-infectious inflammation or perhaps dysanapsis which is thought to increase susceptibility to inhaled pollutants,[35] is a risk factor for COPD,[36] and contribute to increased mortality risk in the elderly.[37] Regardless the reason, this is the first demonstration of abnormally narrowed airway lumen in female patients with long-COVID, which is consistent

with the finding of airway dysfunction and abnormal SGRQ scores,[27] both of which largely persisted 15-months post-infection.[26]

The finding of thinner airway walls in females with long-COVID, as compared to COPD, is consistent with the finding of thinner airway walls in female never-smokers, compared to ever-smokers.[20] It is well understood that the airway walls in smokers and patients with COPD can be thickened due to inflammatory processes and this wall thickening on CT has been previously associated with airflow limitation.[38-41] CT total airway count was similar (P=.050) between females with long-COVID and COPD, which is important because diminished TAC and airway wall thinning was previously demonstrated by COPD severity,[42,43] over time in COPD patients,[44] and by asthma severity.[45] Taken together, the finding of a narrowed airway lumen, similar to COPD, and thin airway walls, similar to ex-smokers, suggests the presence of airway remodelling in females with long-COVID, aligning with previous reports of airways disease in long-COVID despite preserved pulmonary function.[26,27,46] It is possible that airway remodelling is a consequence of COVID-19 infection or perhaps played a role prior to infection or in the predisposition of females to long-COVID; however, this study is not powered to draw such conclusions.

Vascular pruning has been previously reported in patients with COPD,[47-49] contributing evidence for the concept of a pulmonary vascular COPD phenotype.[50] Pulmonary vascular abnormalities have also been reported in acute COVID-19 and long-COVID.[51-54] In the female patients with long-COVD evaluated here, there was greater small vessel volume as compared to ex-smoker and COPD females. It is possible that post-COVID infection, persistent airway inflammation[55] may have resulted in increased vascularization of the smaller airways.[56] This would agree with findings in patients with asthma[56] in whom increased small vessel volume is

a compensatory mechanism for airway dysfunction. Unfortunately, we cannot distinguish post-viral vascular remodelling in long-COVID from augmented vascular pruning in COPD patients and it is certainly possible that either or both are occurring.

Underscoring these important results were the significant relationships for CT airway and pulmonary vascular measurements with clinical measures of quality-of-life and gas-exchange. Thicker airway walls were associated with greater physical activity limitations and with impaired pulmonary gas-exchange in all females investigated here. The linear trends, particularly for SGRQ Activity Score, do not seem to be driven by a specific subgroup. Instead, the females with long-COVID are dispersed among the whole group (**Figure 4-4**), highlighting the similarity in the functional consequences of airway remodelling in all these female patient subgroups. As expected, we also observed that BV_5 correlated with DL_{CO}, and there was a clear delineation between the three subgroups. This suggests a greater extent of vascular abnormalities in COPD as compared to long-COVID, which is consistent with the differences in DL_{CO} and CT pulmonary vascular measurements reported among the three groups. Regardless of the differences in DL_{CO} values among subgroups, SGRQ scores were similar and quite abnormal.

We acknowledge several study limitations, including the relatively small sample size (n=51). Moreover, none of the long-COVID participants had chest CT prior to COVID-19 infection, so the differences measured here may have predated COVID-19 infection or the onset of long-COVID. In addition, it is worth noting that the long-COVID females were significantly younger than the ex-smoker and COPD subgroups. Hence the finding of similar luminal narrowing in long-COVID and COPD females may be a conservative estimate because airway lumens do narrow over time with aging.[57] Indeed, we cannot be certain if the CT airway and

vessel tree measurements reported here for females with long-COVID are “abnormal” based on literature values because previous studies used a variety of CT protocols and airway segmentation methods with inconsistent adjustment of confounding factors.[38-44,47-49] However, the similarities observed here among long-COVID and COPD patients provide an important context for debilitating symptoms experienced by long-COVID patients for whom normal spirometry does not provide any explanation.[26,27] MRI ventilation heterogeneity has previously pointed to the presence of airway dysfunction, which can be mechanistically linked to exercise limitation and persistent symptoms, in patients with long-COVID.[27] In fact, patients who were prescribed airways disease therapy were more likely to experience quality-of-life improvements over one year.[26] Now, we provide evidence of airway remodelling in long-COVID that is similar to ex-smokers with and without COPD, helping to further solidify the concept of an airways disease phenotype in patients with long-COVID.[46]

In summary, in females with long-COVID, airway lumen area was similar to females with COPD, although airway walls were not as thick. Airway lumen differences or remodelling in long-COVID did not coincide with pulmonary vascular redistribution from the small to large vessels, which was observed in female patients with COPD. CT airway findings in long-COVID were similar to those in females with COPD which may help partially explain their highly abnormal quality-of-life scores and respiratory symptoms. Baseline CT airway measurements prior to infection will be required to explain the higher relative risk of long-COVID in females, post-infection.

4.5 References

1. Borges do Nascimento, I.J., *et al.* Novel Coronavirus Infection (COVID-19) in Humans: A Scoping Review and Meta-Analysis. *J Clin Med* **9**(2020).

2. Chakravarty, D., *et al.* Sex differences in SARS-CoV-2 infection rates and the potential link to prostate cancer. *Commun Biol* **3**, 374 (2020).

3. Sylvester, S.V., *et al.* Sex differences in sequelae from COVID-19 infection and in long COVID syndrome: a review. *Curr Med Res Opin* **38**, 1391-1399 (2022).

4. Bowyer, R.C.E., *et al.* Characterising patterns of COVID-19 and long COVID symptoms: evidence from nine UK longitudinal studies. *Eur J Epidemiol* **38**, 199-210 (2023).

5. Nalbandian, A., *et al.* Post-acute COVID-19 syndrome. *Nat Med* **27**, 601-615 (2021).

6. National Institute of Health and Care Excellence. COVID-19 Rapid Guideline: Managing COVID-19. (NICE, 2021).

7. Sharma, G., Volgman, A.S. & Michos, E.D. Sex Differences in Mortality From COVID-19 Pandemic: Are Men Vulnerable and Women Protected? *JACC Case Rep* **2**, 1407-1410 (2020).

8. Klein, S.L. & Flanagan, K.L. Sex differences in immune responses. *Nat Rev Immunol* **16**, 626-638 (2016).

9. Pinkerton, K.E., *et al.* Women and Lung Disease. Sex Differences and Global Health Disparities. *Am J Respir Crit Care Med* **192**, 11-16 (2015).

10. Barnes, P.J. Sex Differences in Chronic Obstructive Pulmonary Disease Mechanisms. *Am J Respir Crit Care Med* **193**, 813-814 (2016).

11. Gan, W.Q., Man, S.F., Postma, D.S., Camp, P. & Sin, D.D. Female smokers beyond the perimenopausal period are at increased risk of chronic obstructive pulmonary disease: a systematic review and meta-analysis. *Respir Res* **7**, 52 (2006).

12. Bjornson, W., *et al.* Gender differences in smoking cessation after 3 years in the Lung Health Study. *Am J Public Health* **85**, 223-230 (1995).

13. Martinez, F.J., *et al.* Sex differences in severe pulmonary emphysema. *Am J Respir Crit Care Med* **176**, 243-252 (2007).

14. Hoffstein, V. Relationship between lung volume, maximal expiratory flow, forced expiratory volume in one second, and tracheal area in normal men and women. *Am Rev Respir Dis* **134**, 956-961 (1986).

15. Mead, J. Dysanapsis in normal lungs assessed by the relationship between maximal flow, static recoil, and vital capacity. *Am Rev Respir Dis* **121**, 339-342 (1980).

16. Martin, T.R., Castile, R.G., Fredberg, J.J., Wohl, M.E. & Mead, J. Airway size is related to sex but not lung size in normal adults. *J Appl Physiol* **63**, 2042-2047 (1987).

17. Sheel, A.W., *et al.* Evidence for dysanapsis using computed tomographic imaging of the airways in older ex-smokers. *J Appl Physiol* **107**, 1622-1628 (2009).

18. Dominelli, P.B., *et al.* Sex differences in large conducting airway anatomy. *J Appl Physiol* **125**, 960-965 (2018).

19. Christou, S., *et al.* Anatomical variability in the upper tracheobronchial tree: sex-based differences and implications for personalized inhalation therapies. *J Appl Physiol* **130**, 678-707 (2021).

20. Bhatt, S.P., *et al.* Sex Differences in Airways at Chest CT: Results from the COPDGene Cohort. *Radiology*, 212985 (2022).

21. Hong, Y., *et al.* Sex differences of COPD phenotypes in nonsmoking patients. *J Chronc Obstruct Pulmon Dis* **11**, 1657-1662 (2016).

22. Zach, J.A., *et al.* Quantitative computed tomography of the lungs and airways in healthy nonsmoking adults. *Invest Radiol* **47**, 596-602 (2012).

23. Camp, P.G., *et al.* Sex differences in emphysema and airway disease in smokers. *Chest* **136**, 1480-1488 (2009).

24. Li, Y., Dai, Y.L., Yu, N. & Guo, Y.M. Sex-related differences in bronchial parameters and pulmonary function test results in patients with chronic obstructive pulmonary disease based on three-dimensional quantitative computed tomography. *J Int Med Res* **46**, 135-142 (2018).

25. Kooner, H., *et al.* Sex Differences in CT Airway Measurements and Their Relationship to Post-Acute COVID-19 Syndrome. in *D109. THE LONG AND THE SHORT OF LONG COVID* A6791-A6791 (American Thoracic Society, 2023).

26. Kooner, H.K., *et al.* Post-Acute COVID-19 Syndrome: (129)Xe MRI Ventilation Defects and Respiratory Outcomes One Year Later. *Radiology*, 222557 (2023).

27. Kooner, H.K., *et al.* (129)Xe MRI ventilation defects in ever-hospitalised and never-hospitalised people with post-acute COVID-19 syndrome. *BMJ Open Respir Res* **9**(2022).

28. Kirby, M., *et al.* Longitudinal Computed Tomography and Magnetic Resonance Imaging of COPD: Thoracic Imaging Network of Canada (TINCan) Study Objectives. *Chronic Obstr Pulm Dis* **1**, 200-211 (2014).

29. Jones, P.W., Quirk, F.H., Baveystock, C.M. & Littlejohns, P. A self-complete measure of health status for chronic airflow limitation. The St. George's Respiratory Questionnaire. *Am Rev Respir Dis* **145**, 1321-1327 (1992).

30. Enright, P.L. The six-minute walk test. *Respir Care* **48**, 783-785 (2003).

31. Miller, M.R., *et al.* Standardisation of spirometry. *Eur Respir J* **26**, 319-338 (2005).

32. Macintyre, N., *et al.* Standardisation of the single-breath determination of carbon monoxide uptake in the lung. *Eur Respir J* **26**, 720-735 (2005).

33. Tschirren, J., Hoffman, E.A., McLennan, G. & Sonka, M. Segmentation and quantitative analysis of intrathoracic airway trees from computed tomography images. *Proc Am Thorac Soc* **2**, 484-487, 503-484 (2005).

34. Estepar, R.S., *et al.* Computational Vascular Morphometry for the Assessment of Pulmonary Vascular Disease Based on Scale-Space Particles. *Proc IEEE Int Symp Biomed Imaging*, 1479-1482 (2012).

35. Bourbeau, J., *et al.* Ambient Air Pollution and Dysanapsis: Associations with Lung Function and Chronic Obstructive Pulmonary Disease in the Canadian Cohort Obstructive Lung Disease Study. *Am J Respir Crit Care Med* **206**, 44-55 (2022).

36. Smith, B.M., *et al.* Association of Dysanapsis With Chronic Obstructive Pulmonary Disease Among Older Adults. *JAMA* **323**, 2268-2280 (2020).

37. Vameghestahbanati, M., *et al.* Association of dysanapsis with mortality among older adults. *Eur Respir J* **61**(2023).

38. Charbonnier, J.P., *et al.* Airway wall thickening on CT: Relation to smoking status and severity of COPD. *Respir Med* **146**, 36-41 (2019).

39. Hasegawa, M., *et al.* Airflow limitation and airway dimensions in chronic obstructive pulmonary disease. *Am J Respir Crit Care Med* **173**, 1309-1315 (2006).

40. Nakano, Y., *et al.* Computed tomographic measurements of airway dimensions and emphysema in smokers. Correlation with lung function. *Am J Respir Crit Care Med* **162**, 1102-1108 (2000).

41. Telenga, E.D., *et al.* Airway wall thickness on HRCT scans decreases with age and increases with smoking. *BMC Pulm Med* **17**, 27 (2017).

42. Kirby, M., *et al.* Total Airway Count on Computed Tomography and the Risk of Chronic Obstructive Pulmonary Disease Progression. Findings from a Population-based Study. *Am J Respir Crit Care Med* **197**, 56-65 (2018).

43. Smith, B.M., *et al.* Comparison of spatially matched airways reveals thinner airway walls in COPD. The Multi-Ethnic Study of Atherosclerosis (MESA) COPD Study and

the Subpopulations and Intermediate Outcomes in COPD Study (SPIROMICS). *Thorax* **69**, 987-996 (2014).

44. Wyszkiewicz, P.V., *et al.* Reduced Total Airway Count and Airway Wall Tapering after Three-Years in Ex-Smokers. *COPD* **20**, 186-196 (2023).

45. Eddy, R.L., *et al.* Is Computed Tomography Airway Count Related to Asthma Severity and Airway Structure and Function? *Am J Respir Crit Care Med* **201**, 923-933 (2020).

46. Adeloye, D., *et al.* The long-term sequelae of COVID-19: an international consensus on research priorities for patients with pre-existing and new-onset airways disease. *Lancet Respir Med* **9**, 1467-1478 (2021).

47. Washko, G.R., *et al.* Arterial Vascular Pruning, Right Ventricular Size, and Clinical Outcomes in Chronic Obstructive Pulmonary Disease. A Longitudinal Observational Study. *Am J Respir Crit Care Med* **200**, 454-461 (2019).

48. Tang, G., *et al.* Correlations of Computed Tomography Measurement of Distal Pulmonary Vascular Pruning with Airflow Limitation and Emphysema in COPD Patients. *J Chron Obstruct Pulmon Dis* **17**, 2241-2252 (2022).

49. Pistenmaa, C.L., *et al.* Pulmonary Arterial Pruning and Longitudinal Change in Percent Emphysema and Lung Function: The Genetic Epidemiology of COPD Study. *Chest* **160**, 470-480 (2021).

50. Kovacs, G., *et al.* Pulmonary Vascular Involvement in Chronic Obstructive Pulmonary Disease. Is There a Pulmonary Vascular Phenotype? *Am J Respir Crit Care Med* **198**, 1000-1011 (2018).

51. Lang, M., *et al.* Pulmonary Vascular Manifestations of COVID-19 Pneumonia. *Radiol Cardiothorac Imaging* **2**, e200277 (2020).

52. Yong, S.J., *et al.* Inflammatory and vascular biomarkers in post-COVID-19 syndrome: A systematic review and meta-analysis of over 20 biomarkers. *Rev Med Virol* **33**, e2424 (2023).

53. Grist, J.T., *et al.* Lung Abnormalities Depicted with Hyperpolarized Xenon MRI in Patients with Long COVID. *Radiology*, 220069 (2022).

54. Matheson, A.M., *et al.* Persistent (129)Xe MRI Pulmonary and CT Vascular Abnormalities in Symptomatic Individuals with Post-Acute COVID-19 Syndrome. *Radiology*, 220492 (2022).

55. Proud, D. Upper airway viral infections. *Pulm Pharmacol Ther* **21**, 468-473 (2008).

56. Zanini, A., Chetta, A., Imperatori, A.S., Spanevello, A. & Olivieri, D. The role of the bronchial microvasculature in the airway remodelling in asthma and COPD. *Respir Res* **11**, 132 (2010).

57. Niewoehner, D.E. & Kleinerman, J. Morphologic basis of pulmonary resistance in the human lung and effects of aging. *J Appl Physiol* **36**, 412-418 (1974).

Chapter 5

5 ^{129}XE MRI VENTILATION TEXTURES AND LONGITUDINAL QUALITY-OF-LIFE IN LONG-COVID

In light of ventilation defect percent not being predictive of longitudinal quality-of-life improvement in patients with long-COVID, we utilized MRI ventilation texture feature analysis and machine-learning to classify long-COVID participants with and without one year St. George's Respiratory Questionnaire score improvement.

The contents of this chapter were accepted for publication by the journal Academic Radiology: HK Kooner, M Sharma, MJ McIntosh, I Dhaliwal, JM Nicholson, M Kirby, S Svenningsen, and G Parraga. ^{129}Xe MRI Ventilation Textures and Longitudinal Quality-of-Life Improvements in Long-COVID. Academic Radiology 2024. doi: 10.1016/j.acra.2024.03.014.

5.1 Introduction

Long-COVID is an umbrella term used to describe the residual symptoms and poor quality-of-life that persist after recovery from SARS-CoV-2 infection, more than four weeks from the onset of acute infection.[1] More than half of COVID-infected patients report at least one long-COVID symptom one[2] and two years[3] post-infection.

Chest computed tomography (CT), the mainstay imaging approach for acute and long-COVID,[4] has been used for diagnosis, to determine infection severity, and to predict prognosis and mortality.[5,6] While machine-learning, in combination with clinical features, has been used to predict long-COVID development in patients post-infection,[7,8] to our knowledge this approach has not yet exploited chest imaging measurements. In addition, clustering methods have been harnessed to "phenotype" long-COVID,[9-11] where clinical features and symptoms were used to stratify patients' impairment and sequelae severity. However, even with such approaches, it remains difficult to provide a timeline or prognosis for long-COVID improvement. This, and the clinical management of long-COVID patients in the presence of normal pulmonary function measurements, remain very challenging.

Hyperpolarized ^{129}Xe magnetic resonance imaging (MRI)[12] provides a way to quantify airway dysfunction via inhaled gas distribution. MRI ventilation defect percent (VDP)[13] uniquely predicts asthma control[14] and quality-of-life in patients with chronic obstructive pulmonary disease (COPD).[15] ^{129}Xe MRI has also revealed ventilation defects[16,17] and their improvement over time[18,19] in patients with long-COVID. In a recent study in patients with long-COVID, MRI ventilation defects improved 15-months post-infection.[17] While MRI ventilation defects did explain improved exercise capacity, they did not help explain improved (but still abnormal) quality-of-life[18] 12 months after a baseline visit.

Beyond the binary classification and measurement of ventilation abnormalities using MRI VDP, ^{129}Xe ventilation MRI texture features provide a way to extract spatial and voxel intensity values to quantify ventilation heterogeneity and patchiness due to airways disease including inflammation and occlusions. ^{129}Xe ventilation MRI texture features were previously shown to explain response to bronchodilator therapy in patients with asthma,[20] as well as predict lung function decline[21] and mortality[22] in ex-smokers.

Here, we aimed to use a combination of machine-learning and MRI ventilation textures (reflecting coarse and fine ventilation signal patchiness) to predict clinically relevant, longitudinal quality-of-life improvements (≥4 points decrease in the St. George's Respiratory Questionnaire [SGRQ] total score) in patients with long-COVID. The SGRQ score provides a quality-of-life measurement which accounts for symptoms, activity limitations, and impact in people with airways disease.[23] In people with COPD, poor SGRQ scores are linked to COPD exacerbations, risk of hospital admissions, and mortality.[24] SGRQ score was also highly abnormal in patients with long-COVID[17] with some improvement one year later,[18] but remaining persistently abnormal.

We hypothesized that MRI ventilation texture features at a baseline visit, 3-months post-infection, would improve the performance of machine-learning models aimed at predicting those long-COVID patients who would experience quality-of-life improvements one year later. We also explored if MRI texture features might provide mechanistic insights by exploring correlations for these textures with pulmonary function test measurements.

5.2 Methods

5.2.1 Study Participants and Design

In this prospective study, participants were enrolled between July 2020 and August 2021 from two research sites (Site 1: Robarts Research Institute, London Canada; Site 2: St Joseph's Healthcare Hamilton, Hamilton Canada) and all provided written-informed consent to ethics board (HSREB #113224 London; HiREB #12672, Hamilton), Health Canada-approved protocols (www.clinicaltrials.gov NCT05014516). Participants were recruited from a local quaternary care post-COVID-19 clinic at Site 1 and through referral from healthcare providers or self-referral through advertising at Site 2. Inclusion criteria consisted of age 18 to 80 years, a local public health office confirmed (positive-test) case of COVID-19, persistent symptoms up to three-months post infection, including but not limited to respiratory, neurological, and metabolic systems, and a clinical diagnosis of long-COVID.

During the 3-month and 15-month visits, participants completed fractional exhaled nitric oxide, spirometry, diffusing capacity of the lungs for carbon monoxide (DL_{CO}), oscillometry, and ^{129}Xe ventilation MRI. SGRQ[23] and six-minute walk test[25] were also completed. ^{129}Xe MRI VDP results acquired 3-months and 15-months post-COVID-19 infection in all participants were previously reported.[17,18]

5.2.2 Pulmonary Function Tests and Questionnaires

Participants completed spirometry for forced expiratory volume in 1 second (FEV_1) and forced vital capacity (FVC), according to American Thoracic Society guidelines,[26] using the EasyOne Pro LAB system (ndd Medical Technologies, Zurich, Switzerland) or a whole-body plethysmograph (MedGraphics Corporation, St. Paul, MN, USA). DL_{CO} was also measured using the EasyOne Pro LAB system or the plethysmograph, according to European Respiratory Society guidelines.[27] Oscillometry was performed according to European Respiratory Society guidelines[28] using a tremoFlo C-100 Airwave Oscillometry System (Thorasys, Montreal, Canada) to measure resistance and reactance between 5 and 37 Hz. Post-bronchodilator measurements were performed 15 minutes after inhalation of 4×100 µg Salbutamol sulfate norflurane (Ivax Pharmaceuticals, Waterford, Ireland) using an AeroChamber (Trudell Medical International, London, Canada). Participants withheld respiratory medications before each study visit according to American Thoracic Society guidelines.[26] SGRQ and six-minute walk test were administered under the supervision of study personnel.

5.2.3 Thoracic Imaging and Analysis

Anatomic ^{1}H and ^{129}Xe static ventilation MRI were acquired at both sites using 3.0 Tesla scanners (Discovery MR750; GE Healthcare, Milwaukee, USA), as previously described.[17] Anatomic ^{1}H MRI was acquired using a fast-spoiled gradient-recalled-echo sequence (partial-echo acquisition; total acquisition time, 8 seconds; repetition-time msec/echo time msec, 4.7/1.2; flip-angle, 30°; field-of-view, 40×40cm^2; bandwidth, 24.4kHz; 128×80 matrix, zero-filled to 128×128; partial-echo percent, 62.5%; 15-17×15mm slices). ^{129}Xe MRI was acquired using a three-dimensional fast-spoiled gradient-recalled echo sequence (total acquisition time, 14s; repetition-time msec/echo time msec, 6.7/1.5; variable flip-angle; field-of-view,

40×40cm^2; bandwidth, 15.63kHz; 128×128 matrix; 14×15mm slices) and a flexible vest coil (Clinical MR Solutions, USA; Site 1) or asymmetric quadrature bird cage coil (custom built; Site 2). Supine participants were coached to inhale a 1.0L bag (Tedlar; Jensen Inert Products, Coral Springs, FL, USA) as previously described.[18] ^{129}Xe gas was polarized to 15-55% (Site 1: Xenispin 9820, Site 2: Xenispin 9800; Polarean, Durham, NC, USA).[17] Quantitative MRI VDP analysis was performed using MATLAB 2021b (MathWorks, Natick, MA, USA), as previously described.[13]

5.2.4 Texture Feature Extraction, Selection, and Modelling

The regions-of-interest from the baseline MR images were generated using the lung mask from the ^{1}H MRI acquisition, where the thoracic cavity was segmented using a seeded region-growing algorithm.[13] This lung mask was applied to the ventilation MR images to identify ventilated regions of the lung for texture feature extraction. Open-source Pyradiomics[29] (version 2.2.0) was utilized to extract 120 unique, unfiltered texture features in a voxel-by-voxel manner. Histogram and shape, first- and higher-order texture features from run-length, gap-length, size-zone, neighbourhood-dependence, and co-occurrence matrices were computed.[29]

All variables for the machine-learning models, including texture features and clinical measurements, were subjected to Boruta analysis[30] for ranking. Boruta used a two-step correction for multiple testing and an optimizable Random Forest classifier for iterations (number of trees in the forest=100, maximum iterations=150, maximum tree depth=5, percentage of shadow feature threshold=95%, alpha level=0.05). The top-ranked texture features were then used to train the machine-learning models to classify participants reporting

an SGRQ improvement greater than the minimal clinically important difference (MCID) of four points[31] from 3- to 15-months post-COVID infection.

Five-fold cross-validation was performed where all the data was randomly and evenly divided into five groups and for each fold, one group was held back for testing and the remaining groups were used for training. Each fold utilized different combinations of testing and training groups and no information was carried over from training to testing. Single and ensemble machine-learning classifiers were implemented. The data was standardized and hyperparameter search was performed using MATLAB2021b Classification Learner App (MathWorks, Natick, MA, USA) for every machine-learning model.

5.2.5 Statistical Analysis

SPSS (SPSS Statistics 25.0; IBM, Armonk, NJ, USA) was used for all statistical analyses. Data were tested for normality using Shapiro-Wilk tests and nonparametric tests were performed for non-normally distributed data. Temporal differences were evaluated using paired samples tests and differences between subgroups were evaluated using independent samples tests. The Holm-Bonferroni correction was used for multiple comparisons. Univariate relationships were evaluated using Pearson (r) and Spearman (ρ) correlations. Classification performance was evaluated using the mean cross-validation area under the receiver-operator curve (AUC), as well as sensitivity and specificity metrics calculated from the confusion matrix. Results were considered statistically significant when the probability of making a type I error was less than 5% ($P<0.05$).

5.3 Results

5.3.1 Participant Characteristics

A CONSORT diagram provided in **Figure 5-1** shows that 76 participants with long-COVID were evaluated at 3-months, as previously described.[17] Of these, 17 were lost-to-follow-up, three declined, two declined COVID-19 vaccination so were excluded from follow-up due to institutional guidelines, and one became pregnant in the time between visits and was withdrawn. Thus, 53 participants were evaluated at 15-months. Of these, nine participants did not complete SGRQ at one of the two visits and hence, 44 participants (mean age, 54 years ±14[SD]; 23 males; 21 females) were included in this evaluation.

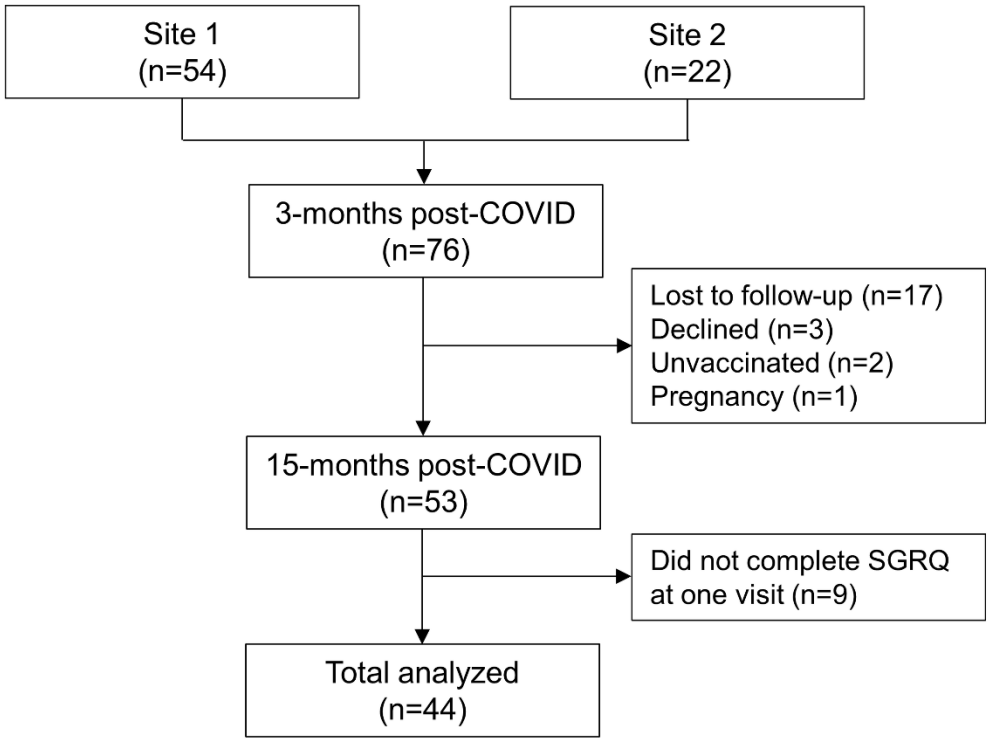

Figure 5-1. CONSORT Diagram
Of the 76 participants enrolled at 3-months post-COVID infection, 54 were from Site 1 and 22 were from Site 2. Of those participants, 17 were lost to follow-up, three declined, two were unvaccinated and unable to complete a visit due to institutional COVID-19 guidelines, and one became pregnant in the time between visits and was withdrawn. Of the 53 participants who completed a follow-up visit, 44 completed SGRQ at both time points and were included in the analysis.
SGRQ=St. George's Respiratory Questionnaire

Table 5-1 provides the demographic characteristics, pulmonary function, questionnaire and imaging measurements at 3-months post-COVID-infection for all participants and those dichotomized by ΔSGRQ<MCID (n=14 [32%]; mean age, 58 years ±18[SD]; 9 male; 5 female) and ΔSGRQ≥MCID (n=30 [68%]; mean age, 52 years ±12[SD]; 14 male; 16 female). There were no baseline differences between the two subgroups. **Table 5-2** shows that there were also no differences between these subgroups based on baseline qualitative CT findings. As previously reported,[18] MRI VDP (6±8%, 5±7%; *P*=.01), SGRQ (35±19, 25±19; *P*<.001), six-minute walk distance (444±85m, 463±66m; *P*=.04), FEV_1 (83±22%$_{pred}$, 89±20%$_{pred}$; *P*=.003), FEV_1/FVC (75±11%, 78±12%; *P*=.02), and DL_{CO} (85±21%$_{pred}$, 100±21%$_{pred}$; *P*=.002) were significantly improved 12-months after the baseline 3-month visit.

Table 5-1. Baseline Demographic Characteristics, Pulmonary Function, Questionnaire and Imaging Measurements

Parameter	All (n=44)	ΔSGRQ<MCID (n=14)	ΔSGRQ≥MCID (n=30)	Sig. *P*
Age years	54 (14)	58 (18)	52 (12)	>.99
Age range years	25-84	25-84	31-74	-
Female sex n (%)	21 (48)	5 (36)	16 (53)	>.99
Male sex n (%)	23 (52)	9 (64)	14 (47)	>.99
BMI kg/m^2	30 (5)	28 (5)	31 (4)	.9
Months Since + COVID Test	3 (2)	3 (2)	3 (1)	>.99
Smoking history pack-years	11 (21)	13 (24)	10 (20)	>.99
Previous Respiratory Disease n (%)	13 (30)	4 (29)	9 (30)	>.99
Asthma n (%)	10 (23)	3 (21)	7 (23)	>.99
COPD n (%)	3 (7)	1 (7)	2 (7)	.9
Hospitalized n (%)	12 (27)	12 (29)	12 (27)	>.99
Hospital Admission days	8 (6)	7 (4)	9 (7)	>.99
Pulmonary function				
FEV_1 $\%_{pred}$	83 (22)	82 (17)	83 (24)	.9
FVC $\%_{pred}$	86 (20)	87 (17)	86 (22)	>.99
FEV_1/FVC %	75 (11)	74 (15)	76 (10)	>.99
FeNO* ppb	24 (15)	24 (20)	24 (12)	>.99
DL_{CO}* $\%_{pred}$	85 (21)	92 (20)	83 (21)	>.99
R_5* $cmH_2O•s/L$	3.7 (1.7)	3.2 (1.6)	4.0 (1.7)	.9
R_{19}* $cmH_2O•s/L$	2.9 (1.1)	2.4 (0.9)	3.1 (1.1)	.7
R_{5-19}* $cmH_2O•s/L$	0.8 (0.7)	0.8 (0.8)	0.9 (0.6)	>.99
Exercise capacity and quality-of-life				
6MWD m	444 (85)	437 (124)	448 (61)	.5
SGRQ	35 (19)	27 (18)	39 (18)	.1
MRI				
VDP %	6 (8)	8 (12)	5 (6)	.7

All data are reported as mean (SD).
Δ=change from 3- to 15-months post-COVID; SGRQ=St. George's Respiratory Questionnaire; MCID=minimal clinically important difference; BMI=body mass index; COPD=chronic obstructive pulmonary disease. FEV_1=forced expiratory volume in 1 second; $\%_{pred}$=percent of predicted value; FVC=forced vital capacity; FeNO=fractional exhaled nitric oxide; DL_{CO}=diffusing capacity of the lungs for carbon monoxide; R_5=oscillometry measurement of total airway resistance; R_{19}=oscillometry measurement of central airway resistance; R_{5-19}=oscillometry measurement of distal airway resistance; 6MWD=six-minute walk distance; MRI=magnetic resonance imaging; VDP=ventilation defect percent.
P=Holm-Bonferroni corrected significance value.
FeNO*: All n=31, ΔSGRQ<MCID n=10, ΔSGRQ≥MCID n=21
DL_{CO}*: All n=33, ΔSGRQ<MCID n=8, ΔSGRQ≥MCID n=25
R_5*, R_{19}*, R_{5-19}*: All n=33, ΔSGRQ<MCID n=11, ΔSGRQ≥MCID n=22

Table 5-2. Qualitative CT Findings at 3-Months

Parameter	All (n=32)	ΔSGRQ<MCID (n=11)	ΔSGRQ≥MCID (n=21)	Sig. *P*
CT Finding n (%)	19 (59)	9 (82)	10 (48)	.3
Ground-Glass Opacity n (%)	11 (34)	6 (55)	5 (24)	.3
Consolidation n (%)	4 (13)	1 (9)	3 (14)	.7
Mosaic Attenuation n (%)	4 (13)	0 (0)	4 (19)	.4
Bronchiectasis n (%)	4 (13)	2 (18)	2 (10)	>.99

All data are reported as n (%)
Δ=change from 3- to 15-months post-COVID; SGRQ=St. George's Respiratory Questionnaire; MCID=minimal clinically important difference.
P=Holm-Bonferroni corrected significance value.

5.3.2 Texture Extraction and Selection

Table 5-3 provides descriptions of the top-performing coarse and fine MRI texture features and summarizes the highest-performing texture predictors of SGRQ improvement 12 months later in all participants and by subgroup. Minor axis length, a coarse texture, was significantly different between the two subgroups (70±6, 62±5; *P*<.001).

Table 5-3. MRI Texture Features

Parameter	Description	All (n=44)	ΔSGRQ<MCID (n=14)	ΔSGRQ≥MCID (n=30)	Sig. *P*
Maximum 2D diameter column	Coarse Texture: The largest pairwise Euclidean distance between the surface mesh vertices in the row-slice plane.	78 (7)	80 (6)	75 (7)	.1
Minor axis length	Coarse Texture: The second-largest axis length of the ROI-enclosing ellipsoid.	65 (6)	70 (6)	62 (5)	<.001
FO mean absolute deviation	Coarse Texture: The mean distance of all intensity values from the mean value of the image array.	1038 (216)	990 (201)	1060 (223)	.3
FO variance	Coarse Texture: The mean of the squared distances of each intensity value from the mean value, a measure of the spread of the distribution about the mean.	1808859 (657496)	1633185 (625761)	1890841 (666043)	.9
GLRLM gray level variance	Fine Texture: The variance in gray level intensity for the runs.	18110 (6577)	16356 (6263)	18929 (6662)	.7
NGTDM complexity	Coarse Texture: An image is considered complex when there are many primitive components in the image, i.e. the image is non-uniform and there are many rapid changes in gray level intensity.	5672789 (2603851)	4334094 (1878540)	6297513 (2683718)	.1
NGTDM contrast	Coarse Texture: A measure of the spatial intensity change but is also dependent on the overall gray level dynamic range. Contrast is high when both the dynamic range and the spatial change rate are high.	1.22 (0.33)	1.07 (0.31)	1.29 (0.32)	.2
GLCM cluster tendency	Fine Texture: A measure of groupings of voxels with similar gray-level values.	67211 (24449)	61255 (23549)	69990 (24751)	.5

All data are reported as mean (SD).
ROI=region-of-interest; FO=first order; GLRLM=gray-level run-length matrix; NGTDM=neighbourhood gray tone difference matrix; GLCM=gray-level co-occurrence matrix.
P=Holm-Bonferroni corrected significance value.

Figure 5-2 provides representative MRI ventilation images at the two timepoints 3- and 15-months post-COVID for two participants. Participant P11 was a 47-year-old female who reported ΔSGRQ<MCID, while participant P08 was a 58-year-old male who reported ΔSGRQ≥MCID. At both 3- and 15-months post-COVID, the MRI ventilation appears visually similar with relatively homogenous distribution. MRI VDP was within normal limits [32] and was not significantly different between timepoints. MRI ventilation texture minor axis length was 73 for participant P11 and 53 for participant P08.

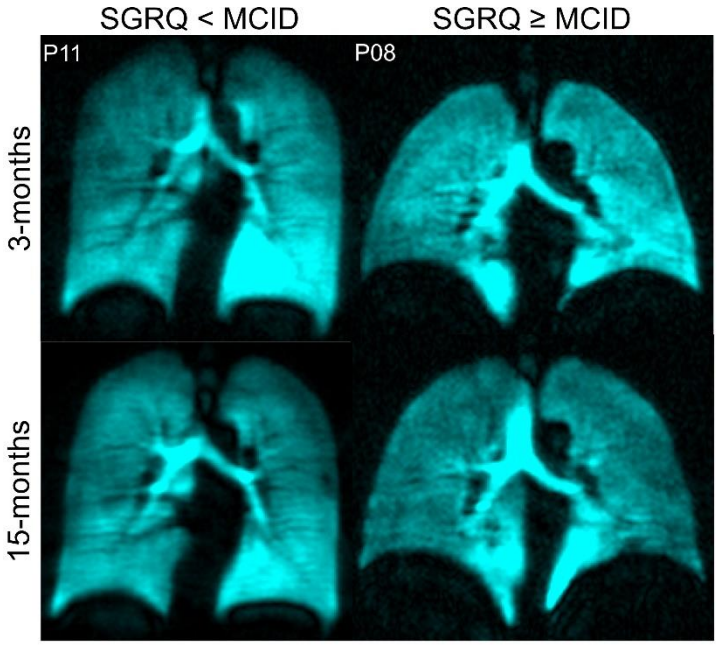

Figure 5-2. Representative ^{129}Xe MRI Ventilation
Coronal ^{129}Xe MRI slices (cyan) at 3- and 15-months post-COVID infection illustrate visually similar ventilation patterns for both participants. Participant P11 is a 47-year-old female who was not hospitalized during acute infection and with 3-months/15-months post-COVID FEV_1=75%/84%, SGRQ=12/11, and VDP=2%/0%. At 3-months, the MRI texture feature values for participant P11 were minor axis length=73, NGTDM complexity=5850371, maximum 2D diameter column=81, NGTDM contrast=0.90, FO mean absolute deviation=1126, FO variance=2066028, and GLRLM gray level variance=20691. Participant P08 is a 58-year-old male who was hospitalized for four days during acute infection and with 3-months/15-months post-COVID FEV_1=79%/85%, SGRQ=35/0, and VDP=1%/1%. At 3-months, the MRI texture feature values for participant P08 were minor axis length=53, NGTDM complexity=5891309, maximum 2D diameter column=68, NGTDM contrast=1.14, FO mean absolute deviation=926, FO variance=1445144, and GLRLM gray level variance=14490.
SGRQ=St. George's Respiratory Questionnaire; MCID=minimal clinically important difference; FEV_1=forced expiratory volume in 1-second; VDP=ventilation defect percent; NGTDM= neighbourhood gray tone difference matrix; FO=first order; GLRLM=gray-level run-length matrix.

5.3.3 Predicting SGRQ Improvement

As shown in **Table 5-4**, machine-learning classification models for SGRQ improvement were generated using: 1) clinical features, 2) MR imaging and texture features, and, 3) a combination of clinical and imaging features. The clinical model included as predictors: age, sex, hospitalization status during acute infection, time between COVID-19 diagnosis and baseline study visit, body mass index, the presence of previously diagnosed chronic lung disease, and FEV_1. The MRI-based model included the following top-ranking MRI ventilation texture features: original shape (OS) maximum 2D diameter column, OS minor axis length, first order (FO) mean absolute deviation, FO variance, gray-level run-length matrix (GLRLM) gray level variance, neighbourhood gray tone difference matrix (NGTDM) complexity, and NGTDM contrast. For the combined model, all clinical and texture measurements underwent feature selection and the following were selected: baseline SGRQ score, OS minor axis length, FO mean absolute deviation, gray-level co-occurrence matrix (GLCM) cluster tendency, NGTDM complexity, and NGTDM contrast.

Table 5-4. Machine-learning models to predict the change in SGRQ score ≥ MCID

Best Performing Models	AUC	Sensitivity (%)	Specificity (%)	Accuracy (%)
Clinical Model				
Quadratic SVM[‡]	0.72	90.0	42.9	75.0
MRI-based Model				
Kernel Naïve Bayes[†]	0.89	90.0	71.4	84.1
Combined Model				
Weighted KNN[§]	0.87	96.7	78.6	90.9

St. George's Respiratory Questionnaire; AUC=area under the receiver-operating curve; SVM=support vector machine, KNN=K-nearest neighbours.
[‡]Model includes: age, sex, hospitalization status, time since positive COVID-19 test, BMI, chronic lung disease, and forced expiratory volume in 1 second.
[†]Model includes: original shape maximum 2D diameter column, original shape minor axis length, first order mean absolute deviation, first order variance, gray-level run-length matrix gray level variance, neighbourhood gray tone difference matrix complexity, and neighbourhood gray tone difference matrix contrast.
[§]Model includes: baseline SGRQ score, original shape minor axis length, first order mean absolute deviation, gray-level co-occurrence matrix cluster tendency, gray-level run-length matrix gray level variance, neighbourhood gray tone difference matrix complexity, and neighbourhood gray tone difference matrix contrast.

The best performing of the clinical or MRI models was the MRI-based model (AUC=0.89, sensitivity=90.0%, specificity=71.4%, accuracy=84.1%), while the clinical model (AUC=0.72, sensitivity=90.0%, specificity=42.9%, accuracy=75.0%) did not perform as well. The combined model (AUC=0.87, sensitivity=96.7%, specificity=78.6%, accuracy=90.9%) had superior sensitivity, specificity, and accuracy with similar AUC as the MRI model.

Figure 5-3 shows the receiver-operator characteristic curves for the individual variables included in the three models. In the clinical model, the top performing measurement was body mass index (AUC=0.64), while minor axis length (AUC=0.85) was the top performing measurement for both the MRI-based and combined models. Of all the features included in all the models, minor axis length outperformed all other clinical and imaging variables, while the presence of previous chronic lung disease and FEV_1 were the worst performing features (AUC=0.50).

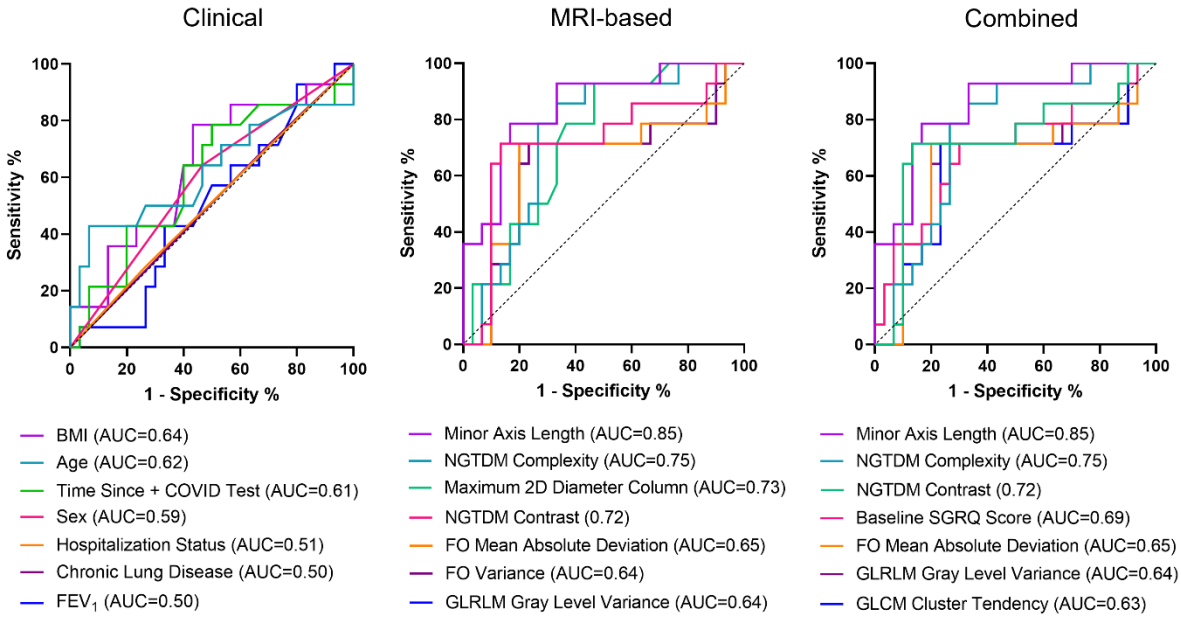

Figure 5-3. Receiver-operator characteristic curves of texture features and clinical variables
Left plot is a logistic analysis of individual clinical variables, middle plot is a logistic analysis of MRI ventilation texture features, and right plot is a logistic analysis of both clinical and texture features at predicting SGRQ improvement ≥MCID between 3- and 15-months post-COVID infection.
BMI=body mass index; AUC=area-under-the-curve; FEV_1=forced expiratory volume in 1-second; NGTDM=neighbourhood gray tone difference matrix; FO=first order; GLRLM=gray-level run-length matrix; GLCM=gray-level co-occurrence matrix.

5.3.4 Correlations with MRI Ventilation Texture Features

Figure 5-4 shows correlations of top-performing MRI texture features with imaging and clinical measurements. Both OS 2D diameter column and OS minor axis length correlated with MRI VDP measured 3-months post-COVID (ρ=.43, *P*=.003; ρ=.33, *P*=.03, respectively). In addition, OS 2D diameter column correlated with FVC (ρ=.37, *P*=.01), DL_{CO} (ρ=.39, *P*=.03), and central airways resistance or R_{19} (ρ=-.41, *P*=.02) measured 3-months post-COVID infection. OS minor axis length also correlated with R_{19} (ρ=-.37, *P*=.03) measured at the same baseline timepoint. In addition, FO mean absolute deviation and FO variance significantly correlated with FEV_1 (ρ=-.38, *P*=.01; ρ=-.41, *P*=.006, respectively, data not shown) and FVC (ρ=-.46, *P*=.002; ρ=-.44, *P*=.003, respectively data not shown).

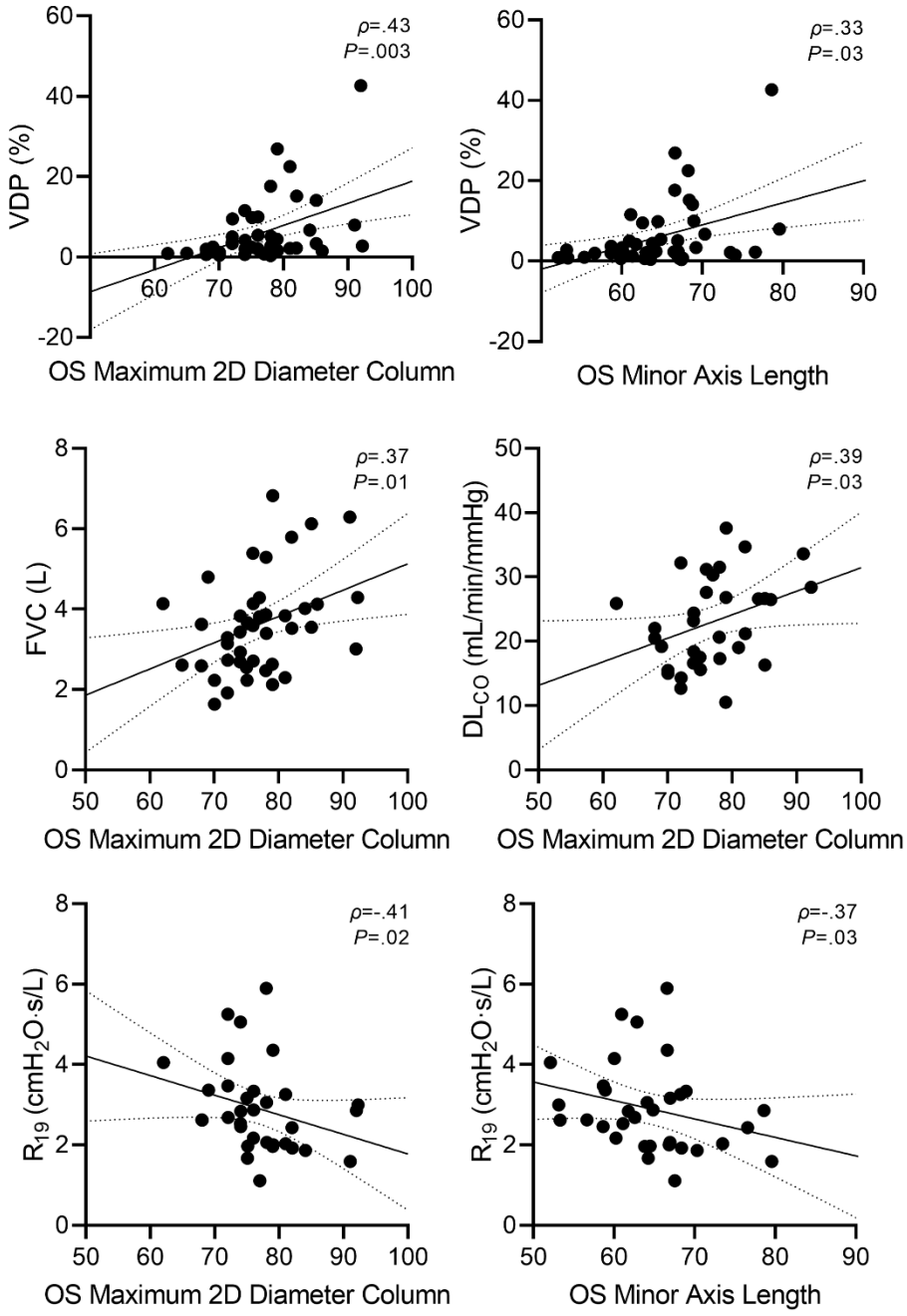

Figure 5-4. Correlations of MRI ventilation texture features with imaging and clinical measurements

Scatter plots show that original shape maximum 2D diameter column (ρ=.43, *P*=.003) and original shape minor axis length (ρ=.33, *P*=.03) significantly correlate with VDP 3-months post-COVID. Original shape maximum 2D diameter column significantly correlates with FVC (ρ=.37, *P*=.01), DL_{CO} (ρ=.39, *P*=.03), and R_{19} (ρ=-.41, *P*=.02) 3-months post-COVID. Original shape minor axis length also significantly correlates with R_{19} (ρ=-.37, *P*=.03) 3-months post-COVID.

VDP=ventilation defect percent; OS=original shape; FVC=forced vital capacity; DL_{CO}=diffusing capacity of the lungs for carbon monoxide; R_{19}=oscillometry measurement of central airway resistance.

5.4 Discussion

We retrospectively evaluated ^{129}Xe ventilation MRI texture features from a group of symptomatic patients with long-COVID to determine if such textures would be helpful in predicting those patients who would experience a clinically relevant quality-of-life improvement after one year. We took advantage of the additional patterns and distribution information available from ^{129}Xe ventilation textures and used these in combination with machine-learning. This work builds upon a previous observation that ^{129}Xe MRI VDP predicted improved 6MWD,[18] but not SGRQ, while the prescription of inhaled respiratory medication was predictive of such clinically relevant SGRQ score improvements.

Our main findings are: 1) a unique model was generated with MRI ventilation textures to predict long-COVID patients who would experience a clinically relevant quality-of-life improvement (AUC=0.89), which outperformed a clinical model (AUC=0.72), and, 2) the top-performing feature, minor axis, correlated with VDP (ρ=.33, *P*=.03) and R_{19} (ρ=-.37, *P*=.03), while another top-performing feature, maximum 2D diameter column, correlated with baseline measurements of VDP (ρ=.43, *P*=.003), FVC (ρ=.37, *P*=.01), DL_{CO} (ρ=.39, *P*=.03), and R_{19} (ρ=-.41, *P*=.02).

Thoracic CT imaging has been critically important for the diagnosis and monitoring of both acute COVID-19 and long-COVID and for predicting short-term outcomes after acute infection.[33,34] Unfortunately, however, none of the currently developed CT biomarkers have been shown to reflect or predict longitudinal changes in clinically relevant outcomes in patients with long-COVID. Here, we illustrate the advantage of using ^{129}Xe MRI ventilation textures to predict longitudinal quality-of-life improvement in patients with long-COVID. Importantly, the study participants who did report clinically relevant improvement in SGRQ at 15-months

did not demonstrate any demographic or other differences at baseline including pulmonary function measurements, exercise capacity, quality-of-life, MRI VDP, or qualitative CT findings as compared to the participants who did not experience improved quality-of-life scores. In addition, every individual MRI ventilation texture feature in the MRI-based model outperformed all features in the clinical model; seven out of eight features included in the combined model were also MRI textures. In fact, although ventilation defects have previously been reported in patients with long-COVID,[17,18] VDP was outranked by texture features and was not included in the models reported here. Thus, MRI ventilation texture features provided additional information, beyond the standard clinical and MRI VDP measurements, which were highly beneficial for the prediction of quality-of-life improvements after one year.

The currently established MRI ventilation biomarker of VDP utilizes five intensity clusters,[13] where the most hypointense cluster is deemed defect and normalized to the total thoracic cavity volume. ^{129}Xe ventilation MRI texture features provide a means to investigate ventilation intensity distribution more deeply in the lungs at the spatial resolution of individual voxels or voxel runs. Two of the top-performing textures, minor axis length and maximum 2D diameter column, are shape-based features and quantify the size of the ventilation distribution in the lungs, providing global pulmonary information comparable to VDP. The second-best performing texture feature, NGTDM complexity, describes the extent of ventilation heterogeneity by quantifying the sum of differences between the intensity of a voxel and the intensity of the directly adjacent neighbouring voxels.[35] In this way, a greater change in intensity values across a ventilated region results in a greater complexity value, indicating patchier ventilation or more ventilation heterogeneity. Relative to VDP, which classifies all

hyperventilation clusters into the same cluster, ventilation texture features extract spatial-intensity relationships that cannot be accessed in another way.

Of all clinical and MRI texture features we evaluated, OS minor axis length was the top-performing feature and was related to central airway resistance (R_{19}). Another high-performing texture feature, OS maximum 2D diameter column, was associated with FVC, DL_{CO}, and R_{19}. Previous work has shown that FVC and DL_{CO} are predictive of disease progression and mortality in patients with interstitial lung disease.[36] Importantly, there are also mounting concerns of interstitial lung disease developing post-COVID in some patients.[37] Because these MRI ventilation textures are related to both FVC and DL_{CO}, these may also be reflective of subclinical fibrosis or gas-exchange abnormalities; additional data over a longer period of time are required to test this hypothesis. In addition, FO mean absolute deviation and FO variance both correlated with FEV_1 and FVC, both of which reflect airways disease. Concurrent with other emerging MRI ventilation texture findings,[21,22] this work helps lay the groundwork for linking texture features with pathophysiology or mechanisms in long-COVID. In the absence of spirometric evidence of airways disease, MRI ventilation texture patterns and heterogeneity reveal subtle airway dysfunction while providing prognostic information about potential for clinically relevant improvements in long-COVID patients.

Several meta-analyses have reported one-year findings following COVID-19 infection,[38-40] where a range of approximately 32% to 50% of patients presented with residual CT abnormalities. Ground-glass opacities are the most commonly reported findings post-COVID, even after one year.[38-40] Although CT was not acquired 15-months post-infection in this group of participants with long-COVID, CT abnormalities were present in 59% (19/32) of participants with 34% (11/32) reporting ground-glass opacities at baseline. However, the

presence of any CT abnormalities or specific CT findings, such as ground-glass opacities or consolidation, were not adequately ranked during feature selection for inclusion in the models and therefore, were not predictive of longitudinal improvement. Hence, MRI ventilation textures also provided information that was not captured using the current COVID-19 imaging standard, which was unexpected given the persistence of CT abnormalities over time in COVID-19 survivors.[38-40]

Previous reports have suggested that the treatment of the airway component of long-COVID is associated with longitudinal recovery.[18,41] Nonetheless, the prescription of respiratory medications by treating physicians at 3-months was also not selected for inclusion in the modelling performed here. There were also no differences in previously diagnosed respiratory disease between those who did and did not report ΔSGRQ$\geq$MCID, suggesting improvement was not influenced by previous or underlying airways disease. Once again, clinical information was outperformed by MRI ventilation textures. However, this does not necessarily negate the importance of the airway component of long-COVID as MRI ventilation defects and textures have been observed to reflect airway inflammation or remodelling.[42] In long-COVID, MRI ventilation defects were observed to relate to exercise limitation and post-exertional dyspnea,[17,18] suggestive of a complex link between airway dysfunction, exercise intolerance, and quality-of-life. The role of pulmonary ventilation texture features in the prediction of longitudinal quality-of-life improvements contributes to the growing body of evidence for an airways disease phenotype in long-COVID.

We acknowledge several study limitations. First, this retrospective analysis had a relatively small sample size with a potential retention bias. This sample size is also smaller in comparison to other machine-learning studies so that the generalizability of these results may be limited.

We note, however, this analysis included multi-centre data, multiple feature selection approaches, and cross-validation to prevent overfitting. Third, not all of our participants consented to CT imaging and thus, CT radiomics could not be included here to complement the MRI data and/or to directly compare results with existing CT radiomics work.

In conclusion, in this investigation in 44 patients with long-COVID, ^{129}Xe MRI ventilation textures outperformed clinical measurements and chest CT findings, for predicting those long-COVID participants who would experience a clinically relevant quality-of-life improvement, 15-months post-infection. ^{129}Xe MRI ventilation textures provided unique information about the spatial and intensity distribution of pulmonary ventilation, which pointed to ventilation heterogeneity and airways disease as a physiologic contributor to long-COVID sequalae. MRI ventilation textures uncovered the functional consequences of these subtle airway pathologies and helped predict long-COVID outcomes.

5.5 References

1. National Institute of Health and Care Excellence. COVID-19 Rapid Guideline: Managing COVID-19. (NICE, 2021).

2. Zeng, N., *et al.* A systematic review and meta-analysis of long term physical and mental sequelae of COVID-19 pandemic: call for research priority and action. *Mol Psychiatry* **28**, 423-433 (2023).

3. Huang, L., *et al.* Health outcomes in people 2 years after surviving hospitalisation with COVID-19: a longitudinal cohort study. *Lancet Respir Med* **10**, 863-876 (2022).

4. Rubin, G.D., *et al.* The Role of Chest Imaging in Patient Management during the COVID-19 Pandemic: A Multinational Consensus Statement from the Fleischner Society. *Radiology* **296**, 172-180 (2020).

5. Cau, R., *et al.* Long-COVID diagnosis: From diagnostic to advanced AI-driven models. *Eur J Radiol* **148**, 110164 (2022).

6. Born, J., *et al.* On the role of artificial intelligence in medical imaging of COVID-19. *Patterns (N Y)* **2**, 100269 (2021).

7. Pfaff, E.R., *et al.* Identifying who has long COVID in the USA: a machine learning approach using N3C data. *Lancet Digit Health* **4**, e532-e541 (2022).

8. Kessler, R., Philipp, J., Wilfer, J. & Kostev, K. Predictive Attributes for Developing Long COVID-A Study Using Machine Learning and Real-World Data from Primary Care Physicians in Germany. *J Clin Med* **12**(2023).

9. Fernandez-de-Las-Penas, C., *et al.* Clustering analysis reveals different profiles associating long-term post-COVID symptoms, COVID-19 symptoms at hospital admission and previous medical co-morbidities in previously hospitalized COVID-19 survivors. *Infection* **51**, 61-69 (2023).

10. Evans, R.A., *et al.* Physical, cognitive, and mental health impacts of COVID-19 after hospitalisation (PHOSP-COVID): a UK multicentre, prospective cohort study. *Lancet Respir Med* **9**, 1275-1287 (2021).

11. Zhao, Y., *et al.* The phenotype and prediction of long-term physical, mental and cognitive COVID-19 sequelae 20 months after recovery, a community-based cohort study in China. *Mol Psychiatry* **28**, 1793-1801 (2023).

12. Albert, M.S., *et al.* Biological magnetic resonance imaging using laser-polarized 129Xe. *Nature* **370**, 199-201 (1994).

13. Kirby, M., *et al.* Hyperpolarized 3He magnetic resonance functional imaging semiautomated segmentation. *Acad Radiol* **19**, 141-152 (2012).

14. Svenningsen, S., Nair, P., Guo, F., McCormack, D.G. & Parraga, G. Is ventilation heterogeneity related to asthma control? *Eur Respir J* **48**, 370-379 (2016).

15. Kirby, M., *et al.* MRI ventilation abnormalities predict quality-of-life and lung function changes in mild-to-moderate COPD: longitudinal TINCan study. *Thorax* **72**, 475-477 (2017).

16. Li, H., *et al.* Damaged lung gas exchange function of discharged COVID-19 patients detected by hyperpolarized (129)Xe MRI. *Sci Adv* **7**(2021).

17. Kooner, H.K., *et al.* (129)Xe MRI ventilation defects in ever-hospitalised and never-hospitalised people with post-acute COVID-19 syndrome. *BMJ Open Respir Res* **9**(2022).

18. Kooner, H.K., *et al.* Post-Acute COVID-19 Syndrome: (129)Xe MRI Ventilation Defects and Respiratory Outcomes One Year Later. *Radiology*, 222557 (2023).

19. Chen, S., *et al.* Relationship between Lung and Brain Injury in COVID-19 Patients: A Hyperpolarized (129)Xe-MRI-based 8-Month Follow-Up. *Biomedicines* **10**(2022).

20. Zha, N., *et al.* Second-order Texture Measurements of (3)He Ventilation MRI: Proof-of-concept Evaluation of Asthma Bronchodilator Response. *Acad Radiol* **23**, 176-185 (2016).

21. Sharma, M., Westcott, A., McCormack, D. & Parraga, G. *Hyperpolarized gas magnetic resonance imaging texture analysis and machine learning to explain accelerated lung function decline in ex-smokers with and without COPD*, (SPIE, 2021).

22. Sharma, M., Wyszkiewicz, P.V., Matheson, A.M., McCormack, D.G. & Parraga, G. Chest MRI and CT Predictors of 10-Year All-Cause Mortality in COPD. *COPD* **20**, 307-320 (2023).

23. Jones, P.W., Quirk, F.H., Baveystock, C.M. & Littlejohns, P. A self-complete measure of health status for chronic airflow limitation. The St. George's Respiratory Questionnaire. *Am Rev Respir Dis* **145**, 1321-1327 (1992).

24. Mullerova, H., *et al.* St George's Respiratory Questionnaire Score Predicts Outcomes in Patients with COPD: Analysis of Individual Patient Data in the COPD Biomarkers Qualification Consortium Database. *Chronic Obstr Pulm Dis* **4**, 141-149 (2017).

25. Enright, P.L. The six-minute walk test. *Respir Care* **48**, 783-785 (2003).

26. Miller, M.R., *et al.* Standardisation of spirometry. *Eur Respir J* **26**, 319-338 (2005).

27. Macintyre, N., *et al.* Standardisation of the single-breath determination of carbon monoxide uptake in the lung. *Eur Respir J* **26**, 720-735 (2005).

28. King, G.G., *et al.* Technical standards for respiratory oscillometry. *Eur Respir J* **55**(2020).

29. Van Griethuysen, J.J., *et al.* Computational radiomics system to decode the radiographic phenotype. *Cancer Res* **77**, e104-e107 (2017).

30. Kursa, M.B. & Rudnicki, W.R. Feature Selection with the Boruta Package. *J Stat Softw* **36**, 1-13 (2010).

31. Jones, P.W., *et al.* Minimal clinically important differences in pharmacological trials. *Am J Respir Crit Care Med* **189**, 250-255 (2014).

32. McIntosh, M.J., *et al.* (129)Xe MRI Ventilation Defects in Asthma: What is the Upper Limit of Normal and Minimal Clinically Important Difference? *Acad Radiol* (2023).

33. Wang, D., *et al.* Study on the prognosis predictive model of COVID-19 patients based on CT radiomics. *Sci Rep* **11**, 11591 (2021).

34. Oi, Y., *et al.* Prediction of prognosis in patients with severe COVID-19 pneumonia using CT score by emergency physicians: a single-center retrospective study. *Sci Rep* **13**, 4045 (2023).

35. Amadasun, M. & King, R. Textural features corresponding to textural properties. *IEEE Transactions on systems, man, and Cybernetics* **19**, 1264-1274 (1989).

36. Caron, M., Hoa, S., Hudson, M., Schwartzman, K. & Steele, R. Pulmonary function tests as outcomes for systemic sclerosis interstitial lung disease. *Eur Respir Rev* **27**(2018).

37. Johnston, J., *et al.* Pulmonary Sequelae of COVID-19: Focus on Interstitial Lung Disease. *Cells* **12**(2023).

38. Fabbri, L., *et al.* Parenchymal lung abnormalities following hospitalisation for COVID-19 and viral pneumonitis: a systematic review and meta-analysis. *Thorax* **78**, 191-201 (2023).

39. Watanabe, A., *et al.* One-year follow-up CT findings in COVID-19 patients: A systematic review and meta-analysis. *Respirol* **27**, 605-616 (2022).

40. Bocchino, M., Rea, G., Capitelli, L., Lieto, R. & Bruzzese, D. Chest CT Lung Abnormalities 1 Year after COVID-19: A Systematic Review and Meta-Analysis. *Radiology* **308**, e230535 (2023).

41. Adeloye, D., *et al.* The long-term sequelae of COVID-19: an international consensus on research priorities for patients with pre-existing and new-onset airways disease. *Lancet Respir Med* **9**, 1467-1478 (2021).

42. Svenningsen, S., *et al*. What are ventilation defects in asthma? *Thorax* **69**, 63-71 (2014).

Chapter 6

6 CONCLUSIONS AND FUTURE DIRECTIONS

*The final chapter of this thesis summarizes the motivation and research questions related to this work and outlines the important observations and conclusions described in **Chapters 2-5**. An overview of the limitations of this research, both chapter-specific and general to this thesis, as well as some potential solutions are also provided. I conclude with possibilities for future research in long-COVID and pulmonary imaging motivated by the work presented in this thesis.*

6.1 Overview of Rationale and Research Questions

In December 2019, the first cases of severe acute respiratory syndrome coronavirus-2 (SARS-CoV-2) or COVID-19 were reported.[1] Initially presenting as viral pneumonia, common symptoms of infection included fever, cough, and myalgia.[1,2] Since then, COVID-19 rapidly has spread and the ensuing pandemic has resulted in millions of global cases of infection.[3,4] Following recovery from acute infection, patients began to report persistent symptoms such as fatigue, dyspnea, chest pain, brain fog, arthralgia, and poor quality-of-life.[5,6] We now know that long-COVID, an umbrella term used to describe this syndrome,[7] has a global pooled prevalence of up to 43% to 45% in COVID-19 patients regardless of hospitalization status.[8,9] Thus, with millions of people reporting long-COVID, there an enormous resultant economic burden consisting of increased healthcare costs, as well as loss of quality-of-life and earning capabilities in these people.[10,11]

Throughout the pandemic, computed tomography (CT) was considered the imaging gold standard for COVID-19 during both the infectious and post-infectious phases.[12-15] Unfortunately, these CT evaluations were limited to qualitative findings or density metrics, which focus primarily on parenchymal abnormalities and do not extensively probe functional consequences of such.[6,13-15] In addition, CT imaging is not ideal for longitudinal imaging or in vulnerable populations, such as children, due to radiation dose constraints. Instead,

hyperpolarized ^{129}Xe gas magnetic resonance imaging (MRI) provides a means to quantify regional inhaled gas distribution and ventilation heterogeneity *in vivo* non-invasively and with minimal effort. Thus, pulmonary imaging provides a method to investigate the structure-function relationships in patients with long-COVID to deepen our understanding of the mechanisms or pathophysiology driving the persistent symptoms and poor quality-of-life, aligning with the overarching objective of this thesis.

The specific research questions addressed were: 1) Is there evidence of pulmonary function and imaging abnormalities in patients with long-COVID? (**Chapter 2**); 2) What is the longitudinal trajectory of ^{129}Xe MRI ventilation abnormalities in long-COVID and how does this relate to changes in pulmonary function, quality-of-life, and exercise capacity? (**Chapter 3**); 3) Can CT airway and pulmonary vasculature measurements explain the prevalence of long-COVID in females and how do these measurements relate to ex-smokers with and without COPD? (**Chapter 4**); and lastly, 4) Can pulmonary imaging measurements help predict the prognosis of patients with long-COVID, outperforming standard clinical measurements? (**Chapter 5**).

6.2 Summary and Conclusions

In **Chapter 2**, we evaluated ^{129}Xe MRI VDP in 76 participants with long-COVID from two sites. We observed significantly worse VDP in ever- as compared to never-COVID participants (P<.001), as well as in ever-hospitalized as compared to never-hospitalized COVID participants (P=.048), who also experienced significantly worse DL_{CO} (P=.009) and 6MWD (P=.005). There were also significant relationships between CT airway and spirometry measurements, which included TAC with FEV_1/FVC (ρ=.30, P=.03), CT wall thickness with FEV_1 (r=.30, P=.046) and CT wall area with FEV_1/FVC (ρ=-.35, P=.04). Post-exertional SpO_2

correlated with two measurements of ventilation heterogeneity, MRI VDP (ρ=-.43; *P*=.002) and LCI (ρ=-.49; *P*=.01), while VDP also correlated with 6MWD (ρ=-.31; *P*=.02). These findings suggest the presence of an airways disease component to long-COVID that can be measured using MRI VDP and that contributes to exercise limitation and abnormal post-exertional SpO_2.

In **Chapter 3**, we investigated the longitudinal changes in MRI VDP for 53 participants with long-COVID who returned for follow-up 15-months post-COVID, one year after a baseline visit. We observed significantly improved VDP (*P*=.003), FEV_1 (*P*=.001), DL_{CO} (*P*=.002), and SGRQ score (*P*<.001) at 15-months as compared to 3-months post-infection. However, both mean VDP and SGRQ remained abnormal one year after baseline. In multivariable models, VDP measured at 3-months (β=-.643, *P*=.006) was the only significant contributor for predicting 6MWD improvement at 15-month whilst the longitudinal change in FVC (β=-.463, *P*=.02) and DL_{CO} (β=-.395, *P*=.04) predicted improvement in SGRQ score. We also observed that participants prescribed respiratory medication at 3-months were four times more likely to report SGRQ score improvement greater than MCID at 15-months post-COVID (odds ratio=4.0, 95% CI: 1.2, 13.8, *P*=.03). These results provide context for the longitudinal trajectory of long-COVID and point to the potential for changes in small airway function driving improved quality-of-life and exercise capacity in some patients with long-COVID.

In **Chapter 4**, based on the propensity for females to experience the persistent symptoms and poor quality-of-life attributed to long-COVID,[16,17] it was observed that females with long-COVID have significantly fewer airways, thinner walls, and smaller lumen compared to males with long-COVID.[18] To better understand these findings and provide context for the observed sex differences, we evaluated and compared CT airway and pulmonary vascular measurements

in females with long-COVID to female ex-smokers with and without COPD. In the absence of differences in quality-of-life scores, we reported narrower airway lumen in females with COVID as compared to female ex-smokers (*P*=.006) and significantly thinner airways walls in females with long-COVID compared to COPD (*P*=.009). Taken together, the finding of narrow lumen and thin airway walls suggests the presence of airway remodelling in females with long-COVID. These results align with our previous observations of MRI ventilation measurements of airway dysfunction in the context of preserved pulmonary function, helping to further solidify the concept of an airways disease phenotype in patients with long-COVID.[19] In addition, there was significantly greater pulmonary small vessel volume (BV_5) in long-COVID as compared to female ex-smokers (*P*=.045) and COPD (*P*=.003) patients and lesser large (BV_{10}) vessel volume as compared to COPD (*P*=.03). This is suggestive of a greater extent of vascular pruning or abnormalities in patients with COPD as compared to long-COVID.

In **Chapter 5**, we aimed to use a combination of machine-learning and MRI ventilation texture analysis to predict clinically relevant quality-of-life improvement, via SGRQ score, in 44 participants with long-COVID. This was motivated by the fact MRI VDP at baseline was unable to predict SGRQ score improvement, whilst the longitudinal change in FVC and DL_{CO} was able to do so. To this end, a unique model with baseline ^{129}Xe MRI ventilation texture features (AUC=0.89) outperformed models based only on clinical features (AUC=0.72) and was similar to a model which included both texture and clinical features (AUC=0.87) for classifying participants with ΔSGRQ≥MCID. In addition, one of the top performing texture features, 2D diameter column, correlated with VDP (ρ=.43, *P*=.003), FVC (ρ=.37, *P*=.01), DL_{CO} (ρ=.39, *P*=.03), and R_{19} (ρ=-.41, *P*=.02) measured at 3-months post-COVID infection.

Moreover, original shape minor axis length was the top-performing feature of all clinical and MRI texture features and correlated with VDP (ρ=.33, *P*=.03) and R_{19} (ρ=-.37, *P*=.03) measured at 3-months post-infection. These results are indicative of ^{129}Xe MRI ventilation textures providing unique information about the spatial and intensity distribution of pulmonary ventilation that cannot be captured by ^{129}Xe VDP. Hence, MRI ventilation texture analysis offers evidence of subtle airway pathologies that may contribute to quality-of-life improvement in long-COVID participants.

To summarize, we have provided: 1) evidence of airways disease in long-COVID via the presence of MRI ventilation abnormalities; 2) data to support longitudinal improvement in MRI VDP, pulmonary function, and quality-of-life in participants with long-COVID and the potential relationship to small airways disease; 3) CT evidence of airway remodelling in females with long-COVID, similar to female ex-smokers with and without COPD; and, 4) evidence that MRI ventilation textures can predict clinically relevant quality-of-life improvement over one year in participants with long-COVID.

6.3 Limitations

The limitations specific to **Chapters 2-5** are detailed here and also provided in the Discussion section of the corresponding thesis chapter. Following this, I provide an overview of the general limitations relevant to the research presented in this thesis.

6.3.1 Study Specific Limitations

Chapter 2: *^{129}Xe MRI Ventilation Defects in Ever- and Never-Hospitalized People with Post-Acute COVID-19 Syndrome*

Our study included a relatively small sample size of participants, as compared to other publications investigating CT or x-ray imaging in COVID-19 or long-COVID patients.

However, we also note this study was the largest multi-centre investigation of long-COVID using hyperpolarized ^{129}Xe MRI. In addition, the majority of participants were recruited from quaternary care long-COVID clinics, which were designed to take a multi-disciplinary approach to treatment of all forms of long-COVID symptoms, including but not limited to respiratory manifestations of long-COVID sequalae. Therefore, there is a possibility for a bias for participants to have a greater number or intensity of symptoms as compared to the general public. Our participants were also enrolled from two relatively diverse regional healthcare systems embedded within a population of 14.7 million people served by a single universal and comprehensive health-care insurance plan. One site enrolled participants from a quaternary care academic health centre serving a mainly rural population, while the other site focused on enrollment from another quaternary care academic health centre, located about 100km away with a mainly urban population. As a result, the generalizability of our findings to other health-care jurisdictions may be limited.

Furthermore, for many of the participants that were not hospitalized during infection and had no history of respiratory illness prior to COVID, we report first-time chest imaging and pulmonary function results. As a result, the impact of any previous clinical history on reported long-COVID symptoms was difficult to untangle. Imaging and pulmonary function measurements prior to COVID-19 infection were also unavailable, which means the impact of COVID-19 on existing lung function remains unclear.

We also acknowledge that the convenience study group we evaluated included a relatively large number of people with previously diagnosed asthma (n=21) and COPD (n=6), which is a greater proportion of patients with co-morbid obstructive lung disease than previous reports.[6,20-24] There are likely complex interactions of this previous obstructive lung disease

with post-COVID pulmonary measurements including MRI VDP. Importantly, we reported that there were no significant differences in SGRQ and IPAQ scores between participants with and without a previous diagnosis of asthma or COPD, which underscores the severity and impact of long-COVID on symptoms and exercise capacity.

Lastly, as previously reported,[25] older people are at greater risk for poor COVID outcomes. There is also a complex relationship between age and MRI VDP[26] and so, age is an important factor to consider in our results. We note that that the ever-COVID group was significantly older than the never-COVID group and thus, this could have influenced VDP measurements in this group. However, MRI VDP was still greater in the ever-COVID group than predicted based on age alone and can still be considered abnormally elevated.[27,28]

Chapter 3: *Post-Acute COVID-19 Syndrome: ^{129}Xe MRI Ventilation Defects and Respiratory Outcomes One Year Later*

We acknowledge once again that this study had a relatively small sample size. In the context of the follow-up data, we note the possibility of a retention bias. Participants with persistent symptoms and poor quality-of-life may have been more inclined to return for repeat imaging, while participants who felt they had recovered were more likely to decline follow-up.

In addition, we did not receive ethics approval for repeat CT imaging and therefore, we were unable to quantify potential changes in CT airway, parenchymal, or pulmonary vascular at 15-months as compared to 3-months post-COVID. We also did not include ^{129}Xe MRI gas exchange measurements, as have been previously reported,[23,24,29-31] which limits our ability to evaluate the interaction between ventilation abnormalities and gas exchange measured on MRI.

Finally, we note all participants enrolled were followed by a multi-disciplinary quaternary care team based at long-COVID clinics and were prescribed treatment plans accordingly, perhaps

based on evidence of airways disease as a potential cause of long-COVID.[19] So, although we reported on prescribed therapies, we did not have any information about the rationale for such patient management decisions. Hence, there may be a selection bias for participants on prescribed therapy based on recruitment from these clinics.

Chapter 4: *Chest CT Airway and Vascular Measurement in Females with Long-COVID, Ex-smokers and COPD Patients*

We again acknowledge the relatively small sample size of participants included in the analysis here, particularly in each of the three subgroups in this study. Moreover, the single plane resolution of the CT acquisition was 0.625×0.625 mm^2 and as a result, we were unable to segment and quantify the small airways and vessels. Therefore, we report quantitative measurements only in larger anatomy evaluable on CT. Moreover, the long-COVID participants studied here did not have chest CT acquired prior to infection and thus, the airway and vessel metrics reported here may be a result of infection or could predate infection or long-COVID onset. In addition, the females with long-COVID were significantly younger than the ex-smokers with and without COPD. Although age was used a confounding variable when determining the differences in CT measurements, some of the differences and/or similarities reported here may be conservative estimates due the changes in the aging lung.[32] Furthermore, differences in CT acquisition protocols, segmentation techniques, and inconsistent methods of statistical comparison in existing literature[33-42] make it difficult to determine whether the CT airway and vessel measurements reported here for females with long-COVID are "abnormal". Lastly, all participants enrolled in the study were infected in the earliest waves of the pandemic, between September 2020 and April 2021. However, we were unable to collect information on

the specific strain of SARS-CoV-2 that caused infection for these study participants. Thus, we cannot parse out whether the strain of infection played a role in the results reported here.

Chapter 5: *^{129}Xe MRI Ventilation Textures and Longitudinal Quality-of-Life Improvements in Long-COVID*

Once again, we note the relatively small sample size with a potential retention bias for persistent symptoms and poor quality-of-life in those participants who consented to follow-up imaging. We also note the limited generalizability of this study due to the smaller sample size in comparison to other machine-learning studies. However, the analysis included multi-centre data, multiple feature selection approaches, and cross-validation to prevent overfitting.

All participants included in the analysis did not consent to CT imaging and so, CT radiomics data could not be included to complement the MRI data and/or to directly compare results with existing CT radiomics work. Finally, the SGRQ score was specifically designed to evaluate patients with COPD[43] and may not be directly applicable to a group of participants with long-COVID. It was used for the purposes of this study due to the lack of questionnaires specific to COVID-19 at the time of study initiation and the comprehensive nature of the different components of SGRQ that consider symptoms, activity limitations, and impact.

6.3.2 General Limitations

A general study limit pertinent to **Chapters 2-5** is the lack of information on the specific COVID-19 variants causing infection in our participants with long-COVID. All of our participants were recruited and enrolled to the study between July 2020 and August 2021. Due to the inclusion criteria of the study, this means COVID-19 infection for these participants could have occurred as early as March 2020. During this time frame in Canada, there were multiple variants of the original strain of COVID-19, including the alpha (arrived by December

2020),[44] beta (arrived by January 2021),[45] gamma (arrived by February 2021)[46] and delta (arrived by April 2021)[47] variants. Compared to the original strain, the variants were reported to be more transmissible, with a higher viral load, and resulted in a greater mortality risk and rate of severe illness.[48-51] There are also contradictory reports on the impact of different variants on eventual long-COVID incidence and symptoms[52-54] and so, it remains unclear what the effect of COVID-19 variants is on the results reported here in patients with long-COVID.

An additional limitation of **Chapters 2-5** is the unknown impact of vaccination status on the results reported. At the time of enrollment, there were no vaccines available for COVID-19 and so, all participants were unvaccinated. However, in the time between baseline and follow-up study visits, vaccines became available in Canada and institutional guidelines at Western University required all personnel on-site to be vaccinated, including study participants. Thus, the majority of participants who attended a follow-up visit 15-months post-infection were vaccinated between visits. There have been reports of vaccination prior to acute COVID-19 infection reducing the subsequent risk of long-COVID;[55] however, all of our participants developed long-COVID prior to vaccination. In the context of vaccination impact on existing long-COVID, there is no consensus with multiple studies reporting contradictory results.[55] In the existing literature, some agree that vaccination results in improvement of long-COVID symptoms, while others report no change or worsening of symptoms.[55] Hence, it is difficult to decipher the role of vaccination on the longitudinal progression of long-COVID in the participants studied.

Another general study limitation for **Chapters 2-5** pertains to the lack of data relating to the infection course for participants who were never hospitalized with acute COVID-19 infection. The majority of data for this time period is entirely self-reported by the participants, during

their initial study visit, which was three months following infection. Participants who were hospitalized were more likely to have had some medical imaging acquired during infection, as well as notes in their online health record regarding their infection. For participants who did not consent to CT imaging at the time of their visit, imaging from their hospital stay may have been used in the analysis and perhaps biased the results towards those with more severe acute disease.

Lastly, the study participants analyzed for **Chapters 2-5** were all recruited as part of the LIVECOVIDFREE study, which included multiple academic centers across Ontario. A large proportion of these participants were recruited from or referred by respirologists working at a long-COVID clinic, which employed a multi-disciplinary team focused specifically on the treatment of patients with long-COVID. The patients attending these clinics may report more severe symptoms or poorer quality-of-life relative to the average person with long-COVID. In this way, the data here may be biased and perhaps not generalizable to the broader long-COVID population.

6.4 Future Directions

6.4.1 Automated Ventilation Defect Segmentation and Analysis

The work presented here used a semi-automated segmentation algorithm to quantify VDP.[56] The development of this algorithm occurred during a time period when hyperpolarized ^{3}He MRI was the primary method of ventilation imaging and has not since been optimized for ^{129}Xe MRI. In fact, ^{129}Xe differs from ^{3}He MRI due to differences in gas distribution in the lungs as a result of greater gas density, viscosity, and solubility of ^{129}Xe.[57,58] Previous work has also explored the greater sensitivity of ^{129}Xe to ventilation abnormalities, as compared to ^{3}He.[59,60] Moreover, the current algorithm specifically quantifies only regions of ventilation "defects" as

defined by a k-means clustering approach,[56] resulting in a binary classification of ventilated versus non-ventilated regions of the lung. In this way, all ventilated regions of the lung are assumed to contribute equally to global lung function. Therefore, the objective of this preliminary work was to create an automated pipeline for quantification of ^{129}Xe MRI ventilation defects, with minimal user input, and to use as a foundation for further image analysis using ventilation texture feature extraction tools.

A multistep segmentation algorithm was generated in a Python environment (Python version 3.10.0). The pipeline was designed to match the proton and ^{129}Xe ventilation MR images in size, generate a whole lung mask by segmenting the thoracic cavity in the proton image, co-register and multiply the lung mask with the ventilation images, and calculate VDP. The pipeline is summarized in **Figure 6-1**. The first step was to normalize both the proton and ^{129}Xe MR images to gray values between 0 and 255. All images were also resized to match one another as 128×128 matrices. Next, the proton images were denoised, k-means clustering was applied to reduce unnecessary information in the image, the total thoracic cavity was automatically contoured, a binary mask was generated for the lungs, and the mask edges were smoothed. Then, the ^{129}Xe ventilation image was denoised before being co-registered with the lung mask using affine transformations and registration. This co-registration removed the background noise in the ventilation images and segmented out the trachea so only the lung regions remained in the image. Lastly, a k-means clustering algorithm was applied to the co-registered ventilation images where the most hypointense cluster was considered ventilation defect and normalized to the entire cavity volume to calculate VDP.

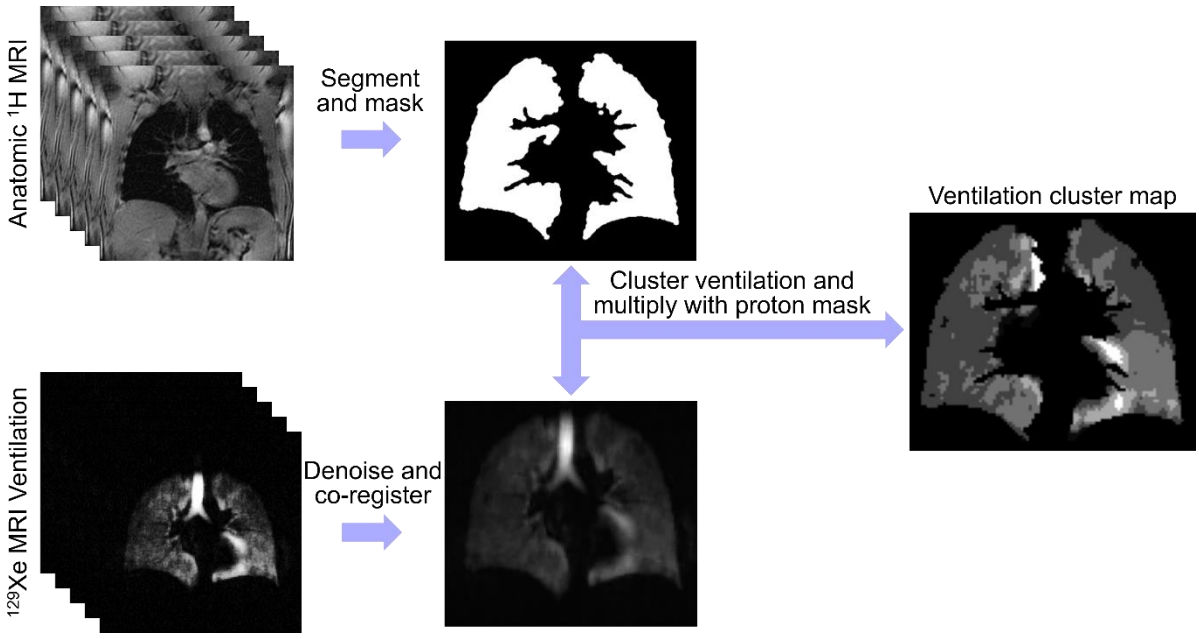

Figure 6-1. Summary of Automated VDP Pipeline
The pipeline begins with segmenting the ^{1}H MR images into binary masks of the thoracic cavity, which is co-registered with the denoised ^{129}Xe MR ventilation images. The subsequent mask is multiplied with the ventilation images before k-means clustering is applied and VDP is calculated.

This preliminary work lays the foundation for creating a fully automated segmentation and analysis pipeline for ^{129}Xe MRI. By eliminating the necessity of any user input throughout the pipeline, variability in VDP calculations as a result of inter- and intra-user reliability is also eliminated. In addition, the new algorithm can be used a base for optimizing VDP calculation for ^{129}Xe rather than ^{3}He images, aligning with the current trajectory of the hyperpolarized noble gas MRI field. Furthermore, additional methods of ventilation analysis can easily be incorporated into the pipeline. This includes new approaches for calculating VDP, as well as integrating texture feature extraction methodology for increased analysis of the images. ^{129}Xe MRI ventilation texture features can provide additional information, beyond the binary calculation of ventilation defects, by exploiting signal intensity differences and spatial pixel locations in the pulmonary ventilation signal. Hence, this proposed future work helps fill existing gaps in hyperpolarized gas ventilation imaging analysis.

6.4.2 Imaging Phenotypes of Long-COVID

Imaging-based phenotypes have previously been established in other respiratory diseases, such as COPD and asthma. Both CT and hyperpolarized gas MRI imaging biomarkers were used to characterize COPD phenotypes in large cohort studies.[61-63] In patients with asthma, quantitative CT and MRI measurements were also used to identify novel imaging phenotypes.[64-66] In this way, imaging was used to classify distinct structure-function pathologies in both COPD and asthma, with the possibility for informing improved clinical decision-making.

Our study included the only paired ^{129}Xe MR and CT imaging for patients with long-COVID to date. Although there is an abundance of literature on CT findings in both COVID-19 and long-COVID, our study is also unique in its use of both quantitative airway and pulmonary vasculature measurements. This opens the door for using these imaging biomarkers to generate imaging phenotypes or clusters of patients with long-COVID to drive an improved understanding of potential disease pathophysiology and how it may differ across patients. This thesis has provided evidence for the utility of pulmonary imaging in long-COVID to investigate airway dysfunction and/or remodelling, thus imaging-based clusters can contribute to clinical care for long-COVID.

One of the most common methods for generating imaging-based phenotypes includes using clustering techniques, as previously described.[65] Briefly, to summarize, variables for the clustering model can be selected using univariate correlations, with the use of the Kaiser-Mayer-Olkin measure of sampling adequacy[67] and Bartlett's test of sphericity[68] to determine common variance between variables.[65] The variable scales are normalized using z-transformation before hierarchal clustering can be performed to determine the likely number

of clusters[65,66] and k-means clustering can be used as the clustering method. The last step would be to use internal cluster validation (silhouette width,[69] Davies-Bouldin index,[70] Dunn's index[71]) to determine the quality of clustering.[65]

6.5 Significance and Impact

The onset of the COVID-19 pandemic set off a cascade of events that would have significant long-term impacts on the global population. One such repercussion is the prevalence of long-COVID, which is an umbrella term used to describe the myriad of post-infection sequelae and impaired quality-of-life affecting millions of people.[5-7,72-74] Despite similar phenomenon occurring following previous infectious outbreaks,[137,138] the relative novelty of this specific syndrome means that its exact mechanisms and pathophysiology are poorly understood. Instead, patients with long-COVID struggled with a lack of complete diagnosis and limited treatment options available to resolve the symptoms inhibiting their return to pre-infection daily life.[75-77] Although CT imaging played a key role in helping to manage and monitor acute COVID-19 disease, it did not provide a method to fully elucidate the pulmonary abnormalities relating to long-COVID, particularly when most CT imaging focused solely on density metrics.[6,13-15]

This thesis advances our understanding of the pulmonary pathophysiology contributing to the manifestation of long-COVID using quantitative MRI and CT measurements. The research presented in this thesis provides evidence for an airways disease phenotype of long-COVID, which may be characterized by airway dysfunction and remodelling. I have demonstrated that ^{129}Xe MRI and CT provide invaluable insight on the structural mechanisms of airways disease in long-COVID and their physiological relevance by allowing for the evaluation of the existing structure-function relationships. Armed with this understanding, there is potential to inform

clinical decision-making to improve treatment options and subsequently, patient outcomes. As this thesis has shown, pulmonary imaging provides sensitive information which can have a real-time clinical impact on helping long-COVID patients recover their quality-of-life.

6.6 References

1. Zhu, N., *et al.* A Novel Coronavirus from Patients with Pneumonia in China, 2019. *N Engl J Med* **382**, 727-733 (2020).

2. Huang, C., *et al.* Clinical features of patients infected with 2019 novel coronavirus in Wuhan, China. *Lancet* **395**, 497-506 (2020).

3. Dong, E., Du, H. & Gardner, L. An interactive web-based dashboard to track COVID-19 in real time. *Lancet Infect Dis* **20**, 533-534 (2020).

4. World Health Organization. WHO Director-General's opening remarks at the media briefing on COVID-19. (2020).

5. Carfi, A., Bernabei, R., Landi, F. & Gemelli Against COVID-19 Post-Acute Care Study Group. Persistent Symptoms in Patients After Acute COVID-19. *JAMA* **324**, 603-605 (2020).

6. Huang, C., *et al.* 6-month consequences of COVID-19 in patients discharged from hospital: a cohort study. *Lancet* **397**, 220-232 (2021).

7. National Institute of Health and Care Excellence. COVID-19 Rapid Guideline: Managing COVID-19. (NICE, 2021).

8. Chen, C., *et al.* Global Prevalence of Post-Coronavirus Disease 2019 (COVID-19) Condition or Long COVID: A Meta-Analysis and Systematic Review. *J Infect Dis* **226**, 1593-1607 (2022).

9. O'Mahoney, L.L., *et al.* The prevalence and long-term health effects of Long Covid among hospitalised and non-hospitalised populations: A systematic review and meta-analysis. *EClinicalMedicine* **55**, 101762 (2023).

10. Cutler, D.M. & Summers, L.H. The COVID-19 Pandemic and the $16 Trillion Virus. *JAMA* **324**, 1495-1496 (2020).

11. Cutler, D.M. The Costs of Long COVID. *JAMA Health Forum* **3**, e221809 (2022).

12. Xiong, Y., *et al.* Clinical and High-Resolution CT Features of the COVID-19 Infection: Comparison of the Initial and Follow-up Changes. *Invest Radiol* **55**, 332-339 (2020).

13. Liu, M., Lv, F., Huang, Y. & Xiao, K. Follow-Up Study of the Chest CT Characteristics of COVID-19 Survivors Seven Months After Recovery. *Front Med (Lausanne)* **8**, 636298 (2021).

14. Caruso, D., *et al.* Post-Acute Sequelae of COVID-19 Pneumonia: Six-month Chest CT Follow-up. *Radiology* **301**, E396-E405 (2021).

15. Han, X., *et al.* Six-month Follow-up Chest CT Findings after Severe COVID-19 Pneumonia. *Radiology* **299**, E177-E186 (2021).

16. Sylvester, S.V., *et al.* Sex differences in sequelae from COVID-19 infection and in long COVID syndrome: a review. *Curr Med Res Opin* **38**, 1391-1399 (2022).

17. Bowyer, R.C.E., *et al.* Characterising patterns of COVID-19 and long COVID symptoms: evidence from nine UK longitudinal studies. *Eur J Epidemiol* **38**, 199-210 (2023).

18. Kooner, H., *et al.* Sex Differences in CT Airway Measurements and Their Relationship to Post-Acute COVID-19 Syndrome. in *D109. THE LONG AND THE SHORT OF LONG COVID* A6791-A6791 (American Thoracic Society, 2023).

19. Adeloye, D., *et al.* The long-term sequelae of COVID-19: an international consensus on research priorities for patients with pre-existing and new-onset airways disease. *Lancet Respir Med* **9**, 1467-1478 (2021).

20. Chopra, V., Flanders, S.A., O'Malley, M., Malani, A.N. & Prescott, H.C. Sixty-Day Outcomes Among Patients Hospitalized With COVID-19. *Ann Intern Med* **174**, 576-578 (2021).

21. Shah, A.S., *et al.* A prospective study of 12-week respiratory outcomes in COVID-19-related hospitalisations. *Thorax* **76**, 402-404 (2021).

22. Mandal, S., *et al.* 'Long-COVID': a cross-sectional study of persisting symptoms, biomarker and imaging abnormalities following hospitalisation for COVID-19. *Thorax* **76**, 396-398 (2021).

23. Li, H., *et al.* Damaged lung gas exchange function of discharged COVID-19 patients detected by hyperpolarized (129)Xe MRI. *Sci Adv* **7**(2021).

24. Grist, J.T., *et al.* Hyperpolarized (129)Xe MRI Abnormalities in Dyspneic Patients 3 Months after COVID-19 Pneumonia: Preliminary Results. *Radiology* **301**, E353-E360 (2021).

25. Yanez, N.D., Weiss, N.S., Romand, J.A. & Treggiari, M.M. COVID-19 mortality risk for older men and women. *BMC public health* **20**, 1742 (2020).

26. Parraga, G., Mathew, L., Etemad-Rezai, R., McCormack, D.G. & Santyr, G.E. Hyperpolarized 3He magnetic resonance imaging of ventilation defects in healthy elderly volunteers: initial findings at 3.0 Tesla. *Acad Radiol* **15**, 776-785 (2008).

27. Sheikh, K., *et al.* Pulmonary ventilation defects in older never-smokers. *J Appl Physiol* **117**, 297-306 (2014).

28. McIntosh, M.J., *et al.* (129)Xe MRI Ventilation Defects in Asthma: What is the Upper Limit of Normal and Minimal Clinically Important Difference? *Acad Radiol* (2023).

29. Grist, J.T., *et al.* Lung Abnormalities Depicted with Hyperpolarized Xenon MRI in Patients with Long COVID. *Radiology*, 220069 (2022).

30. Matheson, A.M., *et al.* Persistent (129)Xe MRI Pulmonary and CT Vascular Abnormalities in Symptomatic Individuals with Post-Acute COVID-19 Syndrome. *Radiology*, 220492 (2022).

31. Matheson, A.M., *et al.* Longitudinal follow-up of postacute COVID-19 syndrome: DL(CO), quality-of-life and MRI pulmonary gas-exchange abnormalities. *Thorax* (2023).

32. Niewoehner, D.E. & Kleinerman, J. Morphologic basis of pulmonary resistance in the human lung and effects of aging. *J Appl Physiol* **36**, 412-418 (1974).

33. Charbonnier, J.P., *et al.* Airway wall thickening on CT: Relation to smoking status and severity of COPD. *Respir Med* **146**, 36-41 (2019).

34. Hasegawa, M., *et al.* Airflow limitation and airway dimensions in chronic obstructive pulmonary disease. *Am J Respir Crit Care Med* **173**, 1309-1315 (2006).

35. Nakano, Y., *et al.* Computed tomographic measurements of airway dimensions and emphysema in smokers. Correlation with lung function. *Am J Respir Crit Care Med* **162**, 1102-1108 (2000).

36. Telenga, E.D., *et al.* Airway wall thickness on HRCT scans decreases with age and increases with smoking. *BMC Pulm Med* **17**, 27 (2017).

37. Kirby, M., *et al.* Total Airway Count on Computed Tomography and the Risk of Chronic Obstructive Pulmonary Disease Progression. Findings from a Population-based Study. *Am J Respir Crit Care Med* **197**, 56-65 (2018).

38. Smith, B.M., *et al.* Comparison of spatially matched airways reveals thinner airway walls in COPD. The Multi-Ethnic Study of Atherosclerosis (MESA) COPD Study and the Subpopulations and Intermediate Outcomes in COPD Study (SPIROMICS). *Thorax* **69**, 987-996 (2014).

39. Wyszkiewicz, P.V., *et al.* Reduced Total Airway Count and Airway Wall Tapering after Three-Years in Ex-Smokers. *COPD* **20**, 186-196 (2023).

40. Washko, G.R., *et al.* Arterial Vascular Pruning, Right Ventricular Size, and Clinical Outcomes in Chronic Obstructive Pulmonary Disease. A Longitudinal Observational Study. *Am J Respir Crit Care Med* **200**, 454-461 (2019).

41. Tang, G., *et al.* Correlations of Computed Tomography Measurement of Distal Pulmonary Vascular Pruning with Airflow Limitation and Emphysema in COPD Patients. *Int J Chron Obstruct Pulmon Dis* **17**, 2241-2252 (2022).

42. Pistenmaa, C.L., *et al.* Pulmonary Arterial Pruning and Longitudinal Change in Percent Emphysema and Lung Function: The Genetic Epidemiology of COPD Study. *Chest* **160**, 470-480 (2021).

43. Jones, P.W., Quirk, F.H., Baveystock, C.M. & Littlejohns, P. A self-complete measure of health status for chronic airflow limitation. The St. George's Respiratory Questionnaire. *Am Rev Respir Dis* **145**, 1321-1327 (1992).

44. Aziz, S. Canada reports first cases of U.K. coronavirus variant. Here's what you need to know. in *Global News* (Corus Entertainment Inc., Online, 2020).

45. Heidenreich, P. & Gibson, C. Officials confirm Canada's 1st case of South African variant of COVID-19 detected in Alberta. in *Global News* (Corus Entertainment Inc, Online, 2021).

46. Favaro, A., Philip, E.S. & Jones, A.M. Third variant detected in Canada, prompting concern from health experts. in *CTV News* (Bell Media, Online, 2021).

47. Little, S. Dozens of cases of 'double mutant' COVID-19 variant confirmed in B.C. in *Global News* (Corus Entertainment Inc., Online, 2021).

48. Davies, N.G., *et al.* Increased mortality in community-tested cases of SARS-CoV-2 lineage B.1.1.7. *Nature* **593**, 270-274 (2021).

49. Li, B., *et al.* Viral infection and transmission in a large, well-traced outbreak caused by the SARS-CoV-2 Delta variant. *Nature Commun* **13**, 460 (2022).

50. Faria, N.R., *et al.* Genomics and epidemiology of the P.1 SARS-CoV-2 lineage in Manaus, Brazil. *Science* **372**, 815-821 (2021).

51. Twohig, K.A., *et al.* Hospital admission and emergency care attendance risk for SARS-CoV-2 delta (B.1.617.2) compared with alpha (B.1.1.7) variants of concern: a cohort study. *Lancet Infect Dis* **22**, 35-42 (2022).

52. Spinicci, M., *et al.* Infection with SARS-CoV-2 Variants Is Associated with Different Long COVID Phenotypes. *Viruses* **14**(2022).

53. Kenny, G., *et al.* Impact of vaccination and variants of concern on long COVID clinical phenotypes. *BMC Infect Dis* **23**, 804 (2023).

54. Saigal, A., *et al.* Cross-sectional study evaluating the impact of SARS-CoV-2 variants on Long COVID outcomes in UK hospital survivors. *BMJ Open Respir Res* **10**(2023).

55. Notarte, K.I., *et al.* Impact of COVID-19 vaccination on the risk of developing long-COVID and on existing long-COVID symptoms: A systematic review. *EClinicalMedicine* **53**, 101624 (2022).

56. Kirby, M., *et al.* Hyperpolarized 3He magnetic resonance functional imaging semiautomated segmentation. *Acad Radiol* **19**, 141-152 (2012).

57. Chen, R.Y., *et al.* Tissue-blood partition coefficient for xenon: temperature and hematocrit dependence. *J Appl Physiol Respir Environ Exerc Physiol* **49**, 178-183 (1980).

58. Kirby, M., *et al.* Pulmonary ventilation visualized using hyperpolarized helium-3 and xenon-129 magnetic resonance imaging: differences in COPD and relationship to emphysema. *J Appl Physiol* **114**, 707-715 (2013).

59. Kirby, M., *et al.* Hyperpolarized 3He and 129Xe MR imaging in healthy volunteers and patients with chronic obstructive pulmonary disease. *Radiology* **265**, 600-610 (2012).

60. Svenningsen, S., *et al.* Hyperpolarized (3) He and (129) Xe MRI: differences in asthma before bronchodilation. *J Magn Reson Imaging* **38**, 1521-1530 (2013).

61. Vestbo, J., *et al.* Evaluation of COPD Longitudinally to Identify Predictive Surrogate End-points (ECLIPSE). *Eur Respir J* **31**, 869-873 (2008).

62. Hoffman, E.A., *et al.* Pulmonary CT and MRI phenotypes that help explain chronic pulmonary obstruction disease pathophysiology and outcomes. *J Magn Reson Imaging* **43**, 544-557 (2016).

63. Lynch, D.A. & Al-Qaisi, M.A. Quantitative computed tomography in chronic obstructive pulmonary disease. *J Thorac Imaging* **28**, 284-290 (2013).

64. Choi, S., *et al.* Quantitative computed tomographic imaging-based clustering differentiates asthmatic subgroups with distinctive clinical phenotypes. *J Allergy Clin Immunol* **140**, 690-700 e698 (2017).

65. Eddy, R.L., *et al.* Pulmonary MRI and Cluster Analysis Help Identify Novel Asthma Phenotypes. *J Magn Reson Imaging* **56**, 1475-1486 (2022).

66. Gupta, S., *et al.* Quantitative computed tomography-derived clusters: redefining airway remodeling in asthmatic patients. *J Allergy Clin Immunol* **133**, 729-738 e718 (2014).

67. Kaiser, H.F. An index of factorial simplicity. *psychometrika* **39**, 31-36 (1974).

68. Bartlett, M.S. A note on the multiplying factors for various χ 2 approximations. *Journal of the Royal Statistical Society. Series B (Methodological)*, 296-298 (1954).

69. Rousseeuw, P.J. Silhouettes: a graphical aid to the interpretation and validation of cluster analysis. *J Comput Appl Math.* **20**, 53-65 (1987).

70. Davies, D.L. & Bouldin, D.W. A cluster separation measure. *IEEE transactions on pattern analysis and machine intelligence*, 224-227 (1979).

71. Dunn, J.C. Well-separated clusters and optimal fuzzy partitions. *J Cybern* **4**, 95-104 (1974).

72. Nalbandian, A., *et al.* Post-acute COVID-19 syndrome. *Nat Med* **27**, 601-615 (2021).

73. Soriano, J.B., *et al.* A clinical case definition of post-COVID-19 condition by a Delphi consensus. *Lancet Infect Dis* (2021).

74. Al-Aly, Z., Xie, Y. & Bowe, B. High-dimensional characterization of post-acute sequelae of COVID-19. *Nature* **594**, 259-264 (2021).

75. Rudenstine, S., *et al.* Long-COVID and comorbid depression and anxiety two years into the COVID-19 pandemic. *Psychiatry Res* **317**, 114924 (2022).

76. Fernandez-de-Las-Penas, C., *et al.* Anxiety, depression and poor sleep quality as long-term post-COVID sequelae in previously hospitalized patients: A multicenter study. *J Infect* **83**, 496-522 (2021).

77. Davis, H.E., *et al.* Characterizing long COVID in an international cohort: 7 months of symptoms and their impact. *EClinicalMedicine* **38**, 101019 (2021).

Appendices

Appendix A – More Data About ^{129}Xe Ventilation Defects in Long-COVID

In this article, we provided additional information regarding the longitudinal trajectory of ^{129}Xe ventilation defects in long-COVID, specifically in relation to differences in patients with and without a previous diagnosis of respiratory disease.

*The contents of this appendix were previously published in the Radiology journal as a letter to the editor: HK Kooner, MJ McIntosh, AM Matheson, S Svenningsen, and G Parraga. More Data about ^{129}Xe MRI Ventilation Defects in Long COVID-19. Radiology 2023; 307(4): e230749. doi: 10.1148/radiol.230479. Permission to reproduce this article was granted by the Radiological Society of North America (RSNA) and is provided in **Appendix B**.*

To the Editor:

We appreciated the Editorial[1] of our Original Research contribution[2] and would like to thank Dr. Vogel-Claussen for his insightful analysis and commentary. He rightly pointed out that abnormal ^{129}Xe MRI ventilation defect percent (VDP) at 15-months post-infection (n=53, 4.2±6.8%) may derive from PACS participants who self-identified with prior respiratory disease (n=22, 7.4±9.1%).

Based on his excellent comments, we thought it would be important to dig deeper into the data, so we performed additional analyses on the subgroups with and without prior respiratory disease.

In the subgroup with no self-reported previous lung disease, airways-disease medication at 3-months post-COVID infection was associated with a significant and clinically meaningful improvement in the St. George's Respiratory Questionnaire (SGRQ) score (OR=3.7, 95%CI: 1.02-13.14, *P*=.046) at 15-months as compared to 3-months post-infection. This was consistent with results in the entire group (OR=4.0, 95%CI: 1.2-13.8, *P*=.03)[2] and the smaller group of participants with prior respiratory illness (OR=4.5, 95%CI: 0.97-20.83, *P*=.05). Therefore, it appears that both subgroups showed an SGRQ improvement which correlated with airways-

disease treatment at 3-months. This finding supports the notion that there is an airways-disease component of PACS,[3] even in patients with no previous diagnosis of asthma or chronic obstructive pulmonary disease.

In the subgroup without respiratory disease, there was significantly improved forced expiratory volume in 1-second ($89\%_{pred}$, $97\%_{pred}$; P=.009), ratio of forced expiratory volume in 1-second to forced vital-capacity (79%, 84%; P=.008), diffusing capacity of the lungs for carbon-monoxide ($88\%_{pred}$, $105\%_{pred}$; P=.009), SGRQ score (35, 21; P=.003), and MRI VDP (3.2%, 1.5%; P<.001) at 15-months post-COVID as compared to 3-months.[2] Although trending in the right direction, forced expiratory volume in 1-second ($76\%_{pred}$, $82\%_{pred}$; P=.6), diffusing capacity of the lungs for carbon-monoxide ($83\%_{pred}$, $92\%_{pred}$; P>.99), SGRQ score (37, 30; P=.2) and VDP (9.4%, 7.4%; P=.2) were not significantly improved in participants with self-reported prior respiratory disease.

As Dr. Vogel-Claussen appropriately articulated,[1] PACS participants without previous lung disease may be normalizing and improving over time, whereas those with respiratory disease (mainly asthma in this group) may well be improving, but perhaps to a different baseline.

References

1. Vogel-Claussen, J. Ventilation Defects at (129)Xe MRI in Post-acute COVID-19 Syndrome: Back to Normal after 1 year? *Radiology*, 230113 (2023).

2. Kooner, H.K., *et al.* Post-Acute COVID-19 Syndrome: (129)Xe MRI Ventilation Defects and Respiratory Outcomes One Year Later. *Radiology*, 222557 (2023).

3. Adeloye, D., *et al.* The long-term sequelae of COVID-19: an international consensus on research priorities for patients with pre-existing and new-onset airways disease. *Lancet Respir Med* **9**, 1467-1478 (2021).

Appendix B – Permission for Reproduction of Scientific Articles

Chapter 2 was published under Creatives Commons CC BY-NC license. As author of the original article, I do not require permission to reproduce beyond citing the original source.

Chapter 3 is reproduced with permission:

This is a License Agreement between Harkiran K Kooner ("User") and Copyright Clearance Center, Inc. ("CCC") on behalf of the Rightsholder identified in the order details below. The license consists of the order details, the Marketplace Permissions General Terms and Conditions below, and any Rightsholder Terms and Conditions which are included below.

All payments must be made in full to CCC in accordance with the Marketplace Permissions General Terms and Conditions below.

Order Date	11-Jan-2024	Type of Use	Republish in a thesis/dissertation
Order License ID	1436912-1		
ISSN	1527-1315	Publisher	RADIOLOGICAL SOCIETY OF NORTH AMERICAN
		Portion	Chapter/article

LICENSED CONTENT

Publication Title	Radiology	Rightsholder	Radiological Society of North America
Article Title	Post-Acute COVID-19 Syndrome: 129 Xe MRI Ventilation Defects and Respiratory Outcomes One Year Later	Publication Type	e-Journal
		Start Page	222557
		Issue	2
Author/Editor	Radiological Society of North America.	Volume	307
		URL	http://radiology.rsnajnls.org/
Date	01/01/1923		
Language	English		
Country	United States of America		

REQUEST DETAILS

Portion Type	Chapter/article	Rights Requested	Main product
Page Range(s)	1-11	Distribution	Worldwide
Total Number of Pages	11	Translation	Original language of publication
Format (select all that apply)	Print, Electronic	Copies for the Disabled?	No
Who Will Republish the Content?	Academic institution	Minor Editing Privileges?	No
		Incidental Promotional Use?	No
Duration of Use	Life of current and all future editions	Currency	CAD
Lifetime Unit Quantity	Up to 999		

NEW WORK DETAILS

Title	Structure and Function of Long-COVID Evaluated Using Pulmonary Imaging	Institution Name	Western University
		Expected Presentation Date	2024-03-28
Instructor Name	Harkiran K Kooner		

The Requesting Person / Organization to Appear on the License	Harkiran K Kooner

REQUESTED CONTENT DETAILS

Title, Description or Numeric Reference of the Portion(s)	Full Article	**Title of the Article / Chapter the Portion Is From**	Post-Acute COVID-19 Syndrome: 129 Xe MRI Ventilation Defects and Respiratory Outcomes One Year Later
Editor of Portion(s)	Kooner, Harkiran K	**Author of Portion(s)**	Kooner, HK; McIntosh, MJ; Matheson, AM; Abdelrazek, M; Albert, MS; Dhaliwal, I; Kirby, M; Ouriadov, A; Santyr, GE; Venegas, C; Radadia, N; Svenningsen, S; Nicholson, JM; Parraga, G
Volume / Edition	307		
Page or Page Range of Portion	222557	**Publication Date of Portion**	2023-04-01

SPECIAL RIGHTSHOLDER TERMS AND CONDITIONS

full article for reuse in thesis/dissertation in print and electronic format ONLY.

Marketplace Permissions General Terms and Conditions

The following terms and conditions ("General Terms"), together with any applicable Publisher Terms and Conditions, govern User's use of Works pursuant to the Licenses granted by Copyright Clearance Center, Inc. ("CCC") on behalf of the applicable Rightsholders of such Works through CCC's applicable Marketplace transactional licensing services (each, a "Service").

1) **Definitions.** For purposes of these General Terms, the following definitions apply:

"License" is the licensed use the User obtains via the Marketplace platform in a particular licensing transaction, as set forth in the Order Confirmation.

"Order Confirmation" is the confirmation CCC provides to the User at the conclusion of each Marketplace transaction. "Order Confirmation Terms" are additional terms set forth on specific Order Confirmations not set forth in the General Terms that can include terms applicable to a particular CCC transactional licensing service and/or any Rightsholder-specific terms.

"Rightsholder(s)" are the holders of copyright rights in the Works for which a User obtains licenses via the Marketplace platform, which are displayed on specific Order Confirmations.

"Terms" means the terms and conditions set forth in these General Terms and any additional Order Confirmation Terms collectively.

"User" or "you" is the person or entity making the use granted under the relevant License. Where the person accepting the Terms on behalf of a User is a freelancer or other third party who the User authorized to accept the General Terms on the User's behalf, such person shall be deemed jointly a User for purposes of such Terms.

"Work(s)" are the copyright protected works described in relevant Order Confirmations.

2) **Description of Service.** CCC's Marketplace enables Users to obtain Licenses to use one or more Works in accordance with all relevant Terms. CCC grants Licenses as an agent on behalf of the copyright rightsholder identified in the relevant Order Confirmation.

Appendix A – More Data About ^{129Xe} Ventilation Defects in Long-COVID is reproduced with permission:

This is a License Agreement between Harkiran K Kooner ("User") and Copyright Clearance Center, Inc. ("CCC") on behalf of the Rightsholder identified in the order details below. The license consists of the order details, the Marketplace Permissions General Terms and Conditions below, and any Rightsholder Terms and Conditions which are included below.

All payments must be made in full to CCC in accordance with the Marketplace Permissions General Terms and Conditions below.

Order Date	18-Jan-2024	**Type of Use**	Republish in a thesis/dissertation
Order License ID	1439395-1		
ISSN	1527-1315	**Publisher**	RADIOLOGICAL SOCIETY OF NORTH AMERICAN
		Portion	Chapter/article

LICENSED CONTENT

Publication Title	Radiology	**Rightsholder**	Radiological Society of North America
Article Title	More Data about 129Xe MRI Ventilation Defects in Long COVID-19.	**Publication Type**	e-Journal
		Start Page	230479
Author/Editor	Radiological Society of North America.	**Issue**	4
		Volume	307
Date	01/01/1923	**URL**	http://radiology.rsnajnls.org/
Language	English		
Country	United States of America		

REQUEST DETAILS

Portion Type	Chapter/article	**Rights Requested**	Main product
Page Range(s)	1	**Distribution**	Worldwide
Total Number of Pages	1	**Translation**	Original language of publication
Format (select all that apply)	Print, Electronic	**Copies for the Disabled?**	No
Who Will Republish the Content?	Academic institution	**Minor Editing Privileges?**	No
		Incidental Promotional Use?	No
Duration of Use	Life of current and all future editions		
		Currency	CAD
Lifetime Unit Quantity	Up to 999		

NEW WORK DETAILS

Title	Structure and Function of Long-COVID Evaluated Using Pulmonary Imaging	**Institution Name**	Western University
		Expected Presentation Date	2024-03-28
Instructor Name	Harkiran K Kooner		

ADDITIONAL DETAILS

The Requesting Person / Organization to Appear on the License	Harkiran K Kooner

REQUESTED CONTENT DETAILS

Title, Description or Numeric Reference of the Portion(s)	Full Article	**Title of the Article / Chapter the Portion Is From**	More Data about 129Xe MRI Ventilation Defects in Long COVID-19.
Editor of Portion(s)	Kooner, Harkiran K; McIntosh, Marrissa J; Matheson, Alexander M; Svenningsen, Sarah; Parraga, Grace	**Author of Portion(s)**	Kooner, Harkiran K; McIntosh, Marrissa J; Matheson, Alexander M; Svenningsen, Sarah; Parraga, Grace
Volume / Edition	307	**Publication Date of Portion**	2023-05-01
Page or Page Range of Portion	230479		

SPECIAL RIGHTSHOLDER TERMS AND CONDITIONS

Request granted for full text of article for reuse in thesis/dissertation print and electronic format rights ONLY

Marketplace Permissions General Terms and Conditions

The following terms and conditions ("General Terms"), together with any applicable Publisher Terms and Conditions, govern User's use of Works pursuant to the Licenses granted by Copyright Clearance Center, Inc. ("CCC") on behalf of the applicable Rightsholders of such Works through CCC's applicable Marketplace transactional licensing services (each, a "Service").

1) **Definitions.** For purposes of these General Terms, the following definitions apply:

"License" is the licensed use the User obtains via the Marketplace platform in a particular licensing transaction, as set forth in the Order Confirmation.

"Order Confirmation" is the confirmation CCC provides to the User at the conclusion of each Marketplace transaction. "Order Confirmation Terms" are additional terms set forth on specific Order Confirmations not set forth in the General Terms that can include terms applicable to a particular CCC transactional licensing service and/or any Rightsholder-specific terms.

"Rightsholder(s)" are the holders of copyright rights in the Works for which a User obtains licenses via the Marketplace platform, which are displayed on specific Order Confirmations.

"Terms" means the terms and conditions set forth in these General Terms and any additional Order Confirmation Terms collectively.

"User" or "you" is the person or entity making the use granted under the relevant License. Where the person accepting the Terms on behalf of a User is a freelancer or other third party who the User authorized to accept the General Terms on the User's behalf, such person shall be deemed jointly a User for purposes of such Terms.

"Work(s)" are the copyright protected works described in relevant Order Confirmations.

2) **Description of Service.** CCC's Marketplace enables Users to obtain Licenses to use one or more Works in accordance with all relevant Terms. CCC grants Licenses as an agent on behalf of the copyright rightsholder identified in the relevant Order Confirmation.

3) **Applicability of Terms.** The Terms govern User's use of Works in connection with the relevant License. In the event of any conflict between General Terms and Order Confirmation Terms, the latter shall govern. User acknowledges that Rightsholders have complete discretion whether to grant any permission, and whether to place any limitations on any grant, and that CCC has no right to supersede or to modify any such discretionary act by a Rightsholder.

Appendix C – Health Sciences Research Ethics Board Approval Notices

Western Research

Date: 27 November 2020

To: Dr. Grace Parraga

Project ID: 116775

Study Title: Lung Structure-Function In SurVivors of Mild and SEvere COVID19 Infection: 129Xe MRI and CT For Rapid Evaluations and NExt-wave Healthcare Planning (LIVE COVID FREE)

Study Sponsor: Robarts Research Institute

Application Type: HSREB Initial Application

Review Type: Full Board

Meeting Date: 03/Nov/2020 13:00

Date Approval Issued: 27/Nov/2020 13:20

REB Approval Expiry Date: 27/Nov/2021

Dear Dr. Grace Parraga

The Western University Health Science Research Ethics Board (HSREB) has reviewed and approved the above mentioned study as described in the WREM application form, as of the HSREB Initial Approval Date noted above. This research study is to be conducted by the investigator noted above. All other required institutional approvals must also be obtained prior to the conduct of the study.

Documents Approved:

Document Name	Document Type	Document Date	Document Version
2.15 Other Instruments V1 Oct 14 2020	Other Data Collection Instruments	14/Oct/2020	V1
ROB0050 Borg Scale v1 June 18, 2019	Paper Survey	18/Jun/2019	V1
ROB0050 Ad with no tabs V2 November 6 2020	Recruitment Materials	06/Nov/2020	V2
ROB0050 Ad with tabs V2 November 6 2020	Recruitment Materials	06/Nov/2020	V2
ROB0050 Infographic V2 November 6 2020	Recruitment Materials	06/Nov/2020	V2
ROB0050 BDI-TDI-pdf	Paper Survey	19/Nov/1984	V1
ROB0050 CAT - English	Paper Survey	24/Jul/2009	
ROB0050 IPAQ_Elderly_English_self-admin_short (1)	Paper Survey	22/Mar/2015	V1
ROB0050 IPAQ_English_self-admin_long	Paper Survey	06/Nov/2010	V2
ROB0050 IPAQ_English_self-admin_short	Paper Survey	12/Jan/2012	V3
ROB0050 IPAQ_English_telephone_long	Paper Survey	23/Jan/2020	V1
ROB0050 IPAQ_English_telephone_short	Paper Survey	06/Nov/2010	V1
ROB0050 mMRC Dyspnea Score	Paper Survey	29/Sep/1988	
ROB0050 SGRQ 3 months	Paper Survey	03/Mar/2014	
ROB0050 Protocol V11 November 18 2020	Protocol	18/Nov/2020	V11
ROB0050 Letter of Information and Consent V3 Nov 18 2020	Written Consent/Assent	18/Nov/2020	V3

Documents Acknowledged:

Document Name	Document Type	Document Date	Document Version
Robarts IB 129Xe RRI draft revised September 21 2020	Investigator	21/Sep/2020	V8

clean	Brochure		
ROB0050 BUDGET Nov 17 2020	Study budget	17/Nov/2020	1
NOL ROB0050 Nov 27 2020	NOL/NOA/ITA	27/Nov/2020	

No deviations from, or changes to, the protocol or WREM application should be initiated without prior written approval of an appropriate amendment from Western HSREB , except when necessary to eliminate immediate hazard(s) to study participants or when the change(s) involves only administrative or logistical aspects of the trial.

REB members involved in the research project do not participate in the review, discussion or decision.

The Western University HSREB operates in compliance with, and is constituted in accordance with, the requirements of the TriCouncil Policy Statement: Ethical Conduct for Research Involving Humans (TCPS 2); the International Conference on Harmonisation Good Clinical Practice Consolidated Guideline (ICH GCP); Part C, Division 5 of the Food and Drug Regulations; Part 4 of the Natural Health Products Regulations; Part 3 of the Medical Devices Regulations and the provisions of the Ontario Personal Health Information Protection Act (PHIPA 2004) and its applicable regulations. The HSREB is registered with the U.S. Department of Health & Human Services under the IRB registration number IRB 00000940.

Please do not hesitate to contact us if you have any questions.

Sincerely,

Ms. Nicola Geoghegan-Morphet , Ethics Officer on behalf of Dr. Joseph Gilbert, HSREB Chair

Note: This correspondence includes an electronic signature (validation and approval via an online system that is compliant with all regulations).

Western Research

Date: 10 November 2023

To: Dr. Grace Parraga

Project ID: 116775

Review Reference: 2023-116775-85340

Study Title: Lung Structure-Function In SurVivors of Mild and SEvere COVID19 Infection: 129Xe MRI and CT For Rapid Evaluations and NExt-wave Healthcare Planning (LIVE COVID FREE)

Application Type: Continuing Ethics Review (CER) Form

Review Type: Delegated

Date Approval Issued: 10/Nov/2023 20:21

REB Approval Expiry Date: 27/Nov/2024

Dear Dr. Grace Parraga,

The Western University Research Ethics Board has reviewed the application. This study, including all currently approved documents, has been re-approved until the expiry date noted above.

REB members involved in the research project do not participate in the review, discussion or decision.

Western University REB operates in compliance with, and is constituted in accordance with, the requirements of the Tri-Council Policy Statement: Ethical Conduct for Research Involving Humans (TCPS 2); the International Conference on Harmonisation Good Clinical Practice Consolidated Guideline (ICH GCP); Part C, Division 5 of the Food and Drug Regulations; Part 4 of the Natural Health Products Regulations; Part 3 of the Medical Devices Regulations and the provisions of the Ontario Personal Health Information Protection Act (PHIPA 2004) and its applicable regulations. The REB is registered with the U.S. Department of Health & Human Services under the IRB registration number IRB 00000940.

Please do not hesitate to contact us if you have any questions.

Electronically signed by:

Mr. Joshua Hatherley, Ethics Coordinator on behalf of Dr. N. Poonai, HSREB Chair 10/Nov/2023 20:21

Reason: I am approving this document

Note: This correspondence includes an electronic signature (validation and approval via an online system that is compliant with all regulations).

Office of Research Ethics
The University of Western Ontario
Room 4180 Support Services Building, London, ON, Canada N6A 5C1
[redacted]
Website: www.uwo.ca/research/ethics

Use of Human Subjects - Ethics Approval Notice

Principal Investigator: Dr. G. Parraga
Review Number: 15930 **Review Level:** Full Board
Review Date: February 10, 2009

Protocol Title: Longitudinal Study of Helium-3 Magnetic Resonance Imaging of COPD
Department and Institution: Diagnostic Radiology & Nuclear Medicine, Robarts Research Institute
Sponsor: INTERNAL RESEARCH FUND-UWO
Ethics Approval Date: May 25, 2009 **Expiry Date:** November 30, 2013
Documents Reviewed and Approved: UWO Protocol, Letter of information & consent form for Patients dated March 26/09 & Letter of information & consent form for Healthy Volunteers dated March 26/09
Documents Received for Information: Protocol, January 27, 2009; IB, ed 6, 09 Sep. 05

This is to notify you that The University of Western Ontario Research Ethics Board for Health Sciences Research Involving Human Subjects (HSREB) which is organized and operates according to the Tri-Council Policy Statement: Ethical Conduct of Research Involving Humans and the Health Canada/ICH Good Clinical Practice Practices: Consolidated Guidelines; and the applicable laws and regulations of Ontario has reviewed and granted approval to the above referenced study on the approval date noted above. The membership of this REB also complies with the membership requirements for REB's as defined in Division 5 of the Food and Drug Regulations.

The ethics approval for this study shall remain valid until the expiry date noted above assuming timely and acceptable responses to the SREB's periodic requests for surveillance and monitoring information. If you require an updated approval notice prior to that time ou must request it using the UWO Updated Approval Request Form.

During the course of the research, no deviations from, or changes to, the protocol or consent form may be initiated without prior written approval from the HSREB except when necessary to eliminate immediate hazards to the subject or when the change(s) involve only logistical or administrative aspects of the study (e.g. change of monitor, telephone number). Expedited review of minor change(s) in ongoing studies will be considered. Subjects must receive a copy of the signed information/consent documentation.

Investigators must promptly also report to the HSREB:

a) changes increasing the risk to the participant(s) and/or affecting significantly the conduct of the study;
b) all adverse and unexpected experiences or events that are both serious and unexpected;
c) new information that may adversely affect the safety of the subjects or the conduct of the study.

If these changes/adverse events require a change to the information/consent documentation, and/or recruitment advertisement, the newly revised information/consent documentation, and/or advertisement, must be submitted to this office for approval.

Members of the HSREB who are named as investigators in research studies, or declare a conflict of interest, do not participate in discussion related to, nor vote on, such studies when they are presented to the HSREB.

[redacted]

Chair of HSREB: Dr. Joseph Gilbert

Ethics Officer to Contact for Further Information			
☑ Janice Sutherland [redacted]	☐ Elizabeth Wambolt [redacted]	☐ Grace Kelly [redacted]	☐ Denise Grafton [redacted]

This is an official document. Please retain the original in your files.

cc: ORE File
LHRI

Western Research

Date: 13 January 2023

To: Dr. Grace Parraga

Project ID: 6014

Review Reference: 2023-6014-74913

Study Title: Longitudinal Study of Helium-3 Magnetic Resonance Imaging of COPD

Application Type: Continuing Ethics Review (CER) Form

Review Type: Delegated

REB Meeting Date: 24/Jan/2023

Date Approval Issued: 13/Jan/2023 16:19

REB Approval Expiry Date: 10/Feb/2024

Dear Dr. Grace Parraga,

The Western University Research Ethics Board has reviewed the application. This study, including all currently approved documents, has been re-approved until the expiry date noted above.

REB members involved in the research project do not participate in the review, discussion or decision.

Western University REB operates in compliance with, and is constituted in accordance with, the requirements of the Tri-Council Policy Statement: Ethical Conduct for Research Involving Humans (TCPS 2); the International Conference on Harmonisation Good Clinical Practice Consolidated Guideline (ICH GCP); Part C, Division 5 of the Food and Drug Regulations; Part 4 of the Natural Health Products Regulations; Part 3 of the Medical Devices Regulations and the provisions of the Ontario Personal Health Information Protection Act (PHIPA 2004) and its applicable regulations. The REB is registered with the U.S. Department of Health & Human Services under the IRB registration number IRB 00000940.

Please do not hesitate to contact us if you have any questions.

Electronically signed by:

Karen Gopaul, Ethics Officer on behalf of Dr. P. Jones, HSREB Chair 13/Jan/2023 16:19

Reason: I am approving this document

Note: This correspondence includes an electronic signature (validation and approval via an online system that is compliant with all regulations).

Research Western

Use of Human Participants - Ethics Approval Notice

Principal Investigator: Dr. Grace Parraga
Review Number: 18130
Review Level: Full Board
Approved Local Adult Participants: 100
Approved Local Minor Participants: 0
Protocol Title: A Single-center Study Evaluating Hyperpolarized 129Xenon Magnetic Resonance Imaging in Subjects with Chronic Lung Disease
Department & Institution: Imaging,Robarts Research Institute
Sponsor: Canadian Institutes of Health Research

Ethics Approval Date: August 12, 2011 **Expiry Date:** August 31, 2016

Documents Reviewed & Approved & Documents Received for Information:

Document Name	Comments	Version Date
UWO Protocol		
Letter of Information & Consent		2011/07/13
Advertisement		2011/07/13
Protocol	Received for information only	2011/06/22

This is to notify you that the University of Western Ontario Health Sciences Research Ethics Board (HSREB) which is organized and operates according to the Tri-Council Policy Statement: Ethical Conduct of Research Involving Humans and the Health Canada/ICH Good Clinical Practice Practices: Consolidated Guidelines; and the applicable laws and regulations of Ontario has reviewed and granted approval to the above referenced study on the approval date noted above. The membership of this HSREB also complies with the membership requirements for REB's as defined in Division 5 of the Food and Drug Regulations.

The ethics approval for this study shall remain valid until the expiry date noted above assuming timely and acceptable responses to the HSREB's periodic requests for surveillance and monitoring information. If you require an updated approval notice prior to that time you must request it using the UWO Updated Approval Request form.

Member of the HSREB that are named as investigators in research studies, or declare a conflict of interest, do not participate in discussions related to, nor vote on, such studies when they are presented to the HSREB.

The Chair of the HSREB is Dr. Joseph Gilbert. The UWO HSREB is registered with the U.S. Department of Health & Human Services under the IRB registration number IRB 00000940.

[redacted]

Signature

Ethics Officer to Contact for Further Information

X Janice Sutherland [redacted]	Grace Kelly [redacted]	Shantel Walcott [redacted]

This is an official document. Please retain the original in your files.

Western Research

Date: 5 June 2023

To: Dr. Grace Parraga

Project ID: 100974

Review Reference: 2023-100974-80083

Study Title: A Single-center Study Evaluating Hyperpolarized 129Xenon Magnetic Resonance Imaging in Subjects with Chronic Lung Disease (REB #18130)

Application Type: Continuing Ethics Review (CER) Form

Review Type: Delegated

Date Approval Issued: 05/Jun/2023 09:35

REB Approval Expiry Date: 05/Jul/2024

Dear Dr. Grace Parraga,

The Western University Research Ethics Board has reviewed the application. This study, including all currently approved documents, has been re-approved until the expiry date noted above.

REB members involved in the research project do not participate in the review, discussion or decision.

Western University REB operates in compliance with, and is constituted in accordance with, the requirements of the Tri-Council Policy Statement: Ethical Conduct for Research Involving Humans (TCPS 2); the International Conference on Harmonisation Good Clinical Practice Consolidated Guideline (ICH GCP); Part C, Division 5 of the Food and Drug Regulations; Part 4 of the Natural Health Products Regulations; Part 3 of the Medical Devices Regulations and the provisions of the Ontario Personal Health Information Protection Act (PHIPA 2004) and its applicable regulations. The REB is registered with the U.S. Department of Health & Human Services under the IRB registration number IRB 00000940.

Please do not hesitate to contact us if you have any questions.

Electronically signed by:

Mr. Joshua Hatherley, Ethics Coordinator on behalf of Dr. N. Poonai, HSREB Chair 05/Jun/2023 09:35

Reason: I am approving this document

Note: This correspondence includes an electronic signature (validation and approval via an online system that is compliant with all regulations).

Western Research

Research Ethics

Use of Human Participants - Ethics Approval Notice

Principal Investigator: Dr. Grace Parraga
File Number:103516
Review Level: Full Board
Approved Local Adult Participants:200
Approved Local Minor Participants:0
Protocol Title: Structure and Function MRI of Asthma
Department & Institution: Schulich School of Medicine and Dentistry\Imaging,Robarts Research Institute
Sponsor:
Ethics Approval Date: April 08, 2013
Ethics Expiry Date: March 31, 2020

Documents Reviewed & Approved & Documents Received for Information:

Document Name	Comments	Version Date
Protocol	Robarts Protocol - Received for information only	2013/02/06
Instruments	Telephone Script	2013/03/14
Letter of Information & Consent	ROB0037 ICF March 13 2013	2013/03/13
Western University Protocol	(including study instruments & questionnaires)	

This is to notify you that the University of Western Ontario Health Sciences Research Ethics Board (HSREB) which is organized and operates according to the Tri-Council Policy Statement: Ethical Conduct of Research Involving Humans and the Health Canada/ICH Good Clinical Practice Practices: Consolidated Guidelines; and the applicable laws and regulations of Ontario has reviewed and granted approval to the above referenced study on the approval date noted above. The membership of this HSREB also complies with the membership requirements for REB's as defined in Division 5 of the Food and Drug Regulations.

The ethics approval for this study shall remain valid until the expiry date noted above assuming timely and acceptable responses to the HSREB's periodic requests for surveillance and monitoring information. If you require an updated approval notice prior to that time you must request it using the University of Western Ontario Updated Approval Request form.

Member of the HSREB that are named as investigators in research studies, or declare a conflict of interest, do not participate in discussions related to, nor vote on, such studies when they are presented to the HSREB.

The Chair of the HSREB is Dr. Joseph Gilbert. The HSREB is registered with the U.S. Department of Health & Human Services under the IRB registration number IRB 00000940.

[redacted]

Signature

Ethics Officer to Contact for Further Information

☑ Janice Sutherland [redacted]	☐ Grace Kelly [redacted]	☐ Shantel Walcott [redacted]

This is an official document. Please retain the original in your files.

Western University, Research, Support Services Bldg., Rm. 5150
London, ON, Canada N6A 3K7 [redacted]

Western Research

Date: 31 January 2023

To: Dr. Grace Parraga

Project ID: 103516

Review Reference: 2023-103516-75680

Study Title: Structure and Function MRI of Asthma

Application Type: Continuing Ethics Review (CER) Form

Review Type: Delegated

REB Meeting Report Date: 21/Feb/2023

Date Approval Issued: 31/Jan/2023 12:44

REB Approval Expiry Date: 19/Feb/2024

Dear Dr. Grace Parraga,

The Western University Research Ethics Board has reviewed the application. This study, including all currently approved documents, has been re-approved until the expiry date noted above.

REB members involved in the research project do not participate in the review, discussion or decision.

Western University REB operates in compliance with, and is constituted in accordance with, the requirements of the Tri-Council Policy Statement: Ethical Conduct for Research Involving Humans (TCPS 2); the International Conference on Harmonisation Good Clinical Practice Consolidated Guideline (ICH GCP); Part C, Division 5 of the Food and Drug Regulations; Part 4 of the Natural Health Products Regulations; Part 3 of the Medical Devices Regulations and the provisions of the Ontario Personal Health Information Protection Act (PHIPA 2004) and its applicable regulations. The REB is registered with the U.S. Department of Health & Human Services under the IRB registration number IRB 00000940.

Please do not hesitate to contact us if you have any questions.

Electronically signed by:

Patricia Sargeant, Ethics Officer (psargean@uwo.ca) on behalf of Dr. P. Jones, HSREB Chair 31/Jan/2023 12:44

Reason: I am approving this document

Note: This correspondence includes an electronic signature (validation and approval via an online system that is compliant with all regulations).

Research Western

Use of Human Participants - Ethics Approval Notice

Principal Investigator: Dr. Grace Parraga
Review Number: 18131
Review Level: Full Board
Approved Local Adult Participants: 50
Approved Local Minor Participants: 0
Protocol Title: Xenon-129 Magnetic Resonance Imaging of Healthy Subjects: Hardware and Software Development and Reproducibility
Department & Institution: Imaging,Robarts Research Institute
Sponsor: Canadian Institutes of Health Research

Ethics Approval Date: August 12, 2011 **Expiry Date:** August 31, 2016

Documents Reviewed & Approved & Documents Received for Information:

Document Name	Comments	Version Date
UWO Protocol		
Letter of Information & Consent		2011/07/13
Protocol	Received for information only	2011/06/22
Advertisement		2011/07/13

This is to notify you that the University of Western Ontario Health Sciences Research Ethics Board (HSREB) which is organized and operates according to the Tri-Council Policy Statement: Ethical Conduct of Research Involving Humans and the Health Canada/ICH Good Clinical Practice Practices: Consolidated Guidelines; and the applicable laws and regulations of Ontario has reviewed and granted approval to the above referenced study on the approval date noted above. The membership of this HSREB also complies with the membership requirements for REB's as defined in Division 5 of the Food and Drug Regulations.

The ethics approval for this study shall remain valid until the expiry date noted above assuming timely and acceptable responses to the HSREB's periodic requests for surveillance and monitoring information. If you require an updated approval notice prior to that time you must request it using the UWO Updated Approval Request form.

Member of the HSREB that are named as investigators in research studies, or declare a conflict of interest, do not participate in discussions related to, nor vote on, such studies when they are presented to the HSREB.

The Chair of the HSREB is Dr. Joseph Gilbert. The UWO HSREB is registered with the U.S. Department of Health & Human Services under the IRB registration number IRB 00000940.

[redacted]

Signature

Ethics Officer to Contact for Further Information

Janice Sutherland [redacted]	Grace Kelly [redacted]	Shantel Walcott [redacted]

This is an official document. Please retain the original in your files.

Western Research

Date: 5 June 2023

To: Dr. Grace Parraga

Project ID: 100975

Review Reference: 2023-100975-80082

Study Title: Xenon-129 Magnetic Resonance Imaging of Healthy Subjects: Hardware and Software Development and Reproducibility (REB #18131)

Application Type: Continuing Ethics Review (CER) Form

Review Type: Delegated

Date Approval Issued: 05/Jun/2023 09:44

REB Approval Expiry Date: 05/Jul/2024

Dear Dr. Grace Parraga,

The Western University Research Ethics Board has reviewed the application. This study, including all currently approved documents, has been re-approved until the expiry date noted above.

REB members involved in the research project do not participate in the review, discussion or decision.

Western University REB operates in compliance with, and is constituted in accordance with, the requirements of the Tri-Council Policy Statement: Ethical Conduct for Research Involving Humans (TCPS 2); the International Conference on Harmonisation Good Clinical Practice Consolidated Guideline (ICH GCP); Part C, Division 5 of the Food and Drug Regulations; Part 4 of the Natural Health Products Regulations; Part 3 of the Medical Devices Regulations and the provisions of the Ontario Personal Health Information Protection Act (PHIPA 2004) and its applicable regulations. The REB is registered with the U.S. Department of Health & Human Services under the IRB registration number IRB 00000940.

Please do not hesitate to contact us if you have any questions.

Electronically signed by:

Mr. Joshua Hatherley, Ethics Coordinator on behalf of Dr. N. Poonai, HSREB Chair 05/Jun/2023 09:44

Reason: I am approving this document

Note: This correspondence includes an electronic signature (validation and approval via an online system that is compliant with all regulations).

HiREB

Hamilton Integrated Research Ethics Board

March 14 2018

Project Number: 3932

Project Title: Single-centre study exploring the utility of hyperpolarized 129Xe magnetic resonance imaging in healthy volunteers and patients with lung disease

Principal Investigator: Prof Parameswaran Nair

This will acknowledge receipt of your letters dated November 30, 2017 and March 6, 2018 which enclosed revised copies of the Information/Consent Form, Protocol and the Application Form along with a response to the additional queries of the Board for the above-named study. These issues were raised by the Hamilton Integrated Research Ethics Board at their meeting held on November 1, 2017. Based on this additional information, we wish to advise your study had been given ***final*** approval from the full HiREB.

The following documents have been approved on both ethical and scientific grounds:

Document Name	Document Date	Document Version
AQLQ(S)	Oct-05-2017	1
Asthma Control Questionnaire	Oct-05-2017	1
Consent_FIRH_Xe0001 V3 February 28 2018 CLEAN	Feb-28-2018	3
Study Protocol_FIRH_Xe0001 V4 Jan. 17, 2018 CLEAN	Jan-17-2018	4

The following documents have been acknowledged:

Document Name	Document Date	Document Version
Dr. Nair_GCP 2015; Certificate # 17461875	Oct-26-2015	1
NOL; Control #212608	Feb-14-2018	1
Clinical Trial Registration: # NCT03455686		
IRC_scirev_Nair-20171003	Oct-03-2017	1

Please Note: All consent forms and recruitment materials used in this study must be copies of the above referenced documents.

We are pleased to issue final approval for the above-named study for a period of 12 months from the date of the HiREB meeting on November 1, 2017. Continuation beyond that date will require further review and renewal of HiREB approval. Any changes or revisions to the original submission must be submitted on a HiREB amendment form for review and approval by the Hamilton Integrated Research Ethics Board.

PLEASE QUOTE THE ABOVE REFERENCED PROJECT NUMBER ON ALL FUTURE CORRESPONDENCE

Sincerely,

[redacted]

Dr. Frederick A. Spencer, MD
Chair, Hamilton Integrated Research Ethics Board

The Hamilton Integrated Research Ethics Board (HiREB) represents the institutions of Hamilton Health Sciences, St. Joseph's Healthcare Hamilton, and the Faculty of Health Sciences at McMaster University and operates in compliance with and is constituted in accordance with the requirements of: The Tri-Council Policy Statement on Ethical Conduct of Research Involving Humans; The International Conference on Harmonization of Good Clinical Practices; Part C Division 5 of the Food and Drug Regulations of Health Canada, and the provisions of the Ontario Personal Health Information Protection Act 2004 and its applicable Regulations; For studies conducted at St. Joseph's Healthcare Hamilton, HIREB complies with the health ethics guide of the Catholic Alliance of Canada

HiREB

Hamilton Integrated Research Ethics Board

Amendment Approval

May-16-2022

HiREB Project #: 3932

Project Submission Title: Single-centre study exploring the utility of hyperpolarized 129Xe magnetic resonance imaging in healthy volunteers and patients with lung disease

Local Principal Investigator: Dr Sarah Svenningsen

Document(s) Approved:

Document Name	Document Date	Document Version
Study Protocol_FIRH_Xe001 V6 9May2022 CLEAN	May-09-2022	6
Table of changes to Protocol	May-11-2022	1

Document(s) Acknowledged:

Document Name	Document Date	Document Version
CTA-N 11May2022 Correspondance for HiREB	May-11-2022	1

This amendment has been reviewed and approved as submitted:

[ ] Full Research Ethics Board

[X] Research Ethics Board Executive

[ ] Student Research Committee

Conditions:
In light of the current COVID-19 pandemic, while HiREB has reviewed and approved this application, the research must be conducted in accordance with institutional and/or public health requirements.

Sincerely,

[redacted]

Dr. Mark Inman, MD, PhD
Chair, Hamilton Integrated Research Ethics Board

HiREB

Hamilton Integrated Research Ethics Board

Nov-16-2020

Project Number: 12672

Project Title: Lung Structure-Function In Survivors of Mild and Severe COVID19 Infection: 129Xe MRI and CT For Rapid Evaluations and Next-wave Healthcare Planning

Principal Investigator: Dr Sarah Svenningsen

This will acknowledge receipt of your letters dated November 7, 2020 and November 15, 2020 which enclosed revised copies of the Information/Consent Form, Study Key, Case Report Form, Protocol and the Application Form along with a response to the additional queries of the Board for the above-named study. These issues were raised by the Hamilton Integrated Research Ethics Board at their meeting held on November 4, 2020. Based on this additional information, we wish to advise your study had been given ***final*** approval from the full HiREB.

The following documents have been approved on both ethical and scientific grounds:

Document Name	Document Date	Document Version
Borg Scale	Sep-19-2020	1
mMRC Dyspnea Score	Sep-19-2020	1
SGRQ	Sep-19-2020	1
Data Collection List_LiveCovidFree_V1_19Sept2020	Sep-19-2020	1
Email Script_LiveCovidFree_19Sept2020	Sep-19-2020	1
Telephone Script_LiveCovidFree_V1_19Sept2020	Sep-19-2020	1
Poster_LiveCovidFree_V1_19Sept2020	Sep-19-2020	1
Study Protocol_LiveCovidFree_V3_7Nov2020 CLEAN	Nov-07-2020	3
Consent Form_LiveCovidFree_V3_7Nov2020 CLEAN	Nov-07-2020	3
Case Report Form_LiveCovidFree_V2_07Nov2020	Nov-07-2020	2
Study ID Key_LiveCovidFree_V3_15Nov2020	Nov-15-2020	3

The following documents have been acknowledged:

Document Name	Document Date	Document Version
citiCompletionReport7144774 Svenningen; Certificate # 26978796	Mar-11-2020	1
citiCompletionReport7144774; Certificate # 35897918	Mar-11-2020	1
245507nol	Nov-05-2020	1
Clinical Trial Registration # NCT04584671		
LiveCovidFree budget 19September2020	Sep-19-2020	1
IRC_scirev_Svenningsen-2020Sep	Sep-24-2020	1

In light of the current COVID-19 pandemic, while this study has been reviewed by HiREB and given final approval status, the actual conduct of the research needs to be performed in accordance with institutional restrictions with respect to Corona virus (which may mean new subjects cannot be actively enrolled and most research staff will be limited with respect to access to other data sources for the time being).

Please Note: All consent forms and recruitment materials used in this study must be copies of the above referenced documents.

We are pleased to issue final approval for the above-named study for a period of 12 months from the date of the HiREB meeting on November 4, 2020. Continuation beyond that date will require further review and renewal of HiREB approval. Any changes or revisions to the original submission must be submitted on a HiREB amendment form for review and approval by the Hamilton Integrated Research Ethics Board.

PLEASE QUOTE THE ABOVE REFERENCED PROJECT NUMBER ON ALL FUTURE CORRESPONDENCE

HiREB

Hamilton Integrated Research Ethics Board

Amendment Approval

May-10-2022

HiREB Project #: 12672

Project Submission Title: Lung Structure-Function In Survivors of Mild and Severe COVID19 Infection: 129Xe MRI and CT For Rapid Evaluations and Next-wave Healthcare Planning

Local Principal Investigator: Dr Sarah Svenningsen

Document(s) Approved:

Document Name	Document Date	Document Version
Study Protocol_LiveCovidFree_V4_8May2022 CLEAN	May-08-2022	4
Summary of Changes to HiREB_Amendment_9May2022	May-09-2022	1

Document(s) Acknowledged:

Document Name	Document Date	Document Version
CTA-N 8May2022 Correspondance for HiREB	May-08-2022	1

This amendment has been reviewed and approved as submitted:

[ ] Full Research Ethics Board

[X] Research Ethics Board Executive

[ ] Student Research Committee

Conditions:
In light of the current COVID-19 pandemic, while HiREB has reviewed and approved this application, the research must be conducted in accordance with institutional and/or public health requirements.

Sincerely,

[redacted]

Dr. Frederick A. Spencer, MD
Chair, Hamilton Integrated Research Ethics Board

The Hamilton Integrated Research Ethics Board (HiREB) represents the institutions of Hamilton Health Sciences, St. Joseph's Healthcare Hamilton, Research St. Joseph's-Hamilton, the Faculty of Health Sciences at McMaster University, and Niagara Health and operates in compliance with and is constituted in accordance with the requirements of: The Tri-Council Policy Statement on Ethical Conduct of Research Involving Humans; The International Conference on Harmonization of Good Clinical Practice Guideline (ICH GCP), Part C Division 5 of the Food and Drug Regulations of Health Canada, Part 4 of the Natural Health Products Regulations; Part 3 of the Medical Devices Regulations and the provisions of the Ontario Personal Health Information Protection Act 2004 and its applicable Regulations. For studies conducted at St. Joseph's Healthcare Hamilton, HiREB complies with the Health Ethics Guide of the Catholic Alliance of Canada.

Curriculum Vitae
Harkiran Kooner, BSc (Hons)

CAMPEP PhD Candidate
Department of Medical Biophysics
Supervisor: Dr. Grace Parraga
Western University

EDUCATION

2020-Present Doctor of Philosophy in Medical Biophysics (*Candidate*)
Department of Medical Biophysics
Western University, London Canada
Supervisor: Dr. Grace Parraga
Thesis Title: Structure and Function of Long-COVID Evaluated Using Pulmonary Imaging

2015-2020 Bachelor of Science Honours (Medical Physics Co-Op)
McMaster University, Hamilton Canada

ACADEMIC POSITIONS AND EMPLOYMENT

2023-2023 **Western University**
Graduate Teaching Assistant
BIOPHYS 9713 – Professional Development for Clinical Medical Physicists

2020-Present **Western University**
Graduate Fellowship

2020 **Robarts Research Institute**
Summer Student Research Trainee

2019-2020 **McMaster Nuclear Reactor**
Lab Assistant

2018 **GlaxoSmithKline**
Process Technologist Summer Student

2018 **Canadian Nuclear Laboratories**
Radiological Software Implementation Specialist

MENTORSHIP DEVELOPMENT AND EXPERIENCES

09/2023-Present **Graduate Student Mentor**
Graduate Student: Sam Tcherner MSc Candidate
Project: "CT Mucus Score Predicts Treatment Response in Moderate Asthma"

09/2023-Present **Graduate Student Mentor**
Graduate Student: Ali Mozaffaripour MSc Candidate
Project: "^{129}Xe MRI Texture Analysis and Machine Learning to Predict Treatment Response in Moderate Asthma"

09/2023-12/2023 **Graduate Student Mentor**
Graduate Student: Yibeltal Aseffa MSc Candidate (International Exchange)
Project: "Automated CT Mucus Scoring Using a Convolutional Neural Network"

09/2022-04/2023 **Graduate Student Mentor**
Undergraduate Thesis Student: Vedanth Desaigoudar BSc Candidate
Project: "Mucus Score in a Healthy Aging Study Group"

09/2021-03/2023 **Graduate Student Mentor**
Graduate Student: Paulina Wyszkiewicz MSc Candidate
Project: "CT Airway Measurements in Longitudinal TINCan Study"

09/2021-04/2022 **Graduate Student Mentor**
Undergraduate Thesis Student: Muhammad Faran BSc Candidate
Project: "Examining Post-Acute COVID-19 using Quantitative CT"

06/2021-08/2021 **Graduate Student Mentor**
Medical Student: Swati Sood MD Candidate
Project: "Quantitative CT of Post-Acute COVID-19 Syndrome"

06/2021-08/2021 **Graduate Student Mentor**
Medical Student: Hammad Saif MD Candidate
Project: "Pulmonary Function of Post-Acute COVID-19 Syndrome"

05/2021-04/2022 **Graduate Student Mentor**
Undergraduate Student: Vedanth Desaigoudar BSc Candidate
Project: "Pulmonary Imaging Biomarkers of Post-Acute COVID-19 Syndrome"

HONOURS, AWARDS, AND RECOGNITIONS

2024 **Top Downloaded Article in Respirology**
Awarded to "Pulmonary Functional MRI: Detecting the structure-function pathologies that drive asthma symptoms and quality of life" for being the in the top 10% of papers downloaded in the first 12 months of publication
International

Assembly on Respiratory Structure and Function of the American Thoracic Society (ATS) Abstract Scholarship
Awarded to an ATS member who submitted an outstanding abstract to the ATS Annual Meeting
International
$395 USD

Canadian Thoracic Society (CTS) Poster Award at the Annual American Thoracic Society (ATS) Conference
Awarded to the top 30 abstract submissions to the ATS Conference by Canadian-based trainees
National

2023 **Natural Sciences and Engineering Research Council of Canada (NSERC) Post-Graduate Scholarship – Doctoral**
Awarded to high-calibre scholars who are engaged in a doctoral program in the natural sciences or engineering
National
$21,000

Western Graduate Research Scholarship, Western University
Awarded to a full-time graduate student for stipend support who maintained an average of 80% or more
Institutional
$5,000

Robarts Research Retreat Poster Presentation Award
Awarded to the presenter with the best poster presentation in their session
Institutional
$50

International Society for Magnetic Resonance in Medicine (ISMRM) Hyperpolarized Media MR Study Group Trainee Poster Award
Awarded to second place HP Media MR Study Group trainee member who submitted an outstanding abstract to the ISMRM Annual Meeting & Exhibition
International
$75 USD

International Society for Magnetic Resonance in Medicine (ISMRM) Educational Stipend
Awarded to ISMRM trainee members who submitted an outstanding abstract to the ISMRM Annual Meeting & Exhibition
International
$475 USD

Canadian Institutes of Health Research – Institute of Circulatory and Respiratory Health (CIHR-ICRH) Spring Travel Award
Awarded to trainees as travel funds in support of knowledge mobilization activities aligned with the CIHR-ICRH vision, mandate, and strategic directions
National
$1,500

2022 **International Workshop on Pulmonary Functional Imaging (IWPFI) Hatabu-Gefter Prize**
Awarded to the IWPFI trainee who placed first in the Young Investigator Award Session oral presentation session at the International Workshop on Pulmonary Functional Imaging
International
500 €

Western Graduate Research Scholarship, Western University
Awarded to a full-time graduate student for stipend support who maintained an average of 80% or more
Institutional
$5,000

International Workshop on Pulmonary Functional Imaging (IWPFI) Young Investigator Travel Stipend
Awarded to IWPFI trainees who submitted an outstanding abstract to the International Workshop on Pulmonary Functional Imaging
International
500 €

Graduate Student Award in Asthma Research on behalf of Asthma Canada, the Canadian Allergy, Asthma and Immunology Foundation (CAAIF) and the Canadian Institutes of Health Research – Institute of Circulatory and Respiratory Health (CIHR-ICRH)
Awarded to students pursuing research for an improved understanding of the causes, mechanisms, treatment, management or cure of asthma
National
$15,000

Canadian Respiratory Research Network Studentship
Awarded to PhD students in order to build Canadian research capacity that contributes to the field of respiratory health with a focus on understanding the origins and progression of airways diseases
National
$10,500 - declined

Natural Sciences and Engineering Research Council of Canada (NSERC) Post-Graduate Scholarship – Doctoral
Awarded to high-calibre scholars who are engaged in a doctoral program in the natural sciences or engineering
National
$21,000

Robarts Research Retreat Oral Presentation Award
Awarded to the presenter with the best oral presentation in their session
Institutional
$200

London Imaging Discovery Day Magna Cum Laude Award
Awarded to the oral presenter in recognition of the distinction of their talk
Institutional

International Society for Magnetic Resonance in Medicine (ISMRM) Educational Stipend
Awarded to ISMRM trainee members who submitted an outstanding abstract to the ISMRM Annual Meeting & Exhibition
International
$655 USD

2021 **Western Graduate Research Scholarship, Western University**
Awarded to a full-time graduate student for stipend support who maintained an average of 80% or more
Institutional
$5,000

International Society for Magnetic Resonance in Medicine (ISMRM) Magna Cum Laude Merit Award
Awarded to trainee members whose abstracts score in the top 15% within a major subject review category
International

Robarts Research Retreat Poster Award
Awarded to the presenter with the best poster in their session
Institutional
$100

Assembly on Respiratory Structure and Function of the American Thoracic Society (ATS) Abstract Scholarship
Awarded to an ATS member who submitted an outstanding abstract to the ATS Annual Meeting
International
$325 USD

International Society for Magnetic Resonance in Medicine (ISMRM) Educational Stipend
Awarded to ISMRM trainee members who submitted an outstanding abstract to the ISMRM Annual Meeting & Exhibition
International
$250 USD

2020 **Western Graduate Research Scholarship, Western University**
Awarded to a full-time graduate student for stipend support who maintained an average of 80% or more
Institutional
$5,000

2019 **Dean's Honour List, McMaster University**
Institutional

2018 **Bronze Global Employee Recognition Award, GlaxoSmithKline**
Awarded to an employee for outstanding contributions to their work
Institutional
$100

2016 **Dean's Honour List, McMaster University**
Institutional

2015 **Honour Entrance Scholarship, McMaster University**
Awarded to an incoming student with a final admission average of 90-94.99%
Institutional
$1,000

Modern Languages Award, St. Augustine Secondary School
Awarded to a graduating student for proficiency in four years of French studies
Institutional
$100

Michael Krupa Memorial Award, St. Augustine Secondary School
Awarded to a graduating student for excellence in science studies
Institutional
$500

COMMUNITY AND VOLUNTEER ACTIVITIES

2021-Present	**St. John's Hospitality Services** Volunteer
2021-2023	**Thames Valley Science & Engineering Fair** Judge
2015-2018	**Brampton Youth Soccer Club** Soccer Referee
2015	**The 2015 Toronto Pan American Games** Events and Venue Management Volunteer
2014-2017	**Credit Valley Hospital** Youth Volunteer
2014-2016	**SEVA Food Bank** Volunteer
2014-2015	**St. Augustine Secondary School** Student Council Secretary
2013-2015	**St. Augustine Secondary School** Girls' Leadership Club President
2013-2015	**St. Augustine Secondary School** Leader of Local Rotary Club Student Group

INVITED TALKS *denotes presenter

1. **HK Kooner*,** MJ McIntosh, I Dhaliwal, JM Nicholson, and G Parraga. Post-Acute COVID-19 Syndrome: Imaging Research Update. London Health Sciences Centre Respirology Rounds. Virtual. June 14, 2023.
2. **HK Kooner*,** M Sharma, MJ McIntosh, I Dhaliwal, JM Nicholson, and G Parraga. ^{129}Xe MRI Ventilation Predicts Longitudinal Quality-of-Life Improvement in Post-Acute COVID-19 Syndrome. Hyperpolarized Study Group Business Meeting, Toronto, Canada. June 7, 2023.
3. **HK Kooner***, MJ McIntosh, RL Eddy, A Gendron, C Licskai, C Yamashita and G Parraga. CT Mucus Score Predicts Benralizumab Response in Severe Asthma. American Thoracic Society Respiratory Structure and Function Mini-Symposia: Illuminating Lung Structure and Function via Novel Imaging, Virtual. November 16, 2021.

MEDIA CONTRIBUTIONS

1. Women with Post-Acute COVID-19 Syndrome Have Worse Airway Structure Than Men. *Healio Pulmonology*. Lay Article. https://www.healio.com/news/pulmonology/20230531/women-with-postacute-covid19-syndrome-have-worse-airway-structure-than-men. May 31, 2023.

2. ^{129}Xe MRI Offers Detailed View of Pulmonary Function and Huge Clinical Potential. *Pulmonology Advisor*. Lay Article. https://www.pulmonologyadvisor.com/home/general-pulmonology/129xe-mri-offers-detailed-view-of-pulmonary-function-and-huge-clinical-potential/. August 19, 2022.

PUBLICATIONS AND PRESENTATIONS

A Peer-Reviewed Journal Manuscripts

Published (13 total, 7 first-author) **denotes co-primary authors*

1. **HK Kooner**, M Sharma, MJ McIntosh, I Dhaliwal, JM Nicholson, M Kirby, S Svenningsen, and G Parraga. ^{129}Xe MRI Ventilation Textures and Longitudinal Quality-of-Life Improvements in Long-COVID. *Academic Radiology* 2024. doi: 10.1016/j.acra.2024.03.014.
2. A Mozaffaripour, **HK Kooner**, and G Parraga. Reply to Leung *et al*: Dose Modulation, BMI and CT-Air Trapping. *American Journal of Respiratory and Critical Care Medicine* 2024. doi: 10.1164/rccm.202402-0353LE.
3. MJ McIntosh, JJ Hofmann, **HK Kooner**, RL Eddy, and G Parraga. ^{129}Xe MRI and Oscillometry in Irritant-Induced Asthma following Bronchial Thermoplasty. *Chest* 2024; 165(2):e27-e31. doi: 10.1016/j.chest.2023.09.10
4. MJ McIntosh, AM Matheson, **HK Kooner**, RL Eddy, H Serajeddini, C Yamashita, and G Parraga. Pulmonary Vascular Differences in Eosinophilic Asthma after 2.5-years anti-IL-5Rα Treatment. *American Journal of Respiratory and Critical Care Medicine* 2023; 208(9): 998-1001. doi: 10.1164/rccm.202305-0849LE
5. **HK Kooner**, MJ McIntosh, AM Matheson, S Svenningsen, and G Parraga. More Data about ^{129}Xe MRI Ventilation Defects in Long COVID-19. *Radiology* 2023; 307(4): e230749. doi: 10.1148/radiol.230479
6. MJ McIntosh, A Biancaniello, **HK Kooner**, A Bhalla, C Yamashita, G Parraga, H Serajeddini and RL Eddy. ^{129}Xe MRI Ventilation Defects: What is the Upper Limit of Normal and Minimal Clinically Important Difference? *Academic Radiology* 2023. doi: 10.1016/j.acra.2023.03.010
7. MJ McIntosh*, **HK Kooner***, RL Eddy, A Wilson, H Serajeddini, A Bhalla, C Licskai, CA Mackenzie, C Yamashita and G Parraga. Mucus and ^{129}Xe MRI Ventilation Defects after 2.5-years anti-IL-5Rα in Eosinophilic Asthma. *Chest* 2023; 164(1): 27-38. doi: 10.1016/j.chest.2023.02.009. **Editorialized**
8. **HK Kooner**, MJ McIntosh, AM Matheson, M Abdelrazek, MS Albert, I Dhaliwal, M Kirby, A Ouriadov, GE Santyr, C Venegas, N Radadia, S Svenningsen, JM Nicholson, and G Parraga. Post-Acute COVID-19 Syndrome: ^{129}Xe MRI Ventilation Defects and Respiratory Outcomes One Year Later. *Radiology* 2023; 307(2): e222557. doi: 10.1148/radiol.222557 **Editorialized**
9. AM Matheson, MJ McIntosh, **HK Kooner**, M Abdelrazek, MS Albert, I Dhaliwal, JM Nicholson, A Ouriadov, S Svenningsen and G Parraga. Longitudinal follow-up of post-acute COVID-19 syndrome: Improved DL_{CO}, Quality-of-life and MRI pulmonary gas-exchange abnormalities. *Thorax* 2023; 78: 418-421. doi: 10.1136/thorax-2022-219378
10. AM Matheson, MJ McIntosh, **HK Kooner**, J Lee, V Desaigoudar, E Bier, B Driehuys, S Svenningsen, GE Santyr, M Kirby, MS Albert, Y Shepelytskyi, V Grynko, A Ouriadov, M Abdelrazek, I Dhaliwal, JM Nicholson and G Parraga. Persistent Lung Vascular Abnormalities in Never-hospitalized people with post-acute COVID19 syndrome. *Radiology* 2022; 305(2): 466-477. doi: 10.1148/radiol.220492. **Editorialized**
11. **HK Kooner***, MJ McIntosh*, AM Matheson, C Venegas, N Radadia, T Ho, E Haider, NB Konyer, GE Santyr, MS Albert, A Ouriadov, M Abdelrazek, M Kirby, I Dhaliwal, JM Nicholson, P Nair, S Svenningsen and G Parraga. ^{129}Xe MRI Ventilation Defects in ever- and never-hospitalised people with post-acute COVID-19 syndrome. *BMJ Open Respiratory Research* 2022; 9: e001235. doi: 10.1136/bmjresp-2022-001235
12. MJ McIntosh*, **HK Kooner***, RL Eddy, S Jeimy, C Licskai, CA MacKenzie, S Svenningsen, P Nair, C Yamashita and G Parraga. Mucus plugs, ^{129}Xe ventilation defects and asthma control

after one dose of Benralizumab. *Chest 2022*; 162(3): 520-533. doi: 10.1016/j.chest.2022.03.003.

13. **HK Kooner**, MJ McIntosh, V Desaigoudar, JH Rayment, RL Eddy, B Driehuys and G Parraga. Pulmonary functional MRI: Detecting the structure-function pathologies that drive asthma symptoms and quality of life. *Respirology* 2022; 27(2): 114-133. doi: 10.1111/resp.14197 **Cover of Journal.**

Submitted (5 total, 2 first-author)

1. AM Matheson, MJ McIntosh, **HK Kooner**, S Svenningsen, RL Eddy, J Rayment, and G Parraga. Multi-site Validation of Fully-automated Convolutional Neural Networks for Hyperpolarized Gas MRI Ventilation Quantification. *Submitted to J Magn Reson Imaging* (Manuscript ID JMRI-23-1973).
2. **HK Kooner**, H Serajeddini, RL Eddy, C Yamashita, S Svenningsen, and G Parraga. CT Airway Mucus in Older People without Chronic Respiratory Illness. *Submitted to Chest* (Manuscript ID CHEST-D-24-00406).
3. VC Poulos, S Kassarian, M Sharma, **HK Kooner**, MJ McIntosh, G Parraga and MA Mitchell. Oscillometry, Lung Clearance Index and ^{129}Xe MRI Detect Small Airways Dysfunction in Sarcoidosis. *Submitted to Thorax* (Manuscript ID thorax-2023-221198).
4. **HK Kooner**, PV Wyszkiewicz, AM Matheson, MJ McIntosh, M Abdelrazek, I Dhaliwal, JM Nicholson, M Kirby, S Svenningsen, and G Parraga. Chest CT Airway and Vascular Measurements in Females with Long-COVID, Ex-smokers and COPD Patients. *Submitted to Respirology* (Manuscript ID RES-24-007).
5. A Mozaffaripour*, S Tcherner*, M Sharma, **HK Kooner**, MJ McIntosh, M Sherwood, N Paul, JM Nicholson, I Dhaliwal, S Jeimy, C Licskai, CA Mackenzie, M Kuprowski, A Bhalla, C Yamashita and G Parraga. Hyperpolarized ^{129}Xe Ventilation MRI Response to ICS/LABA/LAMA and Role of Type-2 Inflammation in Poorly-Controlled Asthma. *Submitted to Thorax* (Manuscript ID thorax-2024-221681).

B Published Conference Abstracts

Accepted (10 total, 3 first-author)

International & National (10 total, 3 first-author)

1. **HK Kooner**, M Sharma, A Mozaffaripour, S Tcherner, MJ McIntosh, N Paul, C Yamashita, and G Parraga. Are There Pulmonary Vascular Differences in GINA 4 and GINA 5 Asthma Severity? American Thoracic Society Annual Scientific Meeting. San Diego, CA, USA. May 17-24, 2024. *Accepted Oral Presentation.*
2. **HK Kooner**, S Tcherner, H Serajeddini, A Mozaffaripour, M Sharma, Y Aseffa, N Paul, C Yamashita, and G Parraga. Does CT Mucus Burden Differ in Mild-moderate Asthma Compared to Severe Asthma? American Thoracic Society Annual Scientific Meeting. San Diego, CA, USA. May 17-24, 2024. *Accepted Poster Presentation.*
3. M Sharma, **HK Kooner**, S Tcherner, A Mozaffaripour, N Paul, C Yamashita, and G Parraga. ^{129}Xe MR Evidence of Abnormal Gas-exchange in Mild-moderate and Severe Asthma. American Thoracic Society Annual Scientific Meeting. San Diego, CA, USA. May 17-24, 2024. *Accepted Poster Presentation.*
4. M Sharma, **HK Kooner**, S Tcherner, A Mozaffaripour, N Paul, C Yamashita, and G Parraga. Rapid and Persistent 6-week Response to ICS/LABA/LAMA in Mild-Moderate Asthma. American Thoracic Society Annual Scientific Meeting. San Diego, CA, USA. May 17-24, 2024. *Accepted Poster Presentation.*
5. MJ McIntosh, **HK Kooner,** RL Eddy, C Licskai, C Yamashita, and G Parraga. Poorly controlled eosinophilic Asthma: Relationships of Airwave Oscillometry Resistance with CT Airway Measurements. American Thoracic Society Annual Scientific Meeting. San Diego, CA, USA. May 17-24, 2024. *Accepted Poster Presentation.*

6. S Tcherner, A Mozaffaripour, **HK Kooner**, M Sharma, MJ McIntosh, Y Aseffa, N Paul, C Yamashita, and G Parraga. CT Mucus Score predicts Response to ICS/LABA/LAMA in Moderate Asthma. American Thoracic Society Annual Scientific Meeting. San Diego, CA, USA. May 17-24, 2024. *Accepted Poster Presentation.*
7. A Mozaffaripour, S Tcherner, M Sharma, **HK Kooner**, MJ McIntosh, N Paul, C Yamashita, and G Parraga. ^{129}Xe MRI and Oscillometry Evidence of Improved Small Airways Dysfunction after 6-Weeks ICS/LABA/LAMA Therapy in Moderate Asthma. American Thoracic Society Annual Scientific Meeting. San Diego, CA, USA. May 17-24, 2024. *Accepted Poster Presentation.*
8. **HK Kooner**, M Sharma, A Mozaffaripour, S Tcherner, C Yamashita, and G Parraga. ^{129}Xe MRS Biomarkers Predict 6-week Response to ICS/LAMA/LABA in Moderate Asthma. Annual International Society of Magnetic Resonance in Medicine Scientific Meeting 2024. Singapore. May 4-9, 2024. *Accepted Poster Presentation.*
9. M Sharma, **HK Kooner**, A Mozaffaripour, S Tcherner, C Yamashita, and G Parraga. ^{129}Xe MR Spectroscopy Reveals Abnormal Gas-exchange in Moderate and Severe Asthma. Annual International Society of Magnetic Resonance in Medicine Scientific Meeting 2024. Singapore. May 04-09, 2023. *Accepted Poster Presentation.*
10. A Mozaffaripour, S Tcherner, M Sharma, **HK Kooner**, MJ McIntosh, Cory Yamashita, and G Parraga. ^{129}Xe MRI Ventilation Texture Features and Machine Learning to Predict Response to ICS/LAMA/LABA in Moderate Asthma. Annual International Society of Magnetic Resonance in Medicine Scientific Meeting 2024. Singapore. May 4-9, 2024. *Accepted Poster Presentation.*

C Proffered Oral Presentations (18 total, 5 first-author) **presenter*

International & National (12 total, 3 first-author)

1. MJ McIntosh*, AM Matheson, **HK Kooner,** RL Eddy, C Yamashita and G Parraga. Pulmonary Vascular Redistribution following 2.5-years anti-IL5-Rα treatment in Eosinophilic Asthma. American Thoracic Society Annual Scientific Meeting. Washington, DC. May 19-24, 2023.
2. M Sharma*, PV Wyszkiewicz, MJ McIntosh, **HK Kooner,** AM Matheson, DG McCormack and G Parraga. MRI and CT Measurements Uniquely Explain All-cause Mortality in Ex-smokers with and without COPD. American Thoracic Society Annual Scientific Meeting. Washington, DC. May 19-24, 2023.
3. MJ McIntosh*, AM Matheson, **HK Kooner,** RL Eddy, C Yamashita and G Parraga. Pulmonary Vascular Redistribution following 2.5-years anti-IL5-Rα treatment in Eosinophilic Asthma. The 2023 International Workshop on Pulmonary Imaging. Philadelphia, PA. February 23-25, 2023.
4. V Desaigoudar*, PV Wyszkiewicz, AM Matheson, M Sharma, MJ McIntosh, **HK Kooner**, DG McCormack and G Parraga. CT Pulmonary Vascular, Airway, Pulmonary Artery and Aorta Measurements in Ex-Smokers with and without COPD. Canadian Undergraduate Medical Physics Conference. August 25 2022. Virtual.
5. **HK Kooner*** and G Parraga. Post-acute COVID-19 Syndrome: ^{129}Xe MRI Ventilation Defects One Year Later. Canadian Respiratory Research Network Annual Meeting 2022, Ottawa, Canada. October 20-21, 2022.
6. **HK Kooner***, MJ McIntosh, AM Matheson, M Abdelrazek, I Dhaliwal, JM Nicholson and G Parraga. ^{129}Xe MRI Ventilation Improvements 15 Months Post-COVID Infection. International Workshop on Pulmonary Functional Imaging 2022. Hannover, Germany. September 15-17, 2022.
7. M Sharma*, MJ McIntosh, **HK Kooner**, DG McCormack and G Parraga. Machine-learning and Texture Analysis of Hyperpolarized ^{3}He MRI Ventilation Predict Quality-of-Life Worsening in Ex-smokers with and without COPD. Canadian Organization of Medical Physicists Annual Scientific Meeting, Quebec City, Canada. June 22-25, 2022.
8. AM Matheson*, **HK Kooner,** E Bier, J Lu, B Driehuys, M Kirby, G Santyr, MS Albert, Y Shepelytskyi, V Grynko, S Svenningsen, A Ouriadov, I Dhaliwal, JM Nicholson and G Parraga. ^{129}Xe Gas-Transfer MRI RBC-to-Barrier Ratio in Post-Acute COVID19 Syndrome. Polarization in Noble Gases Workshop 2021, Virtual. December 6-10, 2021.

9. MJ McIntosh*, AM Matheson, M Sharma, **HK Kooner**, RL Eddy, DG McCormack, C Yamashita and G Parraga. Pulmonary ^{1}H MRI Lobar Classification Using Convolutional Neural Networks. Canadian Organization of Medical Physicists Annual Scientific Meeting, Virtual. June 22-25, 2021.
10. **HK Kooner***, MJ McIntosh, M Sharma, AM Matheson, Y Rajapaksa, I Dhaliwal, JM Nicholson and G Parraga. Hyperpolarized ^{129}Xe MRI Ventilation Texture Features to Characterize Long-haul COVID-19 Survivors. International Society for Magnetic Resonance in Medicine Annual Meeting & Exhibition, Virtual. May 15-20, 2021.
11. MJ McIntosh*, **HK Kooner**, RL Eddy, C Licskai, C Yamashita, A Gendron and G Parraga. Response to Benralizumab in Severe Asthma: Oscillometry and MRI Ventilation Defect Improvements in Participants with Abnormal FeNO. American Thoracic Society Annual Scientific Meeting, Virtual. May 14-19, 2021.
12. M Sharma*, MJ McIntosh, AM Matheson, **HK Kooner**, DG McCormack, DA Palma and G Parraga. 6MWD Worsening in COPD Predicted using CT and MRI Texture Features and Machine Learning. American Thoracic Society Annual Scientific Meeting, Virtual. May 14-19, 2021.

Regional & Local (6 total, 2 first-author)

1. MJ McIntosh*, M Sharma, **HK Kooner,** H Serajeddini, A Bhalla, C Yamashita, and G Parraga. Hyperpolarized ^{129}Xe MRI ventilation textures predict short and long-term response to Anti-IL-5Rα Biologic Therapy in Eosinophilic Asthma. Imaging Network of Ontario Annual Symposium, London Ontario. March 23-24, 2023.
2. **HK Kooner***, MJ McIntosh, AM Matheson, M Sharma, PV Wyszkiewicz, I Dhaliwal, M Abdelrazek, JM Nicholson, and G Parraga. ^{129}Xe MRI Ventilation Defects in People with Post-Acute COVID-19 Syndrome. Robarts Research Retreat. London ON, Canada. June 16, 2022.
3. **HK Kooner***, MJ McIntosh, AM Matheson, M Sharma, PV Wyszkiewicz, I Dhaliwal, JM Nicholson, M Abdelrazek, and G Parraga. ^{129}Xe MRI Ventilation Defects in People with Post-Acute COVID-19 Syndrome. London Imaging Discovery Day. London ON, Canada. June 9, 2022.
4. MJ McIntosh*, **HK Kooner**, RL Eddy, C Licskai, C Yamashita and G Parraga. ^{129}Xe MRI Ventilation Response to Benralizumab in Severe Asthma. London Imaging Discovery Day. London ON, Canada. June 9, 2022.
5. AM Matheson*, MJ McIntosh, **HK Kooner**, J Lee, V Desaigoudar, A Ouriadov, M Abdelrazek, I Dhaliwal, JM Nicholson and G Parraga. ^{129}Xe Gas-Transfer MRI RBC-to-Barrier Ratio in Post-Acute COVID19 Syndrome: Clinically-relevant? London Imaging Discovery Day. London ON, Canada. June 9, 2022.
6. M Sharma*, MJ McIntosh, **HK Kooner**, AM Matheson, PV Wyszkiewicz, DG McCormack, and G Parraga. Texture Analysis and Machine Learning of Hyperpolarized ^{3}He MRI Ventilation Predicts Quality-of-life Worsening in Ex-smokers with and without COPD. London Imaging Discovery Day. London ON, Canada. June 9, 2022.

D Proffered Poster Presentations (24 total, 7 first-author) **denotes presenter*

International & National (12 total, 4 first-author)

1. **HK Kooner*,** M Sharma, MJ McIntosh, I Dhaliwal, JM Nicholson, and G Parraga. ^{129}Xe MRI Ventilation Predicts Longitudinal Quality-of-Life Improvement in Post-Acute COVID-19 Syndrome. Annual International Society of Magnetic Resonance in Medicine Scientific Meeting 2023, Toronto, Canada. June 3-8, 2023.
2. MJ McIntosh*, M Sharma, **HK Kooner,** H Serajeddini, A Bhalla, C Yamashita, and G Parraga. Hyperpolarized ^{129}Xe MRI ventilation textures predict short and long-term response to Anti-IL-5Rα Biologic Therapy in Eosinophilic Asthma. Annual International Society of Magnetic Resonance in Medicine Scientific Meeting 2023, Toronto, Canada. June 3-8, 2023.

3. PV Wyszkiewicz*, M Sharma, **HK Kooner,** DG McCormack, M Kirby and G Parraga. Terminal Airspace Enlargement Measured Using Pulmonary Functional MRI Predicts CT Airway Loss in COPD. Annual International Society of Magnetic Resonance in Medicine Scientific Meeting 2023, Toronto, Canada. June 3-8, 2023.
4. **HK Kooner*,** M Faran, MJ McIntosh, AM Matheson, PV Wyszkiewicz, I Dhaliwal, M Abdelrazek, JM Nicholson, and G Parraga. Sex Differences in CT Airway Measurements and their Relationship to Post-Acute COVID-19 Syndrome. American Thoracic Society Annual Scientific Meeting. Washington, DC. May 19-24, 2023.
5. JM Nicholson, AM Matheson*, **HK Kooner,** MJ McIntosh, S Svenningsen and G Parraga. Unique MRI Phenotypes Help Explain Post-Acute COVID-19 Syndrome. American Thoracic Society Annual Scientific Meeting. Washington, DC. May 19-24, 2023.
6. A Biancaniello*, MJ McIntosh, **HK Kooner,** A Bhalla, C Yamashita, G Parraga, RL Eddy, and H Serajeddini. Minimal Clinically Important Difference for ^{129}Xe MRI Ventilation Defect Percent in Patients with Asthma. American Thoracic Society Annual Scientific Meeting. Washington, DC. May 19-24, 2023.
7. AM Matheson*, MJ McIntosh, **HK Kooner**, C Yamashita, and G Parraga. ^{129}Xe Magnetic Resonance Spectroscopy: Abnormal Cardiogenic Oscillations in Severe Asthma. International Workshop on Pulmonary Functional Imaging 2022. Hannover, Germany. September 15-17, 2022.
8. **HK Kooner***, MJ McIntosh, M Sharma, GV Singh, N Nasir, E Blake, I Dhaliwal, JM Nicholson, M Kirby, and G Parraga. Post-Acute COVID-19 Syndrome: Longitudinal ^{129}Xe MRI Ventilation Heterogeneity Measurements. Joint Annual International Society of Magnetic Resonance in Medicine-European Society for Magnetic Resonance in Medicine and Biology Scientific Meeting 2022, London, England, UK. May 7-12, 2022.
9. AM Matheson*, **HK Kooner,** E Bier, J Lu, B Driehuys, M Kirby, G Santyr, MS Albert, Y Shepelytskyi, V Grynko, S Svenningsen, A Ouriadov, I Dhaliwal, JM Nicholson, and G Parraga. ^{129}Xe Gas-Transfer MRI RBC-to-Barrier Ratio in Post-Acute COVID19 Syndrome: Clinically-relevant? Joint Annual International Society of Magnetic Resonance in Medicine-European Society for Magnetic Resonance in Medicine and Biology Scientific Meeting 2022, London, England, UK. May 7-12, 2022.
10. M Sharma*, **HK Kooner**, MJ McIntosh, DG McCormack, and G Parraga. Quality-of-life Worsening Predicted Using Baseline Hyperpolarized ^{3}He MRI Ventilation Texture Features and Machine-Learning. Joint Annual International Society of Magnetic Resonance in Medicine-European Society for Magnetic Resonance in Medicine and Biology Scientific Meeting 2022, London, England, UK, Virtual. May 7-12, 2022.
11. MJ McIntosh*, M Sharma, AM Matheson, **HK Kooner**, RL Eddy, C Licksai, DG McCormack, JM Nicholson, C Yamashita and G Parraga. Respiratory System Resistance Explained using Hyperpolarized ^{129}Xe MRI Texture Features and Machine Learning. Joint Annual International Society of Magnetic Resonance in Medicine-European Society for Magnetic Resonance in Medicine and Biology Scientific Meeting 2022, London, England, UK. May 7-12, 2022.
12. **HK Kooner***, MJ McIntosh, RL Eddy, A Gendron, C Licskai, C Yamashita and G Parraga. CT Mucus Score Predicts Benralizumab Response in Severe Asthma. American Thoracic Society Annual Scientific Meeting, Virtual. May 14-19, 2021.

Regional & Local (12 total, 3 first-author)

1. **HK Kooner*,** M Faran, MJ McIntosh, AM Matheson, PV Wyszkiewicz, I Dhaliwal, M Abdelrazek, JM Nicholson, and G Parraga. Sex Differences in CT Airway Measurements and their Relationship to Post-Acute COVID-19 Syndrome. Robarts Research Retreat. London, ON. June 28, 2023.
2. MJ McIntosh*, AM Matheson, **HK Kooner,** RL Eddy, C Yamashita and G Parraga. Pulmonary Vascular Redistribution following 2.5-years anti-IL5-Rα treatment in Eosinophilic Asthma. Robarts Research Retreat. London, ON. June 28, 2023.

3. A Biancaniello*, MJ McIntosh, **HK Kooner,** A Bhalla, C Yamashita, G Parraga, RL Eddy, and H Serajeddini. Minimal Clinically Important Difference for ^{129}Xe MRI Ventilation Defect Percent in Patients with Asthma. Robarts Research Retreat. London, ON. June 28, 2023.
4. M Sharma*, PV Wyszkiewicz, MJ McIntosh, **HK Kooner,** AM Matheson, DG McCormack and G Parraga. MRI and CT Measurements Uniquely Explain All-cause Mortality in Ex-smokers with and without COPD. Robarts Research Retreat. London, ON. June 28, 2023.
5. **HK Kooner*,** M Faran, MJ McIntosh, AM Matheson, PV Wyszkiewicz, I Dhaliwal, M Abdelrazek, JM Nicholson, and G Parraga. Sex Differences in CT Airway Measurements and their Relationship to Post-Acute COVID-19 Syndrome. Imaging Network of Ontario Annual Symposium, London Ontario. March 23-24, 2023.
6. M Sharma*, PV Wyszkiewicz, MJ McIntosh, **HK Kooner,** AM Matheson, DG McCormack and G Parraga. CT and MRI Measurements Uniquely Explain All-cause Mortality in Ex-smokers. Imaging Network of Ontario Annual Symposium, London Ontario. March 23-24, 2023.
7. A Biancaniello*, H Serajeddini, MJ McIntosh, **HK Kooner**, A Bhalla, C Yamashita, RL Eddy, and G Parraga. Minimal Clinically Important Difference for ^{129}Xe MRI Ventilation Defect Percent in Patients with Asthma. Imaging Network of Ontario Annual Symposium, London Ontario. March 23-24, 2023.
8. V Desaigoudar*, PV Wyszkiewicz, AM Matheson, M Sharma, MJ McIntosh, **HK Kooner,** DG McCormack and G Parraga. Pulmonary Small Vessel Worsening in Ex-smokers with COPD. Imaging Network of Ontario Annual Symposium, London Ontario. March 23-24, 2023.
9. MJ McIntosh*, **HK Kooner**, RL Eddy, C Licskai, C Yamashita and G Parraga. ^{129}Xe MRI Ventilation Response to Benralizumab in Severe Asthma. Robarts Research Retreat. London ON, Canada. June 16, 2022.
10. AM Matheson*, MJ McIntosh, **HK Kooner**, J Lee, V Desaigoudar, A Ouriadov, M Abdelrazek, I Dhaliwal, JM Nicholson and G Parraga. ^{129}Xe Gas-Transfer MRI RBC-to-Barrier Ratio in Post-Acute COVID19 Syndrome: Clinically-relevant? Robarts Research Retreat. London ON, Canada. June 16, 2022.
11. M Sharma*, MJ McIntosh, **HK Kooner**, AM Matheson, PV Wyszkiewicz, DG McCormack, and G Parraga. Texture Analysis and Machine Learning of Hyperpolarized ^{3}He MRI Ventilation Predicts Quality-of-life Worsening in Ex-smokers with and without COPD. Robarts Research Retreat. London ON, Canada. June 16, 2022.
12. **HK Kooner*** and G Parraga. Hyperpolarized ^{129}Xe MRI Ventilation Texture Features to Characterize Post-Acute COVID-19 Syndrome. Robarts Research Retreat, Virtual. June 15, 2021.

COMMITTEES AND PROFESSIONAL ACTIVITIES

2020-Present
Western University Medical Biophysics CAMPEP Student Club
MEMBER

2019-2020
McMaster Science Cooperative Education
MEMBER: Peer Mentor

PROFESSIONAL SOCIETIES

2023-Present American Association of Physicists in Medicine (AAPM)
Student Member

2020-Present Canadian Organization of Medical Physicists (COMP)
Student Member

2020-Present	Canadian Thoracic Society (CTS) *Student Member*
2020-Present	American Thoracic Society (ATS) *Trainee Member*
2020-Present	European Respiratory Society (ERS) *Student Member*
2020-Present	International Society for Magnetic Resonance in Medicine (ISMRM) *Trainee Member*